CRANFIELD UNIVERSITY

TAREQ A. ALAWADI

Investigation of the Effects of Cloud Attenuation on Satellite Communication Systems

School of Engineering
Department of Engineering Physics

Submitted for the Degree of PhD
Academic Year: 2011 - 2012

Supervisor: Dr A. Savvaris
July 2012

CRANFIELD UNIVERSITY

School of Engineering

PhD Thesis

Academic Year 2011 - 2012

TAREQ A. ALAWADI

Investigation of the Effects of Cloud Attenuation on Satellite Communication Systems

Supervisor: Dr A. Savvaris

July 2012

This thesis is submitted in partial fulfilment of the requirements
for the degree of PhD

ABSTRACT

The aim of this project is to investigate the attenuation due to clouds at 20-50GHz; to develop an accurate long-term prediction model of cloud attenuation applicable to slant-path links and evaluate the impact of cloud attenuation dynamics on the design of future portable EHF earth-space systems. Higher frequencies offer several advantages, for example, greater bandwidth and immunity to ionospheric effects. The EHF band is being targeted for the launch of earth-space communication systems to provide global delivery of bandwidth-intensive services (e.g. interactive HDTV, broadband internet access and multimedia services, television receive-only, etc.) to portable terminal units. Since spectrum shortage and terminal bulk currently preclude the realization of these breakthrough-broadband wireless communication services at lower frequencies, a better understanding is needed in order to optimize their usage.

One major obstacle in the design of EHF earth-space communication systems is the large and variable signal attenuation in the lower atmosphere, due to a range of mechanisms including attenuation (and scattering) due to clouds and rain, tropospheric scintillation caused by atmospheric turbulence and variable attenuation by atmospheric gasses. In particular, cloud attenuation becomes very significant at EHF.

In this thesis, we start with an overview of literature review in the first chapter. Followed next by the theory and description of accepted-up to date- cloud attenuation models in the field (chapter 2). Then followed up by a description of the pre-processing, validations, sources and assumptions made in order to conduct the analysis of the cloud attenuation in this work (chapter 3). Afterwards, a comprehensive analysis of Meteorological and local tropospheric degradation was carried out (chapter 4). That was followed by an overview of cloud fade statistics and suggested methods to counter their effects (chapter 5). And finally the improved cloud attenuation model and the enhancement of the currently accepted cloud attenuation model (ITU-R 840.4) by terms of validating the effective temperature concept and ways of acquiring it (chapter 6).

ACKNOWLEDGEMENTS

First of all, I would like to express my thanks to my supervisor Professor Ali Savvaris for his supervision and advice over the course of this work. He would go out of his way to accommodate and help me on both professional and humanitarian levels even though he might be heavily occupied. I'd also like to thank Dr. Spiro Ventouras from STFC for all his help and invaluable discussions.

I felt that my interaction with my department colleagues added to my experience in Cranfield greatly. Naseem Akhtar, Kashif Iqbal, Guido Monterzino, Ramey Jamal, Solange Baena, Paul Jemitola, Mudassir Lone, Ken Lai, Peter Thomas, Henry Leonardo, Hamid Al-Turbah, Angelina Croft, Ting Ding, Francis Salama, Baba Omar, Yosuke Shimada, Samer Muhi, Shirley Mao, Marco and Pierre, are appreciated for the memories in and out of the office. Your friendship made life in Cranfield that much bearable.

A special thanks goes to Hakim Oheda, for all the good, the bad and the ugly times that we shared together in and out of the office. It was (and still is) my privilege to have known you.

Not forgetting the reason that made me continue my studies, I wish to thank my family. My parents, Amin and Fatt-heyyah, my wife Abrar (we went through a lot while in Cranfield) And my darling children: Soloman, Luluwa, Dawood and Sarah. Your father loves you very much.

None of my achievements would have been possible without the grace and blessings of Allah the almighty. The more I know the less I know, and the more my faith in Allah strengthens. I pray that he continues to bestow his blessings and protection over us, all whom we hold dear and the rest of humanity... Amen.

TAREQ ALAWADI

TABLE OF CONTENTS

LIST OF FIGURES

LIST OF TABLES

List of Symbols

α_m	Mie specific attenuation
α_r	Rayleigh specific attenuation
α_{ci}	specific attenuation for each cloud type
A	attenuation
A_c	attenuation in cloud
A_{ci}	cloud attenuation due to specific cloud type
a_c	critical radius of droplets
a	scatterer radius
Δl	vertical distance between cloud top and base
$\varepsilon(f)$	complex dielectric permittivity of water
ε'	real part of $\varepsilon(f)$
ε''	imaginary part of $\varepsilon(f)$
ε	random errors
$\varepsilon_0, \varepsilon_1, \varepsilon_2$	constants
$E(r)$	electric field
$E_i(r)$	incident electric field
E_b	energy per bit
E_i	amplitude of electric field
f	frequency in Giga Hertz (GHz)

f_p	primary frequency
f_s	secondary frequency
γ_c	specific attenuation within cloud
k_0	wave number (free-space)
K_l	specific attenuation coefficient
λ	wavelength
L	liquid water path (LWP)
L_{red}	reduced LWP (0^o C)
η	$= \frac{2+\varepsilon'}{\varepsilon''}$
N''_w	imaginary part of complex refractivity
N_0	noise density
$n(r)$	refractive index
ρ	water density (g/m^3)
P_o	probability of attenuation due to cloud
p	probability of attenuation exceeding a given value in time
σ_a	absorption extinction
σ_c	standard deviation of A_c
σ_s	scattering extinction
σ_t	total extinction
$\overline{S}$	averaged Poynting vector

θ	elevation angle in degrees
θ_T	reciprocal (inverted) temperature
T	temperature
T_f	effective temperature
u_x	polarization orientation
U_c	critical humidity function
v	cloud liquid water content (g/m^3)
V	volume of scatterer
W_{red}	reduced liquid water content
w	liquid water density (content) in cloud
χ	attenuation amplitude
χ_T	threshold level

1 Satellite Communication (Satcom)

1.1 Synopses

There are various types of satellite systems in operation today; they vary in shape, size, functionality and nationality. For the principle of putting man-made object into orbit was still theoretical until the first satellite released (Sputnik 1) by the Soviet Union on October 4th, 1957 and the United State retaliating with SCORE, launched on December 18th, 1958. The race between the US and the Soviet Union sparked a new era of space exploration [1].

The Satcom concept in the early days was to act as a repeater to connect two points on the globe. There was a debate about two approaches: active and passive satellites. The scales tipped in favor of the active satellites for the reason of signal amplification trait. However, with the technological advancements, commercial and political (military) influence they now include processing equipment and are of many uses (laboratories, TV, Global positioning service, mobile services, internet, espionage…etc.).

This chapter will serve as a concise literature review on satellite communications, their uses, particulars, the atmosphere, clouds and other satcom signal attenuators.

1.1.1 Advantages of Satellite Communications

The use of satellites offers several advantages. As the technology evolves so will the extents of these advantages [2]. Some of those advantages are listed below:

Mobile/Wireless Communication, Independence of Location

1. Wide Area Coverage: Country, Continent, Globe
2. Wide Bandwidth Available Throughout (e.g. C/Ku Satellites have bandwidth of the order of 1 GHz)
3. Independence From Terrestrial Infrastructure
4. Rapid Installation of Ground Networks
5. Low Cost per Added Site

1.1.2 Types of orbit

There are 2 major classifications of Satellite orbits, namely Elliptical Orbits (e.g. MOLNYA, TUNDRA) and Circular Orbits. The choice of any of these orbits is made based on the tasks, services and geographical coverage that are in need of the satellite. A sub-classification exists based on the distance of the satellite from the Earth:

1. Low Earth Orbits:- LEO, for low power and minimum signal path-delay
2. Medium Earth Orbits: - MEO, in-between the LEO and GEO usage.
3. Geostationary Earth Orbits:- GEO, for wide coverage area
4. High (Elliptical) Earth Orbits: - HEO, is rather not-fully exploited for SATCOM yet!

LEO/MEO satellite systems operate at altitudes ranging between 200-1000 km for LEO and around 10000 km for MEO. The period of LEO satellite systems is between 1.5-1.8 hours and the period increases with the altitude. As for MEO systems the period is about 6 hours meaning that the satellite is visible above a given geographical location for that amount of time. Thus, in order to provide continuous 24-hour service a constellation of satellites must be employed and linked together at all times (e.g. Iridium (LEO), ICO (MEO)).

GEO satellite systems operate at an altitude of 35786 km or 22236 miles (5.61 earth radii) from sea level altitude. This type has a circular orbit shape with earth at the center and the satellite coinciding with the equator with a period of 24 hours; Hotbird (Europe) and Arabsat (middle-east) are examples of GEO satellites that provide TV channels to their targeted geographical locations, thus they appear at the same spot in the sky for the users on the ground all the time. GEO satellites are able to see about a third of the earth's surface, by having three satellites arranged at 120^{o} around the orbit a global coverage (except near the poles).

The table below shows some advantages and disadvantages of the LEO/MEO orbits compared to GEO.

Table 1.1 Comparison between LEO/MEO and GEO [3]

GEO	LEO & MEO
Provides continuous coverage	Provides intermittent coverage per satellite
Polar coverage not possible	Can provide coverage to all the globe
System requires few satellite	A constellation of satellites are required for a full coverage system
Satellite has fixed position in the sky for a stationary user on the ground. Ideal for fixed satellite and direct broadcast services.	Satellite moves relative to a stationary user on the earth's surface leading to the need of widebeam or tracking narrowbeam antennas by the user.
Elevation angle can be low (to satellite) however the signal loss increases and higher power is needed.	For high-orbit inclination, the elevation angle is high thus reducing blockage making it ideal for mobile satellite without fixed antenna
Signal propagation loss is high and Doppler effect is negligible. Satellite power need to be high.	Signal propagation loss is low however the Doppler effect must be accounted for. Satellite power can be lower.
Single ground station required for control and monitoring	A ground network is required to coordinate handover between satellites and traffic routing
Energy requirements to reach GEO are high particularly for high latitude launch site	The energy requirements to reach operational orbit are lower than GEO

1.1.3 Space radio communications services

Defined as reception and/or transmission of radio-waves for a specific telecommunication application [4], these services are:

1. Fixed Satellite Services (FSS)
2. Mobile Satellite Services (MSS)
3. Broadcasting Satellite Services (BSS)
4. Earth Exploration Satellite Services (EES)
5. Space Research Services (SRS)
6. Space Operation Services (SOS)
7. Radiodetermination Satellite Services (RSS)
8. Inter-Satellite Services (ISS)
9. Amateur Satellite Services (ASS)

FSS are GEO satellites operating in the C-band (3.7-4.2 GHz), the Ku-bands (11.45-11.7 GHz and 12.5-12.75 GHz in Europe, 11.7-12.2 GHz in the USA) and even operating in the Ka-bands (20-30 GHz) nowadays. These satellites are used to supply broadcast feeds for TV and radio stations, also used for telephony, telecommunications and data communications. The rest of the satellites services can be GEO or non-GEO and have various frequency bands in which they operate in. Some of the frequency bands utilized for these other services are:

1. 420-470 MHz is utilized for fixed, mobile, amateur, radiolocation, mobile-satellite and meteorological satellite services.
2. 1215-1300 MHz is utilized for EES, radiolocation, SRS and amateur.
3. 5250-5570 MHz is utilized for EES, radiolocation, SRS, aeronautical radio navigation, radio navigation maritime and amateur satellite services.
4. 35.5-36.0 GHz is utilized for Meteorological Aids, EES, radiolocation and SRS satellite services.

1.1.4 Satcom Specifics

To place a satellite into orbit involves a lot of work and many aspects to consider from design to deployment. Two major parts of a satellite system are the space segment and the ground segment. The space segment usually consist of satellite deployment (in orbit, the spacecraft) and also includes TT&C (Tracking, Telemetry and Command) which is a station that involve a SCC (Satellite Control Center, could be at the station but usually located at a more convenient place like the headquarters of the satellite operator) and Tracking antenna. The ground segment (Earth stations-transmitters and receivers) facilitates access to the satellite (repeater) from earth stations in order to cater to the needs of the users. An earth station is a term that includes stations located on the ground, on the sea (on ships) or in the air (on airplanes). The services most utilized with the ground segment are FSS, BSS and MSS.

There are many particulars to account for in the field of Satcoms (e.g. network architectures, electronics, spacecraft (antennas, bus and subsystems), launch vehicles…etc.) but this thesis is mainly concerned with the signal propagation issue. Therefore one cannot talk about Satcoms without explaining a few specifics regarding Payload Capacity, Modulation and Coding schemes, Quality of Service, Frequency and mitigation as will follow below.

1.1.4.1 Frequency

The analysis in this project will cover the frequency range 20-50 GHz (Ka to V-band). Mainly targeting wavelengths between λ=15 mm and λ= 6 mm. Most microwave frequencies are not satcom inclusive but are used also by other terrestrial services. The most common frequencies used for the terrestrial links (common-carrier long-haul) are the 4 GHz, 6 GHz and 11 GHz bands whereas the 12 GHz band is utilized as a part of the cable TV system (USA). As For short point-to-point links between buildings the commonly used frequency is 22 GHz band [5]. HAPs (High Altitude Platforms- altitude of 17-22 km) which are quasi-stationary aircrafts are also considered as terrestrial links and now they are about to use high microwave frequencies as well (~48 GHz). Therefore interference is an always an issue to consider when utilizing satcoms [3].

Microwave links are largely characterized by:

- Line-of-sight (LOS) propagation through space and the atmosphere
- Wide bandwidths, compared to the lower frequency bands such as LF, HF, SW, VHF, FM and UHF
- Compact antenna, which can focus energy in a desired direction (directivity)
- Blockage by dense media like hills, tree trunks, solid buildings, metal walls, and at higher frequencies even by heavy rain
- Transmission is carried by waveguide structures

The move to higher frequencies can be explained by both the 1st and 2nd points mentioned above. The LOS trait is apparent in the ionosphere layer effects, lower frequencies would bend and bounce back to earth whilst microwave (above 10 GHz) simply pass-through thus ionospheric effects could be neglected. The bandwidth of commonly used frequencies such as C/X/Ku-bands is about 500 MHz for uplink and downlink each (C-band had an additional 500 MHz spectrum allocated by the ITU in the 1990s for both uplink and downlink due to its popularity); whilst when moving towards the higher frequencies such as Ka-band with bandwidth of about 2.5 GHz along with Q/V-bands, that would be economical (getting more channels and services) and hence feasible to build and maintain systems that deliver the most in terms of communication channels and data through put.

The next generation satcoms are making the transition to yet higher frequencies well into the millimeter wave band (Ka and above). The main disadvantage of these higher frequencies is the high attenuation of the signal due to Tropospheric degradation. Clouds cover of the satellite's signal path (cloud attenuation) is a part of the Tropospheric degradation factors, since not many studies at the Ka-V bands were conducted in the literature; cloud attenuation is investigated in this thesis.

1.1.4.2 Satellite Payload Capacity

Satcom's payload is defined as the system on board the satellite responsible for providing the link for the communication signal path. The link used to be between two ground stations however, payloads nowadays can also provide interconnectivity for a large number of mobile users directly to each other or through the ground stations [3]. Usually the number of transponders is used to indicate the capacity of the satcom.

In the satellite industry the term transponder is referenced to a specified RF channel of communication within the communication payload [2] where the term comes from contracting the words transmitter-responder which originally referred to a single-frequency repeater on the satellite. However, a satellite transponder is more of a microwave relay channel which would also be needed to translate the frequency from the uplink range to the downlink range. Therefore, a transponder is a combination of elements within the payload. For the input side, it can be seen as a share of the common uplink and the receiver equipment within the repeater. Whereas at the downlink side, a transponder would consist of the input filter, power amplifier, and output filter. It is to be noted that there are spare parts (redundant) to ensure no disruption of the service in case of amplifier or receiver malfunction.

Transponders (also known as repeaters) generally can be categorized as either transparent or regenerative, see section 5.5.1.1. The transparent transponder is relatively simple. It converts frequency, flexible (e.g. the transition between analog and digital modulation is straightforward) and is independent of uplink signal format. However, its main disadvantage is that noise and interference are not filtered out. On the other hand the regenerative transponder adds complexity to the payload. The main advantages of a regenerative transponder include adaptation of modulation and coding to specific requirements of uplinks and downlinks, beam scanning, baseband switching and by extension the uplink noise is not retransmitted on the downlink which ultimately can lead to lower complexity and cost of ground stations. However, the added complexity on board necessitates high reliability [4].

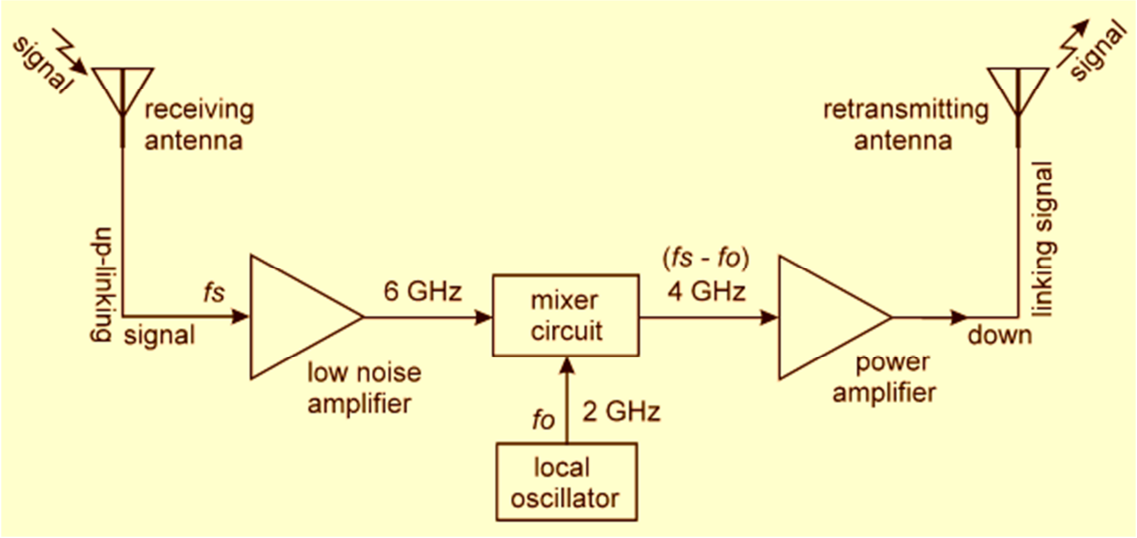

Figure 1.1 Simple block diagram of a transponder (C-band) in satellite [6]

Since transponders can cater to a particular user application network which has led to them being rented and even sold like common property; however in reality it is the microwave channel of communication bandwidth that is rented of sold. Hence a transponder's own capacity (amount of channels that it can handle simultaneously) is a defining factor of a satcom's capacity.

1.1.4.3 Modulation and Coding Schemes

Modulation (and Demodulation) has to do with analog and digital data conversion. To modulate is to raise the base-band signal to the carrier frequency and demodulation is the reverse operation. Coding techniques [7] are used for several reasons: reduction of dc wandering, Suppression of enter-symbol interference, data compression, encryption and self-clocking capability. These will in-turn result in complexities of the hardware used. However coded systems make much more efficient use of bandwidth widening to increase the output signal-to-noise ratio than an un-coded system. Hence coded systems are inherently capable of better transmission efficiency than the un-coded types.

It is needless to say that integrity of data (encryption) has to do with security; there is no point of utilizing a system in which any external (undesired) entity can intercept and hence make use of the data.

Some of the widely used schemes for modulation include:

1. Frequency Modulation (FM): becoming old and obsolete giving way to more channel efficient techniques
2. Phase Modulation (PM): include BPSK, variations of QPSK
3. Amplitude & Phase Modulation: all varieties of QAM (16-QAM, 64-QAM…etc)

As for coding techniques, the most used are:

1. channel coding: block and convolution coding, interleaving, concatenated coding
2. Forward Error Coding (FEC)

In chapter 5 (section 5.3) details on modulation techniques will be further explained in relation to satellite communications.

1.1.4.4 Fade Mitigation Techniques

Fade mitigation techniques can be carried out for both depolarization and attenuation. In the case of attenuation the way to deal with it is by an increase of the EIRP (Effective Isotropic Radiated Power). This requires a higher transmission power to coup with the high attenuation that would be encountered for a small time percentage. As such is the case, the extra power needed can exceed the operational limits of the used equipment. Thus, other solutions [3] are needed like:

- Site diversity

  It is the case to have high attenuations because of regions of rain spanning small geographical area. In order to overcome this hurdle, the concept of utilizing two or more distinctly located stations receiving the same link (site diversity) is introduced. Here, each station would presumably suffer different attenuation levels, and the signals are routed to the link less affected by attenuation.

- Adaptivity

  This solution involves the variation of certain parameters (e.g. signal coding and/or modulation) while the attenuation is taking

place in order to maintain the required carrier to noise power ratio (C/N). Some of the approaches implemented for that purpose include:

- utilizing additional resources usually kept in reserve (frequency allocation to one less affected by attenuation, higher EIRP on the uplink …etc)
- Reduction of capacity as for digital transmission using Forward Error Correction (FEC). This would reduce the necessary (C/N) at the expense of information bit rate (R_b)

The medium with major dynamic impact on satcom links is the atmosphere. It is not of a static nature in terms of its constituents' content and concentration Therefore it is essential to study the properties of the atmosphere if satcom links particulars are to be better understood.

1.2 The Atmosphere

1.2.1 Composition

There are many gases within the atmosphere. The concentrations of these gases at any given altitude would differ due to the difference of their densities. Hydrogen and helium would be the dominant on the edge of the atmosphere (toward outer-space) whilst the heavier gases would be found closer to the surface (Nitrogen, Oxygen, water vapor …etc.). most of the gases content is somewhat fixed. However it contains highly variable water vapor and ozone content (see Table 1.2). Aerosols (solid and liquid matter in suspension) are also considered as part of the atmosphere's composition.

1.2.2 Layers of the Atmosphere

Two major classifications are usually associated with the description of the Atmosphere, Neutral (Isothermal) and Ionized atmosphere. The divisions of spheres are merely shells of the atmosphere around the Earth with given thickness, and regions. More so, the region below the height of 80 km where

the gases are well mixed-up and keep approximately the same proportions is known as the Homosphere, whereas above the 80 km height were the gases tend to stratify due to their weights is called the Heterosphere.

Table 1.2 Composition of the atmosphere [8]

Gas	*Symbol*	*% by volume*	*% by weight*
Nitrogen	N_2	78.09	75.52
Oxygen	O_2	20.95	23.15
Argon	A	0.93	1.28
Carbon dioxide	CO_2	0.035	0.046
Neon	Ne	0.0018	0.012
Helium	He	0.0005	0.0007
Methane	CH_4	0.00015	0.0008
Krypton	Kr	0.0001	0.003
Ozone	O_3	Variable	0-0.01
Water vapor	H_2O	Variable	0-4

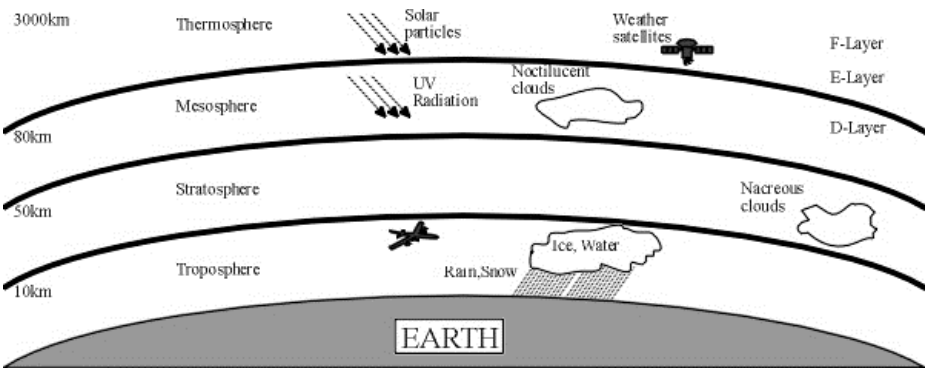

Figure 1.2 Atmospheric layers [9]

1.2.2.1 Ionosphere

The basic Ionospheric layers are identified closest to farthest from the ground as D, E, F (sub-division F1 and F2), and Protonosphere (Plasmasphere). The naming starts with D because at the time it was speculated by E.V Appleton that other layers below it might exist and therefore started with D. these layers are what makes long distance radio wave communications possible (below microwave length).

1.2.2.2 Isothermal spheres

There are four main isothermal spheres (layers), Namely the Troposphere, Stratosphere, Mesosphere and Thermosphere.

The basis of these divisions is mainly the distinct thermal properties of these layers. Which are due to the thermal energy absorption [10] of energy supplied by the Sun (Avg. 1.4 kW/m^2). Below is the vertical profile of the atmosphere.

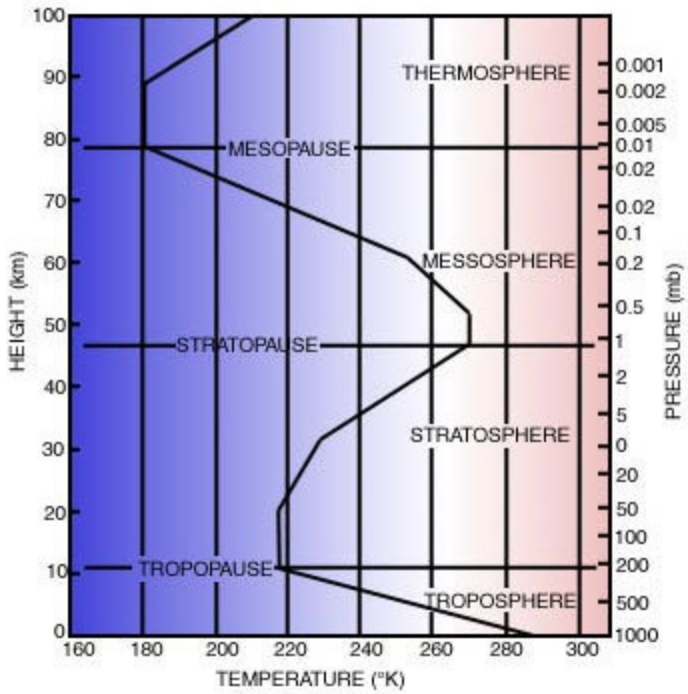

Figure 1.3 Atmosphere's vertical profile [8]

Each layer is characterized by a uniform change in temperature with increasing altitude. In some there is an increase in temperature with altitude, whilst in others there is a decrease in temperature. The upper boundary of each layer is denoted by a "pause" where the temperature profile abruptly changes. As illustrated by Figure 1.3, the main 4 layers are [8]:

- **Thermosphere: -** depending on the degree of solar activity, the temperature in this layer ranges from 500 K to 2,000 K (Kelvin). It is located above the height of 80 km and extends to several hundred kilometers (~500 km). The temperature changes between night and day would reach hundreds of degrees.
- **Mesosphere**: - temperatures decrease with height, towards the higher edge (mesopause) temperature values vary from -120 ^{0}C in the summer to -50 ^{0}C in the winter. In summertime, a special type of clouds may exist as high as 80 km above the surface due to having sufficient lifting (vertical motion). These clouds are known as Noctilucent (seen in the time just before night time) and are very thin.

- **Stratosphere**: - the ozone layer resides here which absorbs Ultraviolet radiation. Temperatures range from -30 C winter time to +20 C summer time. The move from the Troposphere to this layer leads to sudden change in the concentrations of the variable trace constituents. Water vapor would decrease severely whilst ozone concentrations rise-up leading to a mostly dried-up atmosphere. Even so, some clouds (Nacreous) may form during winter months at altitudes of 17 km to 30 km over high latitudes. It is notable to say that both the Stratosphere and Troposphere account for more than 99.8% of the Earth's entire atmosphere.

- **Troposphere**: - it contains about 80% of the entire atmosphere. Weather changes (hence most cloud formation) occurs in this layer. Temperature decreases with height due to pressure (adiabatic cooling). The vertical motions due to convective and turbulent transfer of heat along with the abundant water vapor content make this layer the source of all important weather phenomena. It extends up to 16 km at the equator and 8 km at the poles.

1.3 Clouds

1.3.1 Definition, Form and Dispersal

1.3.1.1 Definition

Clouds are *"a visible aggregate of minute droplets of water or particles of ice or a mixture of both floating in the free air"* [11] they form mostly when moist warm air is ascending to the sky then cooled down. The earth's surface is 50% covered with clouds statistically at any given time which leads us to the impact that they have.

Clouds physical traits are not static but change all the time. Whether it can be perceived clearly like cumulus clouds development, or whether the change is very slow as in cirrus clouds. Change is the dynamic of clouds all the time.

1.3.1.2 Formation of clouds

There are two essential facts that constitute the appearance of a cloud, they are:

1. stability of the atmosphere (in the cloud's vicinity)
2. increasing development of precipitation within the cloud

The mechanism of which clouds form involves a part of the atmosphere being cooled below its dew point, and then excess water vapor (not maintaining saturation) condenses. It follows that there can be no condensation of water vapor (in clean air) unless one of these two conditions happens:

a) Water vapor becomes extremely supersaturated with relative humidity of more than a few hundred percent (i.e. to have small droplets with radii of 0.001 micrometer the relative humidity should reach 340% [12]).
b) Get in contact with existing water or ice surface suspended in the air

The first condition never happens in the physical world in the atmosphere, so it is the later condition that would account for it. However, condensation does occur even with the absence of these conditions which lead to the conclusion of the existence of microscopic air impurities that promote condensation. These specks act as centers (nuclei) that allow condensation to happen, consequently the name condensation nuclei.

Now, talking about cooling, there are three main processes that make the atmosphere cool below its dew point:

1- Adiabatic expansion: air rising to levels of lower pressure in the atmosphere. The cooling rate is at the dry adiabatic drop (lapse) rate up to the point where the air becomes saturated, then onward saturation happens and cooling is now at the saturated adiabatic drop rate. There are five factors that can lead to the process of air ascension and cooling, namely:

- Surface Heating
- Topography
- Frontal
- Convergence
- Turbulence

Note that cloud base would indicate the change-over point of interaction. Also, it takes about a few minutes up to an hour to form a cloud.

2- Contact with a cold body, namely the ground. Having temperature below the dew-point of air.
3- Mixing of two virtually saturated masses of air of distinctly dissimilar temperatures.

Out of these three processes, it is the first that is most important, as the second would make clouds only near the ground (around 500 meters height) while the third is of little value and almost in no way by itself causes natural clouds to form.

1.3.1.3 Dispersal of clouds

There are a couple of processes in which clouds thin out and disappear (disperse), namely:

1- Evaporation: due to rise of temperature making the relative humidity to decrease below 100% or by integrating with its non-humid surroundings, particularly for cumuliform clouds for their relative isolated nature.
2- Fall-out as rain, snow and hail (precipitation): this counts for a large share of water volume removal in precipitation clouds.

In the following section, we move on to the way clouds are classified and some of their qualities.

1.3.2 Classifications

Back in 1803 Luke Howard proposed a simple scheme of classification for clouds in which he identified three principal cloud categories:

1- Stratus: clouds that are arranged in a level sheet
2- Cumulus: clouds consisting of flat bases and rounded tops, usually lumpy in appearance
3- Cirrus: clouds that appear feathery or stringy

Although this system was simple, the variety of clouds that can be associated to any of the three categories can have distinctly different physical traits. Since the study of clouds and their effects (e.g. on the climate) was advancing, the need of a more comprehensive classification was growing. Thus, the International Meteorological Committee published an atlas of clouds in 1895 in the effort to attain some sort of worldwide standardization of both naming and identification of clouds. Many revisions were made since.

The latest, named International Cloud Atlas (still used nowadays), was issued back in 1975 by the World Meteorological Organization (WMO) which is a specialized agency of the United Nations (UN).

There are 10 basic cloud types spanning 3 categories, Low, Medium, and High. These categories are based on the altitude of the cloud's base (bottom) from the ground.

- **Low clouds**: - clouds that have a base below 2,000 m (7,000 ft). Contain high amount of water droplets. Cloud types in this category include:
  1- Cumulus (Cu)
  2- Cumulonimbus (Cb)
  3- Stratus (St)
  4- Stratocumulus (Sc)

- **Medium clouds**: - they have a base range between 2,000~7,000 m (7,000~17,000 ft.). These also contain water droplets. Cloud types include:
  1- Altocumulus (Ac)
  2- Altostratus (As)
  3- Nimbostratus (Ns)

- **High clouds**: - usually made up of ice crystals. Their base ranges between 5,500~14,000 m (17,000~35,000 ft). The final 3 types are
  1- Cirrus (Ci)
  2- Cirrostratus (Cc)
  3- Cirrocumulus (Cs)

In this study of cloud attenuation, the focus will be on the clouds with high water content near the ground (station); Namely the **Stratus & Stratocumulus (St/Sc)**, **Cumulus (Cu)**, **Cumulonimbus (Cb)** and **Nimbostratus (Ns)**. That is because clouds that are forming at other altitudes would consist mostly of ice particles and therefore the attenuation would be negligible at frequencies lower than 100 GHz.

1.4 Atmospheric effects on Satcom signal

As previously mentioned, there are many factors that affect Satcom's signal propagation in the atmosphere. Some are due to the ionosphere and some are due to the troposphere. In our study we will be focusing on the troposphere since high water content clouds reside in that layer and above 10 GHz ionospheric effects could be neglected. Below is a brief description of the main impairments due to the troposphere for frequencies up to 50 GHz.

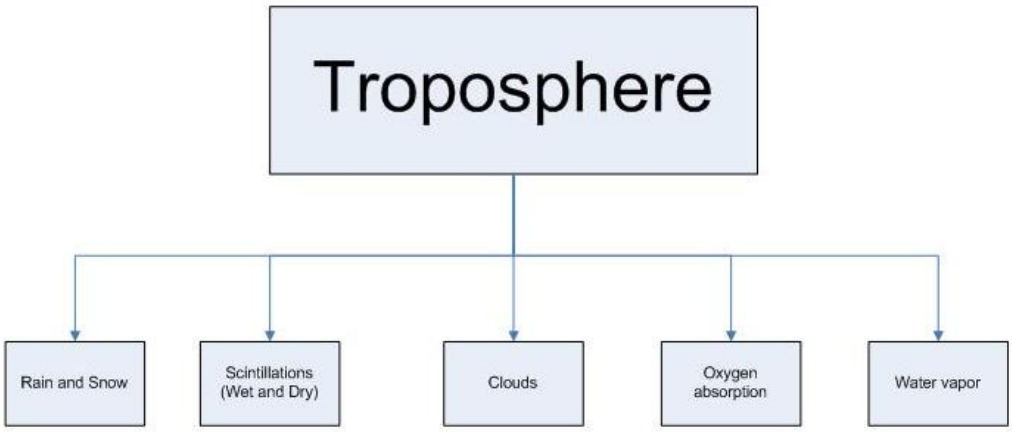

Figure 1.4 Microwave signal attenuation factors in the troposphere

1.4.1 Ionosphere

The ionosphere is a region of ionized plasma that extends from about 50 km to 2000 km towards the sky. Small percentage of molecules are ionized, the majority still remain neutrally charged.

This layer highly impacts RF communications of wavelengths below microwave (up to about 10 GHz). So, for our topic at hand it is of low importance but we state some of the factors affecting radio signals at f<10 GHz in this region:

- Critical frequency
- Total electron content
- faraday rotation

- group delay
- phase advance
- Doppler frequency
- Dispersion

Also, ionospsheric scintillation which is a relatively rapid fluctuation of the signal about a mean level that is either constant or changing much more slowly than the scintillations themselves; is a major phenomenon that affects the integrity of radiowave signals.

1.4.2 Gaseous Absorption (O_2 and H_2O vapor)

Atmospheric attenuation due to gaseous absorption is dependent on frequency, elevation angle (angle of antenna's LOS vs. horizon), and altitude of the station- i.e. total path through the atmosphere which is a function of theta (elevation angle from the horizon) and h (distance traveled by the signal within the medium). When absorbed, RF energy is converted into heat as the signal passes through clear air, smog and water vapor. Oxygen and water vapor are the prime culprits when it comes to Gaseous absorption attenuation of any satcom's signal. Oxygen is a paramagnetic molecule [10] with a permanent magnetic moment, which leads to it having resonant absorption at particular frequencies. More so, for water and water vapor being a polar molecule also leads to resonant absorption at critical frequencies. Figure 1.5 shows the attenuation due to gaseous absorption. It is noted that at around 22.3GHz, attenuation spike is due to water vapor absorption band. And toward +50 GHz rise (up to around 60 GHz) is due to Oxygen absorption.

As for the rest of the gases in the atmosphere, it is not until the higher frequencies >70 GHz that their absorption counts significantly towards the attenuation of the signal.

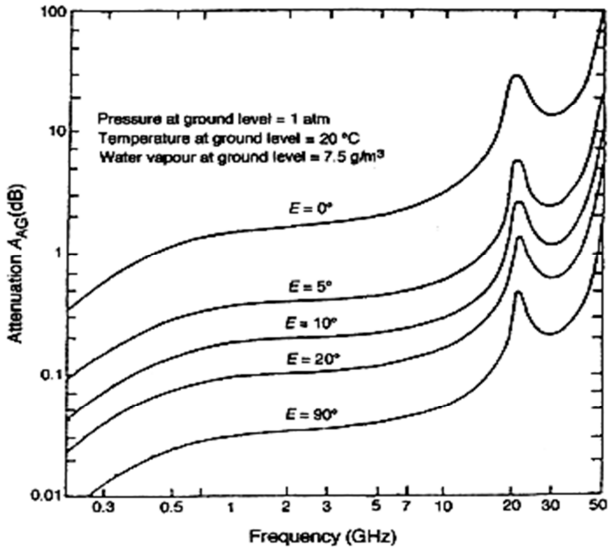

Figure 1.5 Gaseous Absorption Attenuation up to 50 GHz [**4**]

1.4.3 Scintillations

They are in general variations of received signal level amplitude and/or phase caused by the refractive index variations of the troposphere (and ionosphere). When the propagation path (atmosphere) is not turbulent, the refractive index varies very slowly in the horizontal plane and a bit faster with height. But due to the fact of wind, the path becomes a mixture and causes relatively rapid variations in that refractive index over small amount of time which we perceive as scintillations. The major factors in giving the greatest scintillation amplitudes are high temperature and humidity leading to strong seasonal dependence (summer scintillations are about 3 times as severe as winter scintillations) [10].

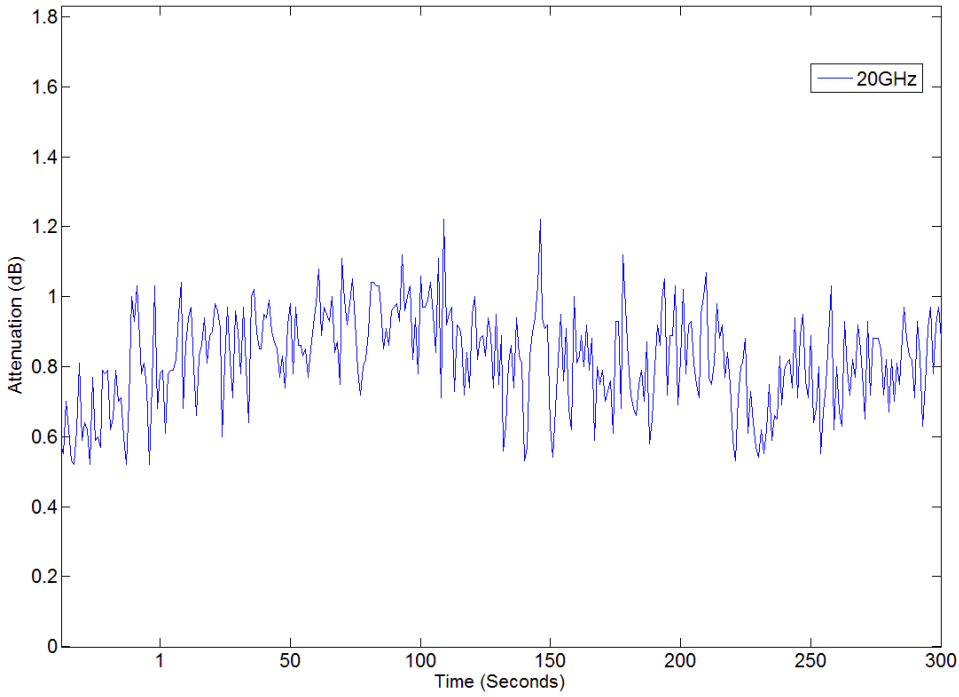

Figure 1.6 sample of signal scintillations at 20 GHz (rapid fluctuations)

1.4.4 Rain and Snow

Rain is the main degradation factor effecting satcoms operating at frequencies above C-band. Rain drops both absorb and -to some extent scatter the RF (microwave) energy. Dry areas and seasons with low rain fall require less link margin in contrast to the rainy, heavy thunderstorm activity locations, such as the tropics. Rain also introduces depolarization; this is due to the non-spherical shape of raindrops [4]. However, snow attenuation only starts to be a concern at frequencies higher than 100 GHz thus it can be neglected.

Rain attenuation has been extensively studied since some of the potential service subscribers would experience rain as both a passing event or they might be located in a heavily rain-afflicted region (e.g. the tropics). Figure 1.7 shows rain impact as the frequency of operation increases (20, 40 and 50 GHz).

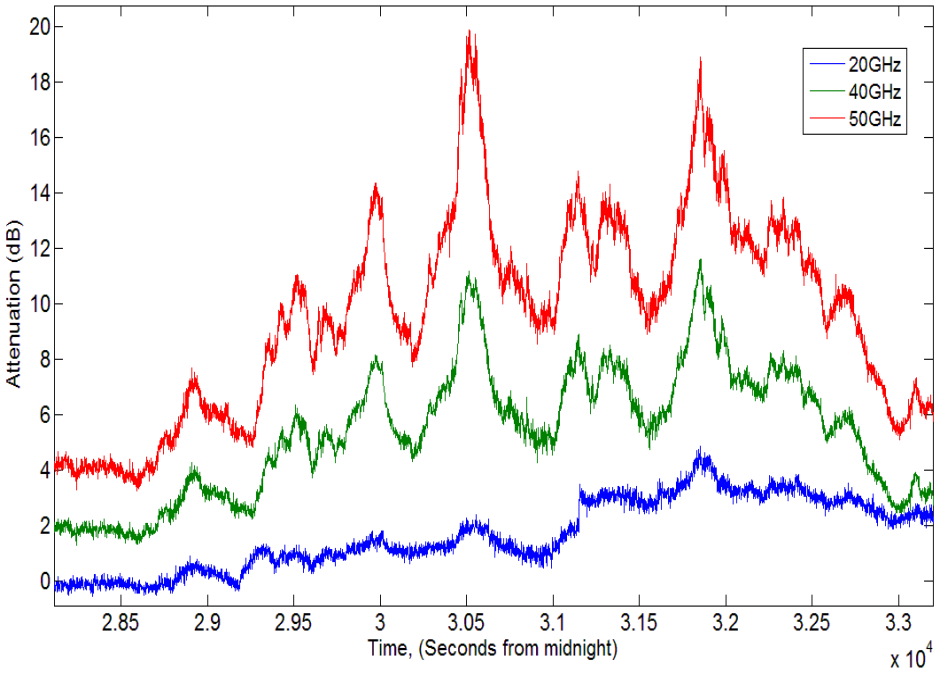

Figure 1.7 attenuation variation during a showery rain event at 20, 40 and 50 GHz (26th of June 1997, Sparsholt, U.K.)

1.4.5 Cloud

This is the main focus of this project. Clouds are considered not too often in the literature and are treated as a relatively new area to explore. Attenuation due to clouds and fog alike is usually small compared with rain. Due to the fact of varying water content and visible time they remain in the sky (along with their thickness and distance from the receiver), the attenuation effect is usually negligible at lower frequencies. However, it is around nonetheless for a greater period of time and at higher frequencies clouds become significant and are the second most important factor. The increasing demand for new services with high link availability (greater than 99.9%) at Ka-band and above requires the system designer though to take those factors into account when designing the system. Table 1.3 below shows attenuation impact of atmospheric gases, clouds and rain for various frequencies.

Table 1.3 Attenuation by Atmospheric gases, clouds and rain [13]

	Attenuation (dB)		
		Clouds	Rain
Frequency	Gases	Thickness (1 km)	Height (1 km)
f (GHz)	Density = 7.5 g m^{-3}	Temp = 0 ^{o}C; density = 1 g m^{-3}	Rate = 12.5 mm/h
5	0.0314	0.023	0.0313
10.7	0.0409	0.106	0.249
15.4	0.066	0.217	0.528
23.8	0.449	0.507	1.114
31.4	0.179	0.859	1.574
90	0.793	4.74	3.17

1.5 Conclusions

Satellites are important in the field of long distance communication as they can traverse geographical obstacles (e.g. mountains) and can provide services for many users with comparably easier setup and lower cost. There are many aspects that can be researched to better the utilization of satcoms for both the space and earth segments. The increasing demand of higher quality of service and increased number of services provided by the satellite has pushed the development of more accurate propagation impairment models. At higher frequencies clouds are the second most impairment degradation factor. For high availability systems, cloud attenuation is an important factor that needs to be considered in the system design and link budget calculations.

The atmosphere is not static, meaning that its condition changes constantly. It can be described by two major properties: thermal and Ionic (for propagation of RF) profile. At higher frequencies the ionospheric effect could be neglected however, it is the constituents of the Troposphere and Stratosphere (thermal profile) that severely attenuate the signals. Attenuation is thus mainly attributed to scintillations, gaseous absorption, clouds, rain and snow. In this project the

focus will be on investigating the effects of cloud attenuation on satellite-earth links.

Cloud attenuation can be attributed to both the density and amount of suspended liquid water droplets within the cloud at microwave and millimeter frequencies. In the next chapter the theoretical foundation is presented, it is the basis from which most cloud attenuation models were developed. Furthermore a description of the most commonly used (recent) models will also be covered.

2 Cloud modeling fundamentals

2.1 Introduction

This chapter first lays down the theoretical foundation of cloud effects on electromagnetic (EM) wave propagation (attenuation) and a collection of mathematical bases found in the literature for implementation in cloud attenuation modeling. The phenomena of absorption and scattering for water particles are discussed to establish the basis of cloud attenuation mechanics (due to absorption and/or scattering depending on the physical characteristics of liquid water in clouds). This is followed by presenting a group of analytical models used to approximate scattering of water droplets are presented afterwards.

Next a review of recent accepted cloud attenuation models is presented. Such review would help in understanding the variables pertaining to cloud attenuation modeling. This would ultimately help in pursuing the thesis's goal of producing an improved cloud attenuation model in both easiness of application and improved accuracy.

2.2 Absorption and single particle scattering

2.2.1 Absorption

A non-conductive, dielectric medium's complex permittivity $\varepsilon*$ describes the effect it has on propagating radiowave through the medium. For a low-loss medium, the real part of permittivity ε' would be sufficient by itself since the imaginary part ε'' is virtually non-existent [10]. By definition, these types of media exhibit symmetry [14] in their atomic (molecular) structure. If ε' and ε'' are plotted vs. frequency of a polar molecule, the critical frequencies (absorption) show up as peaks in ε''. See Figure 2.1.

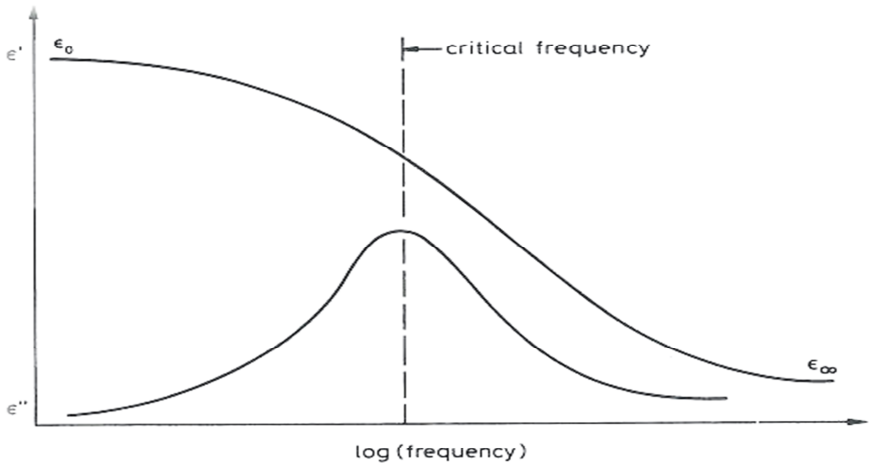

Figure 2.1 ε' and ε'' plotted against log (frequency) for a substance that has one critical frequency [10]

When a molecule is asymmetrical it will have a preferred configuration if placed within an electric field (polar molecule). These polar molecules display much more loss than other molecules [15]. This loss depends noticeably on the frequency of measurement.

The troposphere is composed primarily of nitrogen and oxygen. Both these gases are electrically non-polar and absorption does not occur due to electric dipole resonance. With that said, Oxygen is a paramagnetic molecule with permanent [16] magnetic moment leading to resonance absorption at specific frequencies around 60 GHz, having an isolated absorption at 118.74 GHz. It is important to note that for low pressures such as high altitudes the individual absorption lines become distinguishable. However, at ground atmospheric pressure these lines amalgamate into a broad continuum also known as pressure broadening between the frequencies of 52 and 68 GHz.

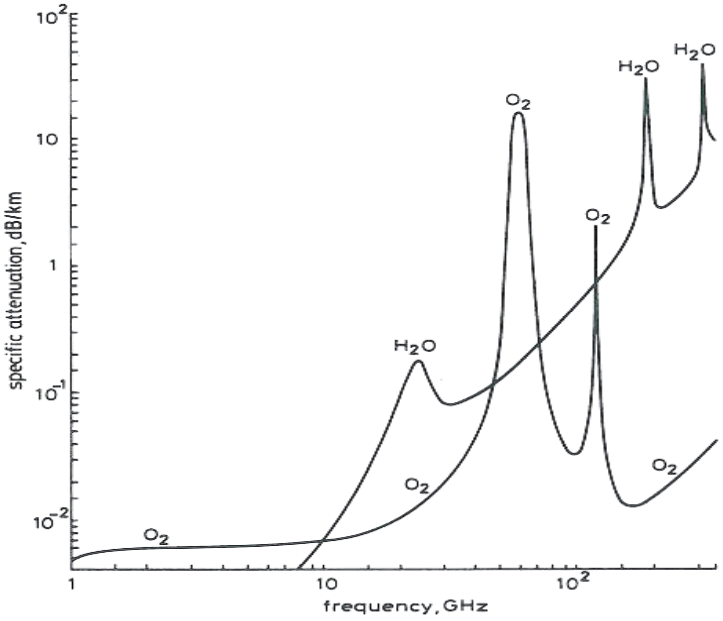

Figure 2.2 Attenuation due to water and oxygen for various frequencies [10]

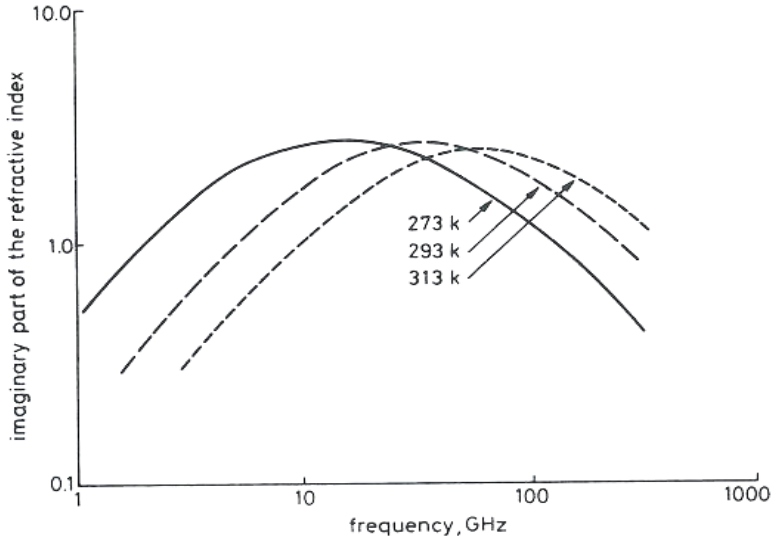

Figure 2.3 Imaginary part of the refractive index of pure water as a function of temperature [10]

H_2O or water is a polar molecule so absorption does occur due to electric dipole resonance. Water molecules tend to associate through hydrogen bonds which have 0.1 strength of molecular bond. This is physically explained by the attraction of the electron-rich end oxygen to electron-poor hydrogen of an adjacent water molecule. This phenomena leads to different results according to the phase (gaseous, liquid, solid) of water molecules; Figure 2.3 shows pure water's imaginary refractive index for three temperatures.

2.2.2 Single-particle scattering

Scattering from single particles theory forms the foundation of attenuation prediction by clouds. There are exceptions for ice-water mixtures and large irregular particles but this theory gives noticeably accurate predictions. So, we'll cover it in more detail.

The primary assumption with this theory is that scattering occurs due to small particle, such as a water drop having spherical shape is valid for a radius up to 1mm [17]. More so, it is assumed the medium surrounding this particle is non-conductive, that is to say no power loss take place in the medium.

2.2.2.1 Definition of Quantities

Both the electric and magnetic fields (EM wave) around the particle can be formulated with the notion of total field, such as

$$E_t = E_i + E_s \qquad \text{(Total complex electric field)}$$

$$H_t = H_i + H_s \qquad \text{(Total complex magnetic field)} \qquad (2.1)$$

Where i is for incident and s is for scattered (fields). See Figure 2.4.

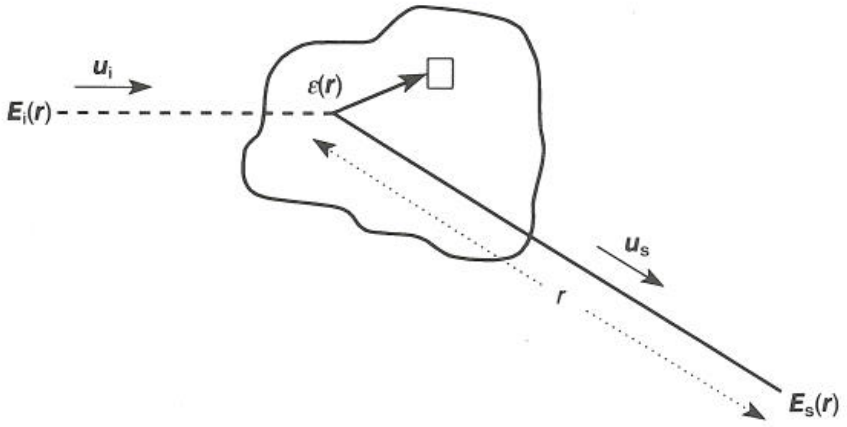

Figure 2.4 Scattering configuration [14]

We will treat the electric component of wave and the same could be carried out for the magnetic field.

For a linearly polarized plane wave having amplitude E_i propagating in the u_i direction:

$$E_i(r) = E_i u_e e^{jk_0 u_i \cdot r} \tag{2.2}$$

r is the vector toward the observer from origin. k_0 is wave number (free-space) and u_e is unit vector defining wave polarization. We'll use this time dependence convention $V(r,t) = \mathrm{Re}[U(r)e^{-j\omega t}]$ where V is the real component of the complex field U . The $e^{-j\omega t}$ will be stricken out. More so, we assume a large distance from the scattering object in which a spherical wave would be propagating (valid configuration) so that

$$E_s(r) = E_i f(u_s, u_i)\frac{e^{jk_0 r}}{r} \tag{2.3}$$

r is the distance between the observer and object. $f(u_s, u_i)$ is the scattering amplitude function which gives u_i and u_s direction from the scatterer to the observation point, it represents amplitude, phase and polarization of the scattered wave in the far-field zone.

The scattering amplitude is attainable from exact calculations of the scattered field. On the other hand, a formula in terms of total field E can be derived [14] resulting in this general integral expression:

$$f(u_s, u_i) = \frac{k_0^2}{4\pi} \int_V \{-u_s \times [u_s \times E(r')]\} [\varepsilon_r(r') - 1]\, e^{-jk_0 r' \cdot u_s}\, dV' \qquad (2.4)$$

The far-field zone is defined as the distance in which a spherical wave would be (locally-have wave front like) as a real plane wave. A generally acceptable distance r for the far-zone is

$$r > {}^{2l^2}\!/_{\lambda} \qquad (2.5)$$

l is the object's diameter and λ is the wavelength.

In order to find a solution for the scattering problem, the cited [14] idea of 'finding a scattered field that, together with the incident field matches on the surface of the scattering object with its internal field' can be applied. Which means that the scattered field is reflecting all of the properties of the scattering particle. Having this idea in mind we now talk about the forward scattering theorem as a solution to the problem.

2.2.2.2 The forward scattering (extinction theorem)

Since the power density is uniform in space for u_i its power loss can be calculated from multiplying a cross-section (2-D as in area) with the power density. Due to this we can rationalize that absorption and scattering by an object is related to the scattered field only. So, for the total power detached from the incident field by means of absorption and scattering it is possible to represent it by the total cross-section or extinction. This is limited to only the in the forward direction. Thus the name forward scattering theory.

Using the averaged Poynting vector $\overline{S}$ to represent the time-averaged energy flow density (power density) we can split it into separate terms as:

$$\overline{S} = \overline{S_i} + \overline{S_s} + \overline{S_d} \qquad (2.6)$$

Where

$$\overline{S_i} = \tfrac{1}{2}\mathrm{Re}\,(E_i \times H_i^*) \tag{2.7}$$

$$\overline{S_s} = \tfrac{1}{2}\mathrm{Re}\,(E_s \times H_s^*) \tag{2.8}$$

$$\overline{S_d} = \tfrac{1}{2}\mathrm{Re}\,(E_i \times H_s^* + E_s \times H_i^*) \tag{2.9}$$

Now, if we imagine a big sphere having radius a surrounding the scatterer, the net power flow through its surface (sphere) can be computed by integration of the radial component of $\overline{S}$ over the sphere. So, for a lossless dielectric the power flow will be zero. But having lossy substance (complex permittivity) the result will not be zero and would stand for the absorption rate P_a of energy by the scatterer. See Figure 2.5.

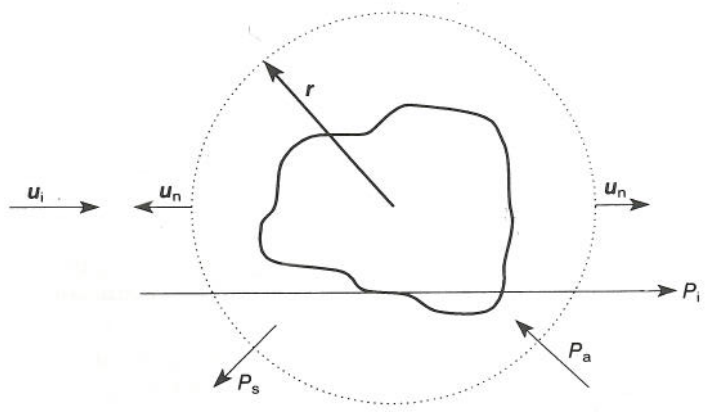

Figure 2.5 illustration of net power and absorption rate by the scatterer [14]

$$-P_a = P_i + P_s + P_d \tag{2.10}$$

P_a is the integral of the radial component of $\overline{S}$. It is assumed the immediate vicinity surrounding the particle is lossless resulting in having the net flow of energy of the incident field equal to zero for all closed surfaces (P_i = 0) so that:

$$P_a + P_s = -P_d = -\tfrac{1}{2}\mathrm{Re}\iint_S (E_i \times H_s^* + E_s \times H_i^*) \cdot u_n \, dS \tag{2.11}$$

u_n is unit vector normal to the surface $\overline{S}$ extending outwards and the dot is the inner product. Implementing Maxwell equations into (5.4) leads to

$$(E_i \times H_s^*) \cdot u_n = \left(\frac{\varepsilon}{\mu}\right)^{1/2} E_i E_s u_e \cdot f^*(u_s, u_i) \frac{e^{-jk_0 a}}{a} e^{jk_0 u_i \cdot u_n} \tag{2.12}$$

$$(E_s \times H_i^*) \cdot u_n =$$

$$\left(\frac{\varepsilon}{\mu}\right) E_i E_s \{u_n \cdot u_i [f(u_s, u_i) \cdot u_e] - u_n \cdot u_e [u_i \cdot f(u_s, u_i)]\} \frac{e^{jk_0 a}}{a} e^{-jk_0 a u_i \cdot u_n}$$

(2.13)

For a choice of large (big enough) sphere radius, the integrals of (2.12) and (2.13) can be evaluated with the stationary phase method. This method's idea is to find points on the scatterer's surface where the phase of the fields does not change drastically. Thus omitting the total contribution of the other points as they will add up to zero since the phase difference between them will lead to them canceling altogether. This is true only for having the amplitude function not changing as much as the phase's sign. In other words, the radius of the sphere a is large enough.

Stationary points are points where the phase is constant and they can be found intuitively. If the vector u_n is parallel to u_i then two solutions are attained

$u_n = u_i$ (forward scattering), $u_n = -u_i$ (back scattering)

(2.14)

Thus;

$$P_s + P_a = \frac{2\pi}{k_0} \left(\frac{\varepsilon}{\mu}\right)^{\frac{1}{2}} E_i^2 \, \mathrm{Im}[u_e \cdot f(u_i, u_i)]$$

(2.15)

Note the stationary point of ($u_n = -u_i$), it gives a purely imaginary contribution to the integral. Since for power balance we need only the real parts (2.9), it is

absent in (2.15). Now as for ($u_n = u_i$) the real part of scatter function is done away with because of the complex conjugate. For that reason, the imaginary part is the only segment of importance in (2.15). We conclude that the imaginary part of the stationary point contribution of forward scattering determines the total absorbed and total scattered power. “Explicitly, the rate at which energy is removed from the incident field is proportional to the imaginary part of the forward scattering amplitude ($u_n = u_i$) in the direction of the electric victor of the incident field.”[14]

The extinction

$$\sigma_t = \frac{P_s + P_a}{P_i} = \frac{4\pi}{k_0} \mathrm{Im}[u_e \cdot f(u_i, u_i)] \tag{2.16}$$

Known as the total cross-section is a ratio of the rate of energy ($P_a + P_s$) removal to that of the incident energy (P_i) on a unit cross-sectional area of the scatterer itself.

Comparably $\sigma_s = \frac{P_s}{P_i}$ (scattering) and $\sigma_a = \frac{P_a}{P_i}$ (absorption) cross-sections are defined, therefore

$$\sigma_t = \sigma_s + \sigma_a \tag{2.17}$$

Although forward scattering theorem is an exact relation, one must be careful if applying it to approximations of the scattered field. For approximations such as Rayleigh scattering it is better to calculate the energy flow through a surface that engulfs scatterer for each solution. As for exact solutions such as Mie scattering the theory is implementable without problems.

It is good now to shed some light on the prominent analytical models pertaining to a spherical particle.

2.2.3 Analytical models for scattering and water cloud calculations

2.2.3.1 Analytical models

Here we will talk about four models namely Mie theory [18], Rayleigh scattering, Born approximation and WKB [19] interior wave-number approximation. These models give a closed expression for the scattering of a plane wave by a spherical particle (water droplet). Direction of propagation of E_i is chosen to be $+z$ direction. Note that due to spherical symmetry of the scattering particle, this does not constitute a restriction.

(a) Mie theory

The first to attain the exact solution for plane wave scattering that is incident on a homogeneous non-magnetic sphere of any diameter and any composition placed in a homogeneous, non-magnetic, non-conducting and isotropic medium.

Mie had done it by utilizing a representation of the fields in potentials and later on solving the boundary value problem by spherical expansion functions. A thorough description of the procedure and solution is given in [20]. Here we are more interested with the solution.

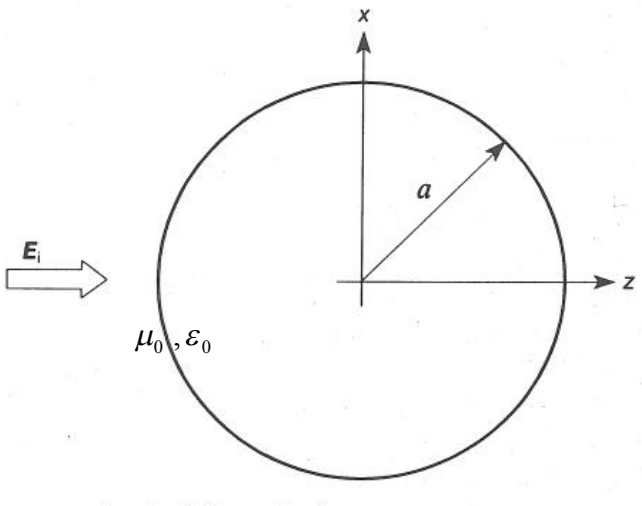

Figure 2.6 Scattering geometry for Mie scattering [14]

For a plane wave E_i travelling in z direction with x direction polarization

$$E_i = \mathrm{E_i} u_x e^{jk_0 z} \tag{2.18}$$

Where E_i is amplitude of field and u_x is polarization orientation.

Here a sphere with $\varepsilon = \varepsilon_r \varepsilon_0$ and radius a is located in the origin of reference frame. The medium has constant ε_0 and μ_0 which is the case for water-droplets in the atmosphere.

The scattered fields are given by

$$E_\psi = -E_i \frac{je^{jk_0 r}}{k_0 r} S_1(\theta)\sin\psi, \quad E_\theta = E_i \frac{je^{jk_0 r}}{k_0 r} S_2(\theta)\cos\psi \tag{2.19}$$

$$S_1(\theta) = \sum_{n=1}^{\infty} \frac{2n+1}{n(n+1)}(a_n \kappa_n + b_n \tau_n)$$

$$S_2(\theta) = \sum_{n=1}^{\infty} \frac{2n+1}{n(n+1)}(a_n \tau_n + b_n \kappa_n) \tag{2.20}$$

$$\kappa_n = \frac{P_n^1(\cos\theta)}{\sin\theta}, \qquad \tau_n = \frac{d}{d\theta} P_n^1(\cos\theta) \tag{2.21}$$

$$a_n = \frac{\psi_n(\alpha)\psi_n'(\beta) - m\psi_n(\beta)\psi_n'(\alpha)}{\zeta_n(\alpha)\psi_n'(\beta) - m\psi_n(\beta)\zeta_n'(\alpha)} \tag{2.22}$$

$$b_n = \frac{m\psi_n(\alpha)\psi_n'(\beta) - \psi_n(\beta)\psi_n'(\alpha)}{m\zeta_n(\alpha)\psi_n'(\beta) - \psi_n(\beta)\zeta_n'(\alpha)} \tag{2.23}$$

$$\beta = k_0 ma, \quad \alpha = k_0 a \tag{2.24}$$

$$\psi_n(x) = x j_n(x) = (\pi x/2)^{1/2} J_{n+1/2}(x) \tag{2.25}$$

$$\zeta_n = x h_n^{(1)}(x) = (\pi x/2)^{1/2} H_{n+1/2}^{(1)}(x) \tag{2.26}$$

Where $P_n^1(\cos\theta)$ is the associated Legendre function of the first kind, $J_n(x)$ is the Bessel function of the first kind and $H_n^{(1)}(x)$ is the Hankel function of the first kind.

Based on this exact solution a number of approximations can be attained. We now move to some of those below.

(b) Rayleigh Scattering

Here an approximation is attained by assuming $k_0 a$ < 1, that is to say the scatterer radius is small compared to wave-length. To get a valid value of this radius a comparison with Mie solution is needed. Kerker [21] concludes a maximum value of a = 0.05λ which results in an error less than 4% for our case of the single scatterer.

A scatterer that is spherical and small (dielectric) in comparison to wavelength has a field inside of it; this field is chosen to be the solution [22] of the equivalent dielectric electrostatic problem. This field (ratio) is given by [23], [24]

$$E = \frac{3}{\varepsilon_r + 2} E_i \tag{2.27}$$

And utilizing (2.4) a solution to the scattering problem would be

$$f(u_s, u_i) = \frac{k_0^2}{4\pi}\left[-u_s \times (u_s \times u_e)\right] V \frac{3(\varepsilon_r - 1)}{\varepsilon_r + 2} \tag{2.28}$$

V is volume of scatterer.

We need to note that a property of Rayleigh scattering is the intensity of $|f(u_s, u_i)|^2$ of the scattered wave is proportional to reciprocal 4th order wavelength k_0^4 yet directly proportional to V^2.

This is an approximation (as the remaining models in discussion)! Leading to forward scattering theorem failing since the scattering field should reflect all the properties of the scatterer in which this is not the case.

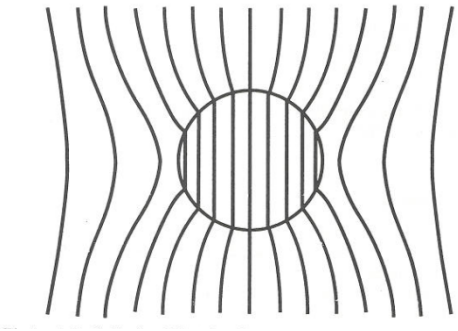

Figure 2.7 Electrostatic field of a dielectric sphere [14]

(c) Born Approximation (Rayleigh-Debye scattering)

This model's validity is attained for

$$(\varepsilon_r - 1)\, k_0\, a << 1 \qquad (2.29)$$

Two possibilities here, either ε_r is close to unity or the radius of the scatterer is small. Both cases mean that very small influence is exerted by the scatterer on the total field. Hence the field inside the scatterer can be approximated by the incident field itself:

$$E(r) \approx E_i(r) \qquad (2.30)$$

And it follows that for a homogeneous sphere with radius a, the scattering amplitude function is

$$f(u_s, u_i) = \frac{k_0^2}{4\pi}\left[-u_s \times (u_s \times u_e)\right](\varepsilon_r - 1)VF(k_1) \qquad (2.31)$$

Having

$$F(k_1) = \frac{3}{k_1^3 a^3}\left[\sin(k_1 a) - k_1 a \cos(k_1 a)\right] \tag{2.32}$$

$$k_1 = k_0 \left| u_i - u_s \right| \tag{2.33}$$

(d) WKB interior wave number approximation

The conditions for this approximation are

$$(\varepsilon_r - 1)\ k_0\ a >> 1, \qquad \varepsilon_r - 1 < 1 \tag{2.34}$$

We note that this model covers the conditions in which the prior approximations are not applicable.

The field inside the scattering object is approximated by a field propagating in the same direction as the incident field but with the wave number of the medium. For normal incidence, the transmission coefficient at the surface is approximated by a plane wave.

So, based on the preceding, the scattering amplitude function now becomes:

$$f(u_s, u_i) = \frac{k_0^2}{4\pi}\left[-u_s \times (u_s \times u_e)\right] VS(u_s, u_z) \tag{2.35}$$

Where

$$S(u_s, u_z) = V^{-1} \int_V 2[n(r') - 1] e^{jk_0 z_1 + jk_0 (z - z_1) - jk_0 r' \cdot u_s}\, dV' \tag{2.36}$$

Having $n(r)$ as the refractive index of the object. V (of sphere), with u_z as the unit vector in $+z$ direction and z_1 as particle surface location in the z-plane.

2.2.3.2 Approaches to calculation for water clouds

Work was done in comparing the critical radius of the Rayleigh approximation with the maximum radii of water particles dominant in clouds. The results are in

favor of applying the approximation up to 100 GHz for a maximum radii size of 50 micrometer. This approximation's condition can be set as:

$$\frac{2\pi a}{\lambda} << 1 \quad \text{and} \quad \frac{2\pi an}{\lambda} << 1 \tag{2.37}$$

Here n is the complex index of refraction of the particle. This condition states the limit for the maximum (critical) radius of which the approximation holds. Table 2.1 shows a compilation for critical radius of water droplet in clouds for different frequencies.

Liebe, Manabe and Hufford [25] have compared both the Rayleigh and Mie scattering approaches for a size distribution [26] corresponding to the case of a heavy cumulus cloud ($\rho = 1\ g\,m^{-3}$, $T = 20°C$, a radius of $6\,\mu$m except now accounting for sizes $\geq 50\mu$m that effect < 1% to ρ). These results support the use of the Rayleigh approximation up to 300 GHz. See Table 2.2.

Table 2.1 Critical radius a_c of droplets [13]

f (GHz)	λ (cm)	ε'	ε''	a_c (μm)
10	3	60	36	571
30	1	24	36	242
60	0.5	11	19	170
90	0.33	7.2	13.5	134

Table 2.2 Comparison between Mie and Rayleigh scattering attenuation values for droplets radius $\leq 50\mu\text{m}$ [25]

f (GHz)	α_m (Mie) (dB km^{-1} (g m^{-3})$^{-1}$)	α_r (Rayleigh) (dB km^{-1} (g m^{-3})$^{-1}$)	$\alpha_r/\alpha_m - 1$ (%)
300	15.0	15.0	0
400	20.5	20.3	-1
500	26	25	-4
800	41	38	-7
1000	50	43	-14

2.3 Existing cloud attenuation models

2.3.1 Overview

As previously mentioned, the bases of cloud attenuation dates back to the mathematical treatment done by Mie and the approximation of Rayleigh thus, old cloud attenuation models were available. But they either treated the cloud attenuation in a pure mathematical way and hence no modification to accommodate empirical data (e.g. Gunn and East [27]), a combination of mathematical and empirical data (e.g. Staelin [28] model based on empirical data for the refractive index of water), localized to a specific region of cloud genre (e.g. Slobin [29] radiometer-radiosonde measurements spanning the continental USA), or attempting to utilize surface parameters to estimate cloud attenuation (e.g. Altshuler-Marr [30] inferred from extinction measurements using the sun as a source in Boston, Massachusetts). A concise description of these models can be found in [31]. Below are some relatively new and accepted working models currently utilized in the field, they are:

- DAH: proposed by A. Dissanayake, J. Allnutt and F. Haidara [32].
- Salonen-Uppala (SU): by E. Salonen and S. Uppala [33].
- ITU-R P.840: published by the International Telecommunication Union [34][35].

These models estimate the clouds attenuation on satellite-earth links to the ground station. In particular, the DAH model is novel in the sense of using cloud coverage parameters that can be acquired from meteorological stations easily to produce fairly accurate annual predictions of attenuation statistics.

DAH model is valid for frequencies up to 35 GHz. As for SU & ITU-R models, both utilize the cloud Liquid Water Content (LWC). However, local radio-sounding profiles and Critical Relative Humidity function for cloud detection are used as input data in SU model whereas ITU-R model provides maps detailing the global statistics of atmospheric LWC based on long-term series of radiometer and radio-sounding data [36].

2.3.2 DAH

This model is based on the cloud cover atlas [37] with grid resolution of 5^{o} x 5^{o}. Investigation of such model was based on the 4 main liquid water bearing cloud types and their average properties in Table 2.3. Using average cloud properties with the assumption of statistical distribution of cloud attenuation following a log-normal probability law and that there is no overlap between occurrence probabilities of the cloud types.

Table 2.3 averaged cloud properties for DAH model [32]

Cloud type	Vertical Extent(km)	Horizontal Extent(km)	Water Content (g/m^3)
Cumulonimbus (Cb)	3.0	4.0	1.0
Cumulus (Cu)	2.0	3.0	0.6
Nimbostratus (Ns)	0.8	10.0	1.0
Stratus (St)	0.6	10.0	0.4

To find the specific attenuation for each cloud type, the Rayleigh [38] approximation for small droplets is utilized thus resulting in

$$\alpha_{ci} = 0.4343\left(\frac{3\pi v}{32\lambda\rho}\right)\mathrm{Im}\left(\frac{1-\varepsilon}{2+\varepsilon}\right) \text{ (dB/km)} \qquad (2.38)$$

Where

v cloud liquid water content (g/m^3)

λ wavelength (m)

ρ water density (g/m^3)…approx. 1 for temperature > 0^o C

ε complex dielectric constant of water $\varepsilon = \varepsilon' - j\varepsilon''$ … from COST 255, see Salonen & Uppala model for formula calculation.

Im imaginary part of a complex number

i index to one of the cloud types in question

The temperature dependency of water dielectric constant is of 2nd order effect and hence it is at 0^o C that this model uses.

So, cloud attenuation due to specific cloud type presence (please note, the assumption is based on no overlapping!) is then

$$A_{ci} = \alpha_{ci} H_{ci} \text{ (dB)} \qquad (2.39)$$

H is the thickness of cloud at elevation of 90^o, in COST 255 a formula for slanted path is introduced assuming the cloud is a vertical cylinder of height H and length L.

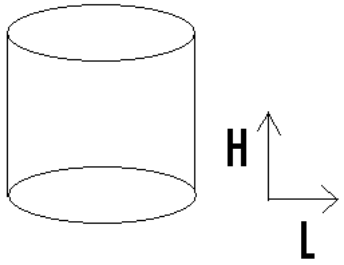

Figure 2.8 Cloud model [32]

The novel approach is in the generating of conditional cloud attenuation distribution curve with cloud cover statistics as input parameters. This is done by arranging the attenuation of the cloud types in rank order of attenuation to get 4 points and using linear regression analysis with the curve

$$P(A > A_c) = \frac{P_o}{2} erfc\left(\frac{\ln A - \ln \overline{A}_c}{\sqrt{2}\sigma_c}\right) \tag{2.40}$$

Where P is the probability of cloud attenuation A_c not exceeding A, and P_o the probability of attenuation due to cloud being present along with σ_c as the standard deviation of A_c. Note that $erfc$ is the complementary error function.

$$erfc(x) = \frac{2}{\sqrt{\pi}} \int_x^\infty e^{-t^2} dt = 1 - erf(x) \tag{2.41}$$

2.3.3 Salonen-Uppala (SU)

This model was an attempt to make a universal prediction regardless of geographical location restrictions. So, the measurements of 40 stations across Europe plus the gridded data of the numerical analyses of European Center for Medium Range Weather Forecast (ECMWF) where tested applying this new method.

The MPM model of Liebe [39] has the specific attenuation of the clouds as

$$\gamma_c = 0.182 f N''_w(f) \quad \text{(dB/km)} \tag{2.42}$$

Where N''_w is the imaginary part of the complex refractivity units (ppm→ 10^{-6}) which is written as

$$N''_w = \frac{9}{2}\frac{w}{\varepsilon''(1+\eta^2)} \tag{2.43}$$

Here w is liquid water density (g/m^3) and $\eta = \left(\frac{2+\varepsilon'}{\varepsilon''}\right)$.

The double Debye relaxation model gives the dielectric spectra for water [40]

$$\varepsilon'(f) = \varepsilon_2 + \frac{\varepsilon_0 - \varepsilon_1}{1+\left(\frac{f}{f_p}\right)^2} + \frac{\varepsilon_1 - \varepsilon_2}{1+\left(\frac{f}{f_s}\right)^2} \tag{2.44}$$

And

$$\varepsilon''(f) = \frac{f(\varepsilon_0 - \varepsilon_1)}{f_p\left[1+\left(\frac{f}{f_p}\right)^2\right]} + \frac{f(\varepsilon_1 - \varepsilon_2)}{f_s\left[1+\left(\frac{f}{f_s}\right)^2\right]} \tag{2.45}$$

With $\varepsilon_0 = 77.66 + 103.3(\theta_T - 1)$, $\varepsilon_1 = 5.48$, $\varepsilon_2 = 3.51$ and the principal with secondary relaxation frequencies as

$$f_p = 20.09 - 142(\theta_T - 1) + 294(\theta_T - 1)^2 \quad GHz, \qquad f_s = 590 - 1500(\theta_T - 1) \quad GHz \tag{2.46}$$

Note that $\theta_T = 300/T$ the inverse temperature parameter with T in Kelvin. These equations can be used for up to 1000 GHz and -10 to 30^o C.

It should be noted that they have applied and tightened the critical humidity as a function of frequency done by Geleyn [41] to detect clouds at each pressure level.

The revised SU cloud detection scheme is as follows [42]

The critical humidity function (spanning 0 to 1) for cloud detection is

$$U_C = 1 - \alpha\,\sigma(1-\sigma)\left[1 + \beta(\sigma - 0.5)\right] \tag{2.47}$$

With $\alpha = 1.0$, $\beta = \sqrt{3}$ and σ is the ratio of the pressure at the considered level to the surface pressure level. When the measured relative humidity is higher than the calculated critical humidity of the same pressure level then this layer is assumed to be within a cloud.

To estimate the density of liquid water w in g/m3 per level both air temperature within the layer and the layer's height with respect to the cloud base is needed, then apply the relations[43]:

$$w = \begin{cases} w_0\,(1 + c\,t)\left(\dfrac{h_c}{h_r}\right) p_w(t) & t \geq 0\ ^\circ C \\ w_0\,e^{ct}\left(\dfrac{h_c}{h_r}\right) p_w(t) & t < 0\ ^\circ C \end{cases} \quad \text{(g/m3)} \tag{2.48}$$

Where

$w_0 =$ 0.17 (g/m3)
c = 0.04 (° C−1)
t = temperature (° C)
hr = 1 500 (m)
hc = height from the cloud base (m).

To approximate the cloud liquid and ice density water fraction $p_w(t)$:

$$p_w(t) = \begin{cases} 1 & 0\ ^\circ C < t \\ 1 + \dfrac{t}{20} & -20\ ^\circ C < t \leq 0\ ^\circ C \\ 0 & t \leq -20\ ^\circ C \end{cases} \tag{2.49}$$

And finally the liquid water path would be obtained by linear integration of w along the profile.

More so, the w is hard to obtain plus the temperature dependence of cloud attenuation, so they worked around that by introducing the reduced liquid water

content w_{red} such as $\gamma_c(f,w,0^\circ C)=\gamma_c(f,w,t)$ around f=43 GHz (COST 255) [44]. And the range of w_{red} (from ECMWF) valid calculations is 10 to 60 GHz.

So, attenuation due to clouds can be written now as

$$A_c=\frac{0.819fW_{red}}{\varepsilon''(1+\eta^2)}\cdot\frac{1}{\sin\theta}=yW_{red}\cdot\frac{1}{\sin\theta} \quad \text{(dB)} \qquad (2.50)$$

With W_{red} in (kg/m^2), and θ is the elevation angle (degrees).

The authors originally suggested the use of this model for mid-latitude climates for elevation angles from 15 to 45°. In the COST 255 it is accepted for all elevation angles of frequencies below 60 GHz.

2.3.4 ITU-R

The ITU-R 840.3 (rev. 1999) and ITU-R 840.4 (rev. 2009) is a recommendation for aiding the engineers in designing of earth-space telecommunication systems that are higher than 10 GHz. The specific attenuation is the same as in Salonen and Uppala model, namely:

$$\gamma_c=K_l\,M \quad \text{(dB/km)} \qquad (2.51)$$

Where M is the liquid water content and K_l is

$$K_l=\frac{0.819f}{\varepsilon''(1+\eta^2)} \quad \text{(dB/km)(g/m}^3\text{)} \qquad (2.52)$$

However, this variable is slightly different

$$\varepsilon_0=77.6+103.3(\theta_T-1) \qquad (2.53)$$

The values of K_l are given in Figure 2.9; note that these are empirical values. Use the Figure with temperature of 0 °C.

More so, cloud attenuation is therefore

$$A_c=\frac{L\,K_l}{\sin\theta} \quad \text{dB} \qquad \text{for elevation of } 90^\circ\geq\theta\geq5^\circ. \qquad (2.54)$$

L is the total columnar content of liquid water (kg/m^2) exceeded for a specified percentage (%) of the year. Four sets of maps are attached to the publication corresponding to 1,5,10 and 20% exceedance of the globe; some other probability values are also available from their website. It is noteworthy to point out that these provided maps are the reduced liquid water content calculated by the method of SU model (setting f=43 GHz and solving for reduced LWP from measurements)… See A.2 for these maps.

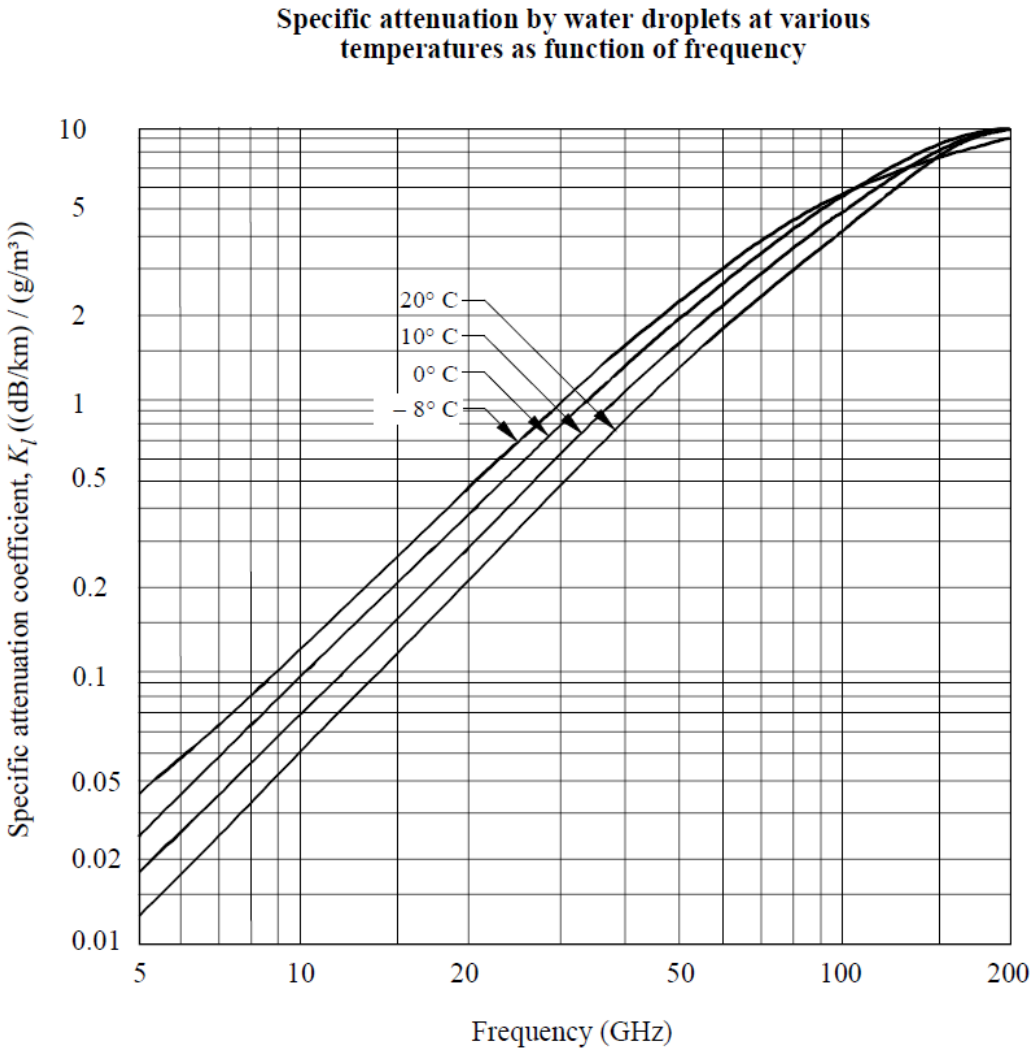

Figure 2.9 ITU-R empirical values of specific attenuation calculation [34]

For locations different from the grid points contours, we are advised to perform bi-linear interpolation on the values of the closest 4 grid points.

2.4 Conclusions

Cloud attenuation can be accurately explained by the scattering of single particle theory (for liquid water droplets) of which the extinction theorem is deduced. An analytical model existed since 1908 (Mie theory) which most other models are based on or approximate. Since cloud formation is complex the use of an analytical model would also be complex. An analytical model could be accurate based on the input parameters utilized and their validity if all circumstances where considered; while an empirical model would be simple to implement however restricted to a particular location. Therefore a semi-empirical model would have the potential to be applied globally and be less complex than the analytical one. The Rayleigh scattering approximation is proven to be adequate and simple to implement for clouds for frequencies up to 300 GHz [25] thus making it an appealing tool to utilize in cloud attenuation models.

Modern accepted cloud attenuation models either sacrifice accuracy for relative ease of use (DAH model with limit of about 35 GHz from synoptic data) or require prolonged (e.g. yearly) measurements of local atmospheric layers profiles by dedicated equipment such as radiometers and radiosonde (SU model) with parameters that might need tweaking per geographical location.

The ITU-R 840 model recommendations have potential as they depend on cloud temperature and LWP as input physical parameters along with the frequency of operation. They are based on the Rayleigh approximation (theoretically valid for up to 300 GHz… see Table 2.2). More so, they provide maps of the various probabilities of the reduced LWP of the globe and are applicable for up to 100 GHz as stated in the recommendations. As for the cloud temperature the models simply assume it to be zero Celsius.

The ITU-R has wide acceptance in the field and the cloud attenuation model is fairly simple to implement. Therefore it would be most beneficial to investigate the accuracy of the model and if possible improve on it in this project.

3 Receiver System and Data Pre-processing

3.1 Introduction (ITALSAT F1 Satellite)

The cloud analysis carried out in this project was performed using beacon data recorded from the ITALSAT satellites. ITALSAT F1 is Italy's first operational communications satellite launched on the 16^{th} of January 1991 by an Ariane booster and stationed in geostationary orbit at 13.2 degrees east and has been maintained at this position within $\pm 0.15^0$ box as seen from the Earth's center.

Developed by a contractor team led by Alenia Spazio, ITALSAT carries ten active transponders plus five spares for 30/20 GHz and 50/40 GHz links with a capacity of 12,000 telephone circuits. The propagation package includes a telemetry-modulated 20 GHz beacon (also used for tracking), a 40 GHz beacon phase modulated by a 505 MHz coherent subcarrier, and a polarization-switched (but otherwise un-modulated) 50 GHz beacon. It supports attenuation and depolarization measurements at 20, 40, and 50 GHz, as well as new measurements of phase and amplitude dispersion. The availability of a polarization-switched signal enables earth stations to fully characterize the matrix depolarization characteristics of the 50 GHz channel [45]

The elevation angle was 29.9^o and will be referred to hereafter as 30^o. The exact propagation beacon frequencies are 18.7, 39.6 and 49.49 GHz; they will hereafter be referred to as 20, 40 and 50 GHz beacons, respectively. The 50 GHz beacon signal is switched between horizontal and vertical polarization at the rate of 933 Hz, had a specified EIRP of 26.8 dBW, after five years of operation.

The 40 GHz beacon, which is fully redundant, consists of an exciter and an impatt amplifier. The beacon is fed by a low-level S-band signal, provided by the L.O. The input signal, after being multiplied by 4 goes to the exciter. The latter is fed also by 505 MHz tone coming from the L.O. and provides 1/4 radian peak phase modulation of the input signal. After modulation, this frequency is again multiplied by 4 giving rise to a 40 GHz signal with 1-rad peak phase modulation.

This signal is fed to an injection locked impatt amplifier providing final amplification with minimum spectrum distortion of the composite signal.

Figure 3.1 Sparsholt location [46]

The modulated signal is radiated by a circular beam antenna with the required polarization characteristics. The beacon is continuously transmitted with the exception of eclipse periods. The average EIRP values of the central 40 GHz beacon are:

30.0 dBW	Edge of coverage, no subcarrier modulation
28.0 dBW	Edge of coverage, with subcarrier modulation

The coverage area (3 dB footprint) of the three beacons includes most of the UK.

3.2 Receiver System

The receiver system shown in Figures 7.3 and 7.4, is located at Sparsholt (51.5850° N, 1.5033° W), U.K. The location of Sparsholt is shown on the map in Figure 3.1. The principal system parameters are summarized in Table 3.1, further details can be found in [47]. The system comprises of:

1. Three earth-station receiving Cassegrain antennas of diameter 1.22m for the 18.68(20) GHz and 0.61m for the 39.59(40) GHz and 49.49(50) GHz, from where ITALSAT was viewed at an elevation angle of 29.9°(30°).
2. Meteorological instruments (temperature, pressure and humidity sensors. Rapid response rain gauge and an impact distrometer).
3. Data logging and storage equipment.

Regular sampling and recording of all the receivers and meteorological parameters is carried-out at a sampling rate of 1 Hz (rain-gauge is at 0.1 Hz). However, enhancements were made to the receiver system during 1997. A modification to the IF section of the 49.49 GHz beacon receiver has meant that it was possible to sample the output at up to 10 Hz; this procedure was performed for periods of 5 minutes every 30 minutes. These extra measurements were first collected in December 1997 [48].

The receiving system (satellite beacon) comprises a 0.61-meter Cassegrain antenna for the 40 and 50 GHz receivers and a 1.22-meter antenna for the 20 GHz feeding into a polarization switch to allow selection of either horizontal or vertical polarization in the case of the 50GHz receiver. Then through single balanced mixer having a noise figure of 6 dB, where the received signal is down-converted to a frequency of 70MHz. The local oscillator (LO) consists of a VHF crystal source that phase locks to an X-band generator (103MHz), then multiplied to 49.42 GHz by a times-four multiplier. The IF signal is then amplified and filtered, before final detection by a conventional phase-lock loop beacon receiver. This simple system resulted in achieving a received signal of 34 dB the noise level in clear sky conditions thus making it adequate for observing related propagation effects. In Figure 3.2 a block diagram of the 50GHz receiver is shown. The 70MHz receiver has a D.C. voltage output proportional to the logarithm of the received signal level.

The 20 GHz dish is mounted outside, on top of the hut and then routed to the data-logging system inside the hut via a cable. The 40 and 50 GHz earth station receiver systems and the data logging units are housed inside the temperature-controlled hut, as shown in Figures 7.3 and 7.4. The system is temperature controlled to 20^0C; the gross weight of each of the 40 and 50GHz receiver systems is around 20 kg. Measured attenuation fidelity is about $\pm$ 0.5 dB [49].

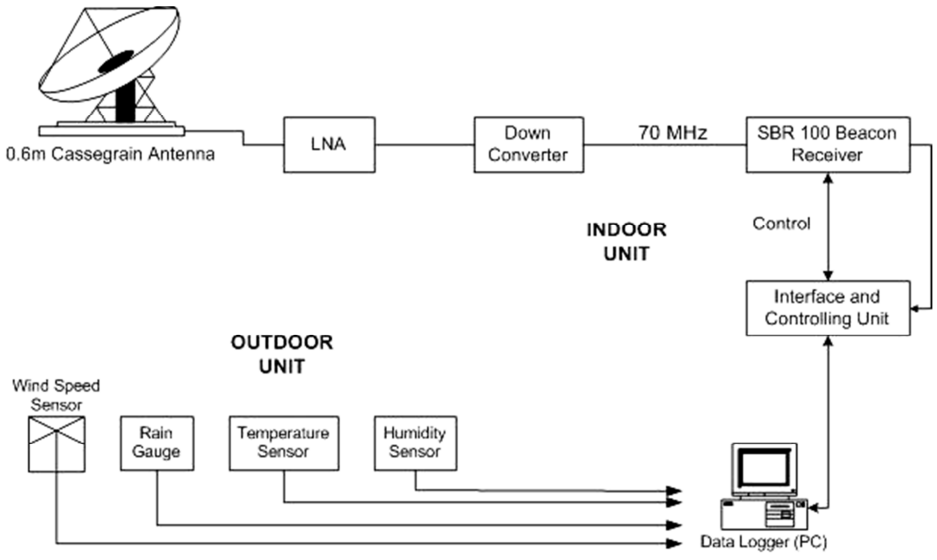

Figure 3.2 Diagram of ITALSAT receiver at 50 GHz [46]

Table 3.1 Main System Parameters

Satellite		
	Name	ITALSAT F1
	Frequency	18.69/39.59/49.49 GHz
	Position	Geostationary, 13.2° East
Earth Station		
	Antenna Diameter	
	(39.59/49.49) 40/50 GHz	0.61 m
	(18.69) 20 GHz	1.22 m
	Antenna gain	
	20 GHz	45.6932 dBi
	40 GHz	46.1896 dBi
	50 GHz	48.1261 dBi
	elevation angle	29.9°
	EIRP	
	20/40GHz	61 dBm
	50 GHz	56.8 dBm
	Free Space Loss (FSL)	
	20 GHz	209.6133 dB
	40 GHz	216.1303 dB
	50 GHz	218.0668 dB
	gaseous absorption	
	20 GHz	0.8554 dB
	40 GHz	1.5735 dB
	50 GHz	4.2755 dB
	Rain rate (0.01%)	37 mm/h
	Rain Attenuation (0.01%)	
	20 GHz	13.4 dB
	40 GHz	25.0 dB
	50 GHz	19.3 dB
	System Noise Temperature	≈-197.4 dBW/Hz

The ITALSAT vehicle was originally designed to operate for five years, but ITALSAT F1 operated beyond its expected life and remained in orbit for almost an additional 5 years. In order to extend the beacons transmission time, a scheme for propellant saving had been adopted in which the North/South station keeping was discarded. Thus a need for the beacon receivers to track the satellite position became apparent through the year and towards the end of 1997. Thus the 50 GHz beacon receiver at Sparsholt was equipped with a tracking unit to counter the problem and the same was done for the 40 GHz receiver in August 1998.

In the next section the data preprocessing is explained.

Figure 3.3 The hut at Sparsholt where the receiving antennas have been installed along with the data logging system [46].

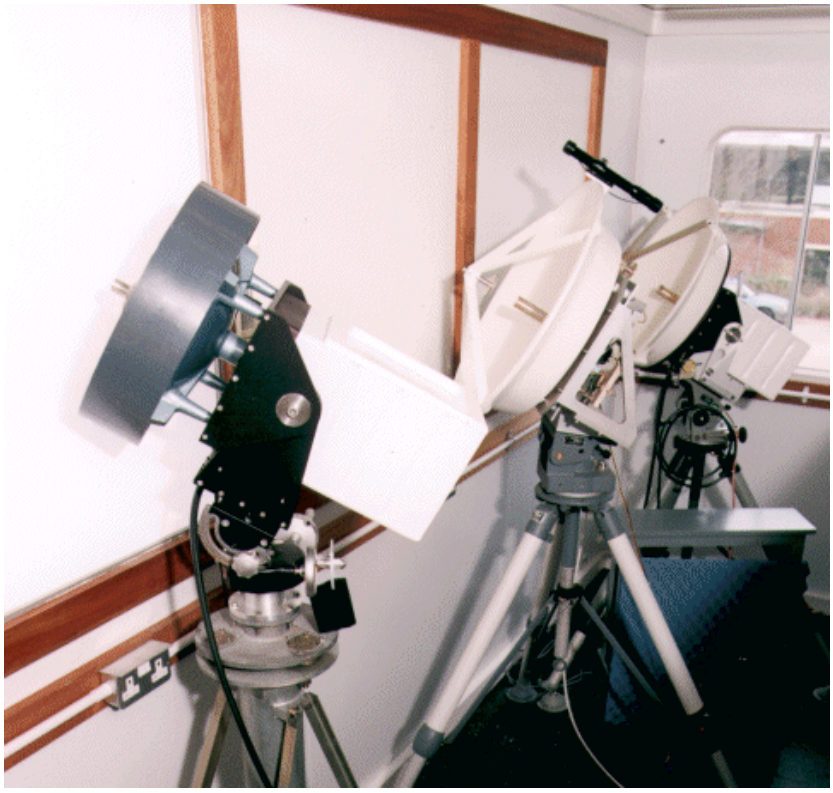

Figure 3.4 From left to right, the 51GHz radiometer, the 50GHz receiver and the 40GHz receiver [46].

3.3 Data Pre-processing

3.3.1 Sparsholt Raw Data

Before the attenuation data could be used in the analysis process, corrupted data had to be removed. Originally data pre-processing were to be performed for the period from April 1997 to March 1999, on the ITALSAT F1 satellite beacon at frequencies 18.68GHz, 39.59GHz and 49.49GHz recorded at Sparsholt. Unfortunately the 18.68GHz beacon data are not useful for the period after March 1998, as a result to satellite movements.

A meticulous visual inspection of plotted raw data at each frequency was crucial to identify and exclude corrupted sample values and data logged during receiver system downtime.

The raw propagation data along with relevant meteorological variables had been saved in daily binary files by the data logging system used at the Sparsholt measurement site. Utilizing MATLAB a program was written to read and calibrate each data channel to give the correct measured parameter, such as rain rate in mm/hr for a rain channel, relative signal level in dB for a propagation channel, relative humidity and so on.

The resulting daily time series of the received signal level of each beacon frequency was plotted and subjected to a careful visual inspection in order to identify gaps and periods of non-genuine signal level, see Figure 3.5. The indices of these gaps (if any) were stored in a separate file. Each propagation data sample that was deemed invalid was replaced by NaN (Not a Number). In this way non-genuine samples are unmistakably marked so they can be excluded from the data analysis keeping the time reference inherent in the index of the vector variable containing the samples of each channel over a one-day period intact. See Figure 3.6.

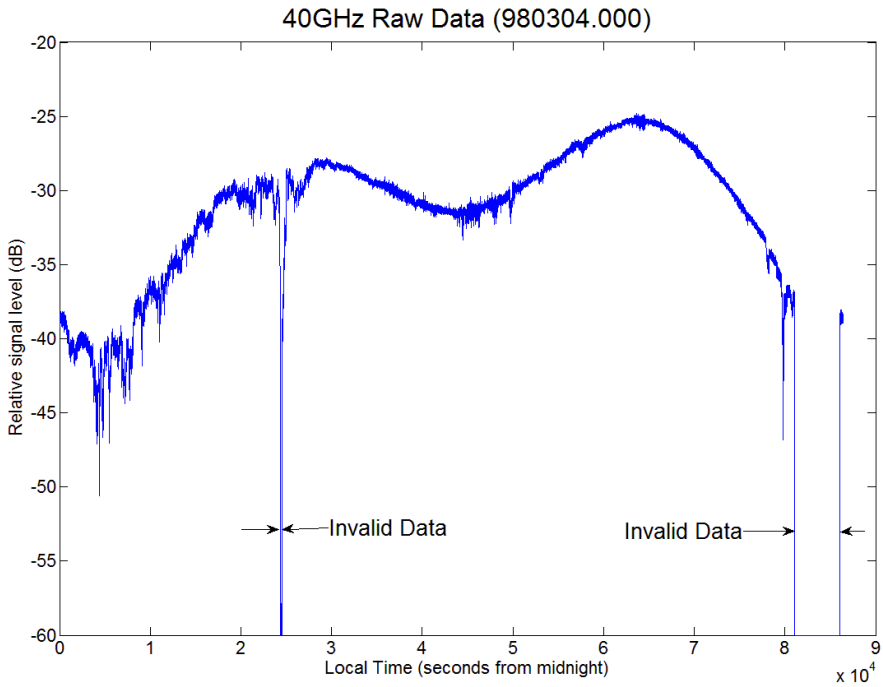

Figure 3.5 Plot of the received raw data for a period of one-day, where *INVALID* data are identified.

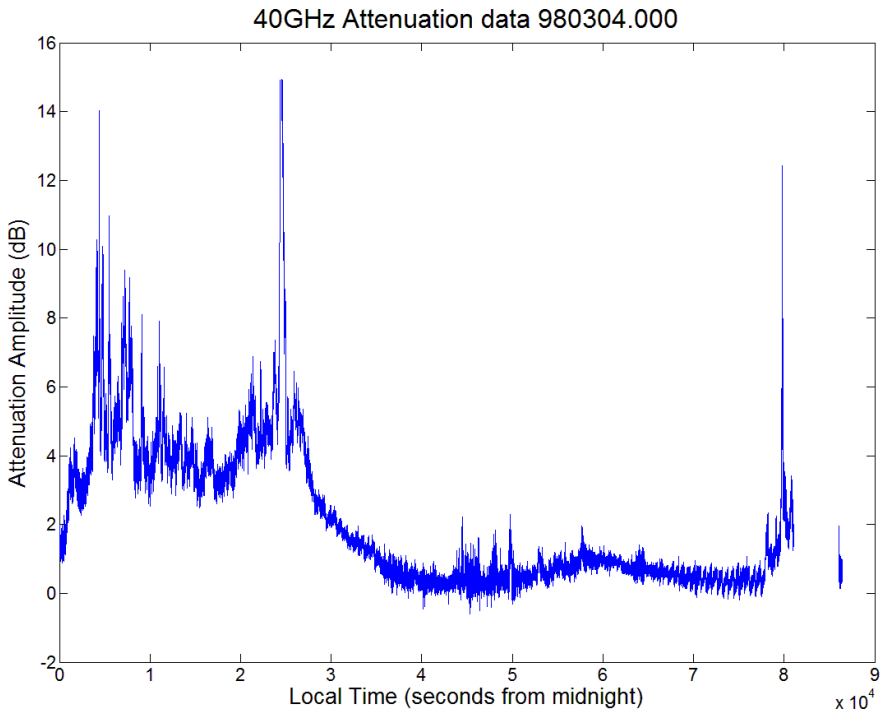

Figure 3.6 Attenuation time series for the same period of one-day as in **Figure 3.5** note that *INVALID* data have been excluded.

3.3.2 Chilbolton ITALSAT Time series

Both Sparsholt raw Data and zero-dB attenuation data where acquired from the British Atmospheric Data Center (BADC) and Chilbolton Facility for Atmospheric and Radio Research (CFARR) at Rutherford Appleton Laboratory (RAL) [50]. The zero-dB level is a reference level by which attenuation is extracted from the beacon signal value and defined (clear sky). The Fourier series method of the Olympus satellite campaign [51] was incorporated in the analysis of the ITALSAT results bearing in mind the particulars of the equipment that were used and the various events that affected the higher frequencies [52].

The zero-dB data consisted of two attenuation flavors, Total and Excess. Total: as the name suggest, include the effect of all impairments. Excess: is the attenuation of all impairments less the gaseous absorption; it is acquired by means of numerical calculation of gaseous attenuation from meteorological parameters obtained from the site and radiosonde, then subtracting it from the Total attenuation.

Having checked these attenuation levels against our own raw data (from the previous section) to make sure the data was indeed valid, we decided to utilize the zero-dB data for attenuation amplitude values-as excess attenuation would indicate cloudy and rainy conditions- along with the temperature, pressure, relative humidity and rain-gauge recorded in the raw data files.

3.4 Resulting Data Sets

Data pre-processing was carried out in order to collect and identify valid (genuine) attenuation some hurdles were encountered, thus resulting in:

All the data after March 1998 recorded from the ITALSAT F1 satellite (20GHz) had to be discarded, due to the satellite North-South movement. Originally we were to process and analysis satellite beacon measurements for the period covering April 1997 to March 2000 for all frequencies of operation.

The Sparsholt raw data were missing a significant period (June-July-August 1999) which meant that the zero-dB files could not be verified. More so, the ability to perform pure cloud attenuation analysis could not be performed for the lack of rain-gauge from the missing period of Sparsholt's Data.

Therefore, in summary the valid data available for use in the analysis were:

a) For the 20GHz: Beacon data for the period from April 1997 to March 1998 (1-year).
b) For both the 40GHz and 50GHz: Beacon data for the period from April 1997 to March 1999 (2-year).

In both Table 3.2 and Table 3.3 we see the invalid data percentages of these years. It is notable that the valid attenuation errors do vary reflecting the effect of implementing the tracking units for the 40 GHz (August 1998) and 50GHz (end of 1997).

Table 3.2 April1997-March1998 Data validity

Frequency (f)	Available Data of whole year (%)	Valid attenuation of available Data (%)	Valid rain-gauge of available Data (%)
20	96.44	79.88	93.94
40	96.44	88.37	93.94
50	96.44	81.90	93.94

Table 3.3 April1998-March1999 Data validity

Frequency (f)	Available Data of whole year (%)	Valid attenuation of available Data (%)	Valid rain-gauge of available Data (%)
40	98.08	84.07	96.52
50	98.08	90.45	96.52

3.5 Sparsholt Data Format

The data were stored on CDs in binary form. For every second the corresponding data are stored in a record containing 52 bytes, see Table 3.4.

The data received are stored as a voltage on a hard disk and are collected once every month. The system is connected via a modem to the Internet, where low quality signal figures of the received data are displayed and can be accessed. It is used mainly to monitor the system on a daily basis to ensure that everything is working fine.

Table 3.4 Sparsholt Data format

Byte	Counter
0	**Year**
1	**Month**
2	**Day**
3	**Hours (GMT)**
4	**Minutes**
5	**Seconds**
6--7	F12 Beacon
8--9	**F20 Beacon**
10--11	R50 Radiometer V
12--13	Radiometer H
14--15	**F40 Beacon, Use this Frequency**
16--17	Don't use
18--19	39 GHz Beacon
20	Don't Use
21	Don't Use
22--23	41 GHz Beacon

24--25	Don't Use
26--27	Don't Use
28--29	**50 GHz Beacon**
30--31	Don't Use
32--33	Don't Use
34--35	Don't Use
36--37	**Air Temperature**
38--39	**Relative Humidity**
40--41	**Pressure**
42--43	Don't Use
44--45	Don't Use
46--47	Don't Use
48	(Rain Gauge)
49	Don't Use
50	Don't Use
51--52	Don't Use

3.6 Calibration

Data received are stored as a voltage hence calibration factors were used to translate those readings into degree Celsius for the temperature, dB for the signal level, obtain the humidity as a percentage and at last to obtain Millibars (hPa) for the pressure.

The calibration is linear and the formulae required are given below:

Linear Calibration

$$Xv = [Xv(0), \quad Xv(1)] \tag{3.1}$$

$$Yv = [Yv(0), \quad Yv(1)] \tag{2.2}$$

$$A = \frac{Yv(0) - Yv(1)}{Xv(0) - Xv(1)} \tag{3.3}$$

$$B = \frac{Yv(1) * Xv(0) - Yv(0) * Xv(1)}{Xv(0) - Xv(1)} \tag{3.4}$$

$$Calibrated \ \ Data = (data \times A) + B \tag{3.5}$$

- **Calibration factors for the 20, 40 and 50 GHz beacons to obtain the signal level in dB**

Xv = [-2048, 2048]

Yv = [-60, -20]

- **Calibration factors for the temperature to obtain it in ^{0}C**

Xv = [0, 1024]

Yv = [-40, 60]

- **Calibration factors for the pressure to obtain it in Millibars (hPa)**

Xv = [0, 2048]

Yv = [900, 1050]

- **Calibration factors for the relative humidity to obtain it in %**

1. If the relative humidity is measured, then the calibration factors are

Xv = [0, 1024]

Yv = [0, 100]

2. If the dew point is measured then the calibration factors are

Xv = [0, 1024]

Yv = [-40, 60]

substituting those calibration factors in the general Equation (3.5) will yield a value say 'RR'.

To estimate the relative humidity from dew point measurements, use the following equations:

Substitute the value of '*RR'* found from Equation 3.5 into Equation 3.6:

$$ww_1 = \frac{RR}{(RR + 238.3)} \tag{3.6}$$

$$ww_2 = \frac{Temperature\,(^oC)}{Temperature\,(^oC) + 238.3} \tag{3.7}$$

*Relative Humidity = 100 * exp [17.2694 * (ww_1-ww_2)]*

Starting from the 3rd of April 1997 relative humidity was measured using dew point. For that reason to obtain the relative humidity for any data obtained after the 3rd of April 1997 utilize the dew point formula.

3.7 Met Office-MIDAS Land Surface Stations Data

The synoptic data set was obtained from the British Atmospheric Data Centre (BADC) [53]. It contains the hourly (period and location dependent) Met office-Land Surface Observation Stations Data from stations around the world for the period from 1853 to current (updated to within 2-months of database access). We needed only the UK Hourly Weather Observations data covering the period from January 1990 to December 2000 recorded at Brize-Norton. Because of the accuracy and valid data availability issue of the years 1990-1993 these years were discarded hence only 1994-2000 years were used. The full content description and format of the data can be found in Appendix B.

This dataset was utilized for the statistical and meteorological analysis (next chapter) of Sparsholt site since the weather station Brize-Norton (12.7 miles) was the closest to it. Cloud genre, Frequency of Occurrence (FoC) and amount recorded with a 1-hour resolution were used in the analysis with emphasis on the year of 1997 since it had all three frequencies of operation (20, 40 and 50 GHz) from ITALSAT Sparsholt Experiment.

3.8 ECMWF ERA-INTERIM data

ERA-interim dataset [54] is the continuation of the reanalysis efforts of global forecast-Numerical Weather Prediction (NWP) at the ECMWF. It follows after their successful ERA-40 which spanned (1957-2002) that has been utilized by the scientific community. Due to the extensiveness of the archives of ERA-interim in comparison to the ERA-40 such as having increased the pressure levels dividing the atmosphere from 23 to 37 and having additional cloud parameters that are freely (publicly) available on the internet, we have decided to use it in this project. A full description of the ERA-interim can be found in [55]. A more detailed review is performed in section 6.3.

3.9 Summary

Acquiring valid measurements of various local meteorological parameters and signal attenuation levels is a time consuming and difficult process. These parameters are validated and filtered of errors in an attempt to make use of them in this project to ultimately produce an improved cloud attenuation model. The period of April 1998 to March 1999 had a percentage of valid samples of 84.07% and 90.45% for both the 40 and 50 GHz, respectively. However, the period of April 1997 to March 1998 was the only period to have all three frequencies (20, 40 and 50 GHz) for utilization. The percentages of valid samples for analysis were 79.88%, 88.37% and 81.90% at 20, 40 and 50 GHz, respectively.

By choosing a data source of meteorological parameters that is accurate and span the globe, the accuracy and validity of the cloud model to be applied globally can be verified. Therefore the use of the latest ECMWF ERA-INTERIM analysis data set is expected to assist in producing and verifying a new (improved) cloud attenuation model.

In the next chapter we lay-out the statistical and meteorological analysis for Sparsholt and other sites of interest.

4 Statistical, Meteorological and Local Tropospheric Analysis

4.1 Statistical tools- Cumulative Distribution Function

4.1.1 Introduction

A lot of research done by various scientists and engineers concentrated on the effect of rain due to its severe effect on microwave communications in comparison to other factors (e.g. Assis and Einloft [56], Bryant [57], Crane [58], Flavin [59], ITU-R 618 [60] to name a few). In the case of rain attenuation the amount of rain rate and the height of the source (cloud) that is producing the rain where found to have a direct impact on signal attenuation. One of the mostly used statistical tools is the Cumulative Distribution Function referred to as CDF.

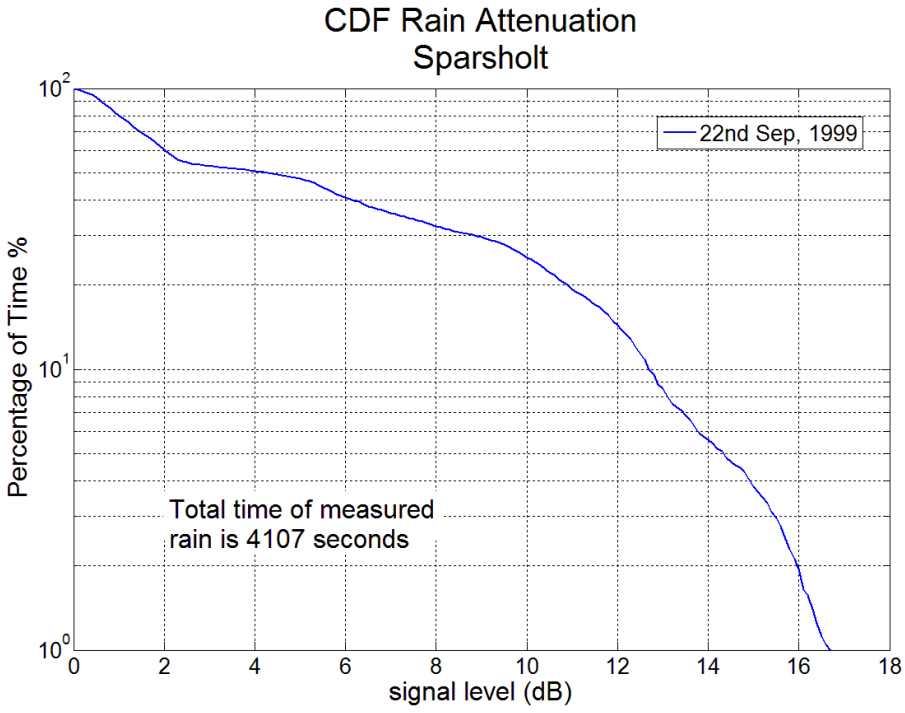

Figure 4.1 Daily CDF of rain attenuation

Figure 4.1 shows the daily CDF at operational frequency of 39.6 GHz in September 1999 is shown. It is noted that at some time in that day the attenuation due to rain reached above 16dB for about 2% (82.14 sec.) and that for about 50% (34.23 minutes) the attenuation was higher than 4 dB.

Therefore, as the demand for the utilization of even higher frequencies is bigger than ever the attenuation due to clouds becomes more significant as previously discussed (section 1.4.5). Thus the CDF tool will be vital in investigating cloud attenuation as the following example illustrates.

If we are to look at a sample day of excess attenuation (section 3.3.2) where clear sky is set to 0 dB; say 25th of April 1997 then we can attest that day's attenuation due to non-clear sky conditions was experienced for 53% of the time (around 12.7 hours) at 20 GHz. However, for the same conditions the signal is attenuated for 86% (around 20.5 hours) for both 40 and 50 GHz frequency. This shows that small amount of liquid water in clouds or suspended in the air begin to show effect on signals with frequencies above 20 GHz.

At 0.1% of the time (86.4 seconds) the attenuation was 1.05, 6.63 and 9 dB at 20, 40 and 50 GHz, respectively. Now for about 10% (2.4 hours) the attenuation was higher than 0.34, 2.74 and 3.33 dB at 20, 40 and 50 GHz, respectively.

Now, if looking at only the cloud attenuation (Figure 4.2 and Figure 4.3) it is noticed that for around 51% of the time (around 12.2 hours) for 20 GHz and 84% of the time (around 20.2 hours) for 40 and 50 GHz, the signal was attenuated due to cloud presence.

Applying the same analysis as for the excess attenuation, the cloud attenuation at 0.1% of the time was 0.8, 5.45 and 7.56 dB for 20, 40 and 50GHz, respectively. And for around 10% the attenuation was higher than 0.27, 2.32 and 2.74 dB for 20, 40 and 50GHz, respectively.

Thus the impact of cloud attenuation is indeed significant at higher frequencies. Clouds are present at much more intervals than rain which makes studying their attenuation effect that more vital in designing satcom links.

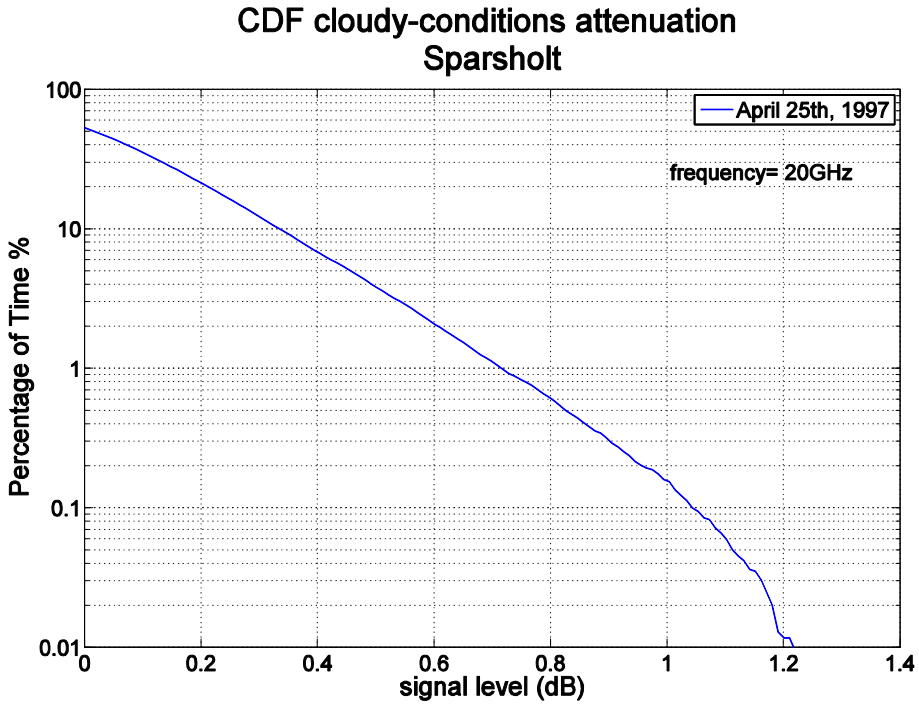

Figure 4.2 Daily CDF of cloudy-conditions attenuation

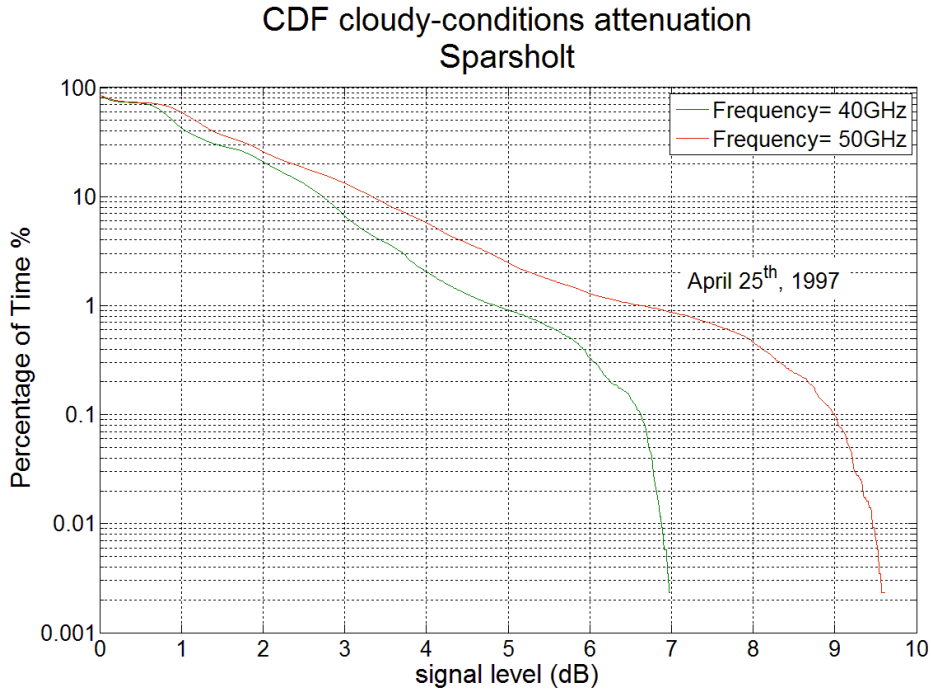

Figure 4.3 Daily CDF of cloudy-conditions attenuation

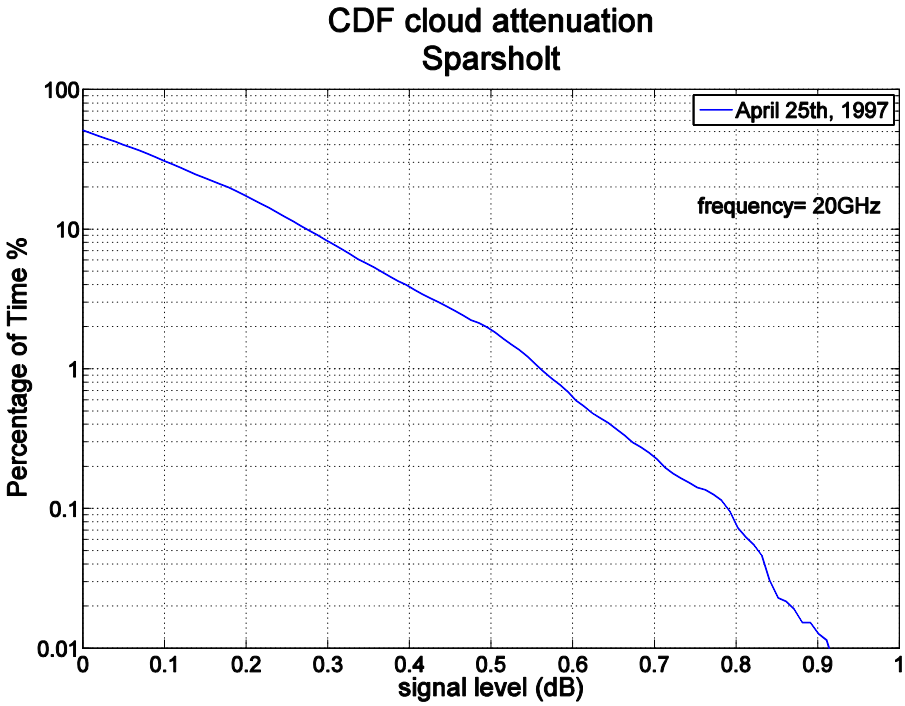

Figure 4.4 Daily CDF of cloud attenuation

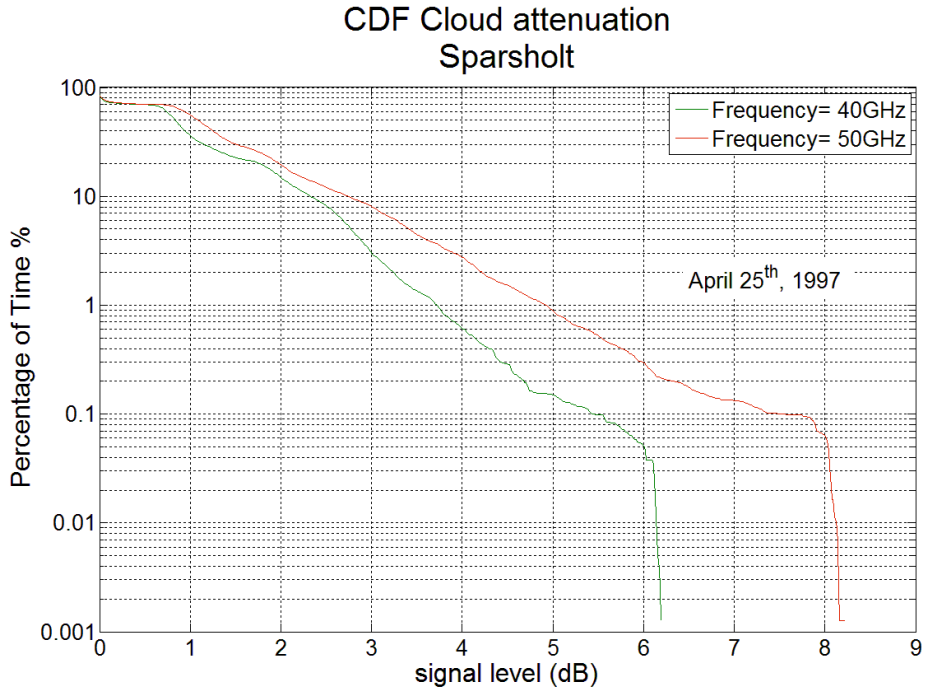

Figure 4.5 Daily CDF of cloud attenuation

4.1.2 Seasonal statistics-Interval of interest

Although one can use any statistical tool (CDF in our case) for any time-scale, making meaning of the processed data is dependent on the period which it has been processed. In the last segment the use of CDFs for diurnal analysis was shown. They can be useful in giving insight into potential variations in service quality due to propagation effects that exist over smaller intervals of time. However, it is impractical to constraint the data on a daily bases since the dynamics of weather (type of cloud, amount of cloud covering the sky, time in which the cloud remains in the propagation path…etc.) varies considerably from day to day and month to month (seasonal change).

Observing the monthly cloud attenuation statistics (April 1997-March 1998) the variation of attenuation per frequency is now visible. Indeed, in southern UK for all of the 20, 40 and 50 GHz monthly statistics the month with the highest attenuation was measured in August. However, the lowest month statistics was in April for the 20 GHz while for both the 40 and 50 GHz statistics the lowest was in February.

The reason for the lowest monthly attenuation not being the same for all frequencies can be accredited to the fact of the 20 GHz signal being unusable at the end of March 1998 as explained back in section 3.4. Hence for the last months of operation of the 20 GHz (See Table 4.1) there were a lot of measurements that were erroneous which means that the status flag was not indicating the data to be valid. Note that the month of September 1997 at 50 GHz the entire month's data had status flag indicating the data to be invalid. However, based on the data of the other frequencies and their high fidelity percentage one can speculate that this month was neither the highest nor the lowest in the cloud attenuation statistics measured.

Table 4.1 Valid data percentage for January to March 1998

Valid data (%) per month	20 GHz	40 GHz	50 GHz
Apr 97	71.26%	76.33%	87.32%
May 97	86.27%	65.90%	97.48%
Jun 97	91.48%	94.65%	94.54%
Jul 97	96.28%	98.72%	98.70%
Aug 97	82.25%	95.14%	86.17%
Sep 97	96.56%	90.58%	not available
Oct 97	95.61%	94.86%	75.90%
Nov 97	78.29%	91.52%	91.02%
Dec 97	29.64%	64.56%	64.50%
Jan 98	66.67%	76.53%	76.50%
Feb 98	61.81%	84.94%	84.87%
Mar 98	67.81%	89.24%	89.53%

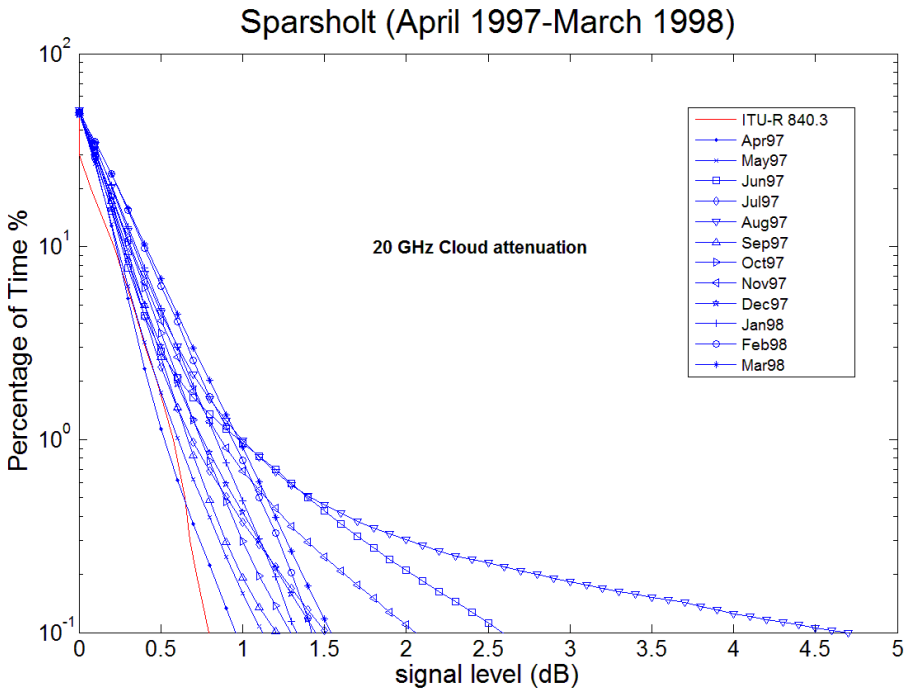

Figure 4.6 Monthly statistics of cloud attenuation for a full year at 20 GHz.

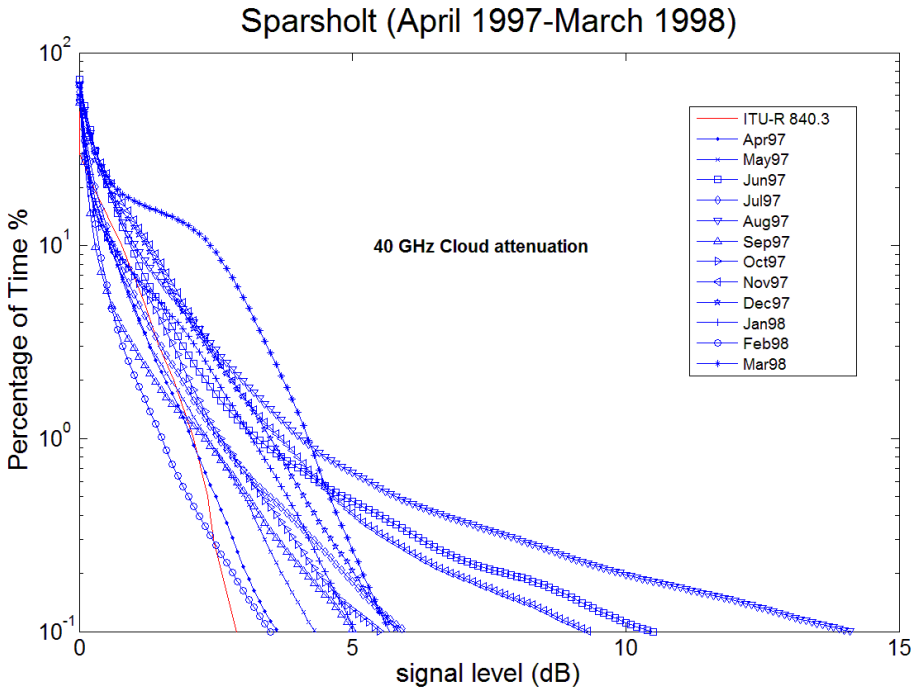

Figure 4.7 Monthly statistics of cloud attenuation for a full year at 40 GHz.

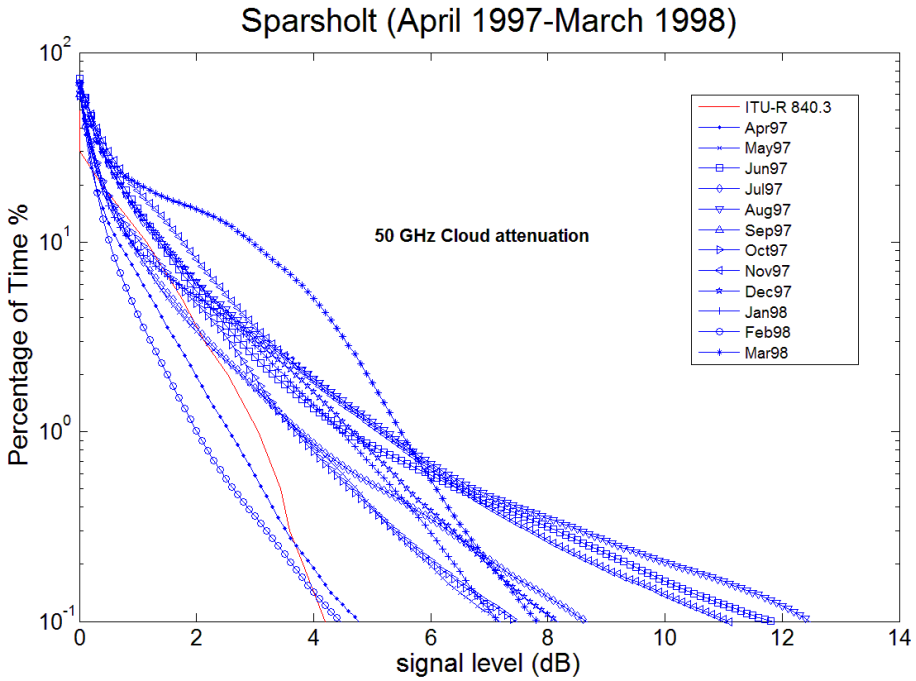

Figure 4.8 Monthly statistics of cloud attenuation for a full year at 50 GHz.

To take into account the full cycle of the climate at the receiver's location of signal reception, annual CDFs were computed. Figure 4.9 and Figure 4.10 show the annual CDFs of total attenuation for all three frequencies for the periods April 1997 to March 1998 and the two upper frequencies for April 1998 to March 1999 at Sparsholt. It is to be noted that total attenuation is the attenuation of all known tropospheric factors namely rain, cloud, scintillations and gaseous absorption. Hence the CDF curves of the total attenuation would have attenuation values at 100% since the gaseous absorption is experienced by signals all the time.

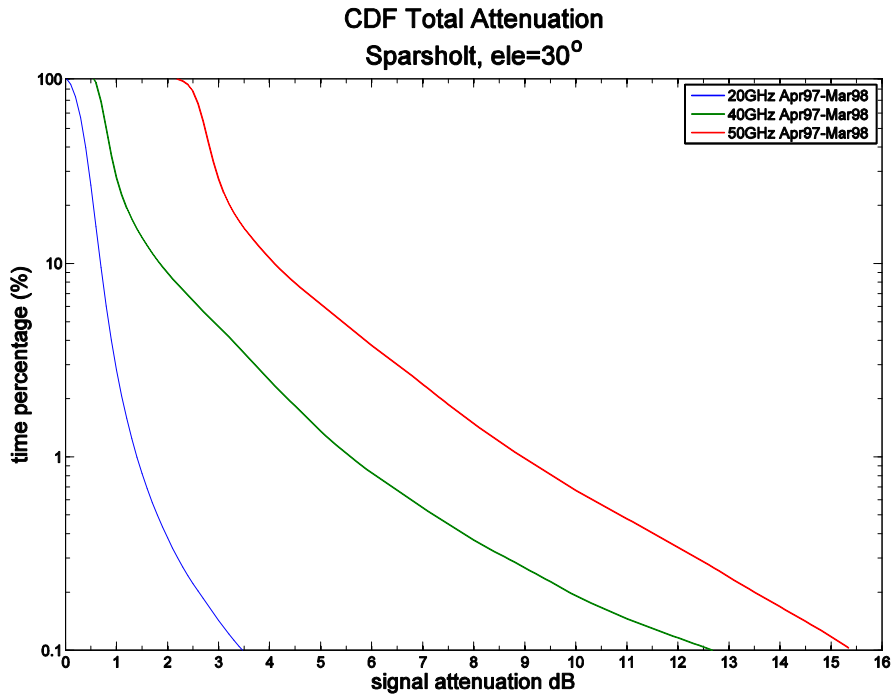

Figure 4.9 Annual CDFs of total attenuation

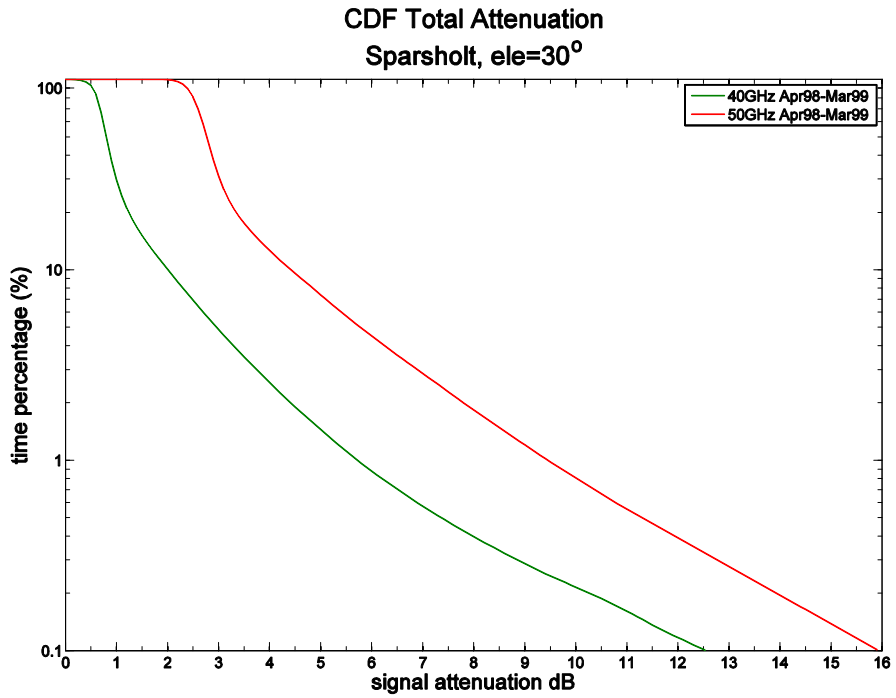

Figure 4.10 Annual CDFs of total attenuation

Indeed, for the period of April 1997 to March 1998 the total attenuation at 20 GHz is much lower than the 40 and 50 GHz total attenuation. For 1% of the year (~ 88 hours) the fade values for the 20, 40 and 50GHz frequencies were 1.4, 5.5 and 8.9 dB, respectively. For 0.1% of the year (~ 8.8 hours) the fade values for the 20, 40 and 50GHz frequencies were 3.5, 12.6 and 15.2 dB, respectively.

Looking at the 40 and 50GHz total attenuation recorded at Sparsholt for the period of April1998 to March1999 one can notice that for 1% of the year the fade values for the 40 and 50 GHz were 5.7 and 9.4 dB, respectively. And for 0.1% of the year the fade values for the 40 and 50GHz were 12.5 and 15.8 dB, respectively.

Considering cloud attenuation alone, then it is clear that cloud attenuation is significant, as seen in Figure 4.11. It no longer can be ignored and constitute a big portion of the total attenuation. For 1% percentage of the time, cloud attenuation fade values at 40 and 50 GHz were 3.8 and 5.1 dB, respectively. This means they contribute more than half of the total measured attenuation.

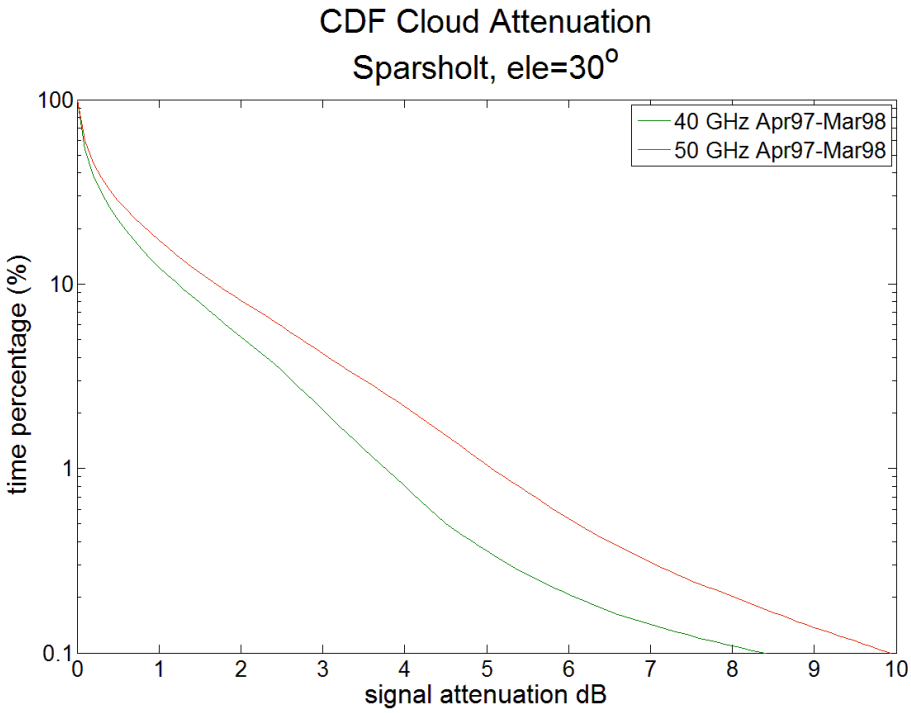

Figure 4.11 Annual CDF of cloud attenuation

In the satcom design field it is helpful to refer to something called worst month CDF. Worst month CDF is computed from the monthly CDFs of a full year by taking the maximum value at each percent of time. The result is an over-estimate of the attenuation percentage values of yearly CDF, see Figure 4.12 and Figure 4.13.

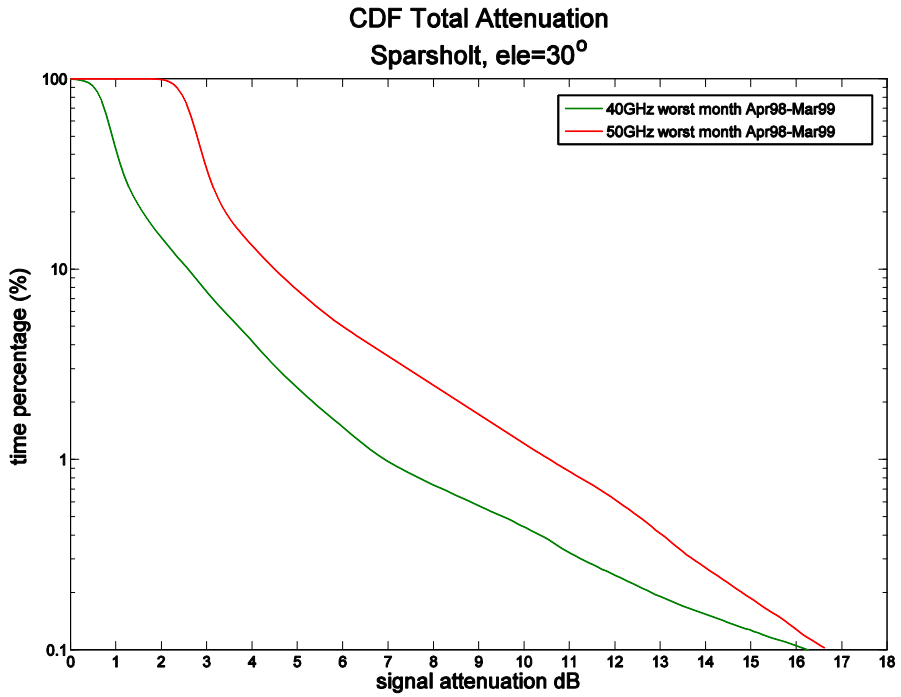

Figure 4.12 Worst month CDFs of total attenuation

The worst month CDF in Figure 4.12 as expected the percentages are higher than the yearly CDF of the same period. For 1% of the time at 40 and 50 GHz the fade values were 7 and 10.6 dB, respectively. While at lower time percentage of 0.1% at 40 and 50 GHz, the measured fade values were 16.5 and 16.8 dB, respectively. As expected, worst month values exceed annual values, for the lower percentage of 0.1% of the worst month fade this represents an increase of 32% and 6.3%, respectively. From Figure 4.13 it is apparent at 0.1% the 50 GHz worst month attenuation is above 2 dB than the yearly. More so, for the 40 GHz worst month at 0.1% the attenuation difference is above 3 dB.

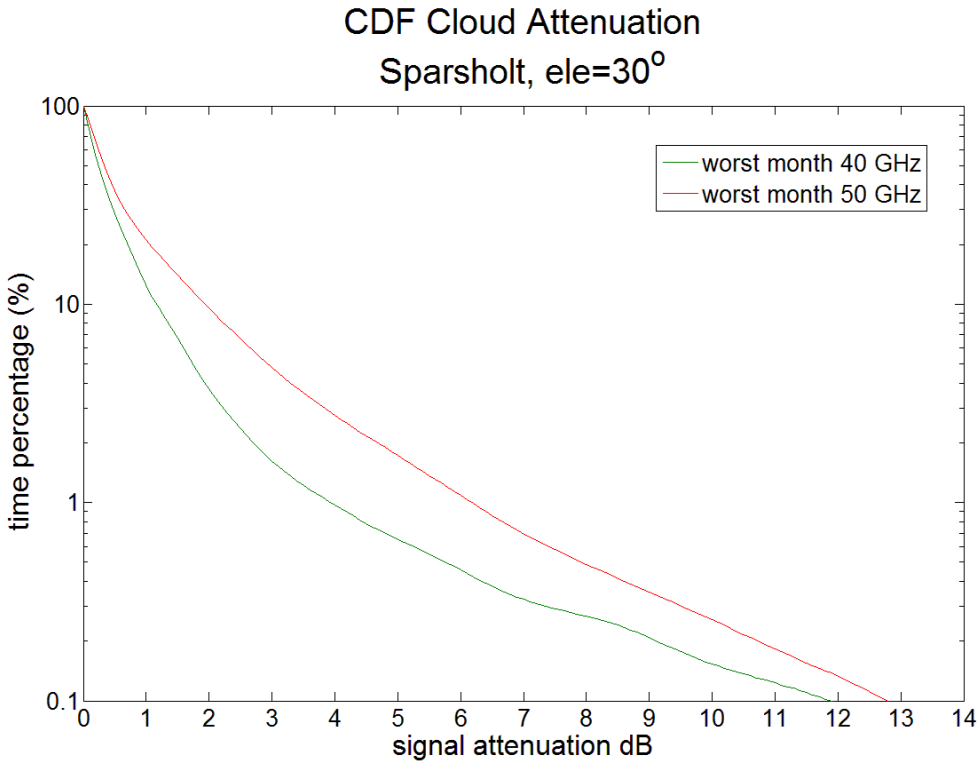

Figure 4.13 Worst month CDF of cloud attenuation

Hence, link budget engineers use annual and worst month cumulative distribution functions to compute the link budget for any new satcom system. These functions would give the system designer information on the probability of any predefined level of fading that would be exceeded in terms of the percentage of the time in a monthly or annual period. Based on these statistics and the mandatory link availability, the system fade margin is calculated.

In section 4.3 (Local Tropospheric Degradation Analysis) the attenuation components extracted from the total attenuations of Sparsholt measurements discussed earlier will be further studied and analyzed.

4.1.3 Global study-locations

Similar to the itu-r 840 recommendations, the main focus is on acquiring yearly cloud attenuation statistics to account for cloud attenuation and model is per geographical (grid-point) location. Hence measurements of verified cloud attenuation (genuine-no scaling or mathematical treatment, published and

above 10 GHz) from different locations spanning different latitudes were collected and used in the analysis in this project.

It is noteworthy to mention that for some sites the elevation angles of measured cloud attenuation were as high as 80^{o} and 90^{o}; that is because these measurements were acquired from radiometers rather than satellite beacons.

4.1.3.1 Malaysia

The location's coordinates is Lat 5.36 x Lon 100.30 having an elevation angle of 40.1^{o} and an operating frequency of 12.255 GHz. Available are the yearly lowest, highest and average of the 5-years measurements period (2000-2004) [61],[62].

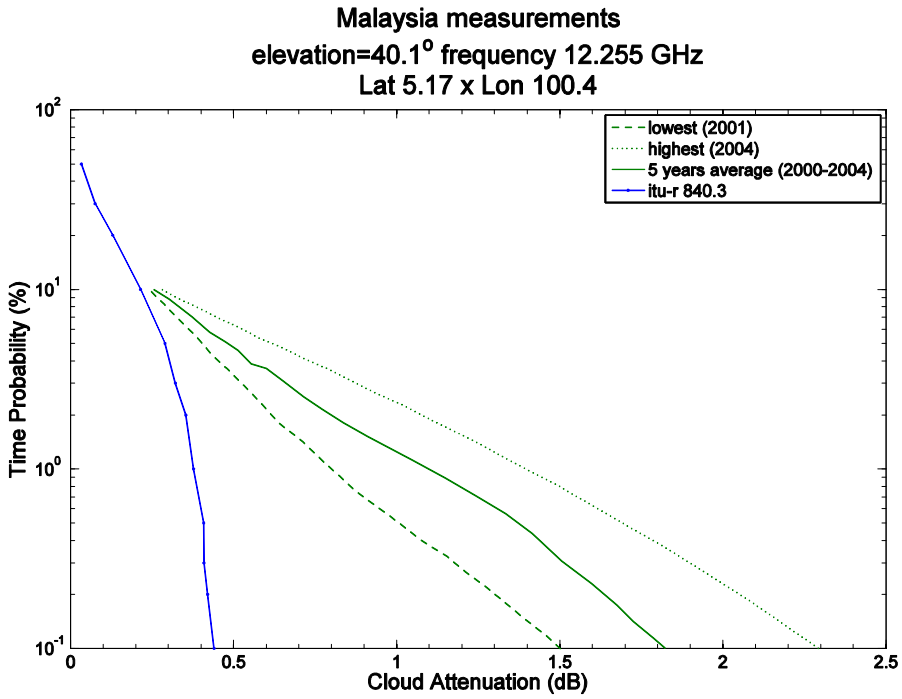

Figure 4.14 Cloud attenuation (Malaysia)

As expected, there is variability in the yearly cloud attenuation. The highest attenuation was recorded in 2004 while the lowest in 2001. For the start of the measurements curves at 10% of the time, year 2001 measurement had a value

of around 0.25 dB; year 2004 measurement had a value of 0.28 dB while the average (2000-2004) had a value of 0.26 dB. However, for 0.1% the values now are 1.5 dB, 2.3 dB and around 1.8 dB for the measurements of year 2001, 2004 and average (2000-2004), respectively. It is obvious that the itu-r 840.3 model heavily underestimates the cloud attenuation at this location; having for 10% and 0.1% of the time attenuation values of 0.21 dB and 0.44 dB, respectively.

The (5 years average) measurements curve will be the curve to utilize in this study.

4.1.3.2 India (New Delhi)

The location's coordinates is Lat 28.64 x Lon 77.27 having an elevation angle of 90^{o} (zenith) and an operating frequency of 19.4 GHz. The measurements of this location are for nearly 2 years (June 1988 to March 1990) [63].

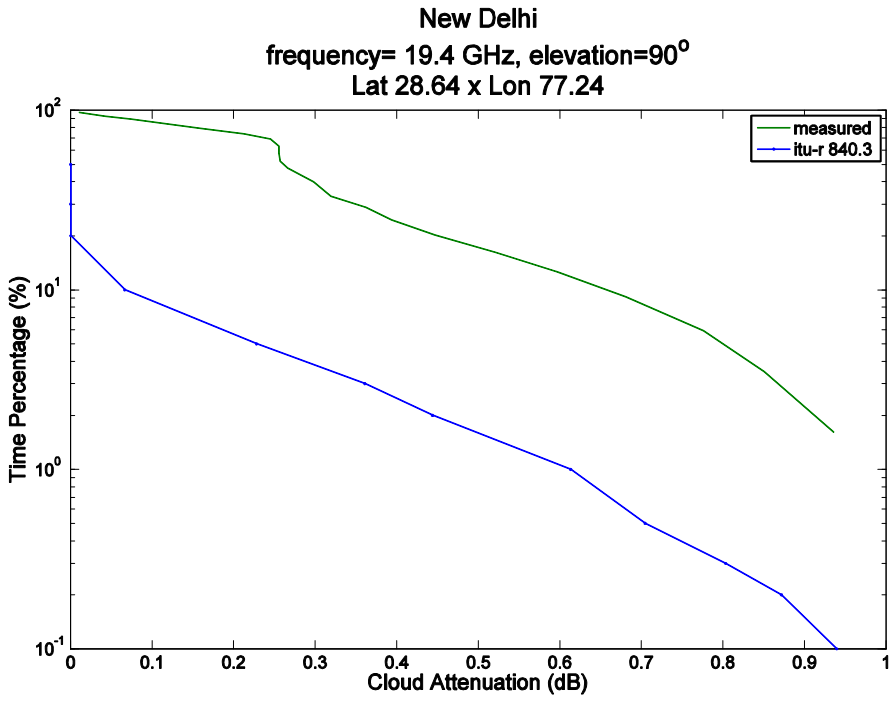

Figure 4.15 Cloud attenuation (New Delhi, India)

For about 10% and 1% of the time the available measured attenuation values were 0.66 dB and 0.94 dB, respectively. By contrast the itu-r 840.3 cloud attenuation model predicts for 10% and 1.6% (same as the measurements) values of 0.066 dB and 0.49 dB, respectively. Again, the itu-r 840.3 model underestimates the cloud attenuation.

4.1.3.3 Singapore

The location's coordinates is around Lat 1.32 x Lon 103.84 having an elevation angle of 80^{o} and an operating frequency of 20 GHz. The measurements of this location are for one year only [64].

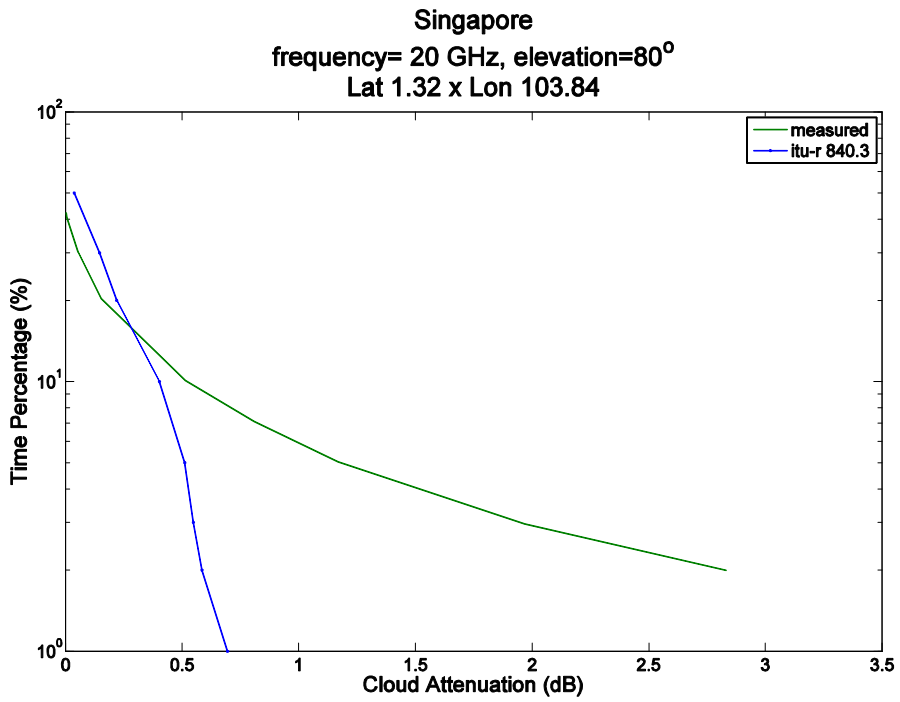

Figure 4.16 Cloud attenuation (Singapore)

Here we notice that the available measured attenuation at 10% and 2% were 0.52 dB and 2.83 dB, respectively. While for the itu-r 840.3 model for the same percentages, 10% and 2% the attenuation values were 0.40 dB and 0.59 dB, respectively. for this location the itu-r 840.3 model seems to overestimate for

higher time percentages (~17%) then severely underestimates the attenuation for lower time percentages (below 16%).

4.1.3.4 USA (New York)

The location's coordinates is around Lat 40.73 x Lon -74 having an elevation angle of 80^{o} and an operating frequency of 20 GHz. The measurements of this location are for one year only [64].

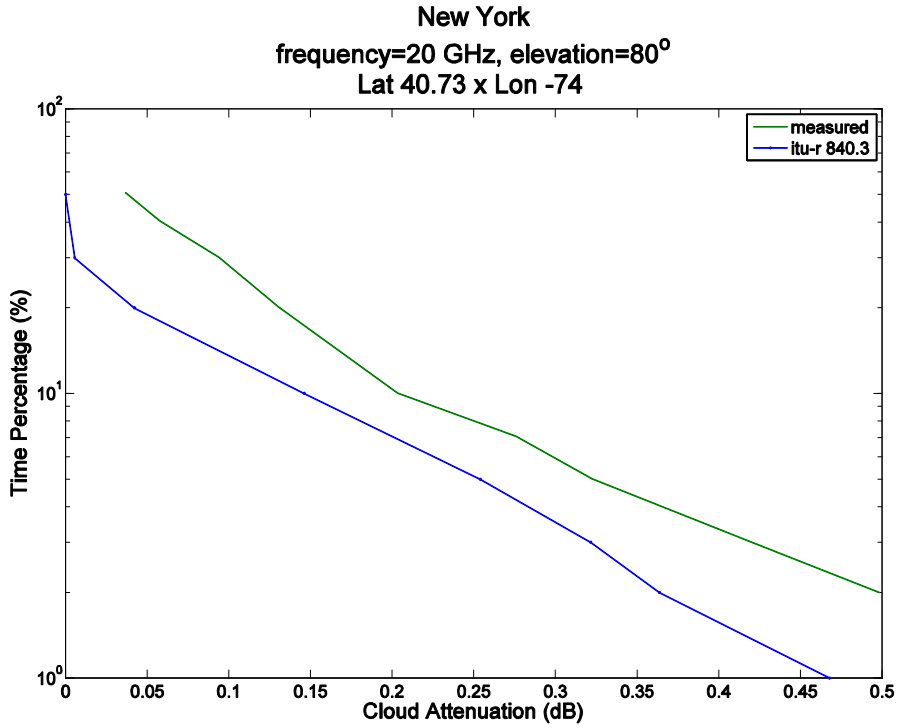

Figure 4.17 Cloud attenuation (New York, USA)

The cloud attenuation values for New York at both 10% and 2% are 0.20 dB and 0.50 dB, respectively. The itu-r 840.3 model slightly underestimates the attenuation on all time percentages. For the same probabilities of 10% and 2% the estimated attenuations are 0.15 dB and 0.36 dB, respectively.

4.1.3.5 India (Kolkata)

The location's coordinates is around Lat 22.57 x Lon 88.48 having an elevation angle of 90^{o} (zenith) and an operating frequency of 40 GHz. The measurements of this location are for one year (January-December 2005) and the monsoon season of the same year [65].

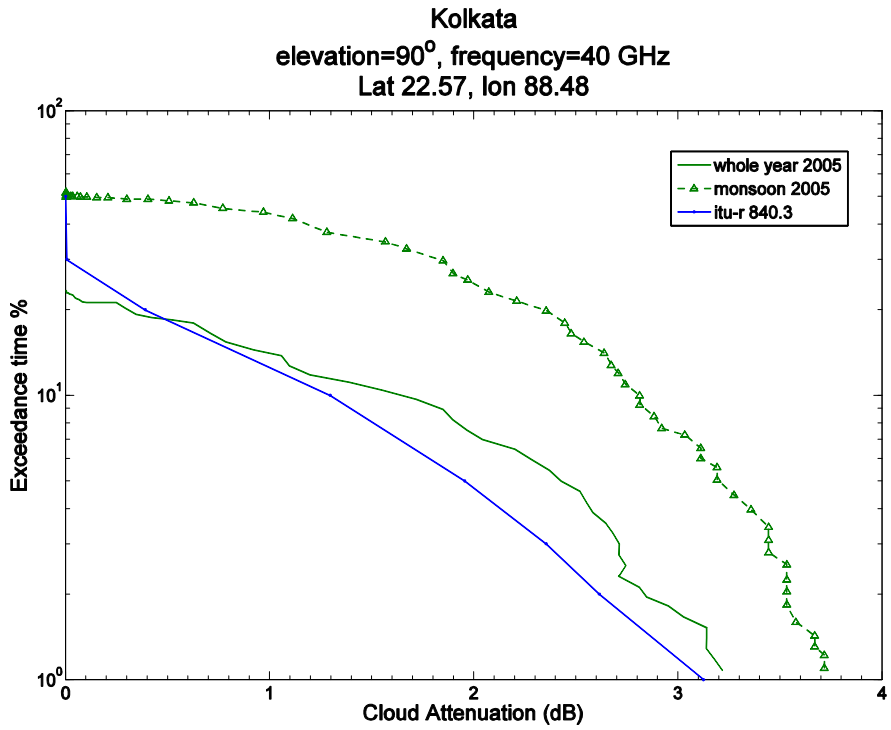

Figure 4.18 Cloud attenuation (Kolkata, India)

There is a big variability between the yearly cloud attenuation and the monsoon season's statistics. For 10% probability the attenuation values for both yearly and monsoon season were 1.62 dB and 2.80 dB, respectively. And for 1% probability they were 3.22 dB and 3.72 dB, respectively. As for the itu-r 840.3 model the attenuation values for the same percentages, 10% and 1% were 1.30 dB and 3.12 dB, respectively.

We will utilize the yearly measurement curve in this study. It looks like the itu-r 840.3 model over estimates the attenuation of the yearly cloud attenuation for

higher probability percentages (~18%) then underestimates the attenuation while following the shape of the attenuation curve.

4.1.3.6 Spain (Madrid)

The cloud attenuation statistics for a full year (2000) were measured in Madrid, Spain. The location coordinates are around Lat 40.42 x Lon -3.69 having an elevation angle of 40^{o} and an operational frequency of 50 GHz [36].

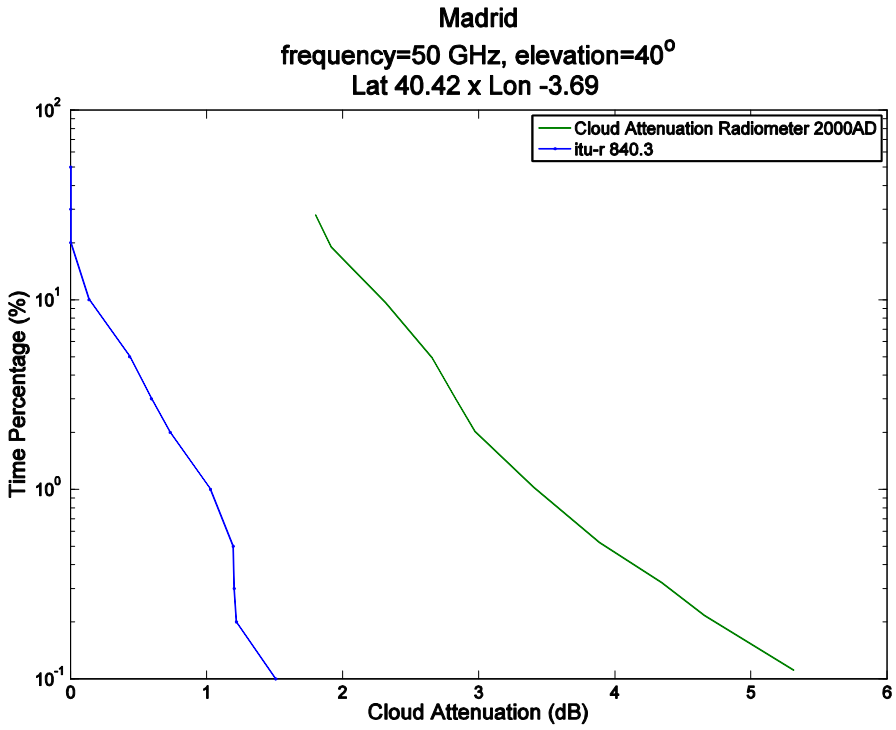

Figure 4.19 Cloud attenuation (Madrid, Spain)

The measured attenuation at probability percentages of 10%, 1% and 0.1% are 2.30 dB, 3.42 dB and 5.32 dB, respectively. The itu-r 840.3 model performs poorly on all probability percentages. For the 10%, 1% and 0.1% probabilities the corresponding attenuation values are 0.14 dB, 1.03 dB and 1.51 dB, respectively.

Although the itu-r 840.4 recommendation supersede the itu-r 840.3 one, it was not approved until December 2009. More so, the main difference between the two is the updating of the reduced Liquid water path maps by utilizing a newer source (ERA-40) and then calculating the probabilities. Hence, better data

sources are crucial in improving cloud attenuation modeling. In the (improved cloud attenuation model chapter) the itu-r 840.4 recommendation is included to show the influence of relaying on more accurate and statistically descriptive data sources (plus 40 years period) on cloud attenuation modeling; and demonstrates the usefulness of the effective temperature (discussed in detail in that chapter) in tweaking the existent itu-r 840.4 recommendation for frequencies above 43 GHz.

4.2 Surface and cloud Synoptic data

4.2.1 Surface parameters

The parameters of temperature, pressure, relative humidity and rain gauge associated with the ITALSAT experiment at Sparsholt were extracted from the raw files and the ECMWF ERA-INTERIM as described in chapter 3. The period of Apr1997-Mar1999 was processed on both daily and monthly bases. From the raw files the rain gauge parameter is used to identify the rainy periods and had a resolution of 0.1 Hertz (one reading every 10 seconds). While the other parameters namely the temperature, relative humidity and pressure had a resolution of 1 Hertz (one reading per second) from the raw files and from ERA-INTERIM were recorded once every 6-hours (4 times a day). The fidelity of the measurements was good and a few samples are shown in Table 4.2 through Table 4.7 for daily analysis and monthly analysis from both Sparsholt's raw data and ERA-INTERIM data set. Note that the ERA-INTERIM data set reported virtually no invalid measurements for the period of the study in this project.

As for the external sites' parameters, there were two sources to consider. Namely the Met-Office MIDAS data set and the ECMWF's ERA-INTERIM. After processing the data of the two sources and comparing their error (instances the parameter values were reported erroneous or non-existent) we were inclined to go with the ERA-INTERIM data set as can be seen by a sample comparison in Table 4.8 and Table 4.9.

Table 4.2 Pressure for May 1997 from Sparsholt's raw files (in hPa)*

Day	Max	Min	Average	Invalid (%)
1	1016.24	1010.89	1013.72	3.48
2	1013.38	1003.78	1009.49	0.02
3	1005.77	995.58	1000.42	0.02
4	997.34	978.44	987.24	0.02
5	980.57	970.39	974.81	0.02
6	989.50	975	982.90	0.02
7	989.21	983.57	986.96	0.02
8	986.43	975.81	981.03	0.02
9	990.38	976.90	984.24	0.02
10	990.53	983.20	986.55	0.02
11	996.17	984.81	988.70	0.02
12	1005.84	993.24	1000.06	0.02
13	1006.86	1001.88	1004.19	0.02
14	1008.84	1003.20	1006.45	0.94
15	1008.33	1000.93	1004.57	0.02
16	1002.25	996.31	998.96	0.02
17	998.22	993.46	996.20	0.02
18	996.61	993.53	995.11	0.02
19	995.58	988.55	991.03	0.02
20	990.89	985.62	987.59	0.02

21	999.61	987.01	994.02	0.02
22	1004.08	998.22	1001.35	0.02
23	1012.65	1002.03	1007.11	0.02
24	1017.92	1011.40	1014.47	0.02
25	1018.07	1014.48	1016.17	0.02
26	1015.94	1011.26	1013.41	0.02
27	1014.04	893.04	951.63	0.02
28	1015.21	903.66	954.05	0.02
29	1014.62	1011.11	1012.96	0.02
30	1014.48	1009.94	1012.25	0.02
31	1011.40	1007.01	1009.07	0.02

* hPa = milliBar

Table 4.3 Relative Humidity for March 1998 from Sparsholt's raw files (%)

Day	Max*	Min	Average	Invalid (%)
1	104.80	31.60	77.73	0.19
2	104.74	35.72	85.74	1.68
3	104.69	36.21	92.62	0.06
4	104.77	10.61	75.27	0.44
5	103.45	23.39	68.60	0.08
6	104.76	9.67	49.61	0.06
7	104.76	8.63	54.47	2.17

8	104.80	42.41	91.50	0.20
9	104.83	27.03	74.98	1.91
10	104.72	14.57	62.81	0.22
11	104.05	11.85	56.13	0.13
12	104.82	0.00	76.43	0.15
13	104.26	49.72	81.60	0.16
14	104.24	51.00	81.49	0.12
15	104.24	50.10	81.53	0.13
16	104.25	54.69	81.47	0.11
17	104.24	54.04	81.43	0.09
18	104.24	54.87	81.26	0.08
19	104.23	55.40	81.14	0.06
20	104.23	57.51	81.36	0.15
21	104.24	54.83	81.33	0.07
22	104.23	57.54	81.26	0.06
23	104.23	51.74	81.29	0.08
24	104.23	32.18	74.31	0.24
25	104.78	68.79	92.09	0.83
26	104.73	84.81	95.14	0.07
27	104.69	78.21	91.42	2.91
28	104.51	61.23	86.48	0.08
29	103.95	67.21	84.58	0.06

30	104.63	74.21	89.61	1.52
31	104.96	55.98	82.56	0.07

* Relative Humidity can reach above 100% (over saturation)

Table 4.4 Temperature for August 1998 from Sparsholt's raw files (in degrees Celsius)

Day	Max	Min	Average	Invalid (%)
1	21.04	10.39	14.23	0.06
2	19.28	10.39	14.85	0.06
3	17.13	11.17	14.53	3.22
4	21.04	12.44	16.54	0.06
5	24.26	10.49	17.05	0.06
6	25.04	8.34	16.03	0.06
7	27.29	12.44	18.63	0.06
8	28.85	10.59	19.97	0.06
9	26.50	14.00	20.37	0.06
10	29.14	12.54	20.55	0.06
11	28.26	12.83	20.10	0.06
12	21.62	11.86	16.47	0.06
13	20.16	10.10	15.30	0.06
14	24.16	12.34	17.39	0.06
15	21.43	12.34	16.74	0.06
16	22.60	9.51	15.97	0.06

17	21.82	11.66	16.73	0.34
18	21.72	11.07	16.07	0.06
19	23.48	9.02	16.14	0.06
20	20.06	10.68	15.61	0.14
21	21.33	11.95	16.82	0.06
22	19.28	10.29	14.48	0.06
23	18.79	8.73	13.80	0.06
24	18.69	10.20	14.71	0.06
25	21.13	6.97	14.32	0.14
26	18.40	8.34	14.24	0.06
27	19.36	5.61	12.79	0.06
28	19.77	7.95	13.62	0.06
29	21.13	7.75	14.93	0.06
30	21.82	9.80	15.59	0.06
31	20.84	11.17	16.07	0.06

Table 4.5 Rain gauge for April 1999 from Sparsholt's raw files (in millimeters)

Day	Max	Min	Average	Invalid (%)
1	0	0	0	5.30
2	0	0	0	0.07
3	5.76	0	0.00	0.07
4	4.32	0	0.00	0.07

5	1.44	0	0.00	0.07
6	5.76	0	0.00	0.07
7	0	0	0	0.07
8	0	0	0	0.07
9	188.48	0	0.03	4.45
10	7.19	0	0.01	0.07
11	8.63	0	0.16	0.07
12	18.70	0	0.16	1.41
13	10.07	0	0.07	0.07
14	0	0	0	0.07
15	20.14	0	0.10	0.07
16	2.88	0	0.00	0.07
17	0	0	0	0.07
18	23.02	0	0.12	0.07
19	2.88	0	0.05	0.07
20	18.70	0	1.04	0.07
21	86.33	0	0.35	0.07
22	61.87	0	0.16	0.07
23	11.51	0	0.49	0.07
24	1.44	0	0.00	0.07
25	2.88	0	0.06	0.07
26	40.29	0	0.15	0.07

27	1.44	0	0.00	0.07
28	0	0	0	0.07
29	0	0	0	0.07
30	0	0	0	2.07

Table 4.6 ERA-INTERIM Temperature (^{o} C) for Sparsholt (Lon 51 x Lat -1.5)

Averages Month\Year	**1997**	**1998**	**1999**	**3-Year Average**
January	2.5	5.9	6.8	5.1
February	7.3	7.0	5.8	6.7
March	8.6	8.4	7.6	8.2
April	9.1	8.0	9.6	8.9
May	12.0	14.0	13.4	13.1
June	14.6	14.6	14.6	14.6
July	17.0	15.9	18.1	17.0
August	19.1	16.6	16.9	17.5
September	14.7	15.2	16.1	15.3
October	10.9	11.4	11.1	11.1
November	9.1	6.8	8.3	8.1
December	6.5	6.6	5.8	6.3

Table 4.7 ERA-INTERIM Relative Humidity (%) for Sparsholt (Lon 51 x Lat -1.5)

Averages Month\Year	1997	1998	1999	3-Year Average
Jan	87.6	82.5	85.3	85.1
Feb	83.4	79.2	80.7	81.1
Mar	81.1	81.1	79.4	80.5
Apr	67.9	80.8	79.9	76.2
May	74.1	70.8	77.5	74.1
Jun	78.7	82.1	73.3	78.0
Jul	74.2	78.8	72.2	75.1
Aug	78.8	73.1	78.2	76.7
Sep	77.9	81.9	79.2	79.7
Oct	78.9	80.6	79.0	79.5
Nov	86.2	81.1	82.1	83.1
Dec	85.7	87.9	81.9	85.2

The values obtained from the ERA-INTERIM are virtually error-free. While the Met-Office MIDAS values are not as solid as we were expecting. In the sample tables below we see that from the study location of Malaysia in 1997 the temperature values were comparable between the two sources. Indeed, the difference of the temperatures recorded by these sources was less than 1.6^{O} C.

However, the maximum difference was 1.59^{O} C was in August which coincidently had a low reported error % by MIDAS of 1.6. As for the relative humidity parameter, we notice that the difference is as high as 20.36%. Again, this high difference was the result of a considerably low reported error % by MIDAS of 3.23. Thus after processing all the parameters for all the locations of study we were more confident with the ERA-INTERIM for the Analysis in this project.

Table 4.8 Monthly measurements Averages of the year 1997 at Malaysian study location (Temperature)

Year 1997	**ERA-INTERIM**		**MIDAS**		**Temp Diff**
Monthly Avg	**Temp (^{o}C)**	**Invalid %**	**Temp (^{o}C)**	**Invalid %**	**Temp (^{o}C)**
Jan	25.74	0.00	27.01	2.42	1.27
Feb	26.26	0.00	27.29	2.68	1.03
Mar	26.73	0.00	27.84	3.23	1.11
Apr	26.69	0.00	27.59	2.50	0.90
May	27.34	0.00	28.48	6.45	1.14
Jun	26.74	0.00	28.09	11.67	1.36
Jul	26.54	0.00	27.60	3.23	1.06
Aug	26.73	0.00	28.32	1.61	1.59
Sep	26.57	0.00	27.62	2.50	1.04
Oct	26.15	0.00	26.96	3.23	0.81
Nov	26.06	0.00	27.16	5.00	1.11
Dec	25.95	0.00	27.34	1.61	1.39

Table 4.9 **Monthly measurements Averages of the year 1997 at Malaysian study location (Relative Humidity)**

Year 1997	ERA-INTERIM		MIDAS		RH Diff
Monthly Avg	RH (%)	Invalid %	RH (%)	Invalid %	RH (%)
Jan	73.19	0.00	93.55	3.23	20.36
Feb	79.43	0.00	94.33	2.68	14.89
Mar	78.00	0.00	93.83	3.23	15.83
Apr	80.52	0.00	94.63	2.50	14.11
May	80.41	0.00	93.99	7.26	13.58
Jun	81.92	0.00	93.87	11.67	11.95
Jul	81.42	0.00	94.23	4.84	12.81
Aug	83.40	0.00	93.37	1.61	9.97
Sep	83.21	0.00	94.72	2.50	11.51
Oct	87.02	0.00	95.38	3.23	8.36
Nov	87.85	0.00	95.63	5.00	7.79
Dec	85.42	0.00	94.90	1.61	9.48

After compiling the data and relating the parameters with the local cloud attenuation at Sparsholt for frequencies of 20, 40 and 50 GHz the connection between the surface parameters and cloud attenuation was found to be weak. The analysis was made on a per second and on a per minute (Average and Median) bases. The analysis spanned April 1997- March 1999 for both daily and monthly cloud attenuation. See samples Figure 4.20 to Figure 4.29.

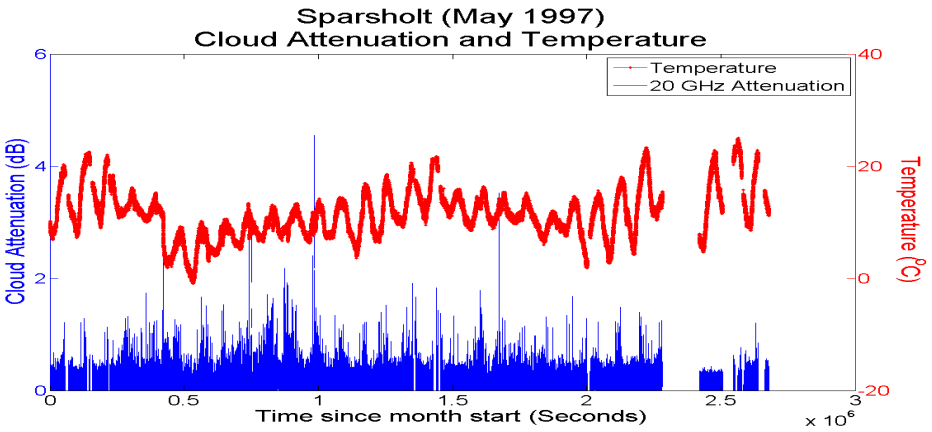

Figure 4.20 Sample analysis of temperature for May 1997 (Sparsholt, 20 GHz)

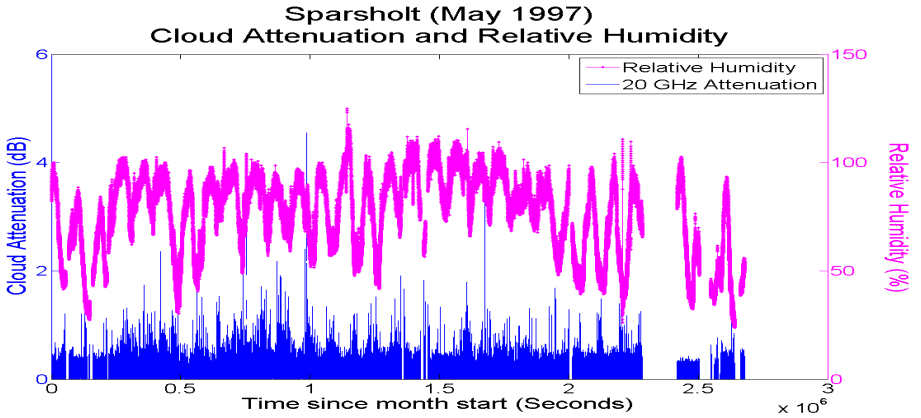

Figure 4.21 Sample analysis of relative humidity for May 1997 (Sparsholt, 20 GHz)

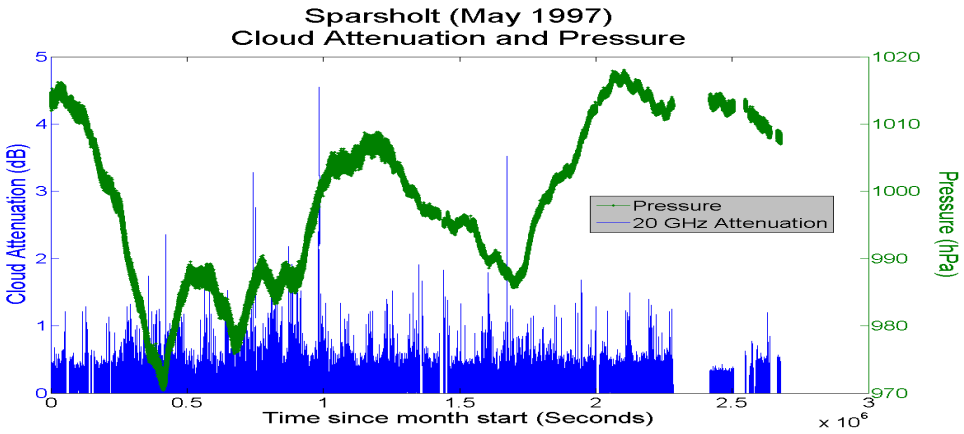

Figure 4.22 Sample analysis of Pressure for May 1997 (Sparsholt, 20 GHz)

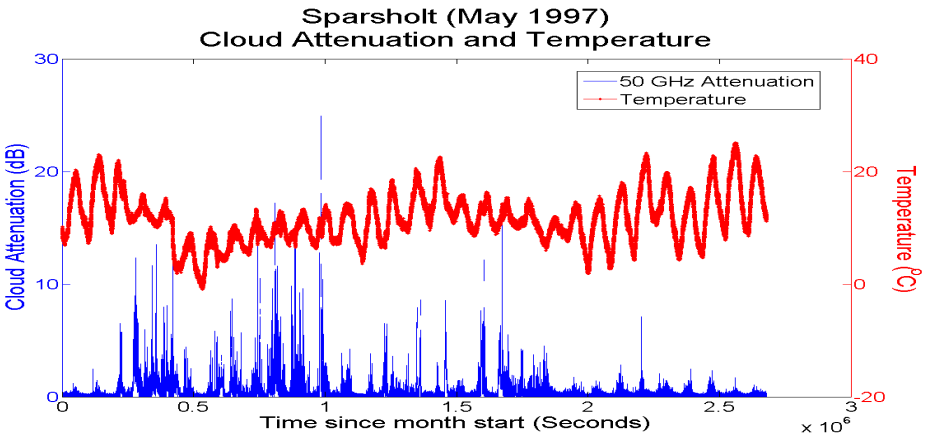

Figure 4.23 Sample analysis of temperature for May 1997 (Sparsholt, 50 GHz)

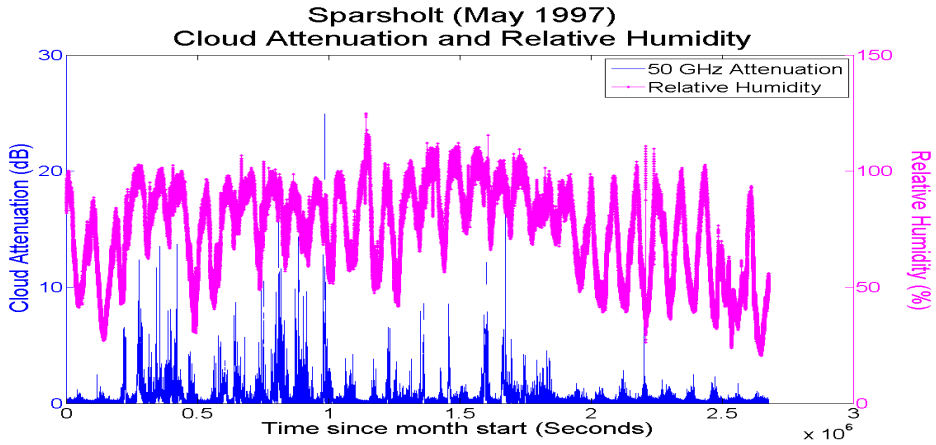

Figure 4.24 Sample analysis of relative humidity for May 1997 (Sparsholt, 50 GHz)

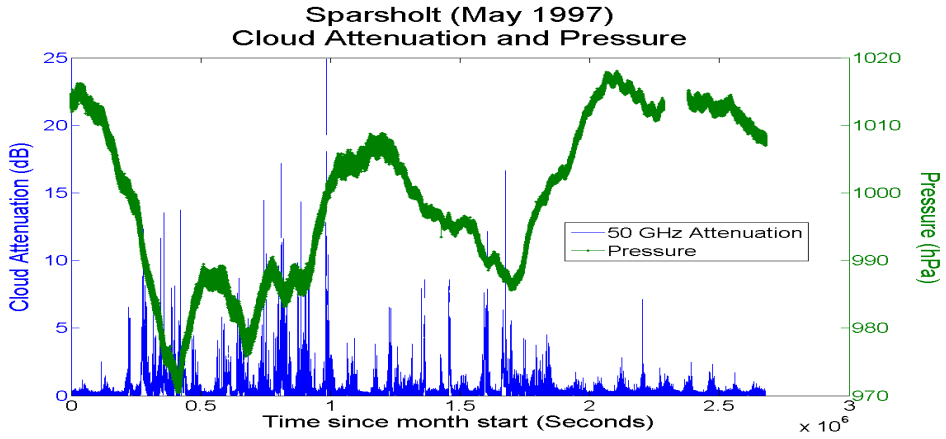

Figure 4.25 Sample analysis of Pressure for May 1997 (Sparsholt, 50 GHz)

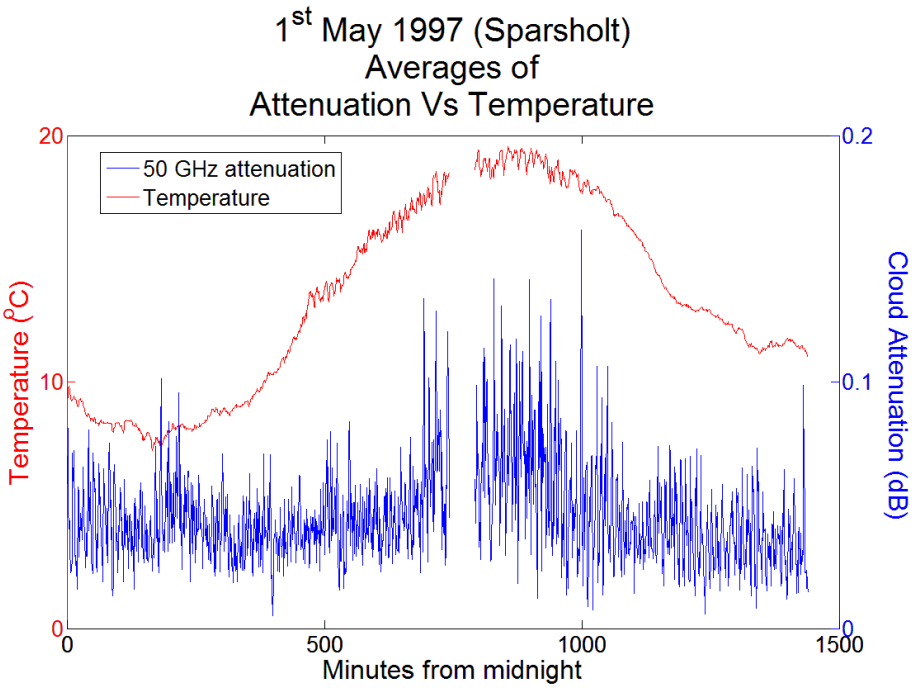

Figure 4.26 Sample analysis of temperature averages for May 1997 (Sparsholt, 50 GHz)

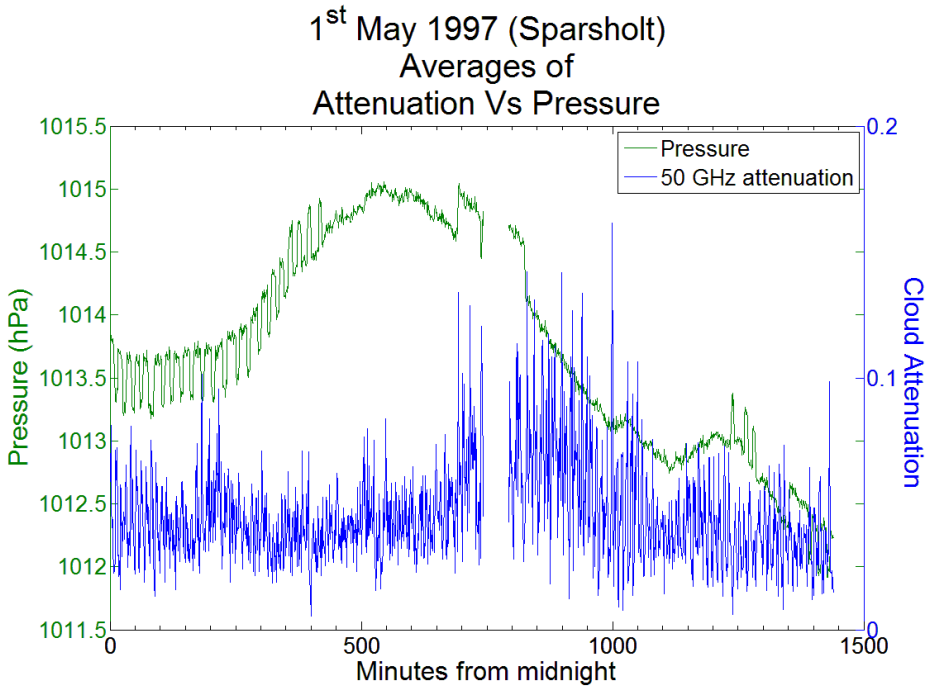

Figure 4.27 Sample analysis of pressure averages for May 1997 (Sparsholt, 50 GHz)

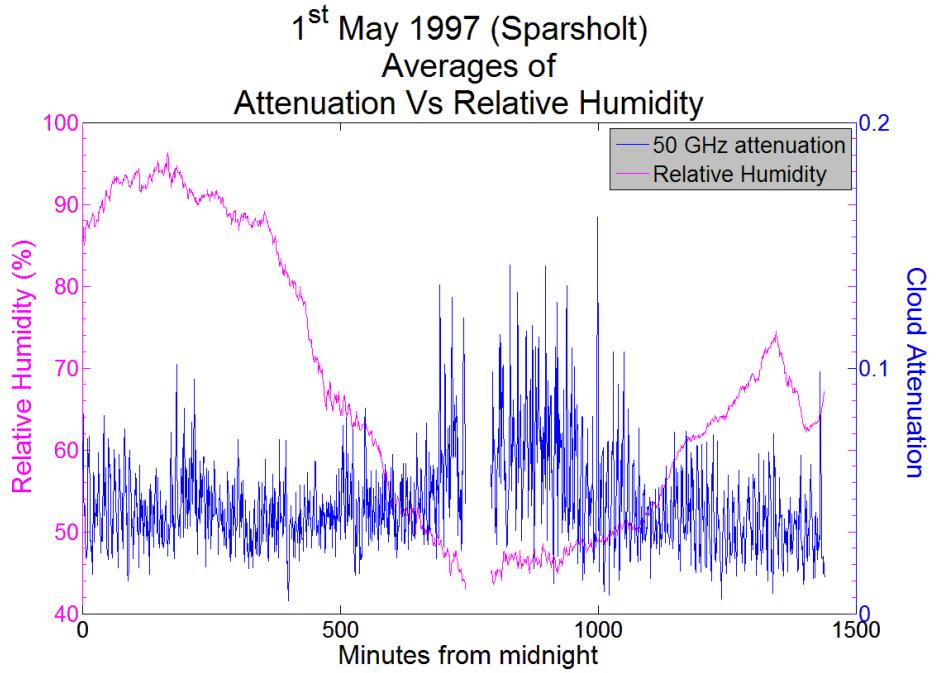

Figure 4.28 Sample analysis of relative humidity averages for May 1997 (Sparsholt, 50 GHz)

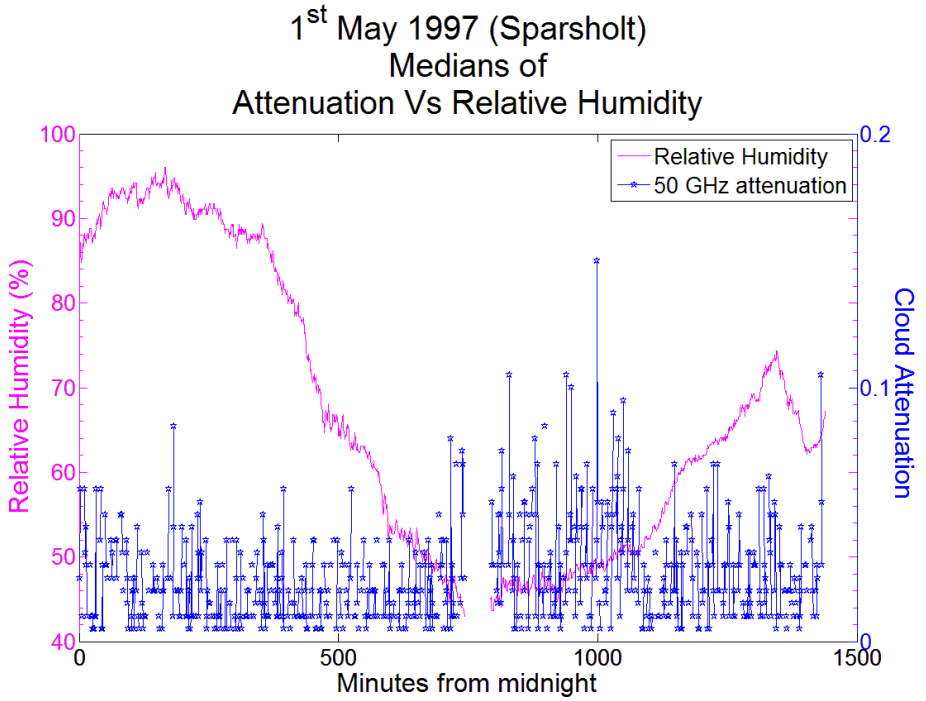

Figure 4.29 Sample analysis of relative humidity median for May1997 (Sparsholt, 50 GHz)

None of the parameters at hand had strong correlation with cloud attenuation. It seems that conditions at the surface do not strongly reflect the type or attributes of clouds in the atmosphere. Sharp pressure changes were found to indicate an alteration in the cloud attenuation intensity however no concrete correlation could be asserted.

Our aim was to see if we could make a connection between the various surface parameters with cloud presence similar to what was done by [30]. However, the results agree with the observations done by [36] and others for models depending on pressure, temperature and relative humidity at the surface. Thus relying on surface parameters for accurate cloud attenuation prediction at high frequencies is discouraged.

4.2.2 Cloud data

One of this project's aims was to correlate the effect of low altitude, water containing clouds (Cu, Cb, Ns and St/Sc) on signal attenuation. In order to do so, knowledge about the statistics of these clouds for an extensive period of time was required. Cloud data used were acquired from the Met Office [53] – MIDAS Land Surface Observation Stations data which contain synoptic (hourly) weather observations as mentioned earlier. The U.K. ground station Brize-Norton (51.75° N, 1.58° W) which is 12.7 miles was selected being the nearest station to Sparsholt where the ITALSAT receivers were operating. The synoptic data of Brize-Norton station for a 7-years cycle spanning 1994 to 2000 have been compiled.

We had to figure out which type of identifier we would use; there were two parameters to identify the presence of clouds, namely LCT (Low Cloud Type) with TCA (Total Cloud Amount) and CT1→CT4 (Cloud Type of up to 4 layers detection) with corresponding CA1→CA4 (Cloud Amount). LCT method was easy to acquire and process however it was inaccurate in detecting targeted cloud types. CT method acquisition was much more involving yet it had the advantage of identifying the specific cloud type occurrence and amount covering the sky. So we did a side by side analysis utilizing both methods and from the results we finally made the choice of carrying on with the CT-CA

method, See Figure 4.30 to Figure 4.32. (Appendix C contains TCA, LCT, CT and CA flag values as utilized in the synoptic data reports while Appendix D contains error bars of all 7-years).

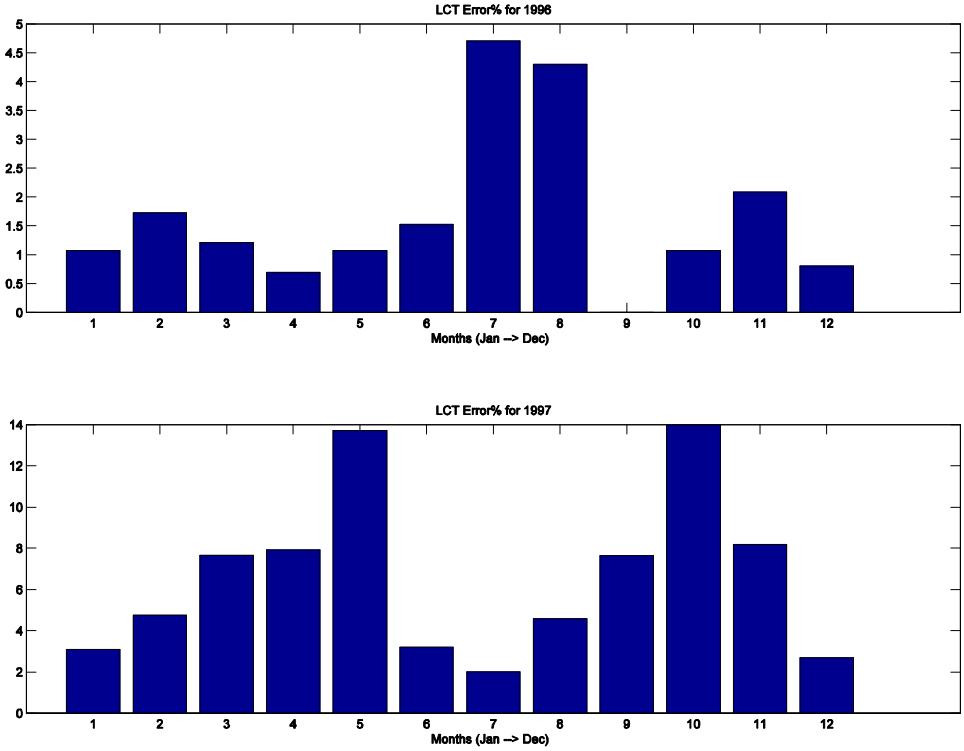

Figure 4.30 Sample LCT monthly invalid data (error)

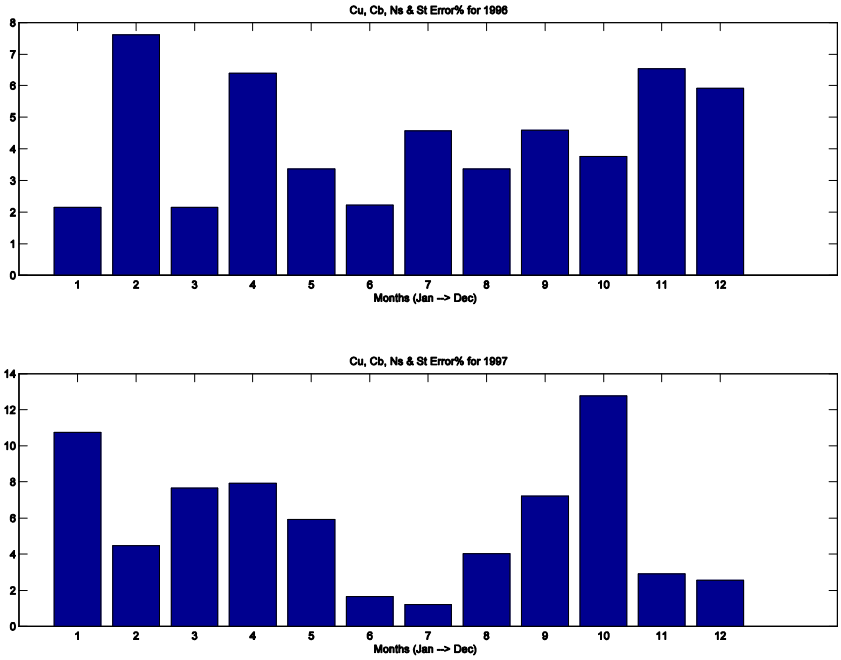

Figure 4.31 Sample CT and CA monthly invalid data (error)

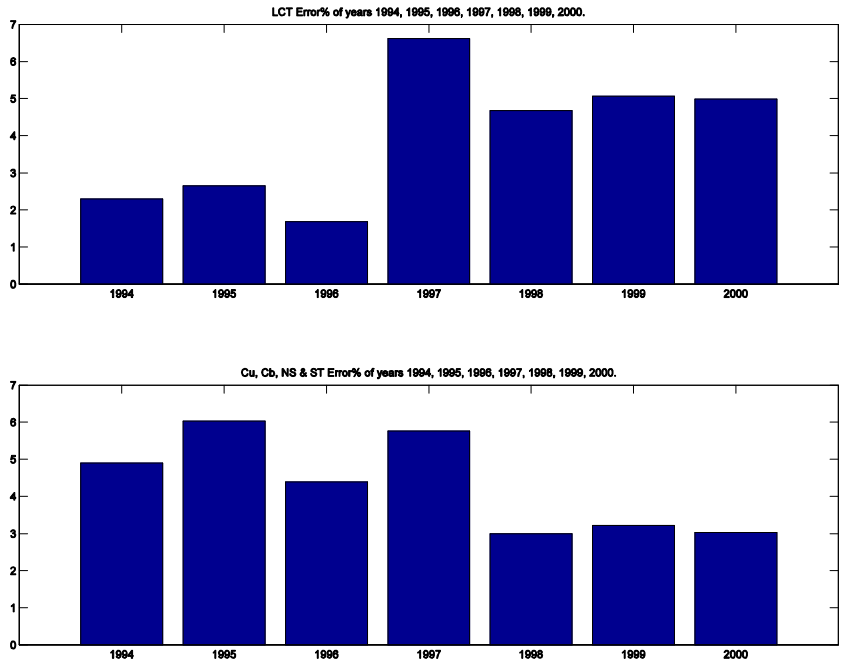

Figure 4.32 Overall invalid data (error) of each year for LCT and CT-CA methods

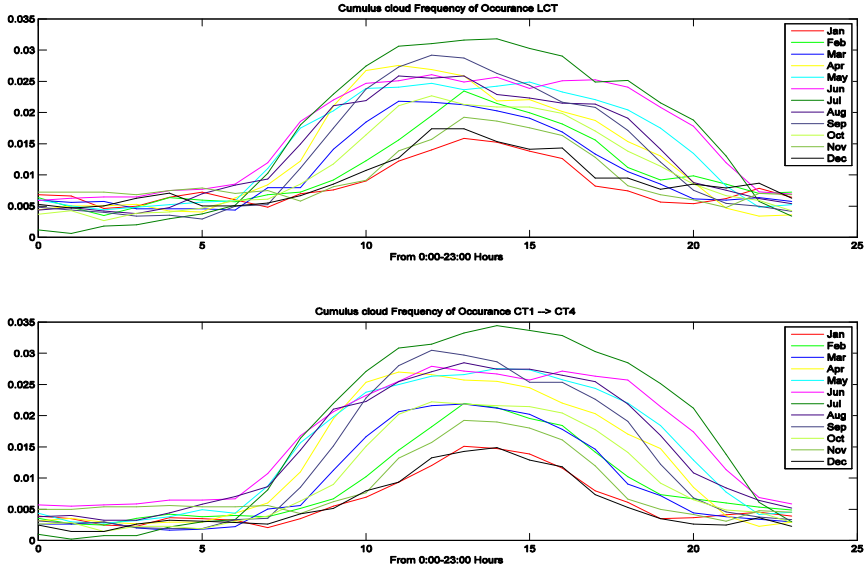

Figure 4.33 Comparison of diurnal freq. of occurrence for Cu cloud type, average of period 1994-2000

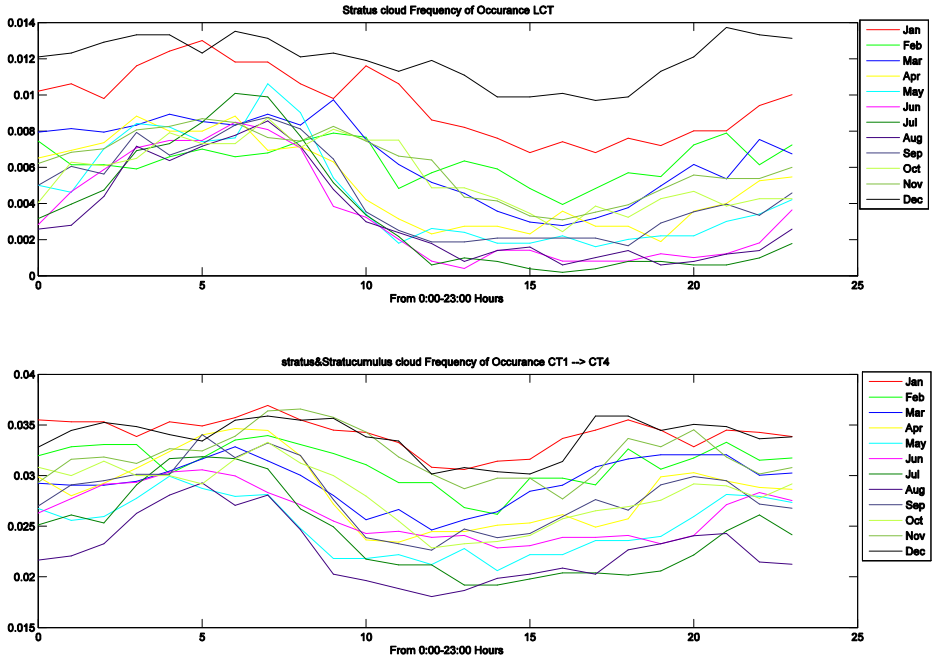

Figure 4.34 Comparison of diurnal freq. of occurrence for St/Sc cloud types, average of period 1994-2000

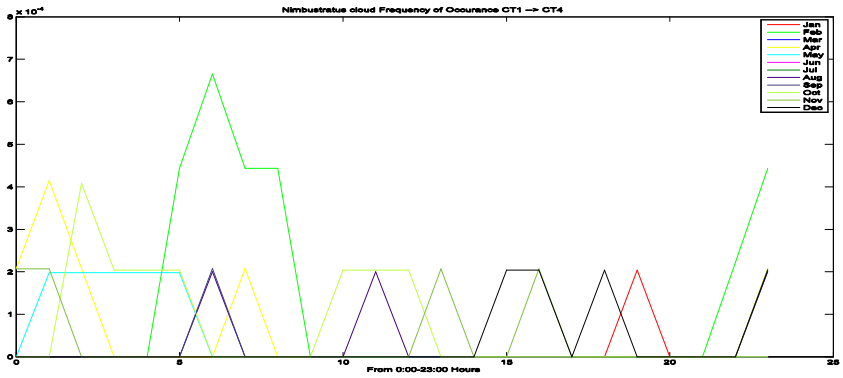

Figure 4.35 Diurnal freq. of Occurrence of Ns cloud type, average of period 1994-2000

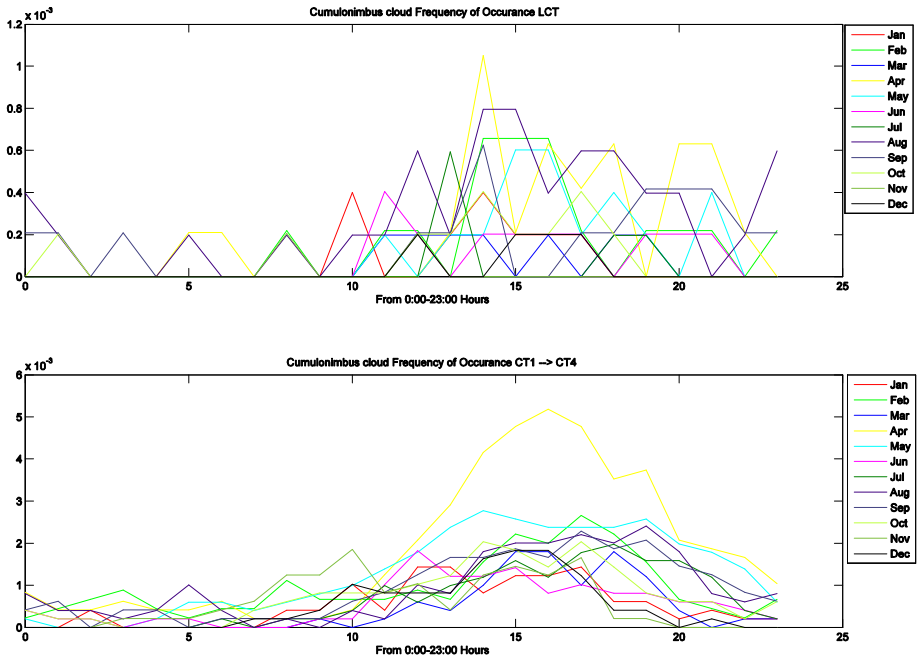

Figure 4.36 Comparison of diurnal freq. of occurrence for Cb cloud, average of period 1994-2000

The diurnal analysis of frequency of occurrence of cumulus cloud type (Figure 4.33) shows that high occurrence is between around 10:00 and 18:00 hours. St/Sc analysis was inconclusive (Figure 4.34) although we can to some extent assert that during 12:00 to 16:00 the occurrence tends to be the lowest for any given month. This is in accordance with the understanding of St/Sc cloud formation process which states that St/Sc clouds are dispersed by day-time sunshine heating the ground (unstable) causing St/Sc clouds to evaporate. This is in essence the opposite of Cu cloud formation and dispersion. As for the cumulonimbus analysis (Figure 4.36), the CT-CA method makes a clearer depiction of the frequency of occurrence and suggests that the high occurrence is somewhat between 13:00 and 19:00 hours. However, for Ns (Figure 4.35) only the CT-CA method had information on this cloud type and it seems that this cloud genre was virtually none existent.

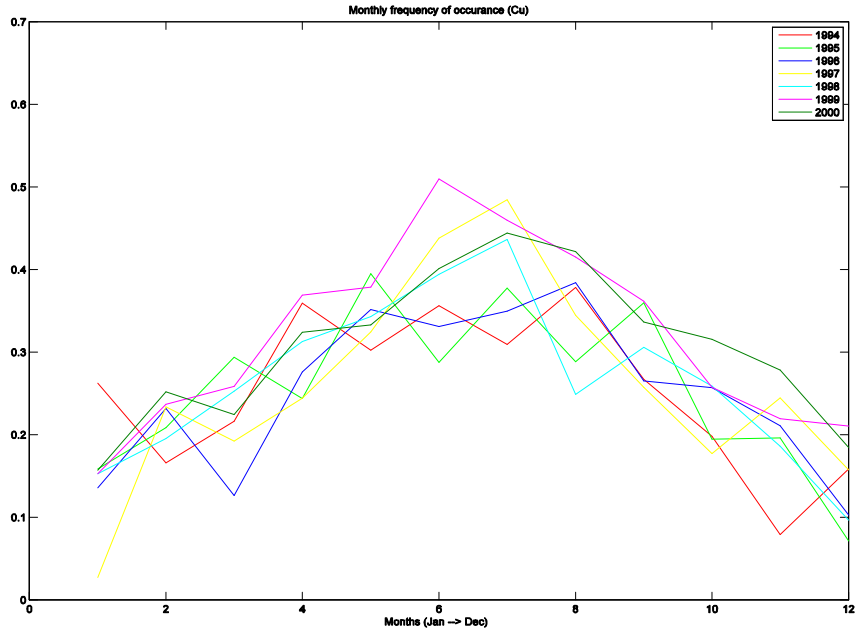

Figure 4.37 Frequency of occurrence of Cu cloud type

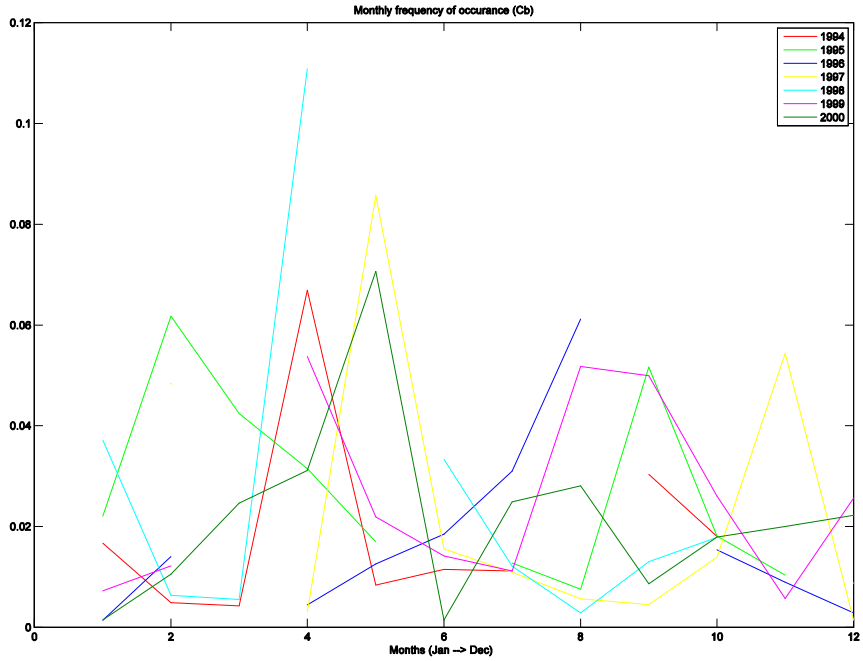

Figure 4.38 Frequency of occurrence of Cb cloud type

From the sample monthly frequency of occurrence of the high water content bearing clouds for Cu and Cb cloud types (Figure 4.37 and Figure 4.38) we notice that Cu clouds had high occurrence rate during the end of spring through the summer season until the start of autumn. While the Cb clouds had high occurrences in somewhat different periods per given year. The month with the highest occurrence rate of Cb clouds would fall between February and May.

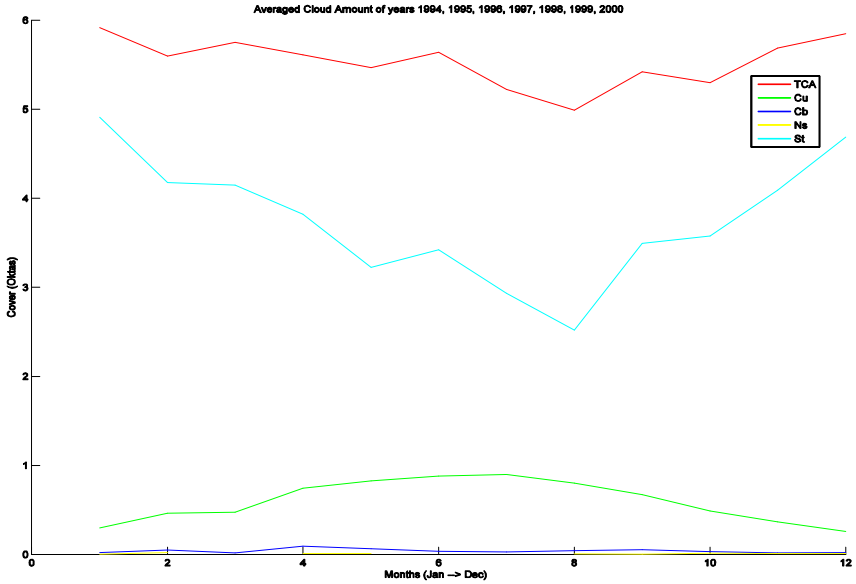

Figure 4.39 TCA and CA of Cu, Cb, Ns and St/Sc

After the processing of the 7-year period of cloud synoptic data the cloud amount and total cloud amount based on the CT-CA method was calculated. As seen from Figure 4.39 when the clouds are covering the sky at the site, the total amount is in general between 5 to 6 Oktas (8 Oktas is full cloud cover while 0 is clear sky). Out of the 4 cloud types investigated in this analysis the most dominant (sky-covering) was the St/Sc cloud type. The second cloud type covering the sky was the Cu. It is noted that the remaining two cloud types cover impact is indeed rare. The diurnal frequency of occurrence analysis suggests the higher occurrences are for the St/Sc and Cu types as well. Thus, this leads to the conclusion of the liquid water path for the Sparsholt site being the result of both the St/Sc and Cu cloud types.

We were expecting to perform the same analysis done on the Sparsholt (Brize-Norton) site on the other sites utilized in this project. However, this was not to be carried out due to two main reasons:

- Available weather stations in MIDAS data were far away from the coordinates of the receivers' locations

- The cloud data availability and resolution were insufficient to perform the anticipated analysis (mixed resolutions of 3-6 hour measurements, non-recorded and erroneous readings were more than 20%)

Thus, by referring to [37] it is found that the dynamics of clouds differ considerably from one location to the next. If we look at the DAH-model we notice that it fails at both higher operational frequencies (upper-limit of application by the model authors of 35 GHz) and accuracy of model at lower time percentages [36]. Hence, it is more viable to try and seek another venue of improving the estimation of cloud attenuation.

4.3 Local Tropospheric degradation analysis

4.3.1 Introduction

A thorough investigation was conducted on the various available data (both synoptic and attenuation) for an entire year spanning Apr1997-Mar1998. This is the only period where the 20 GHz data were available as mentioned earlier. Hence, this will give us a true comparison of the 3 frequencies of study.

The following tropospheric factors were investigated: gaseous, rain and cloud attenuation along with Scintillation. Attenuation comparisons were made mostly against the ITU-R related models. It is worth mentioning that none of the external cloud attenuation measurements used in this thesis (see section 4.1.3 above) had the attenuation treated for scintillation effects thus making our own (scintillation-treated) cloud attenuation measurements the most realistic in terms of approximating true cloud attenuation effects.

4.3.2 Data processing

As indicated earlier, the time resolution of the MIDAS data base is one hour, that is to say observations are made on the hour for every hour starting from midnight local time. The data of interest consisted of low-cloud type and low cloud-amount (see section 4.2.2). The low cloud amount is measured in eighths having a range from 0 (no cloud) to 8 (complete cover of sky). The synoptic data values recorded at Brize-Norton weather station were available for 95% of the time. The missing or errors in the data were less than 5%.

Attenuation data are validated by the status flags (Table 4.10) of the zero-dB data. Correct readings are labeled based on status flag 1 and status flag 3. Flag 1: status is for confirming that the registered attenuation by the equipment is error-free. Flag 3: status is to indicate that data has been interpolated from valid data at another frequency due to the loss of lock of the beacon signal.

Scintillations were extracted from Excess attenuation by applying a 6th order Butterworth high pass filter (HPF) with cut-off frequency of 0.04 Hz [66].

The rain attenuation is acquired by including the Excess attenuation values at corresponding positive rain-gauge readings after being filtered with a low pass Butterworth filter (LPF) to exclude scintillation. Figure 4.40 is a sample of data showing the severity of rain attenuation on the signal.

Gaseous attenuation was calculated simply by subtracting the Excess attenuation from the Total attenuation (see section 3.3.2).

Table 4.10 Status flag values of ITALSAT time series.

Status flag	Description
0	data is not valid
1	data is valid
2	attenuation is not genuine but the data is valid
3	Loss of lock at this frequency. Data has been interpolated from valid data at another frequency.
5	Loss of lock at this frequency and it was not possible to interpolate from another frequency.

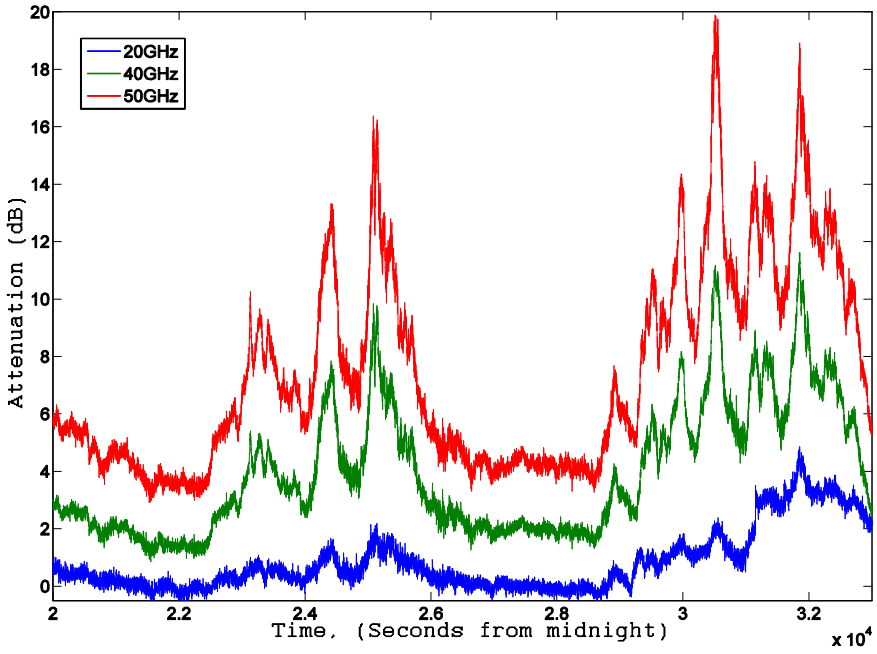

Figure 4.40 Comparative levels of total attenuation during a showery rain event (June 26th, 1997 at Sparsholt, U.K)

Cloud attenuation (section 4.3.7) is obtained applying the same steps as rain attenuation but now excluding the rainy periods based on rain-gauge measurements. There is a drawback of this method not being completely accurate due to factors such as wind conditions and rain drops not reaching the ground (Virga: re-evaporating in midair), the percentage of these events actually occurring is both low and has very little effect when tackling rain attenuation here in the U.K. The rain guard concept is introduced, it is based on actually guarding the immediate rainy periods before and after by a fixed interval and treating them as rain in order to try and only deal with pure cloud attenuation.

However, it is worth mentioning that when comparing with the external sites measurements (chapter 6) we are not using this guard concept, since it is not possible to implement it on the other (external) measurements.

4.3.3 Meteorological parameters

Basic statistics of collected meteorological parameters are presented in Table 4.11 where visual inspection of all meteorological measurements at Sparsholt was carried out. It can be seen that the highest Average temperature was as expected recorded in August whilst the lowest average recorded in January. More so for Sparsholt the maximum averages for both relative humidity and pressure were in November and February, respectively. Minimum averages of relative humidity and pressure were recorded in February and November.

Diurnal variation of low-type clouds is displayed in Figure 4.41 to Figure 4.43. These variations are collected over an interval of one year (Apr1997-Mar1998) rather than the diurnal averages calculated over 7-years in section 4.2.2. From the analysis of Frequency of Occurrence (FO) of cumulus (Cu) clouds we notice that the highest FO is between around 10:00 and 18:00 hours. More so, the peak is during the months of June, July and August (summer time). As for the cumulonimbus (Cb) clouds analysis, high FO values are not that distinct however they generally take place between 8:30 and 19:30 hours. More so, stratus and stratocumulus (St/Sc) tend to have low FO during 11:00 to 19:00 hours.

Table 4.11 Acquired meteorological parameters from Sparsholt

Month	Avg Temperature (C)		Avg Relative Humidity (%)		Avg Pressure (hPa)			Local Raingauge (mm/hour)	
	Sparsholt	Brize-Norton	Sparsholt	Brize-Norton	Sparsholt	MSLP*	Brize-Norton	Avg	Max
Apr-97	9.0	9.17	68.1	83.2	1005.2	1013.95	1002.82	3.34217	15.8
May-97	11.6	11.5	75.2	80.6	995.7	1024.12	994.544	3.21611	97.8
Jun-97	13.7	14.2	80.3	80.1	994.2	1021.62	989.771	2.30729	136.7
Jul-97	16.4	17	75.8	68.4	1004.0	1022.93	999.047	3.29323	67.6
Aug-97	18.5	19.1	81.2	76	1000.7	1014.32	995.906	2.95619	83.5
Sep-97	14.5	14.3	79.9	77.8	1006.7	1009.27	1002.06	2.08169	165.5
Oct-97	10.5	9.9	80.5	72.1	1002.3	1018.54	997.673	2.81284	84.9
Nov-97	8.5	8.12	89.9	76.6	987.7	1015.19	982.799	2.81793	164.0
Dec-97	5.9	5.78	89.0	77	995.8	1021.79	990.823	2.29758	12.9
Jan-98	5.2	5.15	82.0	81.2	1002.6	1017.62	993.738	1.70415	145.3
Feb-98	6.8	6.9	50.9	90.8	1009.5	1002.58	1003.83	2.99475	18.7
Mar-98	8.0	8.02	79.3	88	1006.8	1010.93	1001.46	3.58853	105.0

* mean sea level pressure

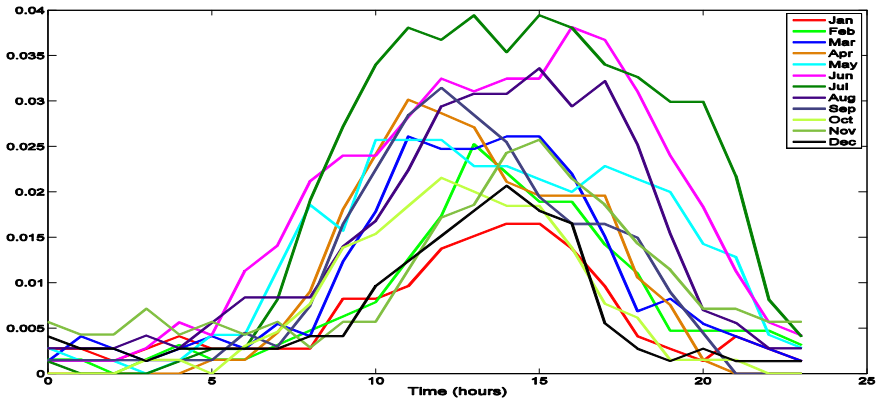

Figure 4.41 Cumulus cloud-type Frequency of Occurrence (Apr97-Mar98)

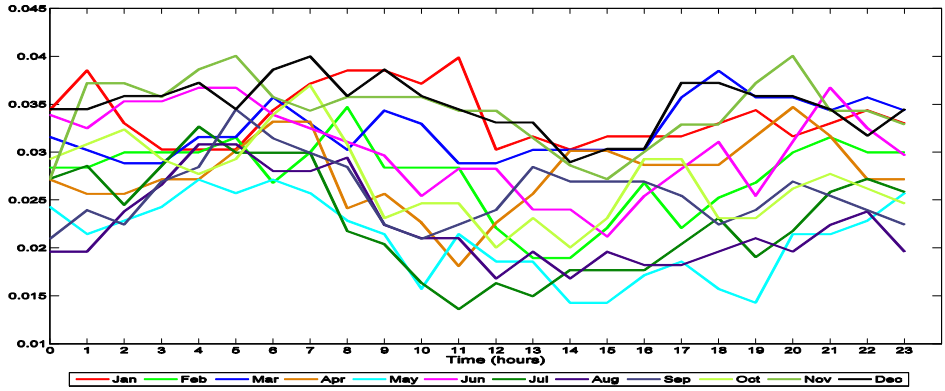

Figure 4.42 Stratus/Stratocumulus cloud-type Frequency of Occurrence (Apr97-Mar98)

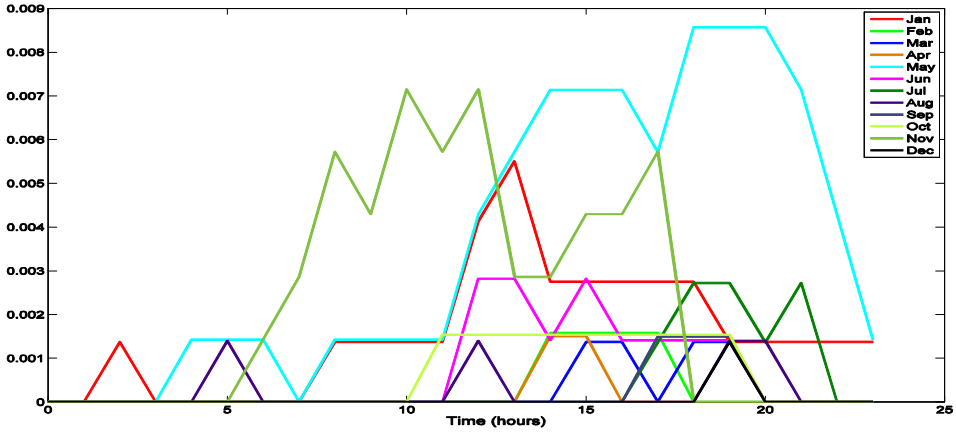

Figure 4.43 Cumulonimbus cloud-type Frequency of Occurrence (Apr97-Mar98)

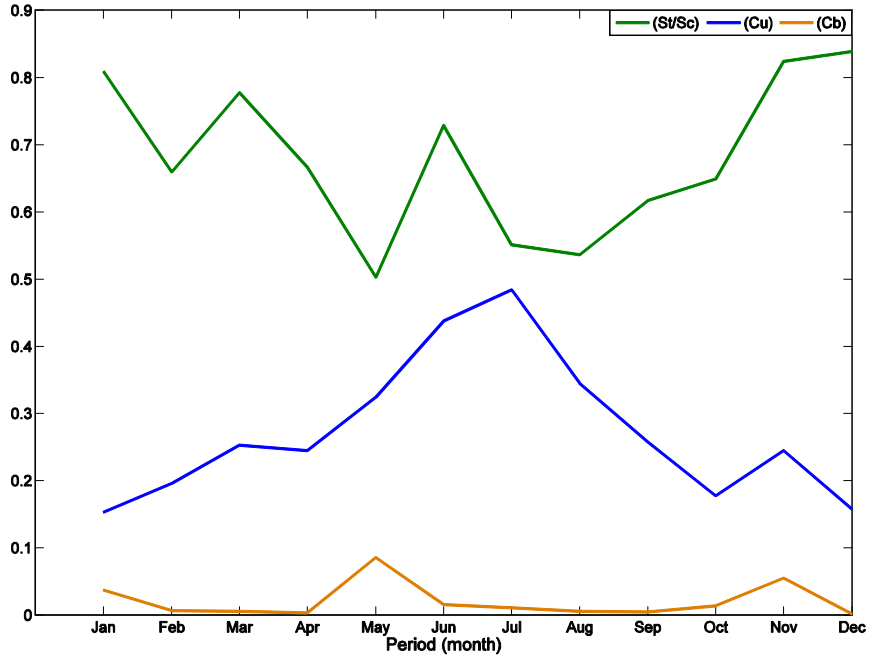

Figure 4.44 Monthly Frequency of Occurrence (Apr97-Mar98)

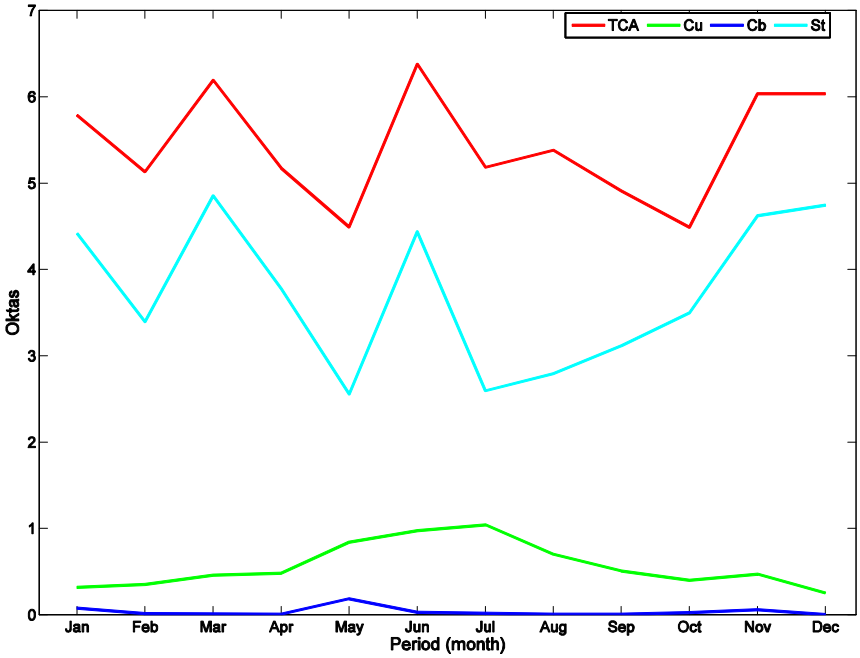

Figure 4.45 Averaged cloud cover (Apr97-Mar98)

From both the monthly average cloud amount and FO figures (Figure 4.44 and Figure 4.45) it is clear that St/Sc clouds are the highest occurring cloud-type in the region. We also note the total amount of cloud cover consist mainly of St/Sc then Cu and finally Cb (Ns is virtually non-existent). The percentage of any of the Cu, Cb, St/Sc and Ns clouds being present in the sky was 80.05% for the period of April 1997-March 1998.

4.3.4 Gaseous attenuation

In the case of gaseous attenuation the variation of attenuation per time percentage is negligible. The difference between the 99% and 1% probabilities at 20 GHz the attenuation was about 0.4 dB. It follows that at 40 GHz the attenuation difference was around 0.51 dB. The highest attenuation difference was at 50 GHz with a value of 0.63 dB.

Gaseous attenuation increases with frequency and so does its variation. For the lower frequency of 20 GHz the attenuation for 0.1% of the time was less than 0.6 dB. Moving towards the higher frequency of 40 GHz at the same probability the attenuation was about 1.1 dB. However at 50 GHz it reached above 3 dB (0.1% of the time). This indicates that the higher the operational frequency the higher the inherent attenuation is on the link. It is expected that the maximum attenuation difference would keep rising when moving towards higher frequencies especially above 70 GHz when the nitrogen absorption starts to contribute to the link attenuation as well.

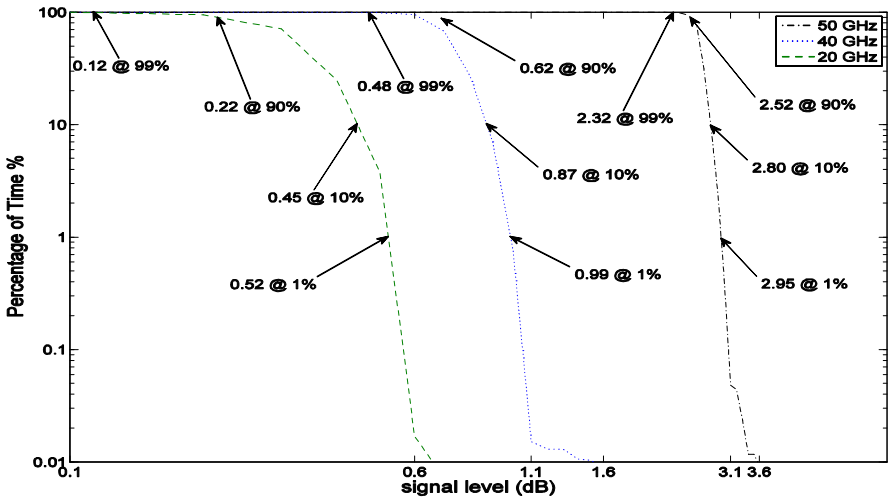

Figure 4.46 Gaseous Attenuation cdf (April 1997-March 1998)

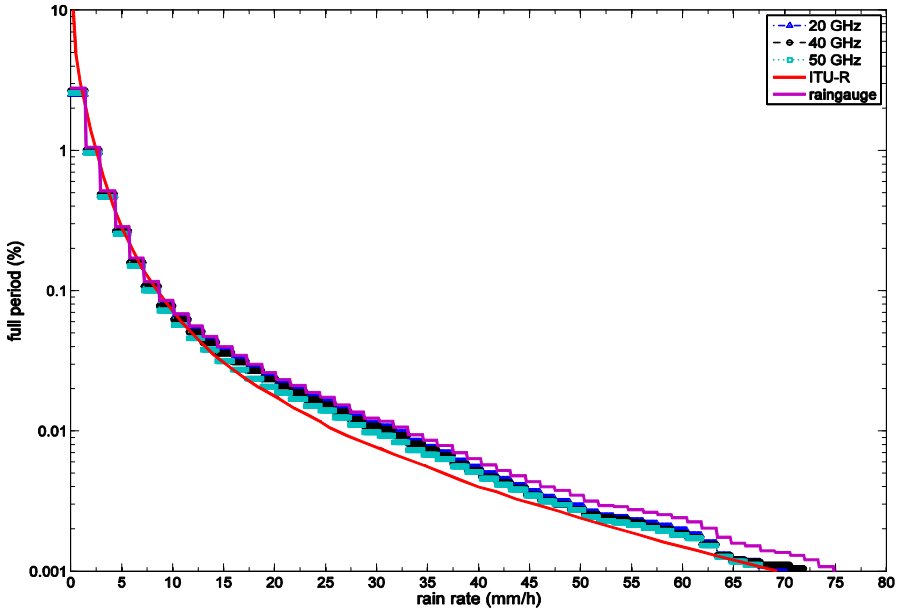

Figure 4.47 Rain-fall rate cdf (April 1997-March 1998)

4.3.5 Rain attenuation

Rain-fall data was obtained from the on-site rain gauge sensor. Rigorous visual inspection of the rain-gauge data was needed since the equipment occasionally malfunctioned and the data files would at times have spikes or no data. In Figure 4.47 the ITU-R estimation is plotted against rain-gauge readings along with specific operational frequency conditions (status flags in effect) for 20, 40 and 50 GHz. The 20 GHz rain-gauge (with status flags readings) was closest to the (rain-gauge only) rain-gauge measurements while the 50 GHz rain-fall rate was the closest to the itu-r curve (high volume of invalid readings compared to the rest during rainy events). Rain attenuation associated with the 20, 40 50 GHz is compared with the ITU-R 618-6 model for Sparsholt site in Figure 4.48. Here the ITU-R 618-6 rain model was good at approximating the attenuation in general. Measured rain attenuation followed the ITU-R curve at the 20 GHz but then started to diverge at higher frequencies. The year's rainy periods did not exceed 3%. The attenuation magnitude increases with frequency (as expected) and can reach about 34 dB and 48 dB (0.01% time) for 40 GHz and 50 GHz links, respectively.

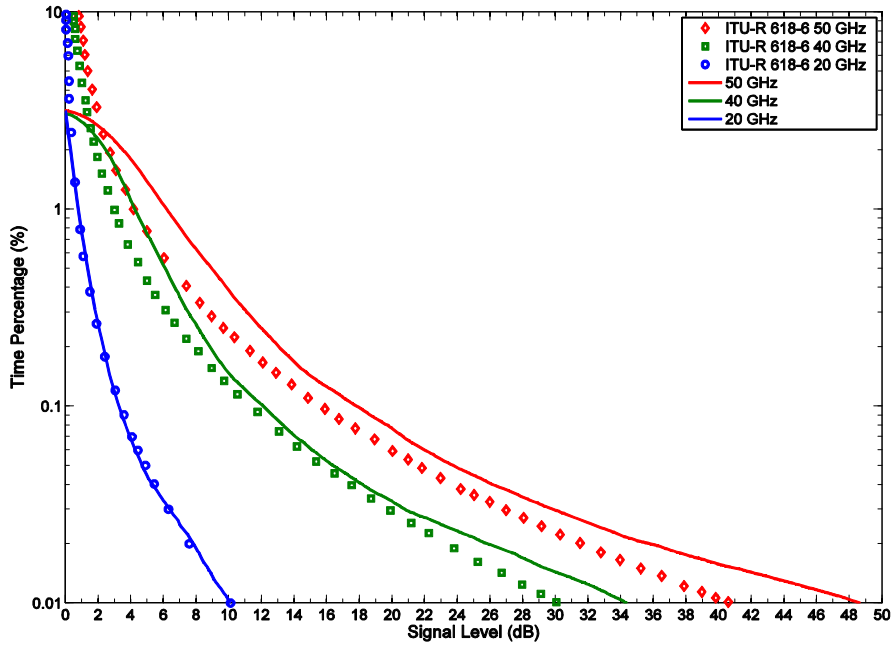

Figure 4.48 Rain attenuation cdf (April 1997- March 1998)

4.3.6 Tropospheric Scintillation

Scintillation severity for the higher frequencies of 40 and 50 GHz can be seen in Figure 4.49. As expected, in general scintillation fluctuations increase with frequency. At 40 GHz scintillation level, for 0.1% of the time the fluctuations were about 0.8 dB. While for 0.01% time percentage it increased to about 1.4 dB. The 50 GHz scintillation is higher, for 0.1% it is now about 1.8 dB. At 0.01% of the time it reached more than 3.1 dB. It is worth mentioning that Tropospheric scintillation shows a strong relationship with convective clouds [67] thus severe scintillation could exist within a rainy event (showers).

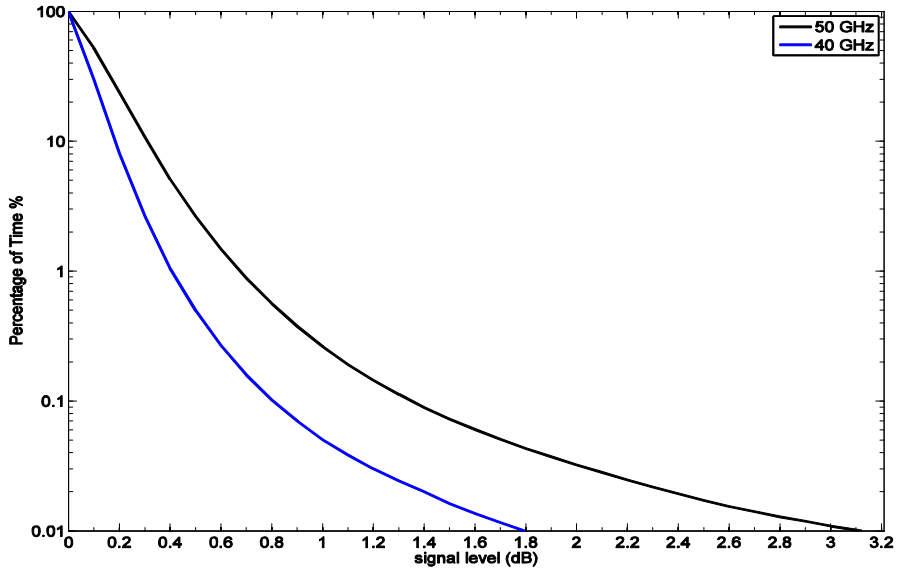

Figure 4.49 Tropospheric scintillation cdf (April 1997-March 1998)

4.3.7 Cloud attenuation

Cloud attenuation presented some difficulty to analyze; rain-gauge sensor is not accurate in flagging rain events: rain drops evaporating in mid-air before reaching the ground, wind intensity that would sway the drops and might not register by the rain-gauge, and having a rain event along the slant path that does not span the receiver's (rain-gauge's) location. From Figure 4.50 to Figure 4.52 the acquired cloud attenuation values of (**cloudy periods**) are rain-

guarded by 0, 10, 20 and 30 Seconds prior to and after a registered rainy event and compared with the ITU-R 840-3 model to get a feel of the attenuation change.

As expected of the ITU-R model, the estimation is comparably lower than actual attained values especially at higher frequencies with a significant difference in regards to the attenuation change at probabilities lower than about 3%. For the 20 GHz statistics the application of guard periods varied the attenuation adjustment from 0.27 dB to about 0.41 dB for 0.1% of the time. Whilst for the 40 and 50 GHz the same periods resulted in an adjustment of attenuation levels of 1.11dB to 1.95dB and 1.7 dB to 2.6 dB, respectively.

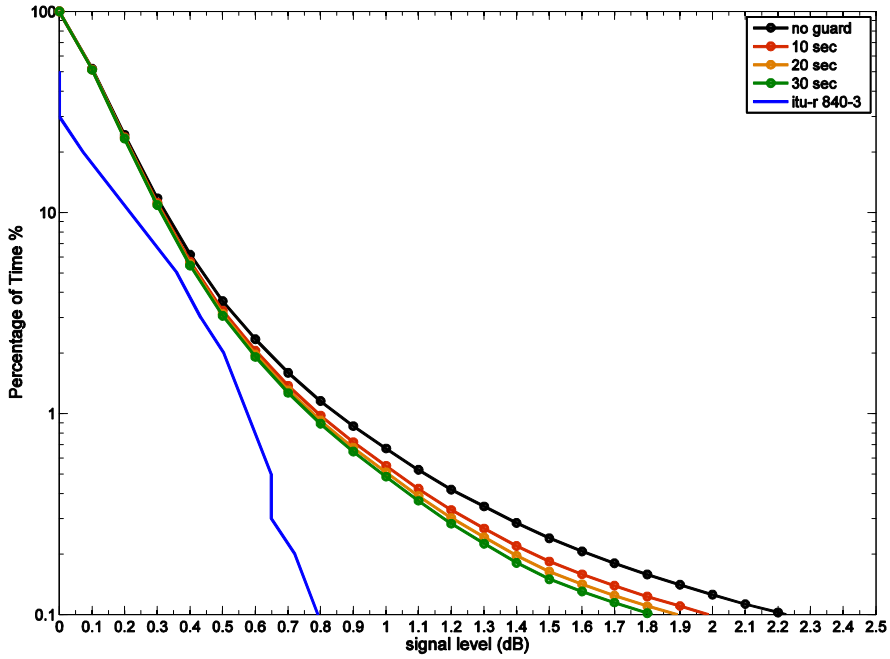

Figure 4.50 20 GHz cloudy periods cloud attenuation (April 1997-March 1998)

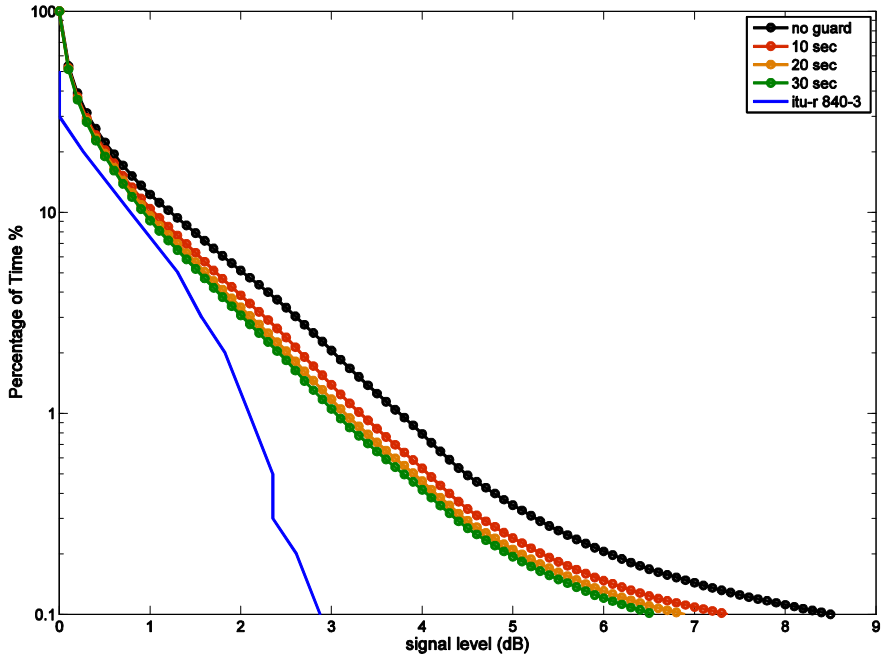

Figure 4.51 40 GHz cloudy periods cloud attenuation (April 1997-March 1998)

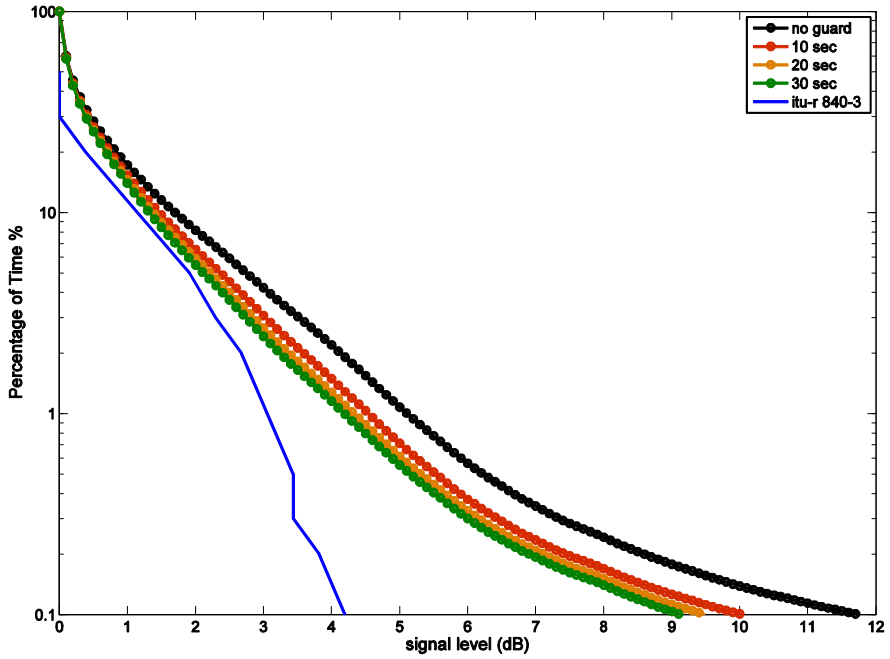

Figure 4.52 50 GHz cloudy periods cloud attenuation (April 1997-March 1998)

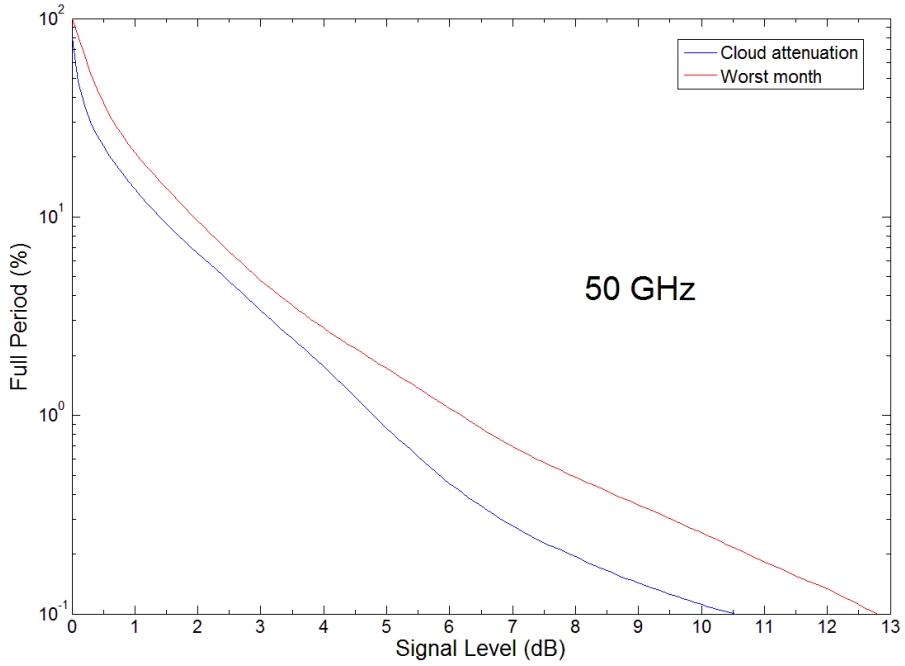

Figure 4.53 Full period-clear sky and cloudy-cloud attenuation (Apr1997-Mar1998)

Now, for the cloud attenuation of the actual full period (measurements with both clear sky and cloudy) compared to the worst month attenuation, it is clear there exists a noticeable difference. Indeed, for the upper frequency of 50 GHz attenuation shown in Figure 4.53 the measured attenuation is now 10.51 dB at 0.1% of the time whereas for the same percentage the worst month has an attenuation of about 12.7 dB. This would indicate the need to take into consideration an additional margin of about 2.2 dB to account for worst-month statistics for calculated attenuation at 0.1% percentage time.

4.3.8 Overview on investigated attenuation factors

The major cloud types available in the region were (Cu), (Cb) and (St/Sc). Both (Cu) and (Cb) cloud-types' FO peaks at around 11:00 AM throughout the day until early night time of around 7:00 PM whereas (St/Sc) cloud-type would on the contrary be at their lowest. Nimbostratus cloud-type was inconclusive.

Rain attenuation is always a key factor in satellite communications; its impact is more severe at higher frequencies. It was noted that measured rain attenuation values were higher than the ITU-R predictions; rain would impact signal

attenuation in the 40 and 50 GHz frequencies by around 4.3 to 6.2 dB for 1% of the full period (about 3.7 days per year). This rises to 12.1 dB and 17.79 dB for 0.1% of the time corresponding to just above 9 hours as compared to the ITU-R model estimation of around 2.98 dB and 4.17 dB for 1% and 11.35 dB to 15.6 dB for 0.1% of the time.

Tropospheric scintillation when compared to other major attenuation impairments (cloud and rain) was much less severe. For the same intervals of 18 days and 3.65 days (5% and 1% of the time) it would have a maximum effect of 0.40 to 0.68 dB at 40 and 50 GHz, respectively. But in very rare occasions (0.01%) the attenuation could reach up to and above 3.12 dB for 50 GHz.

Gaseous attenuation had a higher attenuation values than scintillation for probabilities higher than 0.1% for all frequencies. The variability of the attenuation between 99% and 0.1% of the time is less than 0.5 dB for 20 GHz, less than 0.6 dB for 40 GHz and less than 0.7 dB for 50 GHz.

Cloud attenuation was usually undermined due to its low impact in the lower frequency regions (up to 12 GHz) however, it is apparent to have ever-more significant effects on the higher frequencies well into the 50 GHz operational region. For the 20, 40 and 50 GHz the ITU-R model always underestimates the influence of cloud attenuation; even with the introduction of guard gaps concept the effects are still significant for low-margin systems design. More so, based on the measured attenuation of especially the 40 and 50 GHz readings we see cloud effect is increasing at a fast rate and becoming of more importance. In the case when considering a 30-second gap guard (before and after the rain event) for 5% and 1% of the time (30 second gap) cloud attenuation would be 0.42 to 0.77 dB for the 20 GHz, 1.54 to 3.05 dB for the 40 GHz, and 2.18 to 4.19 dB for the 50 GHz.

4.4 Conclusions

Surface parameters were proved (section 4.2.1, see Figure 4.20 to Figure 4.29) not to have a strong correlation with cloud attenuation as investigated by [36]

and others at high frequencies. This is due to the fact of the atmosphere acting as layered areas with different temperatures, pressure and relative humidity values which would affect the development and sustainability of cloud formation at these layers.

Clouds synoptic data like frequency of occurrence and type (genre) can be acquired with ease from meteorological stations (section 4.2.2). However, the vertical profile of a given cloud genre is not fixed (the concentration of the liquid water droplets, their size and distribution along with the cloud's vertical extent) and changes all the time. In this project the meteorological station was located 12.7 miles from the receiver's, that in turn would also contribute to the measurements difference of what is observed and what is seen by line-of-sight earth-station receiver. Therefore the periods of cloud attenuation and their yearly presence impact can be accurately assessed if the receiver was located at the meteorological station location, and the direction and elevation angle were correlated with the observations. However for the actual attenuation levels experienced by the propagating signal due to the exact amount of liquid water content (from the cloud vertical profile), accurate measurements are not possible; and the need for extra equipment such as Lidar, radiosonde and radiometers becomes apparent. Thus for the utilization of only meteorological station data, statistical values of liquid water content need be implemented and fine-tuned as was done by the DAH model, see section 2.3.2.

Based on Sparsholt's measurements having an elevation of 30° (ITALSAT) it is obvious that the attenuation impairments of rain, cloud and gaseous absorption are dominant. Tropospheric scintillation had the least effect in the statistics. Hence for commercial systems availability (coverage) lossy mechanisms in the troposphere are the key hinderer to look out for (section 4.3, see Figure 4.46 and Figure 4.48 to Figure 4.52).

In the next chapter we deal with the available fade countermeasures and what would be best suited for dealing with cloud attenuation.

5 Cloud fade statistics effect on satcom

5.1 Introduction

Many services like video conferencing and high-speed internet services via satellite for multimedia applications require larger bandwidth. This in combination with the saturation of C-band and the rapidly filling-up Ku-band, led to the exploitation of higher frequencies to provide these services.

The advantages of utilizing higher frequencies include, smaller antennas, increased bandwidth, and smaller satellite footprint that give higher EIRP and permit frequency reuse. The main issue (down-side) for their use is the stronger propagation degradation they experience. In order to prevent a system utilizing higher frequencies (e.g. V-band) from only being deployed in regions of low amount of clouds or to commercially unavailable earth stations (e.g. the military-scientific research), fade countermeasures (FCM) also known in the literature as fade mitigation techniques (FMT) become necessary.

Figure 5.1 shows the levels of total attenuation (compared to clear sky) at 20, 40 and 50 GHz during a rain event logged on the 5th of June 1997. The rain rate had values up to 17mm/hr. As we can see, the attenuation at 20 GHz reached about 6 dB, whereas at 40 and 50 GHz the attenuation levels surpassed 20dB. Therefore, assigning a fixed fade margin for the higher frequencies is not a viable solution. The general approach for handling the large attenuation at those frequencies is to use adaptive methods or fade countermeasures (FCM).

Throughout this chapter we will talk about some general definitions and equations related to satellite communication system design, then an overview of FCM that can be applied to mitigate the severe degradation due to the atmospheric propagation fading. Followed by results from the analysis of cloud fade duration statistics. The percentage of time that information can be transmitted and received with acceptable quality (link availability) is a vital parameter for any VSAT/USAT network. Information quality for digital signals at the demodulator/decoder input is described in terms of both the bit error rate (BER) and carrier-to-equivalent noise spectral density ratio (C/N_0, also CNR).

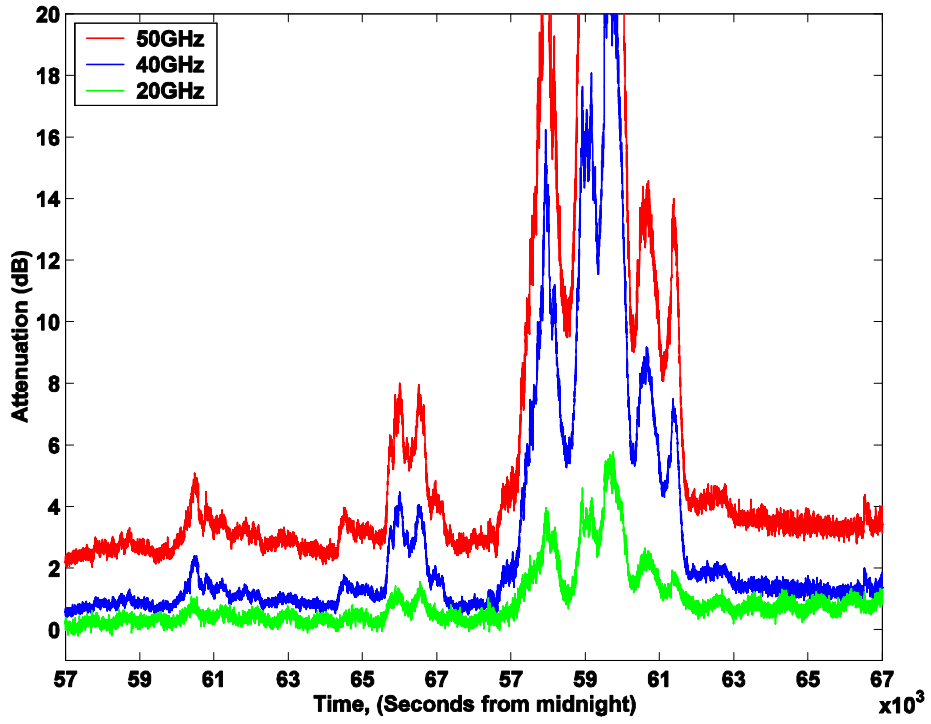

Figure 5.1 Levels of total attenuation (compared to clear sky) measured during a rain event on June 5th, 1997.

5.2 General definitions

5.2.1 BER (Bit Error Rate)

In digital satellite systems the errors in identification of the received symbols (received bits) is the result of phase\amplitude identification errors under the influence of noise. Bit-error-rate (BER) measures the performance of the system by counting the number of bits in error, in a stream of received bits.

BER is a crucial performance criterion for digital data communication systems. In practice, the transmitted symbol is affected by noise as it propagates through the medium until it reaches the receiver. At the receiver a bank of correlators extracts the received vector. With this received data vector, the receiver has to decide on which message point in the signal constellation is most likely to have

been transmitted. Assuming that all M message points are transmitted with equal probability, the maximum likelihood detector will decide which message point has been transmitted in favor of the message point that is closest to the received signal point.

The received symbol will be mistaken for the adjacent one if the noise that the signal encountered is greater than half the distance between the two neighboring message points. As a result a symbol error will occur whenever noise effects shift the received point across the decision boundary between two points in the symbol space. As the space between the signal points shrinks, the possibility of error increases. For example, a probability of symbol error equal to 0.001 means that there is one symbol error per 1000 received symbols on average. This is referred to as the symbol error rate (SER).

Bit and symbol errors for a binary system are identical as each symbol error corresponds to a single bit error. However For M-ary systems (M > 2) this is not true anymore. For example, in the case of a 64-ary scheme conveying six bits per symbol may sustain anything from one bit to six bit errors per incorrectly decoded symbol, depending on which symbol was mistakenly identified. Thus BER depends on the modulation method and of course the SER.

Some symbols, in practice, are more likely to be detected in error than others. It is more likely for a symbol to be mistaken as its neighbor. Therefore to minimize the number of bit errors occurring for every symbol error, it would be good to use reflected binary encoding.

Reflected binary code (also known as Gray coding**)** is the name given to a bit assignment where the bit patterns in adjacent message points only differ in one bit position. For the assumption that the detection process will only mistake symbols for those adjacent to the correct symbol, the bit error probability will then be approximately given by the symbol error probability divided by the number of bits in each symbol. Thus for an M-ary modulation scheme,

$$BER = \frac{Symbol \quad Error \quad Rate}{\log_2 M}$$

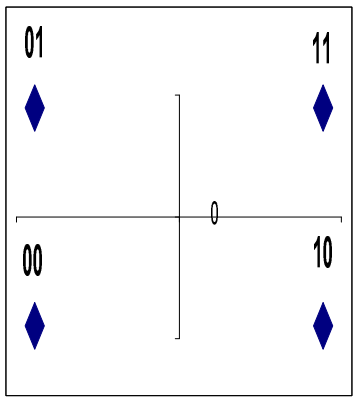

Figure 5.2 Example QPSK signal space (2-D) diagram with Gray coding

5.2.2 Shannon's capacity

A good measure of merit of any communication system is the channel capacity defined by Shannon. That is because it gives the maximum rate of transmission of signals over the used channel. A channel subject to fading will have a varying capacity due to the changes in the propagation medium. So, if we increase the level of modulation, i.e. the number of symbol states, which would allow the bit rate of a system to be increased. However, the ability of the receiver to distinguish between the symbol states in the presence of noise becomes more difficult which results in an increase in error rate. The Shannon capacity parameter for error-free communication is given by:

$$C = B\log_2\left(1+\frac{S}{N}\right) \quad \text{bits/second} \tag{5.1}$$

Here C is the channel capacity, and B the channel bandwidth in Hz with S/N the signal to noise ratio in the channel. In theory, it is possible to transmit at the above specified rate by having the error rate approach zero as closely as wanted. However, a method to achieve this rate was not specified by Shannon, but only showed that complex coding and large delays in transmission would be required. An overview of the theory is provided in the books referenced as [68] and [69].

5.2.3 Outage and availability

If we are to utilize the ITU-R recommendations definition [70], then an outage event occurs in a digital receiver if its BER exceeds a specified threshold (based on the requirement of the service at hand) for not more than 10 succeeding seconds. Thus outage time is the accumulated seconds for all outage events per a predefined time period (e.g. per year). For events that last more than 10 seconds the link status is described as unavailable. The previous distinction between outage time and unavailability arises from the fact that digital trunks often lose framing when high BERs persist over a long period of time.

5.3 Modulation techniques in satcom

The majority of operational satellites are power limited, i.e. the available ratio of energy per bit to noise density (E_b/N_0) is insufficient to enable the utilization of modems which have a spectral efficiency more than 2 b/s/Hz and require a greater E_b/N_0 ratio. Due to their power efficiency, Binary Phase Shift Keying (BPSK) and Quadrature Phase Shift Keying (QPSK) are the more frequently employed modulation techniques. Since the spectral efficiency of such systems is less than 2b/s/Hz [71].

The spectral or bandwidth efficiency of a communication link is a measure of how well a particular modulation format makes use of the available bandwidth. It equals to the ratio between transmission bit rate and the system bandwidth, having units of bits per second per hertz (b/s/Hz).

Amplitude, phase and frequency modulation are all applicable to digital modulation. The digital equivalent of these modulation schemes are known as Amplitude Shift Keying (ASK), Frequency Shift Keying (FSK) and Phase Shift Keying (PSK). Additionally, some modulation schemes have been developed

specifically to optimize digital modulation. These are hybrid phase/amplitude schemes called Quadrature Amplitude Modulation (QAM).

5.3.1 ASK/FSK modulation

Amplitude Shift Keying (ASK) is considered the simplest form of band-pass data modulation. Although extending binary ASK to multilevel ASK (M-ASK) is simple, the bit error rate (BER) of M-ASK is very poor due to the use of strongly correlated sinusoidal pulses. There is no prospect to exploit orthogonality with M-ASK which is an immediate penalty in BER performance. Its poor BER performance means that there are very few practical applications of ASK other than its binary form, even with its excellent bandwidth efficiency. Poor BER and its inherent characteristics of a non-constant envelope makes ASK unsuitable for applications in satellite communications.

On the other hand, with M-ary FSK we have the ability to trade bandwidth for an improved noise performance in a manner that is not possible with M-ary ASK and M-ary PSK. An M-ary FSK signal consists of one of the following M orthogonal sinusoidal pulses in each symbol interval of duration T_s. These pulses differ in frequency, which are spaced at half the symbol rate to achieve mutual orthogonality of the transmitted symbols with minimum required bandwidth [68].

$$g_i(t) = A_c \cos\left[2\pi\left(f_0 + i\Delta f\right)t\right] \qquad \text{i = 0,1,2,…,M-1} \tag{5.2}$$

$$\Delta f = 1/2T_s = R_s/2 \tag{5.3}$$

The frequency f_0 is chosen to place the transmission in the allocated frequency band.

The effect of noise is reduced as the symbol averaging time becomes very large due to the increase in number of symbol states employed. Thus M-ary FSK can be applied in systems where noise immunity is the key issue. However, increasing the number of symbol states causes a rapid reduction in bandwidth efficiency thus making FSK schemes inappropriate for satellite applications.

5.3.2 PSK modulation

In a PSK system the phase of the carrier is altered in accordance with the baseband digital stream. PSK scheme have a general form of

$$v(t) = A\cos(\omega_0 t + \phi_m) \tag{5.4}$$

where ϕ_m is the phase angle changed in accordance with the information signal. The signal space diagram of M-ary PSK consists of message points uniformly spaced, with constant phase shift, along a circle that is centered at the origin. For Binary Phase Shift Keying (BPSK) which is the simplest form of phase modulation, the data is taken one bit at a time and the carrier phase is varied by 0 or π radians to correspond to the data as 1 or 0. The orthogonality between the sine and cosine function suggest that if BPSK is to be used to transmit on a cosine carrier, and simultaneously a second BPSK signal is sent using a sine carrier of the same frequency, then it will be possible to detect each one independently of the other. This setup is referred to as Quadrature Phase Shift Keying (QPSK). By applying Gray encoding to the symbols, the BER of BPSK and the Gray encoded QPSK is the same. The advantage of using QPSK is that it has twice the bandwidth efficiency of BPSK. The theoretical bandwidth efficiency of QPSK = 2 b/s/Hz.

If the number of symbol states for M-ary PSK is increased beyond four that would allow further improvements in bandwidth efficiency. The bandwidth efficiency for M-ary PSK is equal to $\log_2 M$ b/s/Hz. However, the additional symbol states are no longer orthogonal which mean that they do not lie on the sine or cosine axis of the constellation diagram. This leads to the performance in noise for M > 4 degrading rapidly as M increases. The BER performance [68] for M-ary PSK for M > 2 is given by:

$$BER = \frac{1}{\log_2 M} erfc\left(\sqrt{\frac{E_b\left[1-\cos\left(2\pi/M\right)\right]\log_2 M}{2N_0}}\right) \tag{5.5}$$

5.3.3 QAM modulation

Quadrature amplitude modulation (QAM) is a combination of amplitude and phase signaling. By spacing the message states more freely and widely in the two-dimensional signal space the BER performance can be improved over that of PSK. The way to achieve this is by combining two quadrature (sine and cosine) carriers that are modulated in both amplitude and phase. This combination gives us the quadrature amplitude modulation. There are different implementations of QAM, like the square QAM, circular QAM and star QAM.

For a square QAM that carries equal number of bits in the quadrature and in-phase channels [68] the BER is:

$$BER = \frac{2}{\log_2 M}\left(1-\frac{1}{\sqrt{M}}\right) erfc\left(\sqrt{\frac{3E_b \log_2 M}{2\left(M-1\right)N_0}}\right) \tag{5.6}$$

The bandwidth efficiency for both M-ary QAM and M-ary PSK is the same and is equal to $\log_2$M b/s/Hz, however M-ary QAM yields a better BER performance. This is an important feature of the M-ary QAM. QAM however has a non-constant envelope and has therefore not been widely implemented in satellite communication systems. Nonetheless, their excellent bandwidth efficiency and their good BER performance make them attractive for satellite communications. Even high M-arity QAM could be considered for satellite applications where really high bandwidth efficiency is necessary [72]. The main drawback of using QAM techniques is their non-constant envelope. Such a modulation format greatly increases data throughput and hence the revenue produced by a transponder.

5.4 Fade duration statistics

Fade duration statistics are important for the design of high frequency satellite systems. Fade and inter-fade duration statistics are parameters that provide the system designer with useful information for considering various mitigation techniques that can be employed to ensure a given system availability and quality of service.

Statistics of observed durations of pure cloud fades (no scintillation, rain or gaseous) of the ITALSAT satellite measurements at 20, 40 and 50 GHz at Sparsholt are presented for various threshold signal levels below.

5.4.1 Fade duration

Fade duration D_- at threshold level χ_T below the mean level (= 0dB) of χ (cloud attenuation amplitude) was taken as the time interval over which the signal level continuously fell below χ_T.

Inter-fade duration or non-fade duration is the complement of the fade duration. It is defined as the continuous time over which the attenuation is lower than a given threshold value. Figure 5.3 gives the graphical representation of this definition.

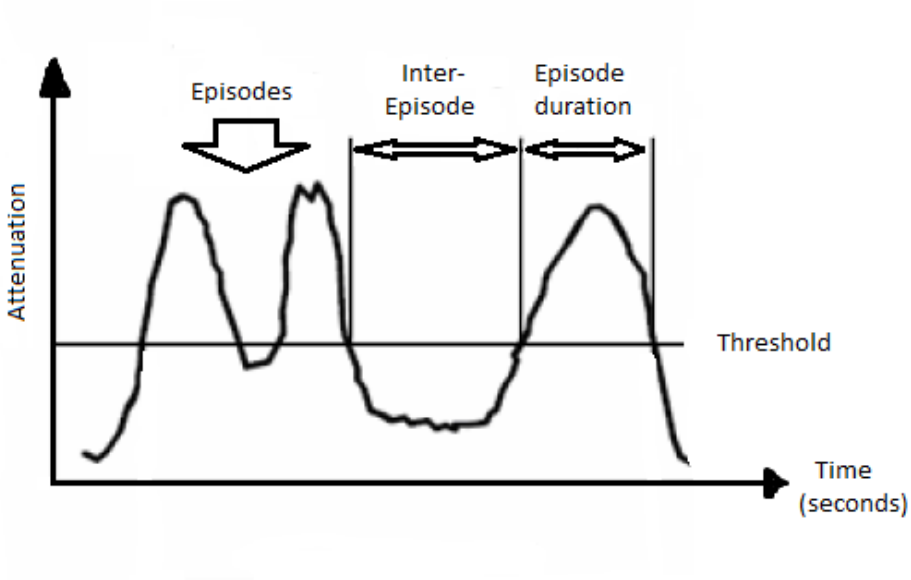

Figure 5.3 Definition of episode and inter-episode, reproduced from [73]

CDFs at 20, 40 and 50 GHz of fade duration at selected threshold levels are shown below (fade distribution). The year of April 1997 to March 1998 measurements was used of cloud attenuation. The fade durations are presented by a logarithmic scale while the probabilities by a linear one. The highest attenuation level at 20 GHz was 16 dB (Maximum fade durations increase with frequency. During the year for the 20 GHz signal, fades length did reach over 1000 seconds (~ 17 minutes). As for the 40 GHz signal the durations could reach about 10000 seconds (close to 3 hours). The same is noted for the 50 GHz with yet an increase of maximum fade durations in excess of 17000 seconds (close to 5 hours).

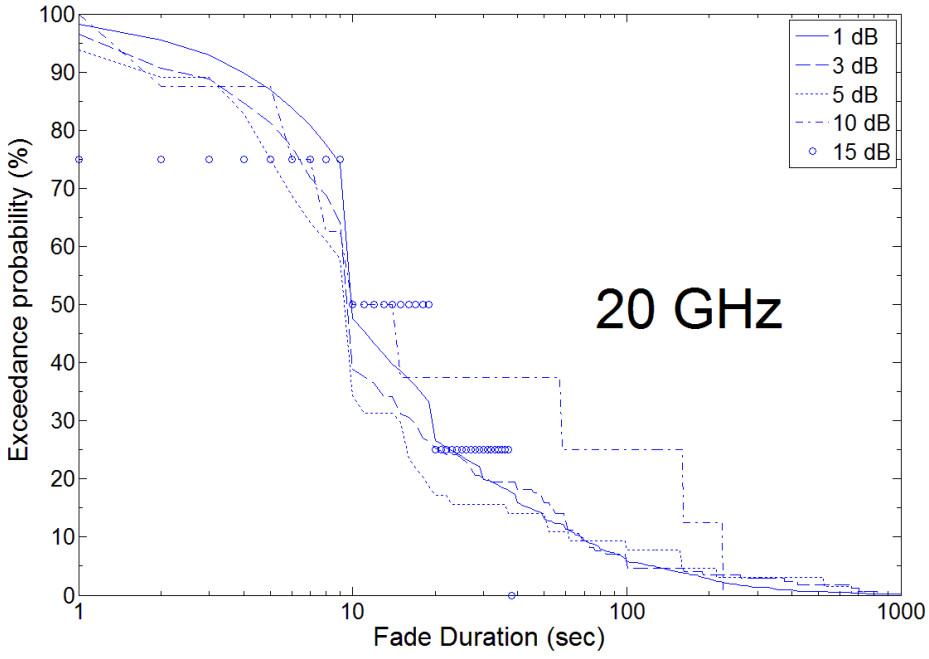

Figure 5.4 Fade duration distribution at 20 GHz

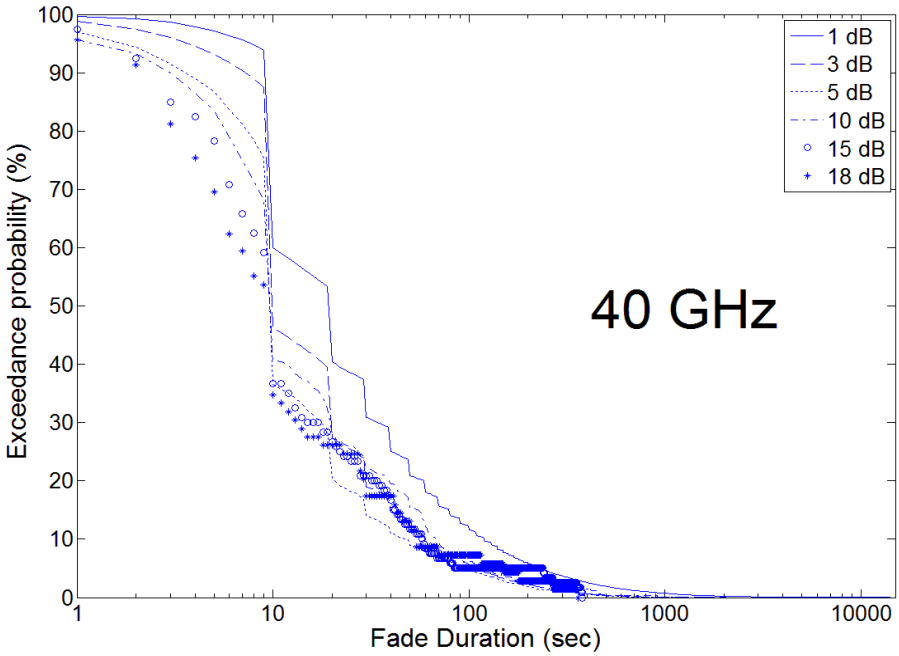

Figure 5.5 Fade duration distribution at 40 GHz

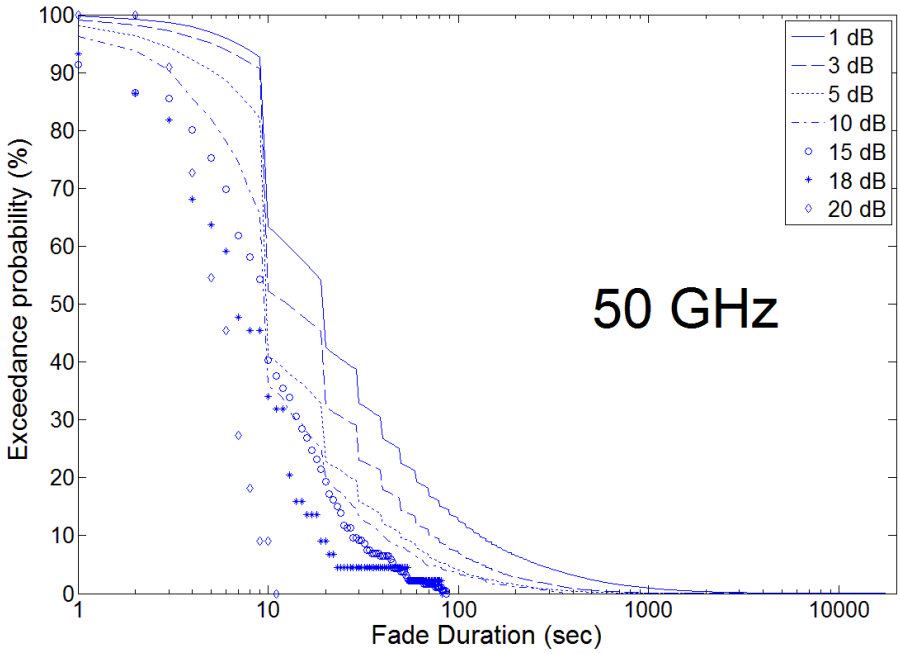

Figure 5.6 Fade duration distribution at 50 GHz

In digital receivers, the synchronization and signal decoding-timing and phase- would be affected by the distribution of fade events. For extended fades the receiver can lose lock leading to the need of re-acquisition. This results in fades and their statistical distribution becoming an influence on service availability, receiver loss of lock and decoder performance. Therefore, it is helpful to plot both the fade durations vs. the number of fades (events) that occurred throughout the year and the fade durations vs. the total duration of events exceeding abscissa. As such plots show the trend of attenuation intensity frequency which help in the decision of choosing the appropriate FMT based on the specific requirements of the service.

In Figure 5.7 it is clear that at 20 GHz, less than 100 events were of 5 dB limit. However, at the 40 and 50 GHz (Figure 5.8 and Figure 5.9) not even the 15 dB limit has that low event count (+103 events). This demonstrates the impact of clouds on attenuation dynamics by just increasing the frequency!

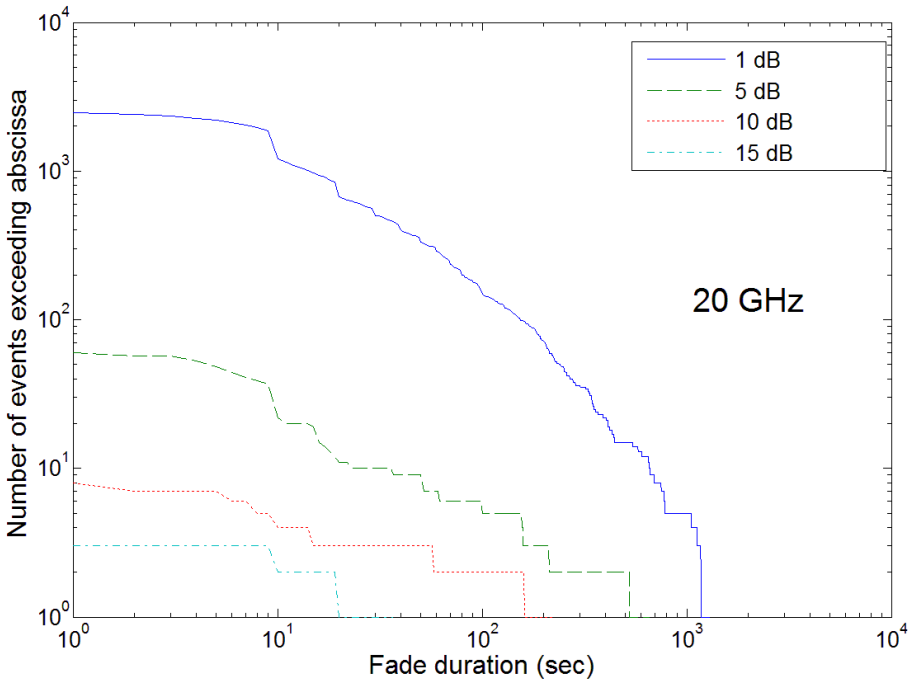

Figure 5.7 Distributions of annual number of fades at 20 GHz

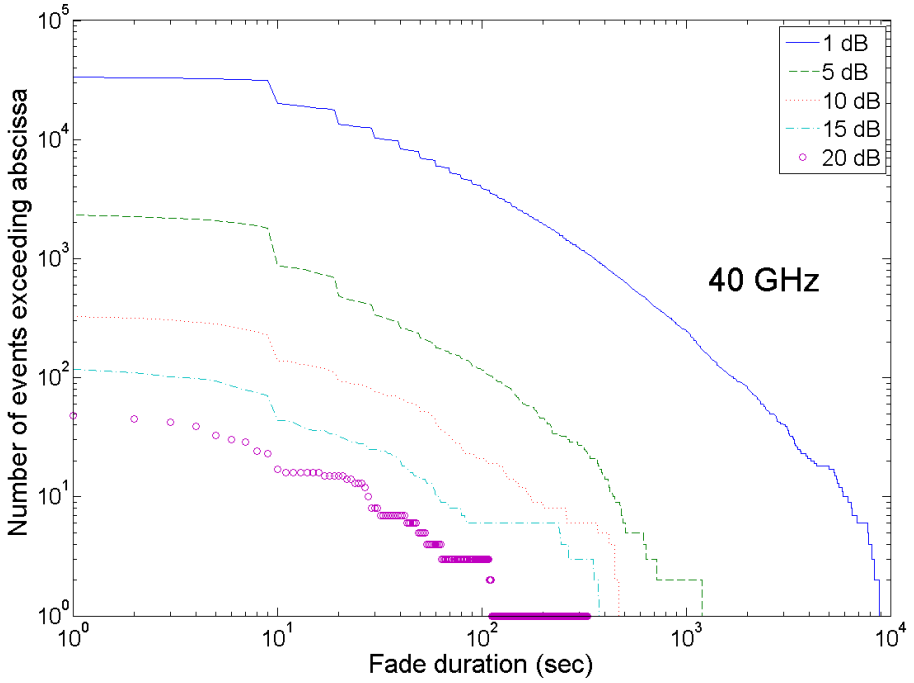

Figure 5.8 Distributions of annual number of fades at 40 GHz

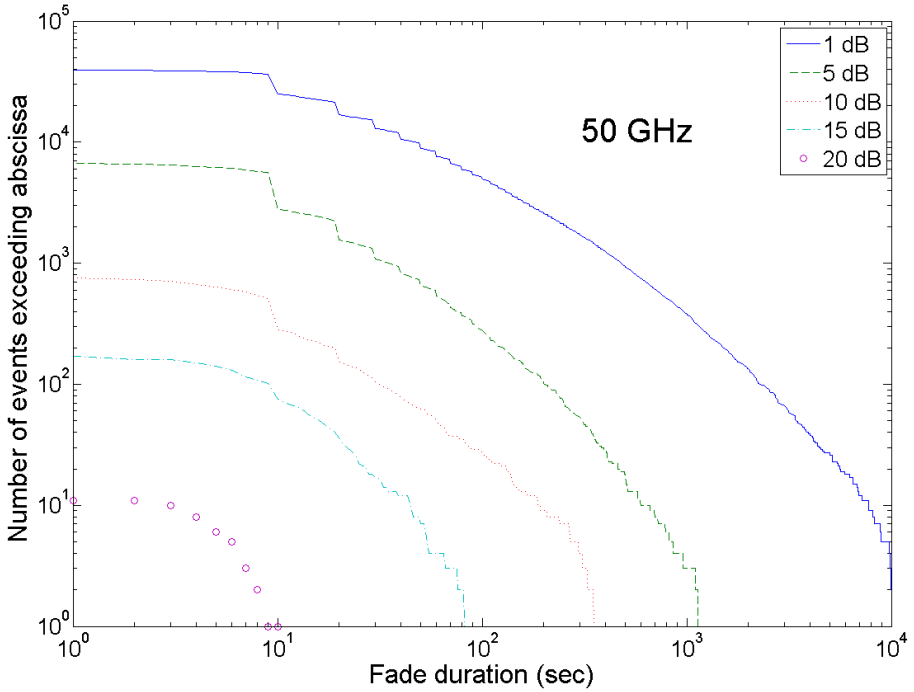

Figure 5.9 Distributions of annual number of fades at 50 GHz

For these events the fade duration at 1 dB for the 20 GHz had a maximum of about 1200 seconds (20 minutes). However it is now about 9000seconds (2.5 hours) and above 10000 seconds (above 2.7 hours) for both 40 and 50 GHz , respectively. As for the 5 dB, the 20 GHz fade duration was about 510 seconds (8.5 minutes) whereas for both the 40 and 50 GHz fades the durations were above 1000 seconds (about 17 minutes). This leads to the conclusion that, moving to a higher frequency of operation would mean dealing with longer fade durations for the same meteorological circumstances at a given site.

From both Figure 5.10 and Figure 5.11 we can see again that the amount of time the signal is attenuated above the specified threshold increases with the frequency. Indeed, total fade durations of 1 second at 1, 5, 10 and 15 dB for the 20 GHz signal were 83665, 2493, 484 and 69 seconds , respectively. As for the 50 GHz now the total fade durations for 1 second for 1, 5, 10 and 15 dB were 2918328, 176440, 16243 and 2599 seconds, respectively.

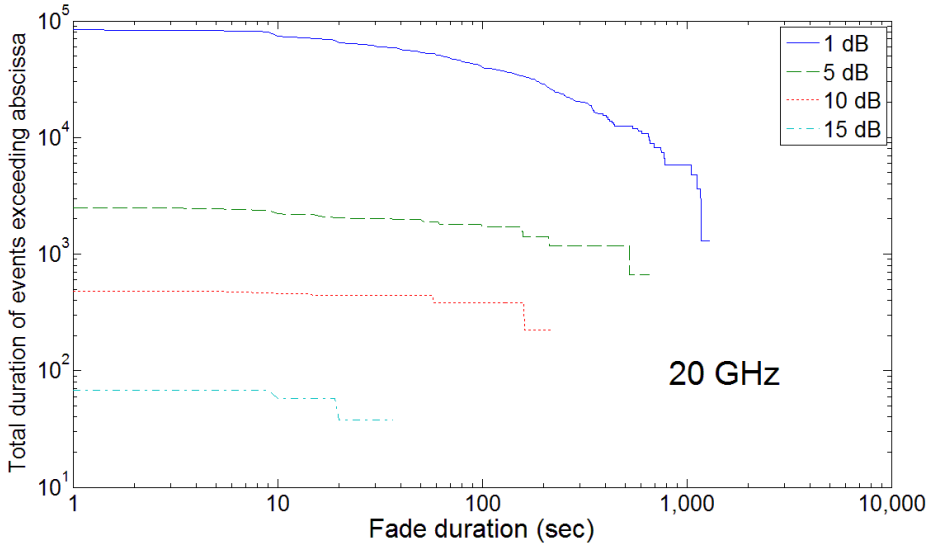

Figure 5.10 Total duration of events exceeding abscissa for 20 GHz

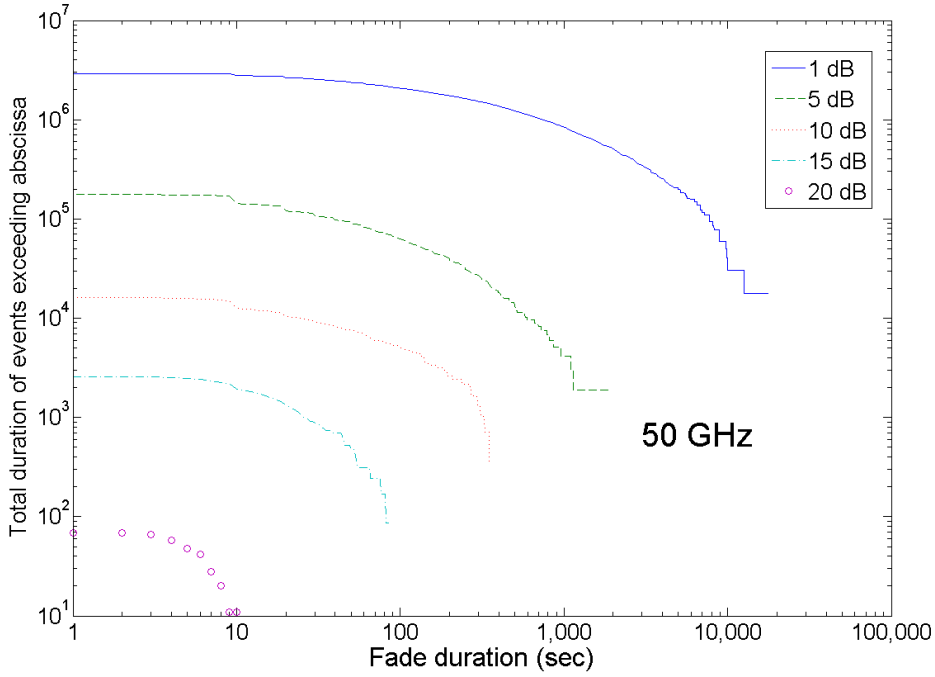

Figure 5.11 Total duration of events exceeding abscissa for 50 GHz

The compilation of total fade duration (in seconds of exceeding fade threshold) per selected attenuation values at 20, 40 and 50 GHz are listed in Table 5.1 and shown in Figure 5.12 for fades up to 20 dB. As expected, the higher frequencies experience extended fade durations. Note that, as explained in section 3.4, due to the higher volume of invalid data of the 50 GHz measurements for the period of April 1997-March 1998, the consequence was lower account of the higher attenuation periods. Therefore the amounts of registered fades above 13 dB limit were heavily affected.

Another aspect in analyzing cloud fade dynamics is to consider the Fade-slope. It is the rate of change of attenuation per time having the units of (dB/s). It can help decide the optimal FMT and fade controller to implement, since it can show the maximum amount of signal drop thus aiding in the configuration of the FMT equipment. As expected, the rate of change (dB/sec) is generally manageable. Nonetheless with higher frequency this rate is affected and starts to increase.

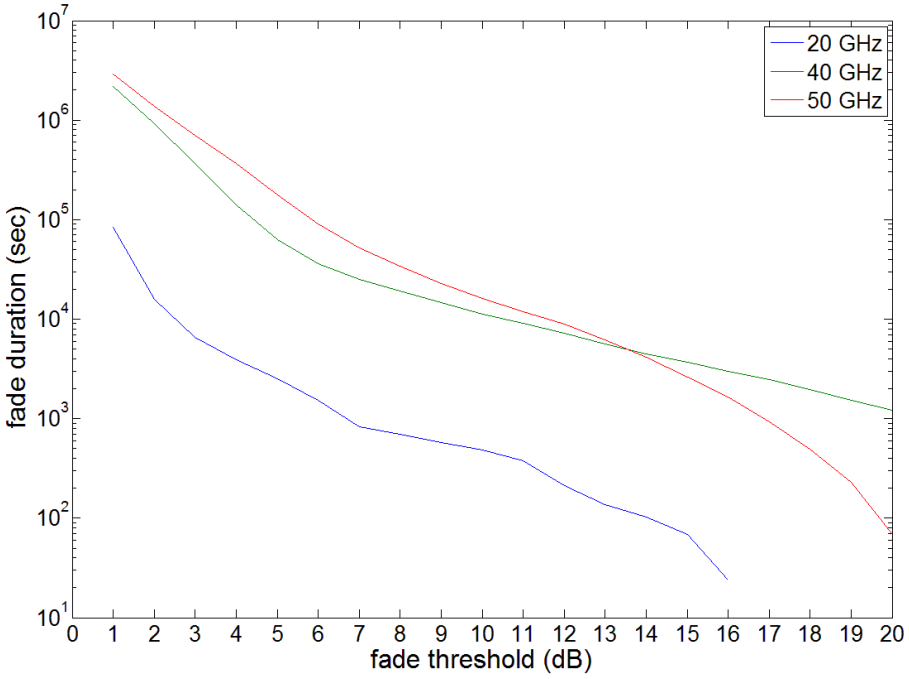

Figure 5.12 fade threshold vs. total fade duration for Sparsholt measurements April 1997-March 1998

Table 5.1 total fade durations (seconds) per fade threshold at 20, 40 and 50 GHz

GHz	1 dB	2dB	3 dB	4 dB	5 dB	10 dB	15 dB	18 dB	20 dB
20	83665	15811	6596	3900	2493	484	69	0	0
40	2165918	911684	366242	141290	62602	11303	3705	1957	1206
50	2918328	1376115	707925	366708	176440	16243	2599	493	69

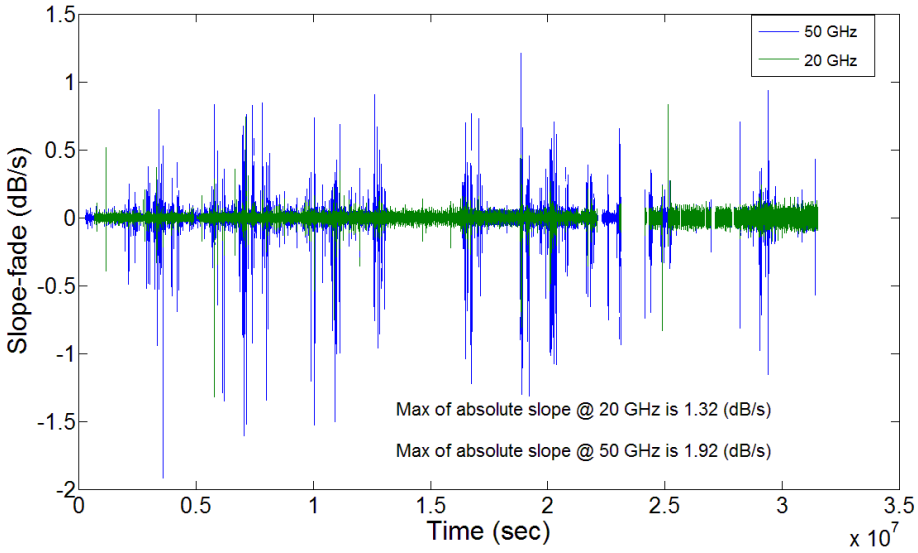

Figure 5.13 Annual fade-slope variations for the 20 and 50 GHz

As can be seen from Figure 5.13 the fade-slope for the 20 GHz was 1.32 dB/s while for the 50 GHz it is now increased to 1.92 dB/s. That is an increase of about 0.6 dB/s, which means the higher frequency, the more the slope-fade variations become.

So, the effect of cloud attenuation as frequencies increase both becomes more severe and lasts longer. Thus cloud presence is indeed significant at Ka/V bands and needs to be accounted for in the design of satcoms.

5.5 Fade countermeasures

It was shown that the excess fade can be large. Hence if a fixed static fade margin (at Ka-band and above) is to be assigned, then the excess margin would be very large thus adding to the cost considerably. Therefore it is encouraged to look at other alternatives to increase the availability of the system with minimum cost. These alternatives are prescribed as Fade Mitigation Techniques (FMT) or Fade Countermeasures (FCM).

By applying these measures, it will be possible to design VSAT Systems [74] with a static margin conforming to the worst case scenario of fading that occurs in clear-sky conditions. Then the application of the FMT will counteract attenuation impairment elements effect that can include scintillation, depolarization, cloud attenuation and even some fraction of rain attenuation.

FMT can be divided into three major categories:

- **Power control:** achieved by adjusting the transmitted power level to match propagation impairments
- **Signal processing:** utilizing a more efficient communication scheme to compensate for the fade
- **Diversity:** making use of another link to avoid fade

Next we briefly review each of these categories focusing on the ones relevant to VSAT/USAT applications with high availability.

5.5.1 Power control techniques

5.5.1.1 Up-link power control (ULPC)

The general idea is to adapt the carrier power level to the propagation conditions. There are two distinct types, namely the transparent and regenerative repeaters.

Transparent repeater

Here the adaptation of the carrier power level aims to control both up-link and downlink budgets by the transmitting Earth station [75]. It can be implemented with relative ease on condition that there is enough power available (i.e. if the satellite power amplifier is not operated at full power). However this would depend on the required dynamic range of fades. Power control attempts to maintain a constant power flux density at the satellite irrespective of fading conditions along the path. That is achieved by either decreasing the power in clear sky conditions or alternatively increasing the power to compensate such fades under fading conditions. ULPC can be seen as a way to keep a constant level of all the carriers at the input of the repeater. Another way to see it is as a manner to maintain the overall link budget of the links in order to optimize the satellite capacity.

Regenerative repeater

With a regenerative repeater carriers are demodulated on-board the satellite prior to the modulation of the downlink carriers, thus making the baseband signals available for specific processing. On-Board Processing (OBP) can be utilized to improve the overall link budget of the system. This technique permits the matching of the waveform (coding rate, data rate, modulation scheme) to the propagation conditions.

Yet it is essential to pay attention to the sensitivity of on-board demodulation to signal dynamic range at the repeater's input. Because Frequency Division Multiple Access (FDMA) is one of the typical choices applied on the uplink, if on-board processing is sensitive to strong variations between carriers, then even in the case of high margin systems, it would be recommended to use ULPC in order to circumvent capture effects of carriers faded by harsh propagation conditions. Therefore the monitoring of all carrier levels would have to be performed on-board the spacecraft, before the spacecraft specifies the necessary adjustments of up-link transmit power to the appropriate Earth station [74],[76]. This is particularly the case for systems operating at or above Ka-band, where a strong relative difference between both up-link and down-link frequencies exists, and for which a strong protection against uplink fading is vital.

Most satellites have beacon sources in the downlink frequency band. While using a down-link beacon for power control, the estimated downlink fade has to be frequency scaled to the up-link frequency. A drawback of up-link power control is that, under non-fade conditions, the quality of the up-link will be worse than the static power scheme for the same maximum power output needed by the dynamic range of the power control scheme. The downlink is unaffected since a new transponder operating point may be chosen to compensate for the reduced up-link power. The reduction in up-link quality leads to a reduction of the total link quality, and thereby decreases the system's tolerance to downlink fading [77].

To sum up, Up-Link Power Control makes use only of transmitted Earth station power; there are no constraints on the sharing of the system resources and no need for any specific delay before mitigation. Additionally, cost considerations and the flexibility of this technique make ULPC a good candidate as an additional technique to be joined with other fade countermeasures.

5.5.1.2 Down-link power control (DLPC)

DLPC aims to allocate a relatively weak extra power on-board, in order to compensate a probable degradation in terms of down-link C/N_0 due to propagation conditions in a particular region [78]. All Earth stations in the same beam coverage benefits from the improvement of EIRP for this situation. However, it is necessary to confirm that ground power flux density specification is not exceeded, in order to both put up with radio regulations and avoid interference problems, bearing in mind no service outages are to occur during changes in power level. If the area covered by the satellite antenna beam extends several hundreds of kilometers, then there might be several earth stations operating in it. At these other stations, this will sometimes result in either under- or overcompensation. The study in [79] was conducted in regards to the correlation of measured rain intensities at 23 locations in the UK. It was found that the correlation decreases rapidly with increasing distance, and that instantaneous rainfall rates at two locations in excess of 100 km apart can be regarded as independent. It was found that the benefit of DLPC is confined to the areas less than about 10 km from the monitor station.

Furthermore, the satellite transponders have to be designed in such a way that very little adjacent channel interference and intermodulation noise would be produced as a consequence of the increased power transmission. Thus adaptive DLPC would complicate the design and operation of the satellite transponder and is constrained by the limited available on-board power.

5.5.1.3 On Board Beam Shaping (OBBS)

OBBS is based on active antenna flexibility thus allowing the adaptation of spot beams to propagation conditions. The objective is to radiate extra power to the region (with the Earth stations) experiencing degraded link quality due to a meteorological event by reducing the size of the spot beam pointing at that affected region. This is possible with the utilization of active antennas.

The main advantage of OBBS is that when implemented, it gives similar results to ULPC or DLPC [80] without actually increasing the power transmission; and it also allows a better design of satellite coverage and the distribution of users in the coverage area as in mobile systems. Though the technique appears to have potential it could nonetheless add to the deployment cost considerably for various factors. More on this method could be found in [74] with additional references.

5.5.2 Signal processing techniques – Adaptive Signal Processing (ASP)

Since the available resources on the satellite rest on the number of users requesting a part of these resources at the same time these techniques would also be considered as Adaptive Resource Sharing. Adaptivity means the ability to adjust to the channel characteristics in order to compensate deep fading when needed. There are two fundamental classes of methods that can be identified which lead to a change in the satellite shared resources by acting on the bandwidth or on the information data rate. The first class aims to reduce the information data rate at constant transmission data rate and as a consequence maintains the BER. While the second class's objective is to introduce additional coding to either maintain the nominal BER or change modulation schemes to implement more robust modulations that require less symbol energy thus compensating additional attenuation on the link.

The quality of the link degrades by reducing the signal to noise ratio (C/N_0) at the receiver input. In digital communication systems, (C/N_0) is related to the bit energy to noise spectral density (E_b/N_0). Figure 5.14 shows the BER of various

modulation techniques plotted against the bit energy per noise spectral density ratio (E_b/N_0) [68]. The lower the ratio is, the higher the BER would be.

ITU regulations dictate that the BER for data transmission in a system should be 10^{-7}. Hence by maintaining (E_b/N_0) constant at the value that is required for a service, it can be ensured that the link quality is at a certain level. Unlike ULPC, which aims to restore the carrier to noise ratio (C/N_0) by means of an increase of the Earth station transmitted power, ASP techniques allow a decrease in the required C/N_0 while maintaining the link performance in terms of the BER. Next we present some methods of ASP techniques.

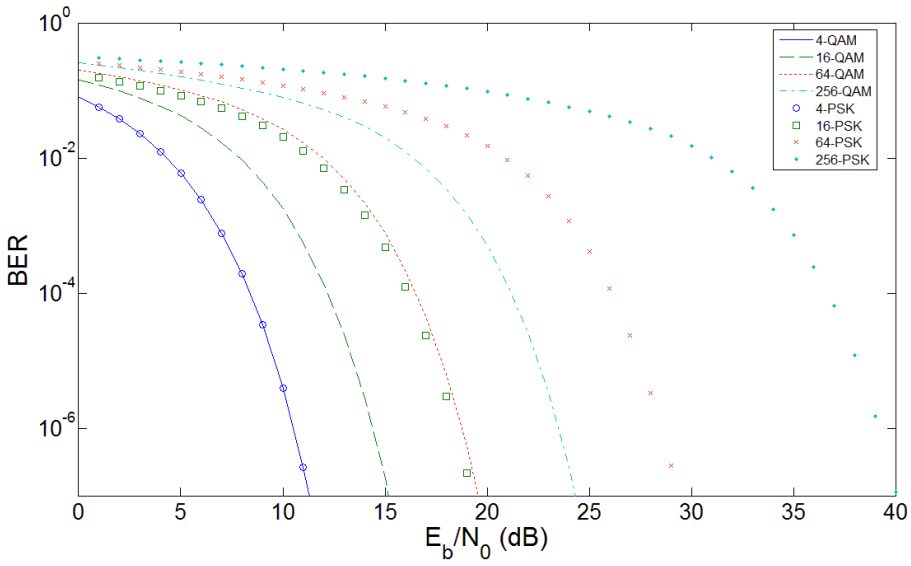

Figure 5.14 BER vs. (E_b/N_0) for M-ary QAM and M-ary PSK

5.5.2.1 Adaptive transmission rate

Adaptive transmission rate is aimed at maintaining the energy per symbol to noise spectral density ratio (E_s/N_0) at a given level by altering the channel symbol rate (speed-up or slow-down) depending on the propagation conditions. Therefore both the transmitter and receiver are aware of the current symbol rate at any given instance. High symbol rates are used under no-fade conditions when the signal to noise is high; it follows that the rate would gradually be

reduced as fading occurs. For example, for implementing a protection margin of 3 dB, the data rate of the system must be reduced by a factor of 2. In order for that to hold the equivalent noise bandwidth must also be reduced by 2 (as bandwidth=symbol rate/spectral efficiency).

By extension, systems operating at or above Ka-band compensating for a moderate fade of 10 dB would require a reduction of the data rate by a factor of 10. Indeed, this dramatic reduction of the information rate may prove to be intolerable to a majority of VSAT\USAT applications. Moreover, if the transmission rate is reduced, it will be essential to reduce the bandwidth of the receiver to that of the data signal to obtain maximum gain by rejecting out-of-band noise. Variable bandwidth filter and the cost associated with a variable rate demodulator are the major disadvantages of this type of FMT and will inevitably increase the system's cost. Therefore an adaptive transmission rate FMT may be a candidate as an additional strategy to be combined with another main FMT system.

5.5.2.2 Adaptive Fade Spreading – Data Rate Reduction (DRR)

This technique works on a similar principle as adaptive transmission rate. It increases the symbol energy at the receiver by reducing the information data rate. However, an important difference is that it maintains the channel data rate at a constant level and as a result avoids interference problems and the need for a variable receiver filter. The user data is multiplied by a pseudo-random code (the spreading function) with fixed chip rate matched to the available spread spectrum bandwidth. This leads to spreading the data signal to the bandwidth of the pseudo-random code [81]. The ratio between the bandwidth of the spread spectrum signal and the bandwidth of the original data stream is the spreading factor; the higher the spreading factor is, the higher would the gain margin be.

This FMT can be applied only for specific services that would accept extra delay and significant reduction of the information rate such as video download or data transmission (through an increase of transfer duration) though it seems to be difficult to use with voice transmission. In summary, adaptive fade spreading is

indeed better and more practical than the not so sophisticated adaptive transmission rate systems on the other hand it is less attractive than other techniques in its class.

5.5.2.3 Adaptive Coding (AC)

Forward Error Correction (FEC) encoding is a method still used in many communication systems to counteract noisy channels. The introduction of coding allows the addition of redundant bits to the information bits, so as to detect and to correct errors caused by propagation impairments and would ultimately lead to a reduction in the required energy per information bit. Each code is characterized by its rate. As a result of the encoding the code rate is the ratio between information bit rate and the channel bit rate, and its gain which is the reduction in the required energy per channel bit to noise density ratio for the same information bit error rate.

AC consists in implementing a variable coding rate in order to match impairments due to propagation conditions. An adaptive FEC system transmits data with no encoding during clear-sky conditions, during fades the system would introduce a level of FEC but would at the same time keep the channel rate (and as a result bandwidth) constant. Owing to the introduction of forward error correction encoding and decoding, the information rate will be reduced in accordance with the rate of the applied code. Whenever adaptive coding is used in a communication link it is important to make sure that both ends of the link are aware of the code rate in use (i.e. before switching code rate the transmitter must alert the receiver).

The fading satcom's channel does not produce independent errors but blocks of errors. Since most forward error correction codes are designed to improve system performances by correcting errors that are considered independent, they are not very efficient in counteracting fading. The performance of FMT can be improved by using block codes (e.g. Reed-Solomon codes) which are more robust to bursts of errors, and with interleaving, which scrambles the coded data in a manner that, after descrambling, errors can be considered independent [82]. Interleaving is efficient only for very short fades and especially for

scintillation. Greater performances can be obtained by the concatenation of a convolutional code (Viterbi algorithm) with a block code (Reed-Solomon code for example), the convolutional code being efficient at correcting random errors, whereas the block code is a good solution to correct error bursts [74].

Systems that utilize encoding make better use of the channel, an adaptive FEC system should not be very costly and difficult to implement, making it an attractive solution for VSAT applications. The main drawbacks of using this FMT are the complex decoding algorithms that have to be implemented in the receiver in order to decode the signal and extract the information, along with the additional bandwidth requirements for Frequency Division Multiple Access (FDMA) and larger bursts in the same frame for Time Division Multiple Access (TDMA), as a hefty penalty to transmission of redundant bytes.

5.5.2.4 Adaptive Modulation (AM)

A system that uses AM would transmit at its most complex modulation during fine propagation conditions and would reduce the complexity of the scheme due to fades accordingly. To achieve higher system capacity for a specified bandwidth, modulation schemes with high spectral efficiency are to be utilized.

Adaptive modulation is a useful technique that can be implemented to improve the energy efficiency and increase the data rate over a fading channel. Just like adaptive coding, the aim of the adaptive modulation technique is to decrease the required bit energy per noise energy ratio (E_b/N_0) corresponding to a given bit error rate (BER), achieved by reducing the spectral efficiency as the *C/N* decreases. The reduction of the spectral efficiency can be obtained by introducing lower level modulation schemes. As an example, if very efficient modulations such as 16-PSK, 16-QAM, 64-PSK, 64-QAM or 256-QAM can be used in clear-sky conditions then in bad propagation conditions AM makes use of more robust modulations such as QPSK or BPSK [83].

A different approach of reducing the required E_b/N_0 is to introduce coding into the modulation. In [84] such a system was proposed based on adaptive pragmatic trellis coded modulation, suitable for services which can accept a

variable user data rate (i.e. satellite bandwidth occupancy is unchanged on a channel basis). It was shown that such a multiple FMT modem could very significantly outperform systems relying on single FMTs such as AC or un-coded AM.

Other FMT such as reserve capacity (adaptive TDMA – FDMA) will not be discussed in this work. Although reserve capacity can be extremely effective, they are more suited to services like trunk telephony rather than data applications.

5.5.3 Diversity

In order to avoid difficulties resulting from atmospheric perturbation a network re-routing strategy is applied. There are three type of diversity recognized in the field: site, orbit and frequency diversity.

5.5.3.1 Site Diversity (SD)

SD is based on the concept of switching the Earth-Space communication from the station affected by fading to another station located at a distant site. Provided that the distance between the Earth station and its back-up(s) is larger than the expected extent of the rain cells (≈ 10 km to 15 km), so that the probability of joint fade occurring at the two sites simultaneously is low [46]. The concept of this is shown in Figure 5.15.

Site diversity (SD) is one of the fade mitigation methods that take advantage of the finite size of rain cells. The high level of fading at high frequencies is due primarily to the passage of convective rainstorms through the satellite link. Meteorological data showed that such events are generally limited in geographical extent and that the stronger the rainstorm the smaller the rain cell is, therefore if two ground stations are separated by a distance greater than that covered by each rain cell, they will experience statistically independent fading. This technique is usually suited for rain fading; by monitoring the performance of the two stations and choosing the better of the two, a site diversity system can be implemented.

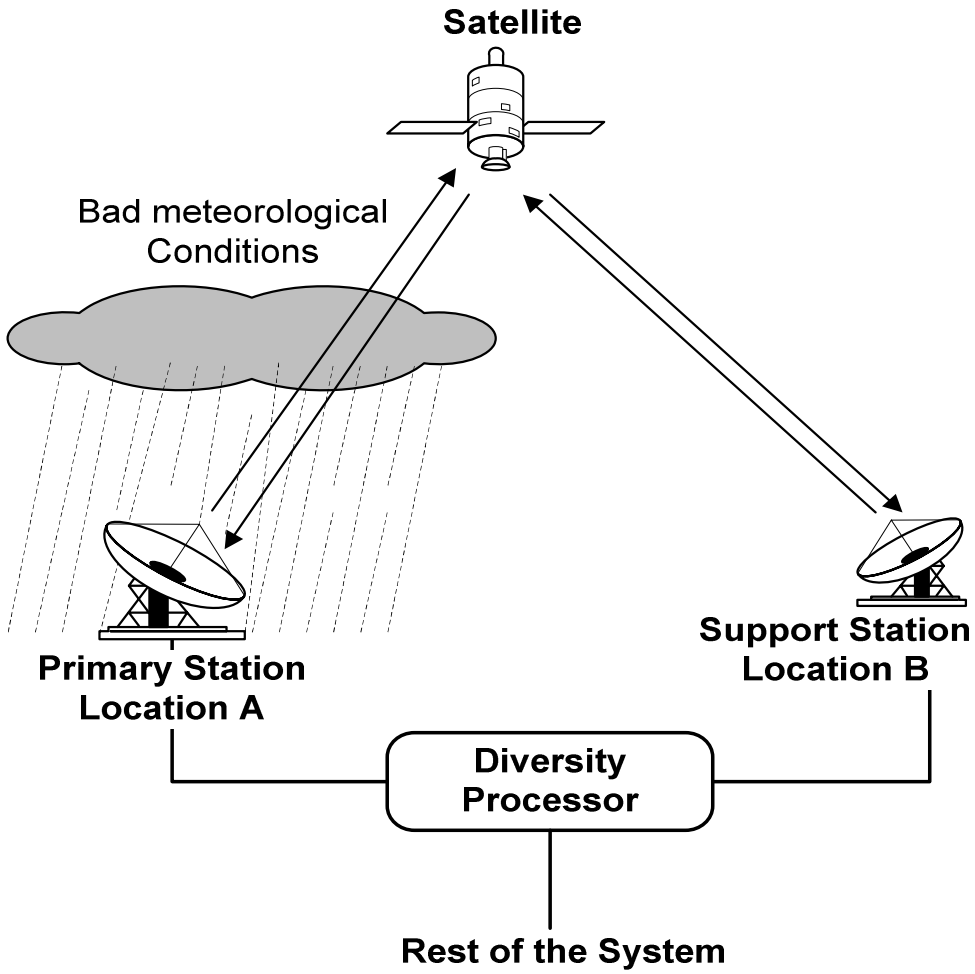

Figure 5.15 Concept of site diversity.

The evaluation of the performance of site diversity (SD) systems requires the knowledge of the joint distribution of attenuation amongst the stations. Diversity models derived from empirical data have been proposed in the literature [85],[86]. They predict a sharp increase of diversity gain for site distances up to 15 km while the improvement stabilizes for greater distances.

Site diversity (SD) is one of the most powerful fade countermeasures techniques, because it is able to counteract deep rain fading occurring at high frequencies and is particularly suited to high availability communication systems. However, various problems arise in the implementation of the site diversity of an operational satellite communication system. Firstly, a suitable

located additional site has to be available and the cost of it must be met. Earth station hardware has to be almost duplicated, a dedicated high reliability terrestrial link of a suitable capacity provided and a monitoring synchronization and switching system implemented. SD is therefore more suitable for systems where quality prevails over price.

5.5.3.2 Frequency and Satellite Diversity (FD and SatD)

SatD consists in setting up two separated spacecraft (or a constellation) so as to provide two separate converging paths to a single ground terminal. In the current Ka-band satellite constellation systems SatD is a big part of keeping degradation away from the service provided. It is considered as a valuable alternative or complement to SD. Although the maximum achievable diversity gain is higher in Site Diversity than in Satellite diversity (SD have Earth stations far enough apart to experience non-correlated fade events which is not the case with SatD and more difficult to attain), SatD is free form terrestrial connections. However, from the operational point of view, the using of SatD implies shifting the antenna pointing from one satellite to another, which ultimately would lead to an interruption of service at some point. This interruption can be minimized if [74] either ephemerides of both spacecraft have been introduced in the Earth station tracking software or if active antennas are used for the ground segment. A dual beam antenna could also be considered.

FD requires payloads using two different frequency band s to available. Whenever fade is detected, the system will switch to the alternative (lower) frequency band payload. There are two techniques that can be implemented with systems utilizing Ka/EHF band as the main carrier and X/Ku as the secondary (back-up) carrier:

- **Cross-shaping frequency diversity:** the up-link and down-link frequency bands are not the same; the transfer is handled by a switch on-board. Both users must be equipped with two terminals (one in each frequency band) in order to counteract propagation conditions.

- **Double-hop frequency diversity:** the information is now sent through a third user that is able to send the message to the original destination in the other frequency band when propagation conditions are becoming extreme.

FD is expensive, because the user must have two terminals. And it is not an optimized method since not all the resources available are used. However, FD can help in guaranteeing extended availability periods on the expense of bandwidth.

5.6 Conclusions

Cloud attenuation is a big contributor to attenuation at Ka/V bands. The clouds attenuation is a slow varying process like rain, which leads to the change of attenuation intensity being steady over even more extended periods.

ULPC is a flexible FMT, since it makes use of only the transmitted Earth station power thus making it possible to utilize for any percentage of time [74]. However, it is governed by the limitations of both the power range (Earth station) and the repeater gain margin for transparent repeaters; which starts to fail for very strong fades. So for areas with low cloud amounts and low LWC it should be applicable (depending on the task and cost, can cope with up to about 15 dB at the hub side).

In practice, for a spot beams size of ($\theta_{3dB} < 0.5^o$) the application of DLPC and OBBS in Ka and EHF bands will allow to lessen the effect of events spread over a landscape of a few hundreds of kilometers. By making the aperture of spot beams not exceeding the rain cell size the efficiency of these FMT would be maximized. Thus making them a good candidate for applying to high time percentages (from large meteorological stratiform configurations, e.g. clouds).

ASP techniques are more suitable for VSAT systems. By using the solid state power amplifiers (SSPA) to the maximum limit of operation that would result in the highest possible data rate available to the user.

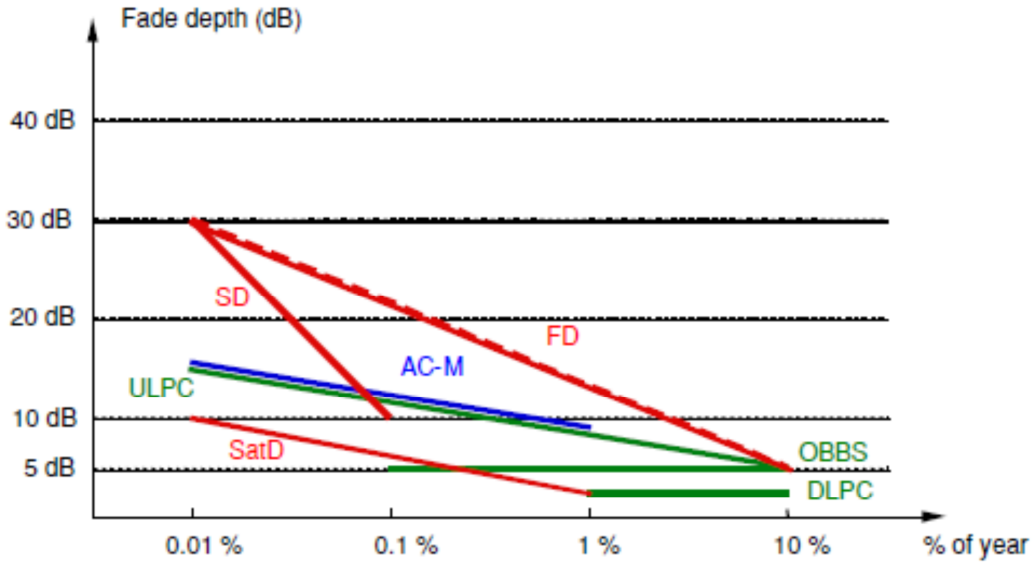

Figure 5.16 Example of FMT availability range at K_a-band [74]

From Figure 5.16 it can be seen that each FMT is adapted to a specific range of availability. Therefore a joint FMT could provide a feasible and powerful method in countering heavy cloud attenuation. Such investigation of joint FMT was carried out by (Chambers, A. [87]) for Ka/V bands (lower frequencies of 11.35-13.87 GHz and V-band of 39.52-80.42 GHz) which asserted the FD and ASP as being both complementary and beneficial for VSAT applications. The FD scheme is inherently good at providing large attenuation margin to a few stations while the ASP scheme has the advantage of providing small attenuation margin to many stations. The ASP is the cheapest while FD or a joint FMT of the two would be more expensive as additional resources (RF equipment) are required at the receiver. Availability percentages of over 99.995% were achieved by implementing FD and ASP. Indeed, the joint FMT of FD and ASP was found not only to perform better for the traffic channel but also would massively benefit the control channel ultimately leading to the control channel being less affected by outage.

SD application is encouraged at the hub for both up-link and down-link (with the appropriate separation distance- for rain it is about 15 km as shown in [85] and [86]) as it would ensure a minimum rate of outage thus allowing for the most time of availability of service. More so, having SD implementation reduces the resources of other FMT need be allocated of the system as well.

There is no simple way of deciding the most appropriate FMTs to utilize as the dynamics of cloud attributes differ considerably from one location to the next and over time (e.g. climate change and sun spots as contributing factors). It is therefore recommended to include cloud statistics for an extended period of time (the more years included the more reflective of the extremes would the results be); thus a period of 11 years (taking into consideration the sun cycle) would be a good time-optimized- interval to describe most of the cloud dynamics at the location of application.

In the next chapter the improved cloud attenuation model is introduced. Data sources treatment and the methodology utilized in the model are explained. Results and verification of the model against the ITU-R model are carried out for both Sparsholt and other global locations.

6 Improved cloud attenuation model

6.1 Introduction

Chapter 2 showed the recent (more accepted) cloud attenuation models in the literature. After comparing these models it was concluded that, the model with potential to deal with higher frequencies based on the ease of use and most flexibility would be the model proposed by ITU-R as will be explained below.

The DAH model has a frequency limitation of up to 35 GHz, needs accurate synoptic data per site of application and has its own preset assumptions regarding the physical attribute of clouds. Whilst the SU model is dependent on the treatment of local radiosonde profiles with a critical humidity function for cloud detection and setting its own assumptions of cloud dimensions making the acquisition of cloud attenuation estimates an involving and expensive process. As for the ITU-R models they consist of preset global maps of normalized LWP probabilities and only the assumption of cloud temperature being set to 0^{o} C thus giving it wide acceptance in the field.

The International Telegraph Union (ITU) cloud attenuation model in-force was ITU-R 840.3 until recently, when the reduced liquid water content maps (L_{red}) source was changed from the ECMWF Numerical Analysis 4 (NA-4) of years 1992-1993 to ECMWF's ERA-40 spanning years 1958-2002. The ITU-R 840.4 is now in-force; ITU-R 840.4 states that the temperature of clouds should be set to 0^{o} C in computing the attenuation (same as ITU-R 840.3). In this chapter this is proven to be inaccurate. Clouds actually have variable temperatures and the net equivalent temperature of the vertical column containing these clouds is not equal to 0^{o} C for many locations.

Here the newest source from ECMWF namely ERA-INTERIM will be utilized. A model that draws on the strengths of the ITU-R models with the aim of having better accuracy than the ITU-R model is introduced. The parameter of concern is the cloud temperature which leads to calculating an *effective temperature* for the site of interest.

6.2 ITU-R 840.4

As previously discussed in section 2.3.4 the ITU-R 840 model recommendations are based on the Rayleigh approximation. To obtain the attenuation due to clouds for a given probability, the statistics of the total columnar content of liquid water L in (kg/m^2) or, equivalently, mm of perceptible water for a given site is needed thus the attenuation is:

$$A_c = \frac{L(p)\, K_l(f,T)}{\sin\theta} \quad \text{dB} \qquad \text{for elevation of } 90^\circ \geq \theta \geq 5^\circ. \tag{6.1}$$

Where θ is the elevation angle in degrees and K_l is the specific attenuation of suspended liquid water droplets (cloud) as a function of frequency and temperature, see Figure 6.1. Because of the dependence of K_l on cloud temperature, the ITU-R 840 statistics of liquid water path were normalized to 0^o C and then the preset value of K_l at 0^o C is used.

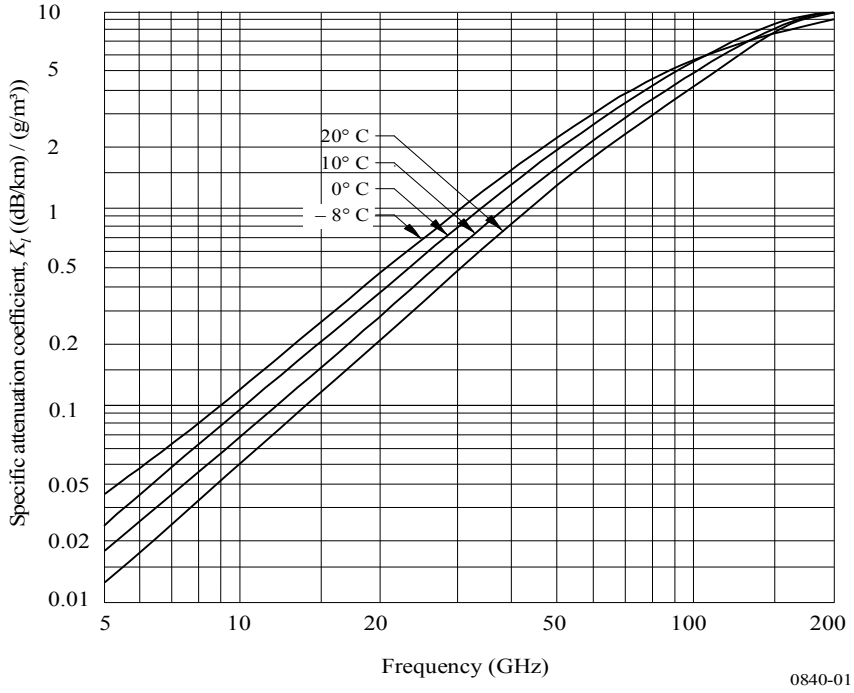

Figure 6.1 Specific attenuation by water droplets at various temperatures as function of Frequency [35]

However, this recommendation still advises (as the previous one) in the case of utilizing regular LWP statistics to still have the K_l parameter calculated based on the setting of cloud temperature dependency to 0^o C. The temperature at which clouds exist is not fixed, as shown for two diverse latitudes cloud temperatures (Figure 6.2 and Figure 6.3) the highest concentration of liquid water is indeed not equal to 0° C. As the latitude increases the physical temperature of clouds (concentration) seems to decrease (Singapore-Sparsholt). Therefore cloud temperature could be an influential factor hence it would need to be incorporated in any prosperous cloud attenuation model.

In the modern era, regular LWP statistics are becoming more abundant and easy to retrieve for different locations across the globe with increased measurement accuracy. There exist various databases sources that span the globe with relatively easy access (some sources are free). For calculating the effective temperature in this project we have opted for the newest publicly (free) available ECMWF data set namely the ERA-INTERM as discussed below.

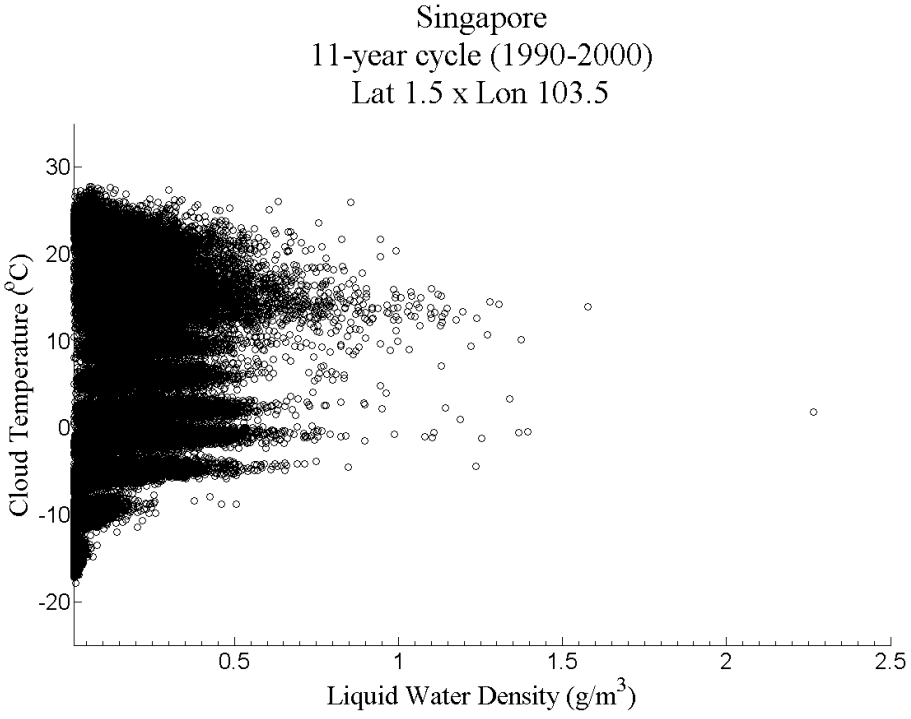

Figure 6.2 Cloud temperature per grid volume (Singapore)

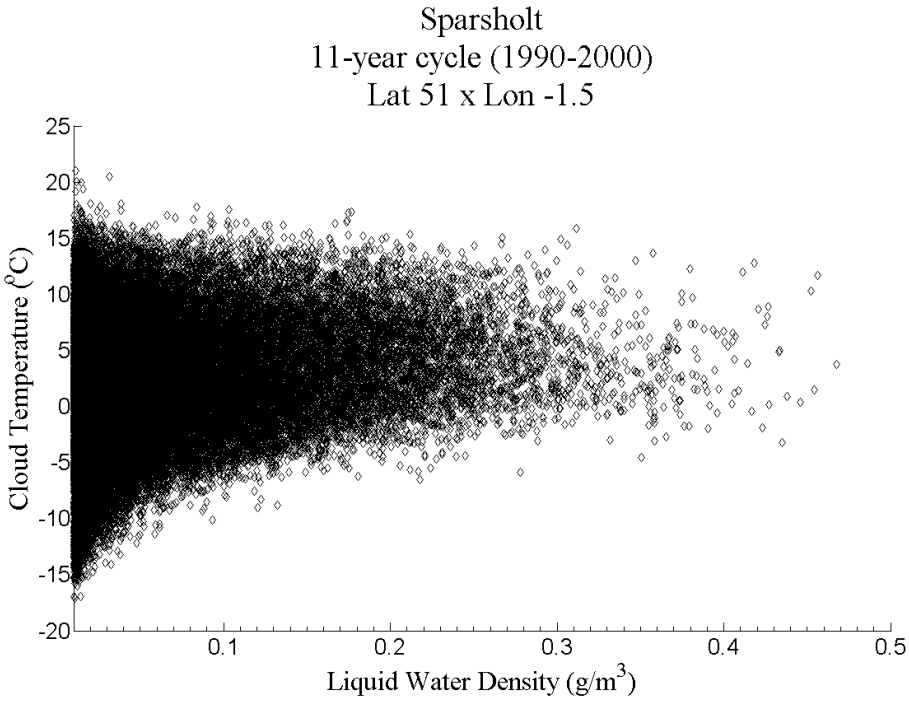

Figure 6.3 Cloud temperature per grid volume (Sparsholt)

6.3 ERA-INTERIM parameters

Based on the qualities of ERA-INTERIM discussed in section 3.8, it was used in calculating the cloud model. There are two main types of the parameters offered by the ECMWF ERA-INTERIM data, namely Analysis and Forecast. Analysis is the reported values by stations all over the globe with quality check on the data and re-tweaking based on the implementation of the ECMWF NWP routines. Forecast is the output of the current forecasting model running at the ECMWF having inputs from reported data of the various meteorological stations. Thus, we have opted in favor of the analysis type. The parameters acquired from this dataset have a resolution of 1.5^{o}x1.5^{o} and are categorized into:

- **Surface level**: parameters acquired or pertaining to surface measurements and observations.
  - Surface pressure (Pa)
  - Total Cloud Cover (prognostic)

- **Upper air pressure level**: parameters acquired of the 37 distinct pressure layers.
  - Temperature (Kelvin)
  - Cloud Liquid Water Content (kg/kg)
  - Cloud Cover (prognostic)

For representation of clouds in large-scale models (NWP), basic simplifications and assumptions are introduced. This stems from the need to define model variables for both clear and cloudy areas within the model grid. Hence, the prognostic variables Total Cloud Cover and Cloud Cover-TCC and CC hereafter- are formulated (computed) [88]. Both parameters have values ranging from 0 (no cloud) to 1 (cloud covering the entire grid-point). We will utilize these parameters in the process of calculating the corrected both cloud Liquid Water Path and Cloud Liquid Water Content –LWP and CLWC, respectively.

It is noteworthy that surface pressure and temperature are directly acquired while the CLWC is in the form of kilograms of liquid water per kilograms of humid air (kg/kg) average of grid-point. Hence in order to get the units of (kg/m^3) of grid-point we need to multiply by the pressure of the corresponding layer P_l and divide by gravity acceleration (g) as defined by the WMO as 9.80665 m/s^2 for all locations and altitudes:

$$CLWC_{\frac{kg}{m^3}} = P_l * CLWC_{\frac{kg}{kg}} * \frac{1}{g} \qquad (6.2)$$

Table 6.1 is provided by the ECMWF in order to supply the coefficients necessary to calculate P_l from model (pressure) levels and hence computing the CLWC. By applying revised and more accurate full pressure level coefficients obtained from the National Center for Atmospheric Research (NCAR) web-site [89] (the information from the website are printed and included at the end of this thesis as an appendix, see Appendix E), we were able to obtain more accurate pressure measurements than the one in the provided

table thus allowing us to have a more trustworthy values of the pressure at any required level. Thus in order to accurately calculate any layer's thickness the coefficients of the upper and lower edges of the layer in question need be acquired first to calculate their pressures then converting them to the equivalent height by:

$$h = \ln(P_o/P) * h_o \quad \text{meters} \qquad (6.3)$$

Where P is pressure in hPa, P_o is the sea level pressure of 1013.25 hPa and h_o the scale height of 7000 meters. Finally subtracting the two calculated heights to acquire the layer thickness in meters.

Table 6.1 ECMWF model and pressure levels

Model levels						Pressure levels (hPa)
k	$A_{k\_1/2}$ **(hP)**	$B_{k\_1/2}$	$p_{k\_1/2}$ **(hPa)**	p_k **(hPa)**	z_k **(km)**	
1	0.00	0.00000	0.00	0.10	64.56	
2	0.20	0.00000	0.20	0.29	57.06	
3	0.38	0.00000	0.38	0.51	53.16	
4	0.64	0.00000	0.64	0.80	50.04	
5	0.96	0.00000	0.96	1.15	47.46	1
6	1.34	0.00000	1.34	1.58	45.27	
7	1.81	0.00000	1.81	2.08	43.33	2
8	2.35	0.00000	2.35	2.67	41.58	3
9	2.98	0.00000	2.98	3.36	39.96	

10	3.74	0.00000	3.74	4.19	38.41	
11	4.65	0.00000	4.65	5.20	36.90	5
12	5.76	0.00000	5.76	6.44	35.40	7
13	7.13	0.00000	7.13	7.98	33.90	
14	8.84	0.00000	8.84	9.89	32.40	10
15	10.95	0.00000	10.95	12.26	30.90	
16	13.56	0.00000	13.56	15.19	29.40	
17	16.81	0.00000	16.81	18.81	27.90	20
18	20.82	0.00000	20.82	23.31	26.40	
19	25.80	0.00000	25.80	28.88	24.90	30
20	31.96	0.00000	31.96	35.78	23.40	
21	39.60	0.00000	39.60	44.33	21.90	
22	49.07	0.00000	49.07	54.62	20.44	50
23	60.18	0.00000	60.18	66.62	19.05	70
24	73.07	0.00000	73.07	80.40	17.74	
25	87.65	0.00008	87.73	95.98	16.50	100
26	103.76	0.00046	104.23	113.42	15.33	125
27	120.77	0.00182	122.61	132.76	14.23	

28	137.75	0.00508	142.90	154.00	13.19	150
29	153.80	0.01114	165.09	177.12	12.21	175
30	168.19	0.02068	189.15	202.09	11.29	200
31	180.45	0.03412	215.03	228.84	10.42	225
32	190.28	0.05169	242.65	257.36	9.59	250
33	197.55	0.07353	272.06	287.64	8.81	300
34	202.22	0.09967	303.22	319.63	8.08	
35	204.30	0.13002	336.04	353.23	7.38	350
36	203.84	0.16438	370.41	388.27	6.71	400
37	200.97	0.20248	406.13	424.57	6.09	
38	195.84	0.24393	443.01	461.90	5.50	450
39	188.65	0.28832	480.79	500.00	4.94	500
40	179.61	0.33515	519.21	538.591	4.42	550
41	168.99	0.38389	557.97	577.38	3.94	
42	157.06	0.43396	596.78	616.04	3.48	600
43	144.11	0.48477	635.31	654.27	3.06	650
44	130.43	0.53571	673.24	691.75	2.67	700
45	116.33	0.58617	710.26	728.16	2.31	750

46	102.10	0.63555	746.06	763.20	1.98	775
47	88.02	0.68327	780.35	796.59	1.68	800
48	74.38	0.72879	812.83	828.05	1.41	825
49	61.44	0.77160	843.26	857.34	1.17	850
50	49.42	0.81125	871.42	884.27	0.95	875
51	38.51	0.84737	897.11	908.65	0.76	900
52	28.88	0.87966	920.19	930.37	0.60	925
53	20.64	0.90788	940.55	949.35	0.46	950
54	13.86	0.93194	958.15	965.57	0.34	
55	8.55	0.95182	972.99	979.06	0.24	975
56	4.67	0.96765	985.14	989.95	0.16	
57	2.10	0.97966	994.75	998.39	0.10	1000
58	0.66	0.98827	1002.02	1004.64	0.06	
59	0.07	0.99402	1007.26	1009.06	0.03	
60	0.00	0.99763	1010.85	1012.05	0.01	
61	0.00	1.00000	1013.25			

6.4 Cloud attenuation model-Effective Temperature

For microwave frequency range the attenuation due to ice is negligible since ice only contributes to signal depolarization. Cloud suspended water particles (liquid) size is small in comparison to the wave-length therefore we can use the Rayleigh approximation of Mie scattering theory. The specific cloud attenuation [39] for a frequency f can be written as

$$\gamma_c = K_l(f, T) \cdot w \qquad (6.4)$$

Where:

γ_c specific attenuation (dB/km) within the cloud.

K_l specific attenuation coefficient as a function of Temperature and frequency (dB/km)/(g/m^3).

w liquid water density in the cloud or fog (g/m^3).

The integrated cloud attenuation is [90]:

$$A = \sum \gamma_{ci} \cdot \Delta l_i = \sum K_l(f, T_i) \cdot w_i \cdot \Delta l_i \qquad (10.5)$$

Where T_i, w_i are the vertical profiles of the specific attenuation coefficient, cloud temperature and liquid water density , respectively. Δl_i (kilometers) is the differential increment of altitude.

In calculating the liquid water density we were faced with a problem. Although ERA-INTERIM is more complex and by contrast better at simulating the processes of the atmosphere, it still has the same limitations inherent in the ERA-40 [91]. Namely the underestimation of liquid content due to its crude resolution and hence a correction of the values needs to be applied. There are two prognostic variables provided, Cloud Cover per profile-layer (CC) and Total Cloud Cover (TCC) that can be utilized. They describe the average portion of the grid-point (layer) affected by clouds in each 6-hour period and account for

the probability of overlapping clouds as seen from the surface. Thus the corrected liquid water density is calculated by dividing the cloud liquid water content provided in ERA-INTERIM (CLWC) by both TCC and CC rather than only by TCC as performed in [91].

Accurate LWP values retrieval would definitely help in producing a better cloud attenuation estimation model. Due to computational rounding and the fact of TCC and CC being *prognostic* and by carefully examining the cloud attenuation at Sparsholt and all other study locations (Figure 6.4 to Figure 6.6), it was found that for optimal liquid water density calculation for all sites of study both TCC and CC should be set to zero for values less than 0.035. This value is the best limit for most of the sites, though near the tropics a lower limit would be better. Nonetheless for a single limit that can be utilized with the ERA-INTERIM data the values 0.035 is recommended.

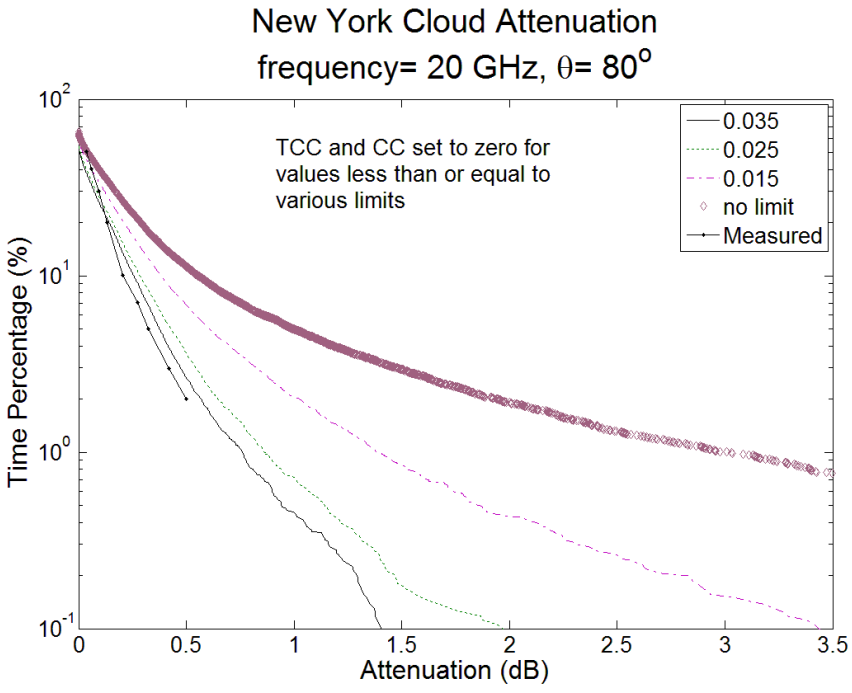

Figure 6.4 TCC & CC limiting effect on cloud attenuation estimation, New York.

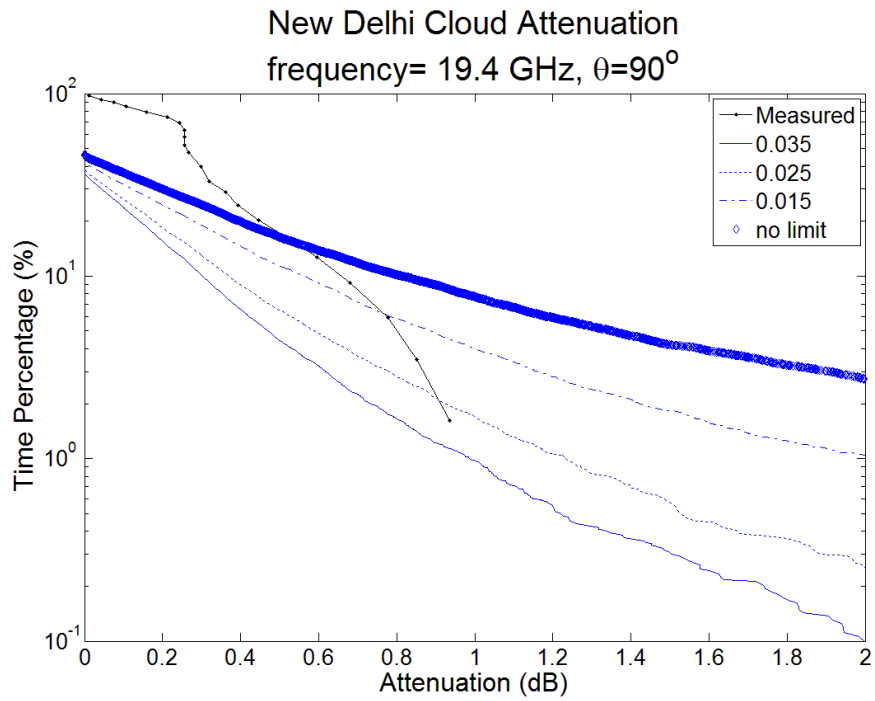

Figure 6.5 TCC & CC limiting effect on cloud attenuation estimation, New Delhi.

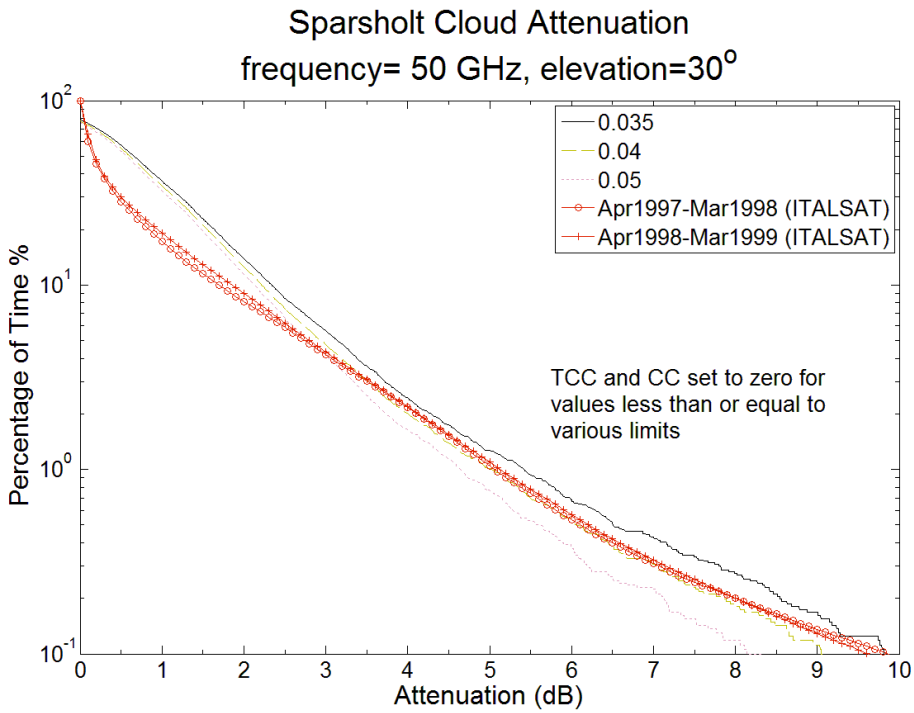

Figure 6.6 TCC & CC limiting effect on cloud attenuation estimation, Sparsholt.

Now, if we look at the spread of the specific attenuation due to variation of temperature values in Figure 6.7 we can consider:

$$\gamma_{ci} = K_l(f, T_f) \cdot w_i + \varepsilon_i \tag{6.6}$$

Here, T_f is an effective cloud temperature and ε_i is random error due to the spread of cloud temperature for the corresponding liquid water density values. Thus by incorporating (6.6) into (6.5) the integrated attenuation is:

$$A = K_l(f, T_f) \cdot L + \varepsilon \tag{6.7}$$

With

$$L = \sum w_i \cdot \Delta l_i \tag{6.8}$$

Where L is LWP and $\varepsilon = \sum \varepsilon_i \cdot \Delta l_i$ is the error which is assumed to be independent and identically distributed and to follow the normal distribution.

Finally, T_f is estimated utilizing the weighted least square regression method. See Figure 6.8 to Figure 6.10.

The above cloud attenuation model is based on zenithal orientation (elevation angle of 90°). Thus, in order to incorporate slant-path propagation when calculating the attenuation the relation [$1/\sin\theta$] is used which is valid for elevations higher than 5°. Thus the cloud model would be:

$$A = K_l(f, T_f).\, L/\sin\theta \tag{6.9}$$

Table 6.2 shows all the values of calculated effective temperatures pertaining to the study sites' frequencies.

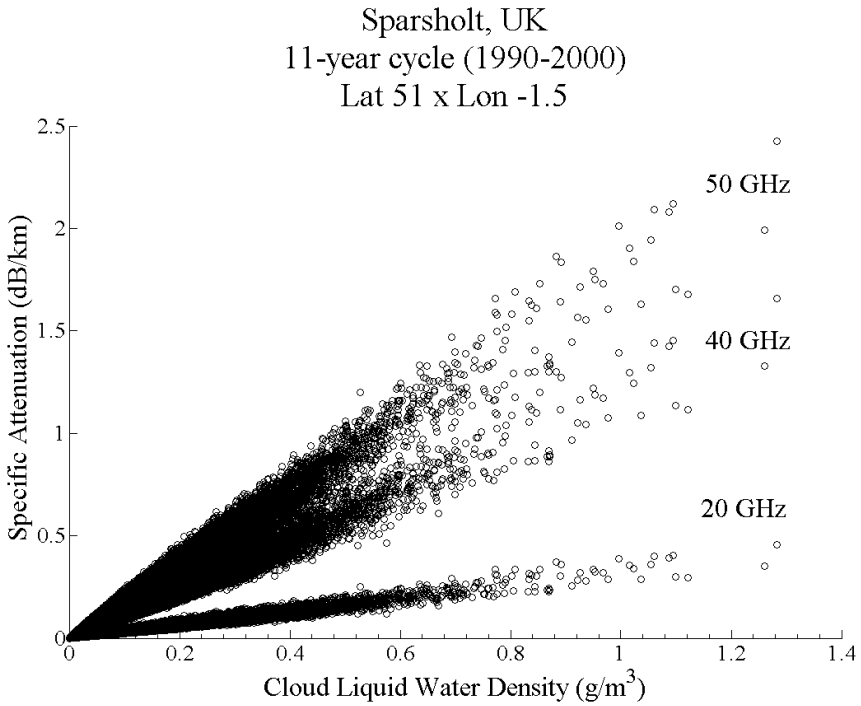

Figure 6.7 Spread of Specific attenuation for different temperatures (Sparsholt)

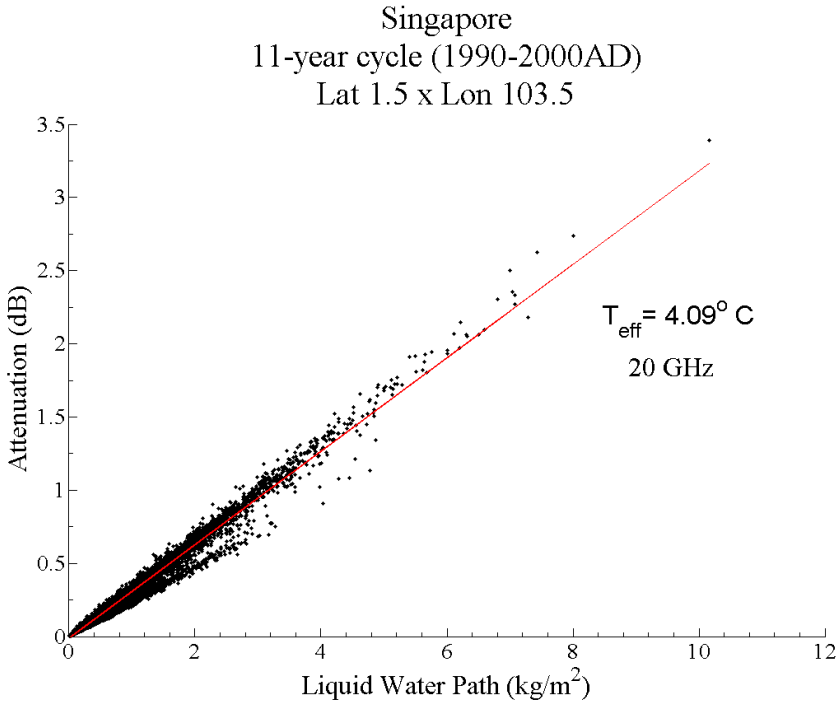

Figure 6.8 Least square regression for effective temperature calculation (Singapore)

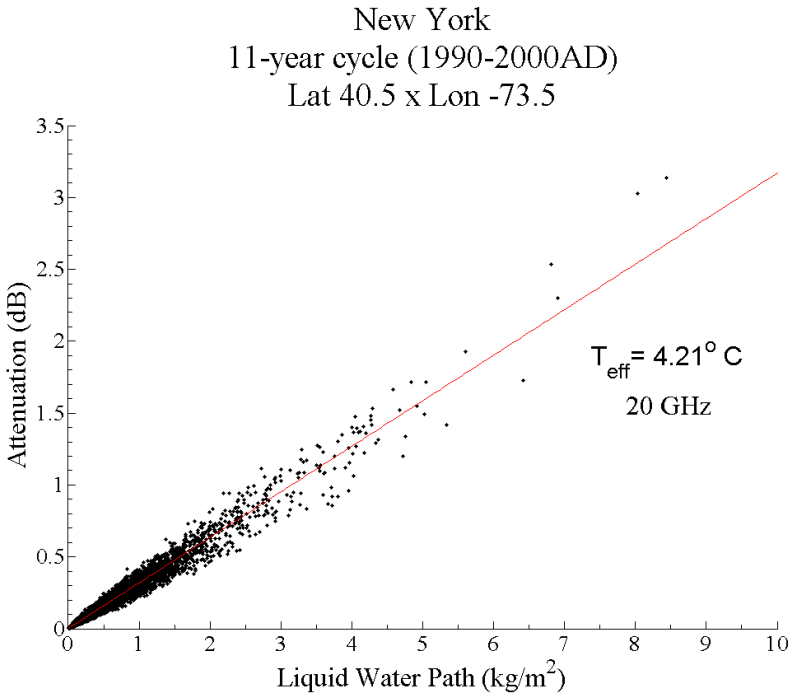

Figure 6.9 Least square regression for effective temperature calculation (New York)

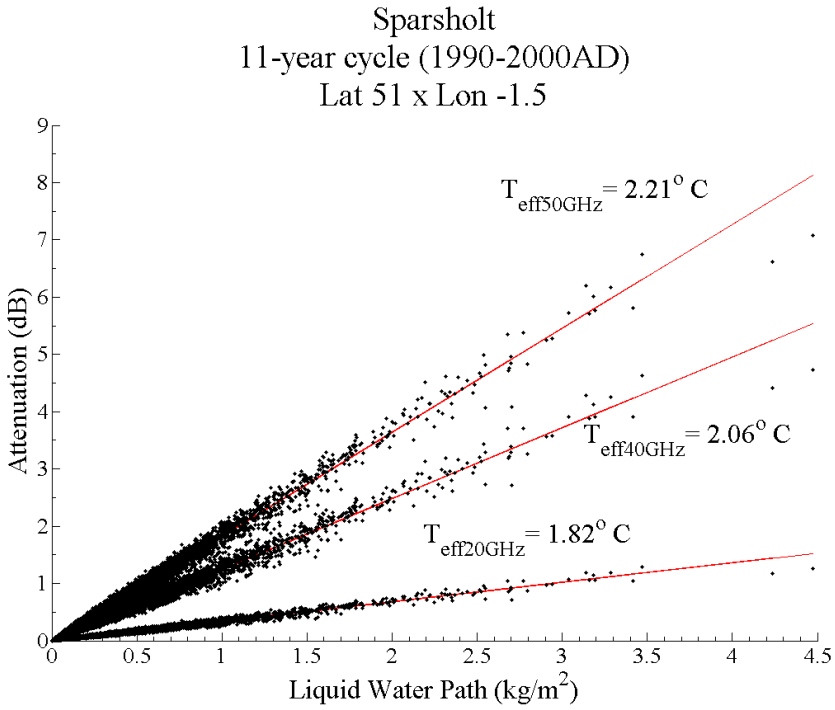

Figure 6.10 Least square regression for effective temperature calculation (Sparsholt)

Table 6.2 Effective Temperatures of study locations

Location	Grid-Point		Measurement Frequency (GHz)	Effective Temperature (^{o}C)
	Lat	Lon		
New Delhi	28.5	76.5	19.4	2.56
Singapore	1.5	103.5	20.0	4.09
Madrid	40.5	-3.0	50.0	2.14
Kolkata	22.5	88.5	40	5.16
Sparsholt	51.0	-1.5	20, 40, 50	1.82, 2.06, 2.21
New York	40.5	-73.5	20.0	4.21
Malaysia	4.5	100.5	12.255	4.65

6.5 Results and comparisons

The cloud model gave good estimations. It can be seen from (Figure 6.11 to Figure 6.19) that the cloud model better estimates than the ITU-R 840.3 on almost all probability percentages. As for ITU-R 840.4 for fairly high probabilities the performance varied for different locations however, the cloud model estimation was better at the lower probability percentages (less than 0.8%) for all locations, as can be seen from Table 6.3 to Table 6.5.

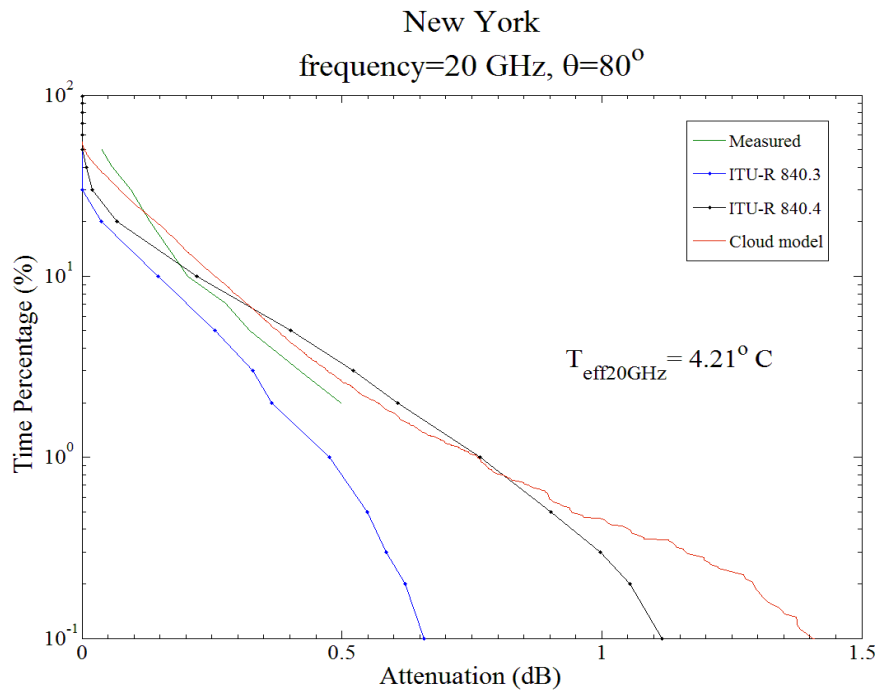

Figure 6.11 Cloud attenuation for New York (20 GHz)

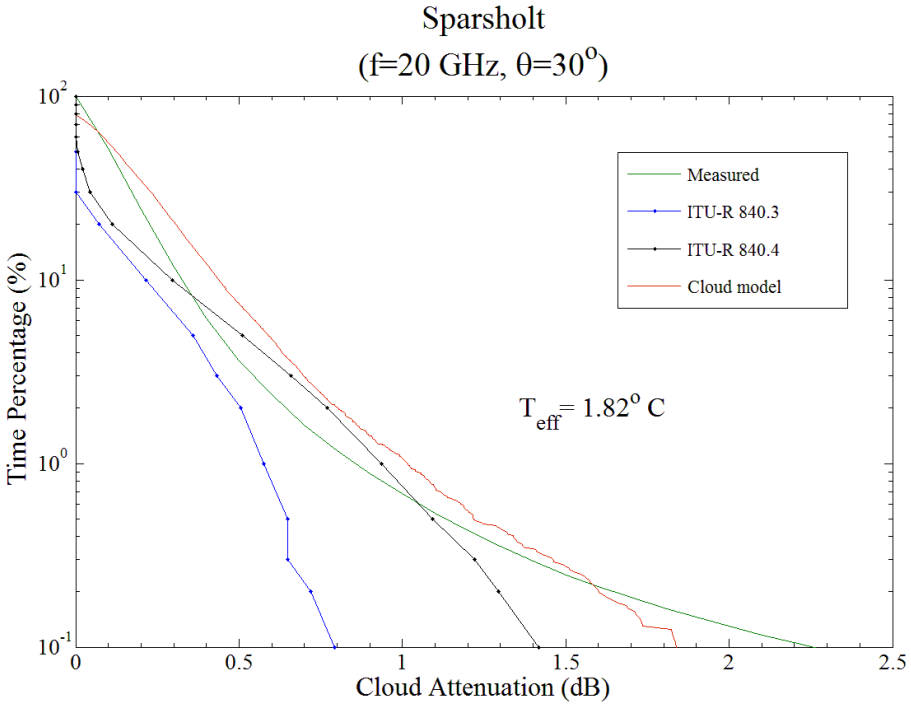

Figure 6.12 Cloud attenuation for Sparsholt (20 GHz)

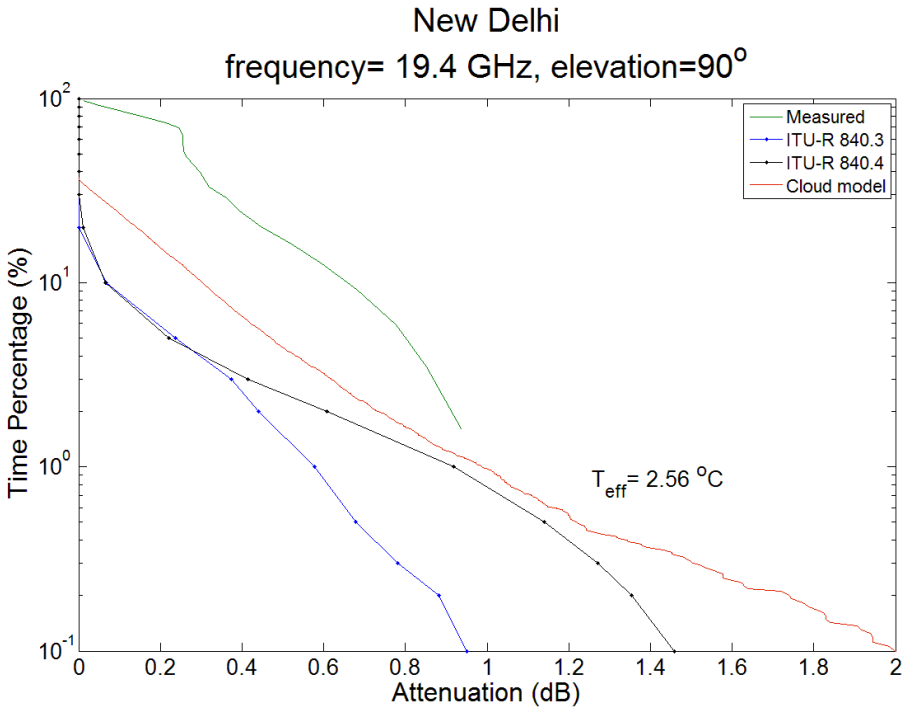

Figure 6.13 Cloud attenuation for New Delhi (19.4 GHz)

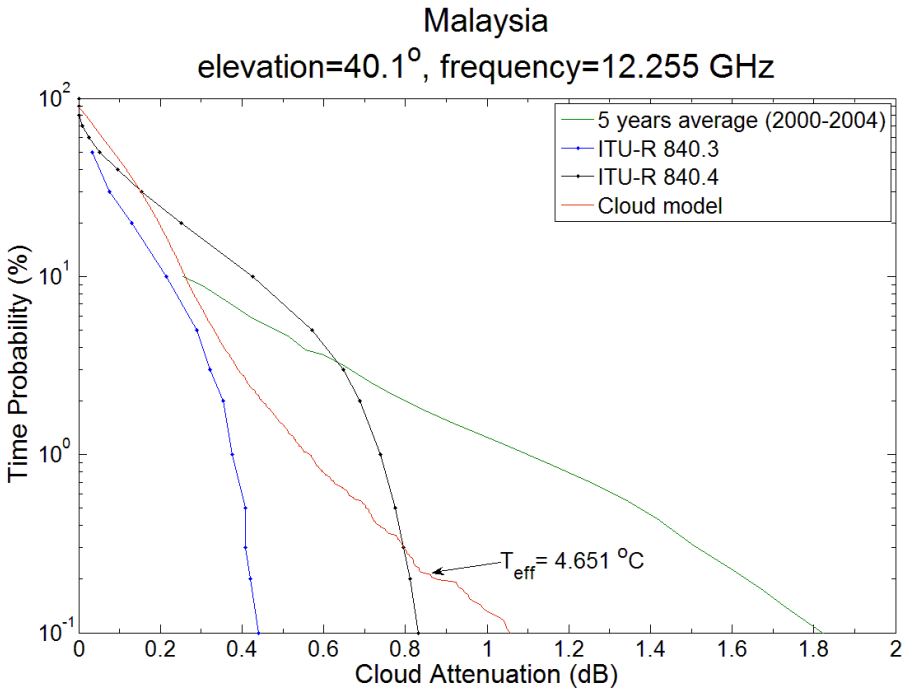

Figure 6.14 Cloud attenuation for Malaysia (12.255 GHz)

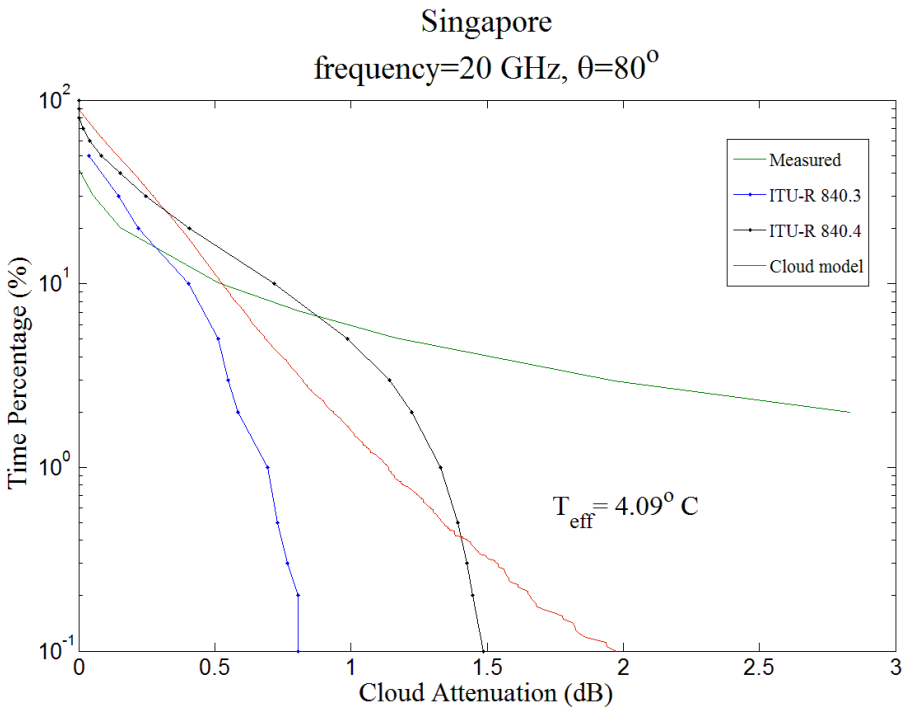

Figure 6.15 Cloud attenuation for Singapore (20 GHz)

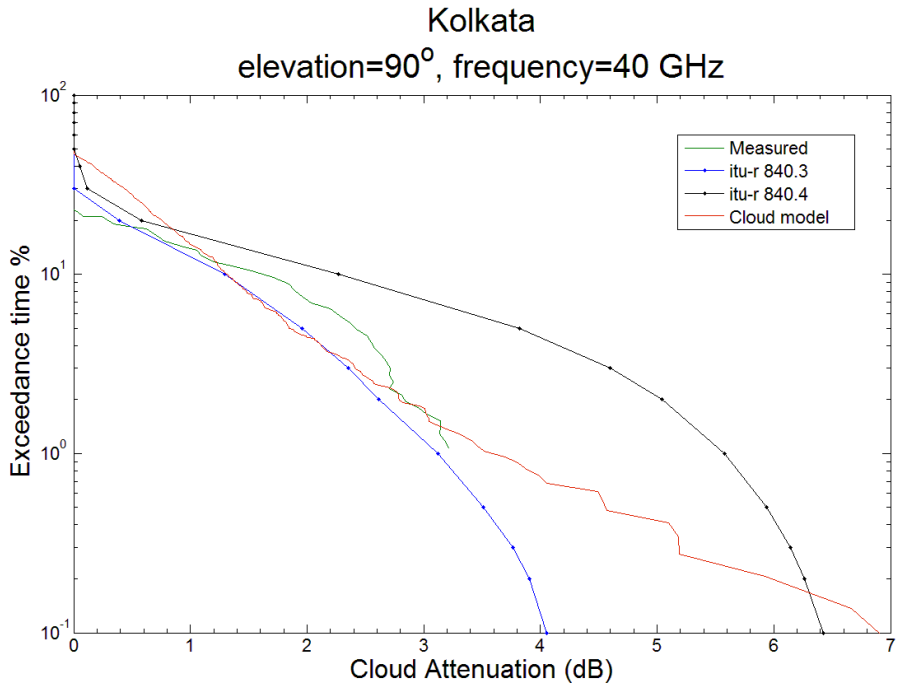

Figure 6.16 Cloud attenuation for Kolkata (40 GHz)

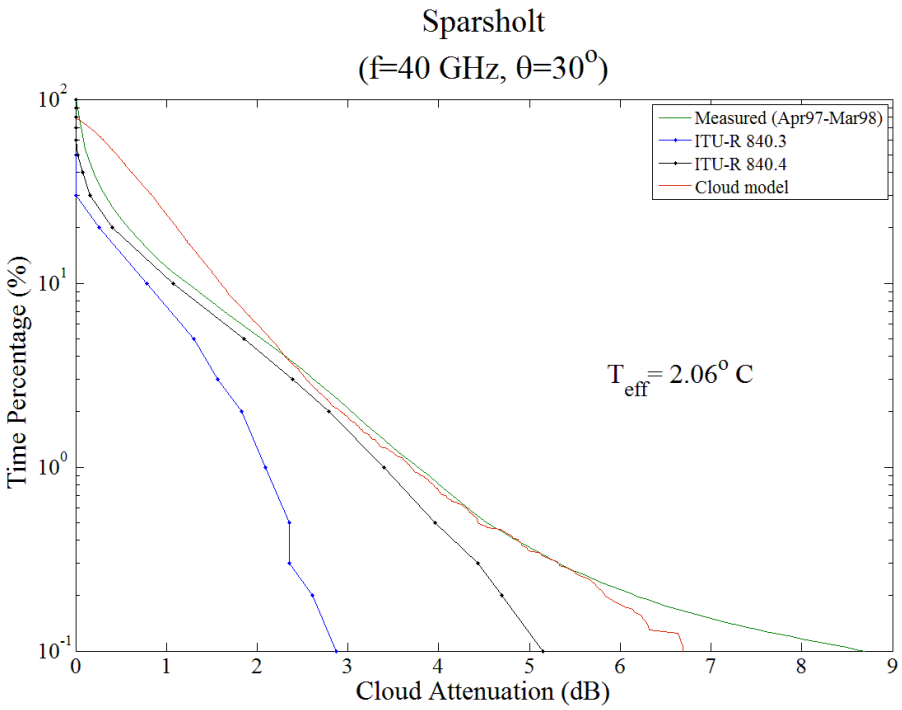

Figure 6.17 Cloud attenuation for Sparsholt (40 GHz)

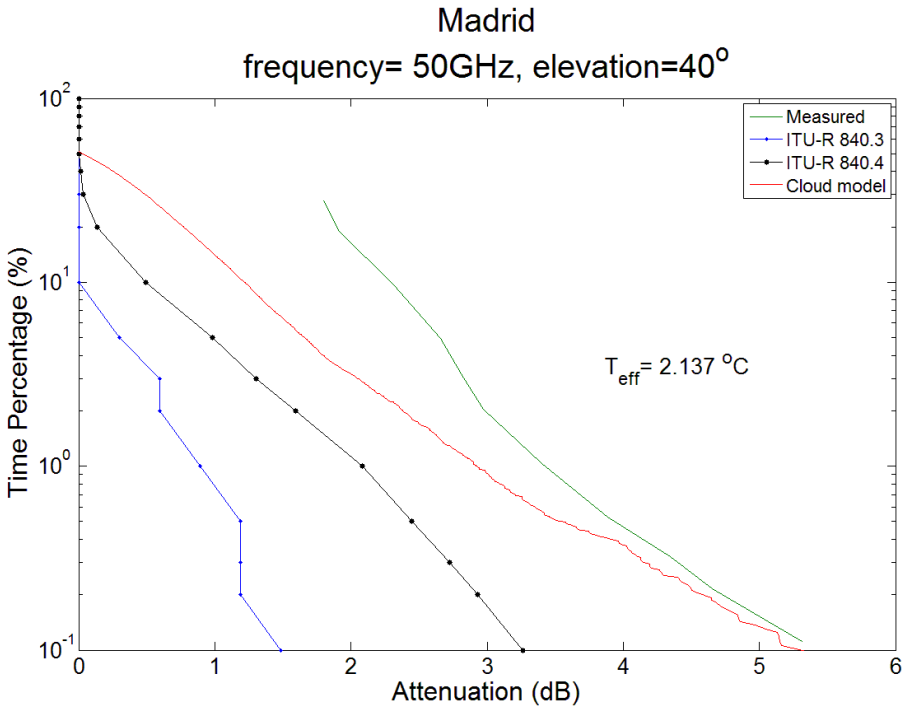

Figure 6.18 Cloud attenuation for Madrid (50 GHz)

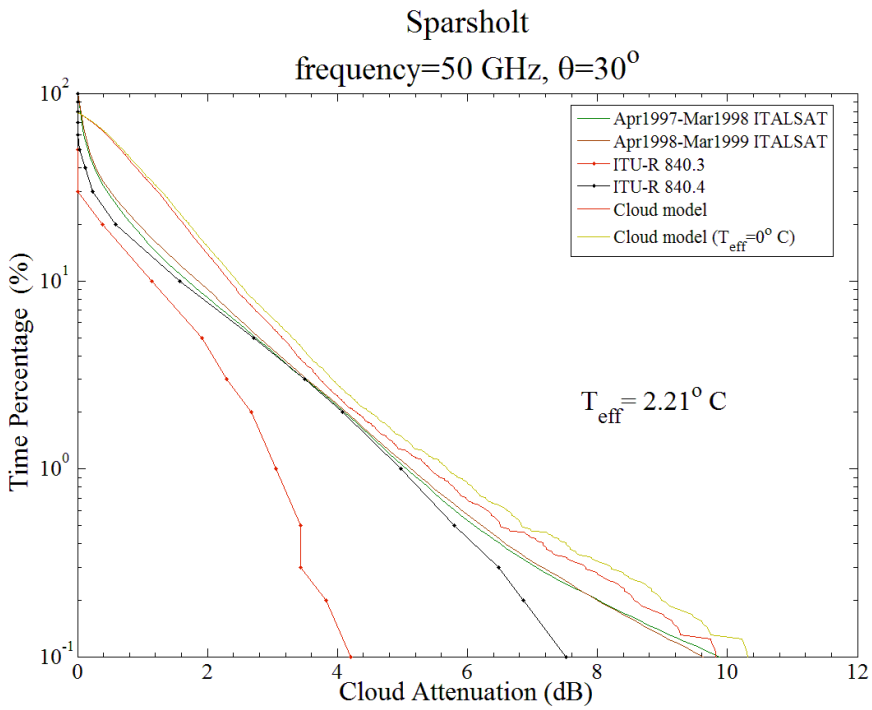

Figure 6.19 Cloud attenuation for Sparsholt (50 GHz)

Table 6.3 Low probability cloud attenuation values (part 1)

Study Location		Frequency GHz	Elevation θ°	Measured (dB) @ 10%	1%	0.10%	ITU-R 840.3 (dB) @ 10%	1%	0.10%
New Delhi		19.4	90	0.66	0.94	N/A	0.07	0.58	0.95
Singapore		20	80	0.52	2.83	N/A	0.4	0.69	0.8
Madrid		50	40	2.3	3.42	5.31	0	0.89	1.49
Kolkata		40	90	1.62	3.22	N/A	1.3	3.13	4.05
Sparsholt	Apr-97	20	30	0.33	0.85	2.24	0.22	0.58	0.79
	to	40	30	1.23	3.77	8.6	0.78	2.09	2.87
	Mar-98	50	30	1.69	5.05	9.6	1.15	3.06	4.2
New York		20	80	0.2	0.5	N/A	0.15	0.48	0.66
Malaysia		12.255	40.1	0.25	1.1	1.82	0.21	0.38	0.44

Table 6.4 Low probability cloud attenuation values (part 2)

Study Location		Frequency GHz	Elevation θ°	ITU-R 840.4 (dB) @ 10%	1%	0.10%	Cloud Model (dB) @ 10%	1%	0.10%
New Delhi		19.4	90	0.07	0.92	1.46	0.3	0.99	2
Singapore		20	80	0.72	1.33	1.49	0.52	1.14	1.97
Madrid		50	40	0.49	2.08	3.27	1.22	2.92	5.3
Kolkata		40	90	2.27	5.58	6.43	1.31	3.58	6.9
	Apr-97	20	30	0.3	0.94	1.42	0.44	1.01	1.84
Sparsholt	to	40	30	1.07	3.4	5.14	1.59	3.7	6.69
	Mar-98	50	30	1.57	4.97	7.52	2.34	5.42	9.81
New York		20	80	0.22	0.77	1.12	0.26	0.76	1.4
Malaysia		12.255	40.1	0.43	0.74	0.84	0.26	0.57	1.06

Table 6.5 Error percentage of models to cloud attenuation measurements at low probability

Study Location	ITU-R 840.3 error (%) 10%	1%	0.10%	ITU-R 840.4 error (%) 10%	1%	0.10%	Cloud Model error (%) 10%	1%	0.10%
New Delhi	89.39	38.30	N/A	89.39	2.13	N/A	54.55	5.32	N/A
Singapore	23.08	75.62	N/A	38.46	53.00	N/A	0.00	59.72	N/A
Madrid	100.00	73.98	71.94	78.70	39.18	38.42	46.96	14.62	0.19
Kolkata	19.75	2.80	N/A	40.12	73.29	N/A	19.14	11.18	N/A
	33.33	31.76	64.73	9.09	10.59	36.61	33.33	18.82	17.86
Sparsholt	36.59	44.56	66.63	13.01	9.81	40.23	29.27	1.86	22.21
	31.95	39.41	56.25	7.10	1.58	21.67	38.46	7.33	2.19
New York	25.00	4.00	N/A	10.00	54.00	N/A	30.00	52.00	N/A
Malaysia	16.00	65.45	75.82	72.00	32.73	53.85	4.00	48.18	41.76

As expected from the attenuation curves of the specific attenuation coefficient (Figure 6.1) if the temperature of 0^o C was to be used in the cloud model, that would have led to an overestimation of the cloud attenuation (e.g. cloud model T_{eff}=0 curve in Figure 6.19). Therefore the combination of effective temperature and accurate LWP would produce more accurate values for cloud attenuation especially at high frequencies.

6.6 Effective temperature and ITU-R maps

In order to utilize the effective temperature values with the ITU-R models we first need to convert the statistics of normalized LWP-section 2.3.3- back to regular (un-normalized) ones provided by the recommendations then plug the effective temperature at the frequency of operation into the specific attenuation coefficient. Since the process in which normalization was performed (to cover the frequency range of 20-60 GHz) is solving for LWP at frequency of 43 GHz [44] at 0 Celsius, to revert it back we solve for the same frequency but now with the new corresponding calculated effective temperature obtained from the cloud model.

$$LWP\ (f,t) = normalized \qquad LWP\ (43_{GHz}, 0^o) = LWP\ (43_{GHz}, T_{eff}) \tag{6.10}$$

And the converted ITU-R model is

$$A_{converted} = \frac{L(p).K_l(f,T_{eff})}{\sin\theta} \tag{6.11}$$

With the LWP statistics recovered from the ITU-R normalized maps, the effective temperature of frequencies higher than 60 GHz can now be used… see below.

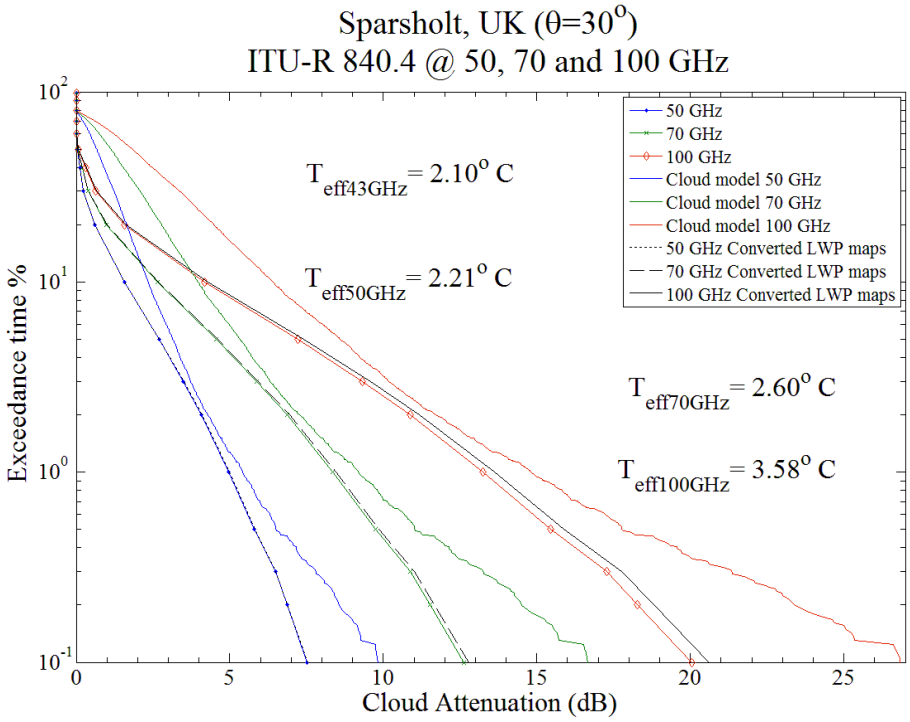

Figure 6.20 Simulation of effective temperature impact at higher frequencies (Sparsholt)

6.7 Conclusions

High availability satellite systems similar to other terrestrial communication systems require high availability percentages as near to 100% as possible. Hence this aspect is taken into consideration in the design of a satellite system in order to give us that little more to reach (if possible) the maximum availability. The model introduced in this thesis (with the better and more accurate performance at these low percentages) provides a better tool for the communication satellite system designer. This model would give the system designer information on the probability of any predefined level of fading that would be exceeded in terms of the percentage of the time in an annual period thus helping in calculating a more accurate system fade margin in conjunction with the mandatory link availability. This new model's accuracy of predicting attenuation at lower probabilities is verified and proven to be better than the ITU-R model. The knowledge of the cloud attenuation at these low percentages

is important as they indicate the maximum theoretical attenuation levels the site is expected to experience at the corresponding frequency. Thus aiding the system designers in calculating the system fade margin. Based on this (depending on service type and availability constraints) the proper FMTs can be implemented leading to optimal design.

The new cloud model is relatively easy to implement as it uses the ECMWF's ERA-INTERIM public (free) data sets. The model shows the potential of NWP data in estimating accurate cloud attenuation for the various global locations. Therefore resources (radiometers, radiosonde) along with money and time can be saved while obtaining accurate results.

In the case of Sparsholt, and other mid-latitude locations the new cloud model gives a very good approximation of cloud attenuation whilst at Singapore (near-tropic) it underestimates the attenuation (same as with the ITU-R model). Note that at lower probabilities (1% and lower) the cloud model seems to better approximate than the ITU-R.

The effective temperature at New York was higher than at Singapore. This can be related to the arrangement and concentration of the suspended water droplets within the clouds in the different layers of the atmosphere. At all locations of study the effective temperatures were more than 1.8^{o} C. It was noted that the higher the frequency, the higher is the effective temperature at the corresponding site (Sparsholt). Again, although Madrid is located at lower latitude than Sparsholt, its effective temperature at 50 GHz was lower.

The new ITU-R 840.4 has better LWP measurements than the previous release (ITU-R 840.3) hence, it is better at estimating the attenuation than the previous one. Looking at the converted ITU-R 840.4 curve that utilizes the effective temperature measured at Sparsholt, it can be observed that for 50 GHz it starts to add to the estimation (compared to the original ITU-R 840.4). This is the direct result of how the normalized LWP was calculated. In order to eliminate the temperature factor from the specific attenuation calculation for frequency range of 20-60 GHz the middle frequency of 43 GHz was utilized. Therefore it is

expected that the converted ITU-R 840 curve will also start underestimating for frequencies less than 43 GHz.

For higher frequencies the effective temperature would start to play an even bigger role in accurately predicting the cloud attenuation (Figure 6.20). The frequency range of 52-68 GHz is where the Oxygen absorption bands are located, therefore it shouldn't be considered for satellite communication. As for ice attenuation, the absorption attenuation of pure ice particles is negligible at microwave frequencies due to its low imaginary component of the refractive index. However, attenuation due to scattering starts to be considerable above 100 GHz (refer to [14] page 170) thus the Rayleigh based models should be sufficient for up to 100 GHz.

The model performed best at non tropic climate sites. Therefore in order to better the prediction accuracy at tropic and near tropic sites more investigation is deemed necessary.

7 Conclusions-further work-Publications

7.1 Conclusions

7.1.1 Introduction

Satellite communications have been in service for over 50 years. In the early 1970's satellite communications operated mainly at C-band. These satellites provided a low capacity at a relatively high cost, and had a short lifespan about 1½ to 2 years only. Nevertheless, since that time there has been an explosive growth for telecommunication services that are either only feasible via satellite or very cost effective if implemented by that means. There were over 700 Ku-band satellites planned or in operation globally at the beginning of the millennium [92].

The need to both provide new services and greater bandwidth has prompted a steady growth in the utilization of higher frequencies in the Ku-band and above. By moving to higher frequencies to introduce new services, many advantages can be attained such as smaller antennas, and smaller satellite footprints that give higher EIRP and permit frequency reuse. The key problem though is that they are now subject to more severe propagation degradation.

In order to provide the same performance as in the lower frequency bands, an unreasonably large margin would be required. Considering that this power margin is needed only occasionally, this is clearly uneconomical. At Ka-band and above atmospheric degradation becomes so severe that the need for adaptive methods or fade countermeasures (FCMs) would be necessary to achieve the high standards of availability [77].

Liquid water bearing clouds are becoming more important in the field of satcoms as they no longer can be considered transparent to the higher frequency microwave link (above 10 GHz). They are present for an extended amount of time and depending on the climate and location they can severely affect satellite-earth links.

Therefore, better understanding and more accurate modeling of cloud attenuation are vital for the reliable design and operation of low availability systems in order to have an accurate link budget.

This project has considered several aspects of cloud attenuation factors. It started with an overview of literature review in the first chapter. Followed by the theory and description of accepted-recent- cloud attenuation models in chapter 2. Then followed up by a description of the pre-processing, validations, sources and assumptions made in order to conduct the analysis of the cloud attenuation in this work (chapter 3). Afterwards a 2 part analysis of Meteorological and local tropospheric degradation was carried out in chapter 4. That was followed by an overview of cloud fade statistics and suggested methods to counter their effects (chapter 5). Finally in chapter 6 the improved cloud attenuation model and the enhancement of the currently accepted cloud attenuation model (ITU-R 840.4) by terms of validating the effective temperature concept and methods of acquiring it.

7.1.2 Cloud attenuation considerations

The classification of clouds is not a fully descriptive one. As was seen in chapter 1, the accepted classification of clouds is based mainly on visual traits and altitude. This in turns leads to ambiguities on the matter of Liquid Water Content (LWC) and its distribution in each identified cloud genre. Therefore the accepted model in the literature that deals with the genre of clouds, namely the DAH-model as a consequence has the limitation of at most being applicable for up to 35 GHz (section 2.3.2). Due to the un-static nature of clouds of the same genre it is concluded that for accurate cloud attenuation modeling the sole dependence on synaptic is discouraged.

The Rayleigh scattering theory approximation is the preferred choice when tackling the issue of suspended water droplets in clouds when attempting to produce viable cloud attenuation models. Indeed, it is easier to utilize than the exact analytical solution by Mie and can for the droplets size of up to 50 microns produce the same attenuation values as the Mie theory for up to 300 GHz. Hence the practice is to incorporate the Rayleigh scattering theory

approximation in the development of accurate (and relatively easy) cloud attenuation models for the millimeter frequency range and above (chapter 2).

7.1.3 Statistical Analysis

The seasonal cloud attenuation at Sparsholt for the period of April 1997 to March 1998 showed that at the higher frequencies of 40 and 50 GHz the maximum cloud attenuation was experienced in August (summer) whilst the lowest cloud attenuation at the same frequencies was measured in February (winter).

Link budget engineers use annual and worst month cumulative distribution functions to compute the link budget for any new satcom system. These functions would give the system designer information on the probability of any predefined level of fading that would be exceeded in terms of the percentage of the time in a monthly or annual period. Based on these statistics and the mandatory link availability, the system fade margin is calculated. Worst month statistics were always higher than the yearly ones as seen in section 4.1.2.

Earlier attempts were made to produce cloud attenuation models that depended on the meteorological parameters at the site of operation, namely the surface temperature, pressure and relative humidity. Not surprisingly, the estimations resulted from such models were always either localized, for a low frequency of operation or was the result of pure mathematical methods needing the actual empirical data in order to fit it per site.

In this project, an attempt to find a strong correlation of the meteorological parameters with signal attenuation was not successful. Neither the daily nor monthly investigation of relative humidity along with surface pressure and temperature resulted in any strong correlation between either of these parameters and the measured cloud attenuation at Sparsholt.

Then a study of synoptic data in an effort to extend the DAH model to higher frequencies was performed however it proved a most difficult task as expected from chapter 4. A full study of localized tropospheric degradation at 20, 40 and 50 GHz for the period of April1997-March1998 was conducted thus proving the

lack of the ITU-R 840.3 cloud attenuation model to accurately predict cloud attenuation at lower probabilities.

7.1.4 Effects of clouds on communications systems

Statistics of observed durations of cloud fades of the ITALSAT satellites at 20, 40 and 50 GHz were presented for various threshold signal levels. The analysis showed that levels of fade reaching 10 dB can last for about 400 seconds (6.7 minutes) while for the same fade level at 20 GHz the attenuation was about 180 seconds (3 minutes). On the larger scale, the annual statistics show that the link at 40 and 50 GHz at the total fade durations at 10 dB level can reach well above 10000 seconds (2.7 hours) as compared with the 20 GHz for the same 10 dB level of less than 500 seconds (8 minutes). This clearly demonstrates the impact of clouds on attenuation dynamics when operating at higher frequencies for the same conditions at the site.

Examination of some adaptive Fade Countermeasures techniques (FCM) also known as Fade Mitigation Techniques (FMT) applicable to satcoms was conducted in chapter 5. Due to the dynamic nature of clouds and their attribute variability at different parts of the world and also at different seasons, there is no simple way of deciding the most appropriate FMTs to utilize as a standard. As some places might not have high liquid water bearing clouds covering them whilst others might be covered by such clouds for an extended amount of time.

Based on the priorities of the system design and services to be provided, for VSAT the combination of Frequency Diversity (FD) and Adaptive Signal Processing (ASP) was reported to achieve acceptable availability for demanding services such as internet access at V-band [87].

As for hubs and Earth stations, the proper implementation of site diversity would lead to minimum outage periods and reduce the resources of other FMT needed to be allocated of the system. However, whether these solutions are feasible economically needs further investigation [85], [86].

7.1.5 Improved prediction model

The improved cloud model presented in chapter 6 was constructed and compared with both ITU-R 840.3 and 840.4. It was found to better estimate all over compared with the ITU-R 840.3. As for the newer ITU-R 840.4 the model was comparable yet at lower probabilities the improved model was better at estimation.

The provided ECMWF ERA-INTERIM parameters were refined by the methods discussed by the National Center for Atmospheric Research (NCAR), see Appendix E. The new model has been validated using long-term measurement results from around the globe from different sites, in different climates and operating at different elevation angles and frequencies.

The model shows the potential of Numerical Weather Prediction (NWP) data in estimating accurate cloud attenuation for the various global locations. Therefore resources (radiometers, radiosonde) along with money and time can be saved while obtaining accurate results.

The cornerstone of the improved model is in the actual consideration of the cloud temperature and calculating an “effective temperature” which would account for the temperatures of all clouds available in the path between the satellite and the receiver rather than setting the temperature to zero Celsius. In order to make use of the already compiled LWP (global) statistics provided by the ITU-R, a method was developed to convert these maps to regular (un-normalized) LWP since these maps inherently have statistical stability (~ 40 years) and in the absence of reliable local LWP statistics would be a viable tool in designing satcom systems.

The model performed best at non tropic climate sites. Therefore in order to better the prediction accuracy at tropic and near tropic sites more investigation is deemed necessary.

7.1.6 Original Aspects of the Research

In summary, the novel aspects of the research carried out in this project are considered to be:

- Pre-processing of RAL's Sparsholt-ITALSAT beacon measurement at 18.7, 39.6 and 49.5 GHz.
- Analysis of beacon data and study of the distribution of cloud attenuation
- Study of the dependence of cloud attenuation on surface parameters namely the relative humidity, temperature and pressure.
- Study of cloud attenuation fade statistics and the implications on the choice and design of fade countermeasures.
- Development of a new improved cloud attenuation prediction model. The model was validated by data acquired from Asia, Europe and the USA.
- Provided a means to utilize the already available ITU-R reduced liquid water path maps in lieu of ECMWF ERA-INTERIM.

7.2 Further work

It will be useful to build a database of effective temperature per grid point location for high frequencies. The suggested frequencies to include would be 43, 50, 70 and 100 GHz. The inclusion of the 43 GHz frequency is for the conversion of the ITU-R normalized LWP maps, thus making use of the statistical stability of these files. That way the engineer could look up the frequency of operation and in lack of local and reliable LWP statistics can utilize the ITU-R model for better estimation of cloud attenuation per location of application.

Another issue to follow is the unified presetting of the Total Cloud Cover (TCC) and Cloud Cover (CC) values to zero for values lower than 0.035. There might be a different value per distinct climate (e.g. tropics, near-tropics, temperate,

arctic…etc.) rather than just a one universal value for all locations. The investigation of this issue would require better attenuation measurements at higher frequencies and more diverse locations to confirm.

Another area to look in to is the possibility of having a frequency dependent factor that would be needed to make the converted ITU-R attenuation model more accurate. As was seen in Figure 6.20 although the converted ITU-R model would start to add to the attenuation, our own cloud model would predict at 0.1% probability a higher attenuation for both the 70 and 100 GHz by about 4 and 6 dB, respectively. Thus the way to confirm is with new measurements at these higher frequencies.

7.3 Publications

Through the course of this work, two conference papers were produced.

They are:

1. Alawadi T., Savvaris A., Ventouras S.: 'Comparative Analysis of Tropospheric Degradation in Southern England', 28th AIAA International Communications Satellite Systems Conference (ICSSC-2010), 30 Aug- 2 Sep 2010, Anaheim, California. (Published)

2. Alawadi T., Savvaris A., Ventouras S.: 'Cloud Attenuation on Satellite Links in the Ka/V-Band and the Effect of Changes in the Effective Cloud Temperature', EuCAP 2012, 26-30 March, Prague. (Published)

See Appendix F for copies of these papers.

REFERENCES

[1] Martin, D. H. (2000), Communication satellites, 4th ed, Aerospace Press, El Segundo, CA.

[2] Elbert, B. R. (1999), Introduction to satellite communication, 2nd ed, Artech House, USA.

[3] Evans, B. G. (2000), Satellite communication systems, 3rd edition, Short Run Press Ltd., UK.

[4] Maral, G. and Bousquet, M. (2002), Satellite communications systems : systems, techniques and technology, 4th ed, Wiley, Chichester.

[5] TechnologyUK, 'Radio and Terrestrial Microwave', (2012), available at: http://www.technologyuk.net/telecommunications/communication_technologies/radio_and_terrestrial_microwave.shtml (accessed 05/17).

[6] Vidyasagar Sir, 'Fundamentals of satellite communication system',(2012), available at: http://vsagar.com/2011/12/10/fundamentals-of-satellite-communication-system/ (accessed 05/18).

[7] Kolawole, M. O. (2002), Satellite communication engineering, Marcel Dekker, New York.

[8] meteorological office, UK. (2008), available at: www.metoffice.gov.uk (accessed 11/23).

[9] Mike Willis, ‘Propagation tutorial’, (2012), available at: http://www.mike-willis.com/Tutorial/propagation.html (accessed 05/09)

[10] Allnutt, J. A. (1989), Satellite-to-ground radiowave propagation, Peter Peregrinus Ltd Company, london, UK.

[11] Great Britain, M. O. (1981), A course in elementary meteorology, Second Impression ed, H.M. Stationery Off, London.

[12] University of Omaha-UNOmaha, ‘Cloud Formation’, (2012), available at: http://maps.unomaha.edu/Peake/3510/cloudform.html (accessed 04/17).

[13] Guissard, A. (1980), Study of the influence of the atmosphere on the performance of an imaging microwave radiometer, ESTEC Contract 4124/79/NL/DG (SC) Rep, Université Catholique de Louvain, European Space Agency.

[14] Brussard, G. and Watson, P. A. (1995), Atmospheric modelling and millimetre wave propagation, 1st ed, Chapman and Hall, London, UK.

[15] Debye, P., (1929), Polar molecules, Chemical Catalogue Company, NY, USA.

[16] Mathews, P. A. (1965), Radio wave propagation, VHF and above, Chapman and Hall.

[17] Pruppacher, H. R. and Pitter, R. L. (1971), "semi-empirical determination of the shape of cloud and raindrops", J. Atmos. Sci., , no. 28, pp. 86-94.

[18] Mie, G. (1908), Ann. Phys., vol. 25, no. 4, pp. 377.

[19] Saxon, D. S. (1955), Lectures on the scattering light, 9, UCLA Department of Meteorological Sciences.

[20] Born, M. and Wolf, E. (1986), Principles of Optics, Pergamon, Oxford.

[21] Kerker, M. (1969), The Scattering of Light, Academia Press, New York.

[22] Ishimaru, A. (1997), Wave propagation and scattering in random media, IEEE press, New York.

[23] Ramo, S., Whinnery, J. R. and Van Duzer, T. (1984), Fields and Waves in Communication Electronics, 2nd ed, Wiley, New York.

[24] Stratton, J. (1941), Electromagnetic Theory, McGraw-Hill, New York.

[25] Liebe, H. J., Manabe, T. and Hufford, G. A. (1989), "Millimeter-wave attenuation and delay rates due to fog/cloud conditions", IEEE Trans. Antennas Propag, vol. 37, no. 12, pp. 1617-23.

[26] Falcone, V.J. and Abreu, L.W., (1979), Atmospheric attenuation of millimeter and submillimeter waves, EASCON ’79 Record. IEEE Publ. 79CH 1476-1 AES ed., IEEE, New York.

[27] Gunn, K.L. and East, T.W., 1954, “The Microwave Properties of Precipitation Particles”, Quart. J. Royal Meteor. Soc., 80, pp. 522-545.

[28] Staelin. D.H., 1966, “Measurements and Interporetation of the Microwave Spectrum of the Terrestrial Atmosphere near 1-Centimeter Wavelength”, J. Geophys. Res., 71, no. 12. June, pp. 2875-2881.

[29] Slobin, S., 1982, “Microwave Noise Temperature and Attenuation of Clouds: Statistics of These Effects at Various Sites in United States, Alaska, and Hawaii”, Radio Science, 17 no. 6. Nov-Dec, pp.1455-1464.

[30] Altshuler, E. And Marr, R., 1989, “Cloud Attenuation at Millimeter Wavelengths”, IEEE Trans. Ant. Prop., 37, no. 11, pp. 1473-1479.

[31] Gerace, G. C. and Smith, E. K. (1990), "A comparison of cloud models (EM wavescattering)", Antennas and Propagation Magazine, IEEE, vol. 32, no. 5, pp. 32-38.

[32] Dissanayake, A., Allnutt, J. and Haidara, F. (1997), "A prediction model that combines rain attenuation and other propagation impairments along Earth-satellite paths", Antennas and Propagation, IEEE Transactions on, vol. 45, no. 10, pp. 1546-1558.

[33] Salonen, E. and Uppala, S. (1991), "New prediction method of cloud attenuation", Electronics Letters, vol. 27, no. 12, pp. 1106-1108.

[34] ITU-R, Recommendation P.840-3, “Attenuation due to clouds and fog”, October 1999.

[35] ITU-R, Recommendation P.840-4, “Attenuation due to clouds and fog”, October 2009.

[36] Al-Ansafi, K., Garcia, P., Riera, J. M. and Benarroch, A. (2003), "One-year cloud attenuation results at 50 GHz", Electronics Letters, vol. 39, no. 1, pp. 136-137.

[37] S.G. Warren, C. J. Hahn, J. London, R. M. Chevrin, and R. L. Jenne, “Global distribution of total cloud cover and cloud type amounts over land,” Nat. Ctr. Atmospheric Res. (NCAR), Tech. Notes, NCAR/TN-273, Oct. 1986.

[38] R. J. Doviak and D. S. Zrnic, Doppler radar and weather observations Orlando. New York: Academic, 1984.

[39] Liebe, H. J. (1989), "MPM-an atmospheric millimeter-wave propagation model", Int. J. Infrared and Millimeter Waves, vol. 10, no. 6, pp. 631-650.

[40] Manabe, T., Liebe, H. J. and Hufford, G. A. (1987), "Complex permittivity of water between 0 and 30 THz", Vol. Twelfth Int. Conf. on Infrared and Millimeter Waves, Lake Buena Vista, Florida, IEEE, pp. 229.

[41] Geleyn, J., F.:'Some diagnostics of the cloud /radiation interaction in ECMWF forecasting model'. ECMWF Workshop on radiation and cloud-radiation interaction in numerical modeling, 15th-17th October 1980, ECMWF, pp. 133-162.

[42] ITU-R website Study Groups SG3, "FASCICLE CONCERNING THE STATISTICAL DISTRIBUTIONS OF INTEGRATED WATER VAPOUR AND LIQUID WATER CONTENTS GIVEN IN RECOMMENDATIONS ITU-R P.836-4 AND ITU-R P.840-4", Dec 2010.

[43] A. Martellucci, "Use and development of climatological and experimental databases for radiowave propagation modelling in SatCom and SatNav systems", invited paper, Proceedings of 3rd European conference on antennas and propagation, EuCAP 2009, 23-27 March 2009, Berlin, Germany, pp. 2002-2006

[44] European Space Agency (ESA) COST Action 255, "Radiowave Propagation Modelling for SatCom Services at Ku-Band and Above", Final Report, ESA Publication Division, 2002, chapter 2.1

[45] ESA, "ITALSAT Propagation Handbook," European Space Agency.

[46] Savvaris, A. (2004), Accurate Prediction of Scintillation Degradation Applicable to Satellite Communication Systems Design (PhD thesis), University of Glamorgan, .

[47] A. Savvaris, "Transfer Report: Accurate Prediction of Scintillation Degradation Applicable to Satellite Communication Systems Design," University of Glamorgan, Pontypridd 2002.

[48] RCRU, "Report of the RCRU at RAL for the Year 1997, Annual report," Rutherford Appleton Laboratory (RAL) 1997.

[49] J. M. Woodroffe, R. C. H. Morgan, and J. R. Newbury, "Preliminary Results from an ITALSAT Propagation Experiment at 49.5GHz in the UK," presented at Olympus Utilisation Conference (WPP-60), Seville, Spain, 1993.

[50] Science and Technology Facilities Council (STFC), Chilbolton Facility for Atmospheric and Radio Research, [Wrench, C.L.

[51] Ventouras, S., P. G. Davies, and J. R. Norbury (1995), “Olympus based propagation measurements in southern UK”, IEE Conf. Publ., 407, 27-31.

[52] S. Ventouras, S. A. Callaghan, and C. L. Wrench (2006), “Long-term statistics of Tropospheric attenuation from the Ka/U band ITALSAT satellite experiment in the United Kingdom”, Radio Sci., 41, RS2007 , doi:10.1029/2005RS003252.

[53] UK Meteorological Office. MIDAS Land Surface Stations data (1853-current), [Internet].NCAS British Atmospheric Data Centre, 2006, April 2010. Available from http://badc.nerc.ac.uk/view/badc.nerc.ac.uk__ATOM__dataent_ukmo-midas/.

[54] , ERA Interim, Daily Fields, Full Resolution , available at: http://data-portal.ecmwf.int/data/d/interim_full_daily (accessed 12/14/2011).

[55] Dee, D. P., Uppala, S. M., Simmons, A. J., Berrisford, P., Poli, P., Kobayashi, S., Andrae, U., Balmaseda, M. A., Balsamo, G., Bauer, P., Bechtold, P., Beljaars, A. C. M., van de Berg, L., Bidlot, J., Bormann, N., Delsol, C., Dragani, R., Fuentes, M., Geer, A. J., Haimberger, L., Healy, S. B., Hersbach, H., Hólm, E. V., Isaksen, L., Kållberg, P., Köhler, M., Matricardi, M., McNally, A. P., Monge-Sanz, B. M., Morcrette, J. -., Park, B. -., Peubey, C., de Rosnay, P., Tavolato, C., Thépaut, J. -. and Vitart, F. (2011), "The ERA-Interim reanalysis: configuration and performance of the data assimilation system", Quarterly Journal of the Royal Meteorological Society, vol. 137, no. 656, pp. 553-597.

[56] Assis, M.S., Einloft, C.M., “A Simple Method for Estimating Rain Attenuation Distributions.” Proc. URSI, La Baule, p.301, 1977.

[57] Bryant G.F., Adimula I., Riva C., and G. Brussaard, “Rain Attenuation Statistics from Rain Cell Diameters and Heights”, submitted to International Journal of Satellite Communications, 1999.

[58] Crane R.K. “Prediction of attenuation by rain”, IEEE Transaction on Communications, COM-28, pp. 1717-1733, 1980.

[59] Flavin R.K., “Satellite link rain attenuation in Brisbane and a proposed new model for Australia”, Telstra Research Laboratories, Report N. 8375, 1996.

[60] ITU-R, “Propagation data and prediction methods required for the design of Earth-space telecommunication systems”, Propagation in Non-Ionised Media, Recommendation 618-1to9, Geneva, (1986-1990-1992-1994-1995-1997-1999-2001-2003-2007).

[61] Mandeep J.S., TANAKA K.: ‘Effects of atmospheric parameters on satellite link’, Int. J. Infrared Millimeter Waves, 2007, 28, (10), pp. 789-795

[62] Mandeep J.S., Ojo J.S., Emiliani L.D.: ‘Statistics of annual and diurnal cloud attenuation over equatorial climate’, IET Commun., 2009, Vol. 3, Iss. 4, pp. 630-635

[63] Raina M. K.: ‘Atmospheric Emission Measurements of Attenuation by Microwave Radiometer at 19.4 GHz’, IEEE Trans. on Antennas and propagation, 1996, Vol. 44, No. 2, pp.188-191

[64] Dissanayake A., Allnutt J., Haidara F.: ‘Cloud attenuation modelling for SHF and EHF applications’, Int. J. Satell. Commun. 2001, Vol. 19, pp. 335-345

[65] Maitra A., Chakraborty S.: ‘Cloud Liquid Water Content and Cloud Attenuation Studies with Radiosonde Data at a Tropical Location’, J. Infrared Milli Terahz Waves, 2009, No. 30, pp. 367-373

[66] Savvaris A., Otung I.E., “Preliminary Preprocessing of ITALSAT Data at 20, 40 and 50 GHz”, URSI 2000 Symposium.

[67] E. Salonen, C.Riva, and J.P.V Poiares Baptista, “A global model for total fade distribution of atmospheric phenomena”, Millennium Conference on Antennas & Propagation, AP2000, ESA SP-444 PROCEEDINGS, 9-14 April 2000, Davos, Switzerland.

[68] I. Otung, Communication Engineering Principles: Palgrave, 2001.

[69] A. Bateman, Digital Communications - Design for the Real World: Addision Wesley, 1999.

[70] ITU-R F.557-4, Geneva, 1997.

[71] C. K. Kassianides, "A Study of the Effects of Scintillation on Digital Satellite Communication Systems," in School of Electronics. Pontypridd: University of Glamorgan, 2002.

[72] F. Xiong, "Modem Techniques in Satellite Communications," IEEE Communications Magazine, pp. 84-98, August 1994.

[73] ITU-R P.1623, “Prediction method of fade dynamics on Earth-space paths”, ITU, Geneva, Switzerland, 2003.

[74] European Space Agency (ESA) COST Action 255, “Radiowave Propagation Modelling for SatCom Services at Ku-Band and Above”, Final Report, ESA Publication Division, 2002, chapter 5.3

[75] Hörle J., ‘Up-link power control of satellite Earth stations as a fade countermeasure of 20/30 GHz communications systems’, Int. Jour. Of Sat. Com., Vol. 6, June 1988, pp. 323-330

[76] R. J. Acosta, "Rain Fade Compensation Alternatives for Ka-band Communication Satellite," presented at 3rd Ka-Band Ultilization Conference, Sorrento, Italy, 15-18 Sep. 1997.

[77] M. J. Willis and B. G. Evans, "Fade Countermeasures at Ka band for Olympus," Int. Journal of Satellite Communication, vol. 3, pp. 301-311, 1988.

[78] L. Castanet, J. Lemonton, and M. Bousquet, "Fade Mitigation Techniques for New SatCom Services at Ku-band and Above: a Review," presented at 5th International Workshop on Radiowave Propagation Modelling for SatCom Services at Ku-band and Above, Netherlands, 28-29 Oct. 1998.

[79] H. Fukuchi, "Quantitative Analysis of the Effect of Adaptive Satellite Power Control as a Rain Attenuation Countermeasure," presented at IEEE International Symposium on Antennas and Propagation, 1994.

[80] Poiares Baptista P., Paraboni A., "Active compensation techniques for spacecraft antennas", ESA publication, "Preparing for the future", vol. 5, n°1, March 1995

[81] C. D. Hughes and M. Tomlinson, "The Use of Spread-Spectrum Coding as a Fading Countermeasure at 20/30 GHz," ESA Journal, vol. 11, pp. 73-81, 1988

[82] J. G. Proakis, Digital Communications, Third Edition ed: Mc Graw-Hill Int. Ed., 1995.

[83] M. Filip and E. Vilar, "Implementation of Adaptive Modulation as a Fade Countermeasure," Int. Journal of Satellite Communication, vol. 8, pp. 33-41, June 1990

[84] B. C. Gremont, M. Filip, and E. Vilar, "Simulation of a High Frequency Satellite Link with a Fade Countermeasure," presented at International Conference on Antennas and Propagation (ICAP 1999), York, UK, 1999

[85] E. Matricciani, "Prediction of Site Diversity Performance in Communications Systems Affected by Rain Attenuation: Extension of Two Layer Rain Model," Euro. Trans. on Telecomms and Related Technologies, vol. 5, pp. 327-336, May-June 1994.

[86] D. B. Hodge, "An Improved Model for Diversity Gain on Earth-Space Propagation Paths," Radio Science, vol. 17, pp. 1393-1399.

[87] Chambers, A. (2008), Viability of High Availability V band Satellite Communication using Hybrid Fade Mitigation (PhD thesis), University of Glamorgan, .

[88] Tiedtke, M. (1993), “Representation of clouds in large-scale models”, Mon. Wea. Rev., 121, 3040-3061.

[89] National Center for Atmospheric Research, ‘ERA-Interim Vertical Coordinate Conventions and Numerical Attributes’, http://dss.ucar.edu/datasets/ds627.0/docs/Eta_coordinate/, 20 Oct. 2008. (accessed 12/14/2011).

[90] D. Vanhoenacker-Janvier, C. J. Gibbins, C. J. Walden, C. L. Wrench, S. Ventouras, J. Spiegel(1), C. Oestges, D. Mertens, A. Martellucc, ‘CHARACTERIZATION AND MODELLING OF PROPAGATION EFFECTS IN 20-50 GHZ BAND’, XXVIIIth General Assembly of International Union of Radio Science Proceedings, new delhi, 2005.

[91] Paraboni, A., Riva, C., Capsoni, C., Luini, L., Castanet, L., Jeannin, N., Martellucci, A., Pontes, M., Schonhuber, M. & Emiliani, L. 2011, ‘Propagation modelling and mapping of rain, clouds and water vapour to cope with spatial and temporal variability’, Proceedings of the 5th European Conference on Antennas and Propagation, EUCAP 2011, pp. 3242.

[92] I. E. Otung, "Accurate prediction of scintillation degradation applicable to satellite communication system design," University of Glamorgan 1998.

APPENDICES

Appendix A

A.1 Normalized LWP maps (ITU-R 840.3)

Figure A. 1 Normalized LWP for 20% probability (840.3)

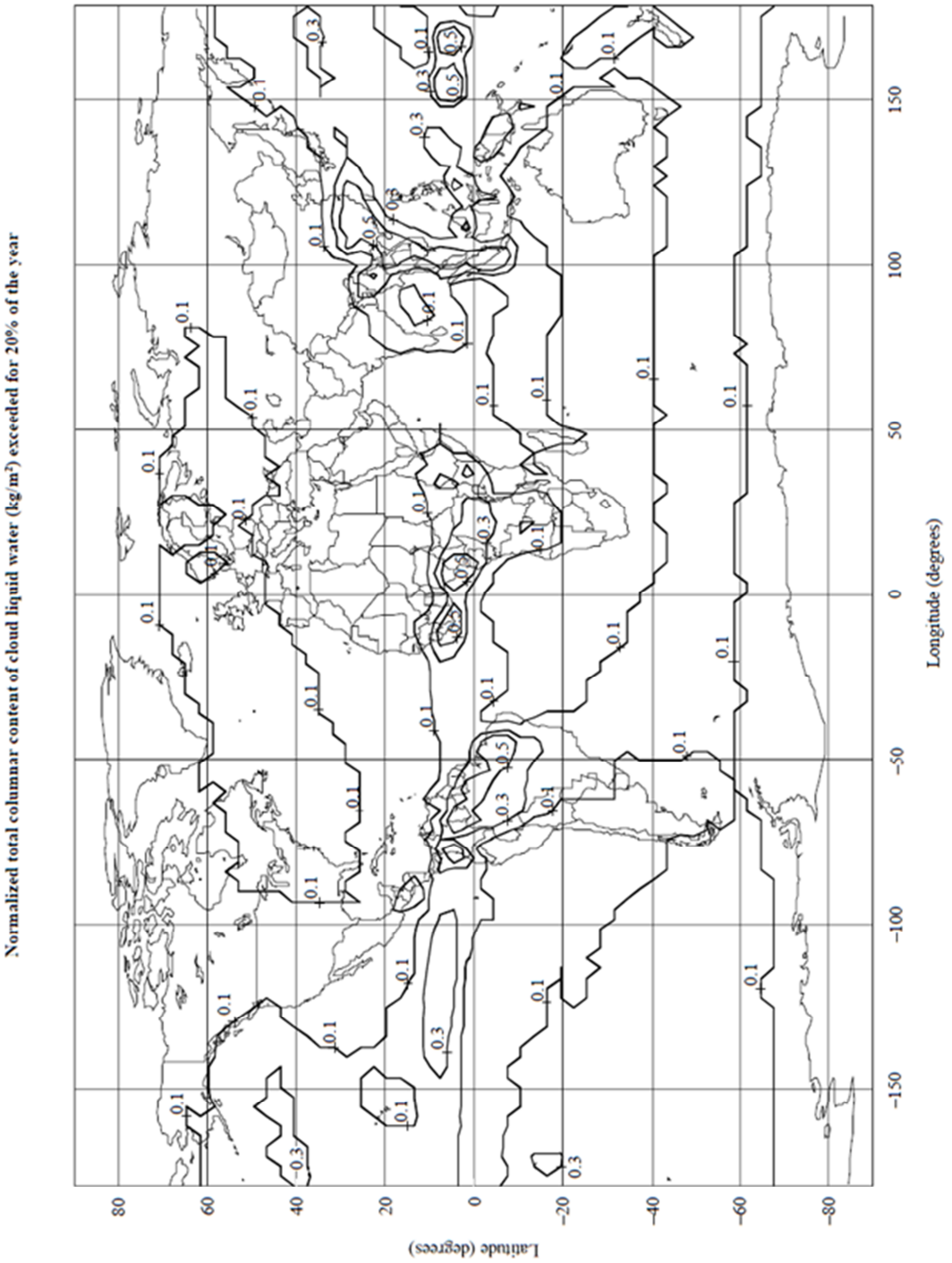

Figure A. 2 Normalized LWP for 10% probability (840.3)

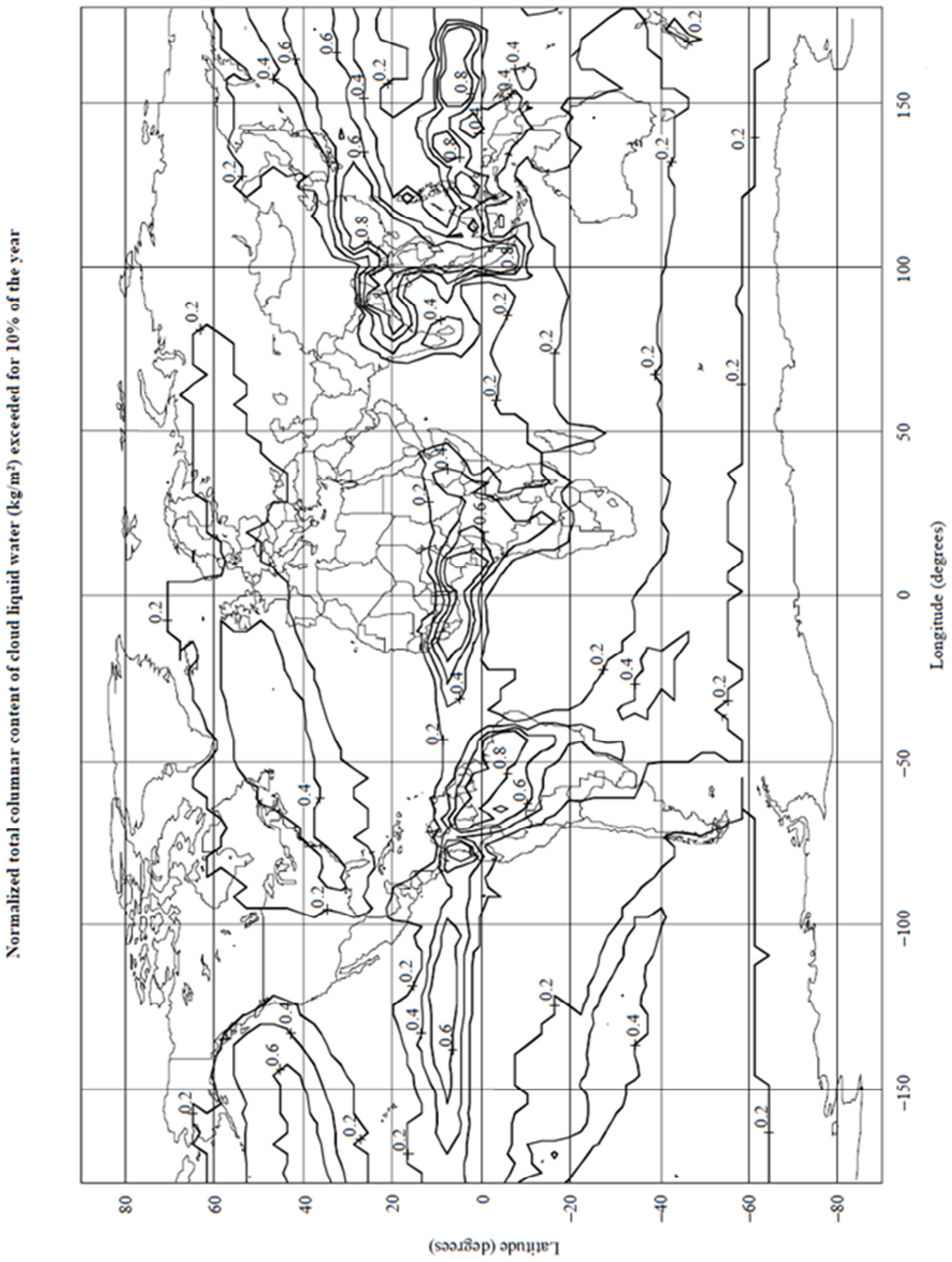

Figure A. 3 Normalized LWP for 5% probability (840.3)

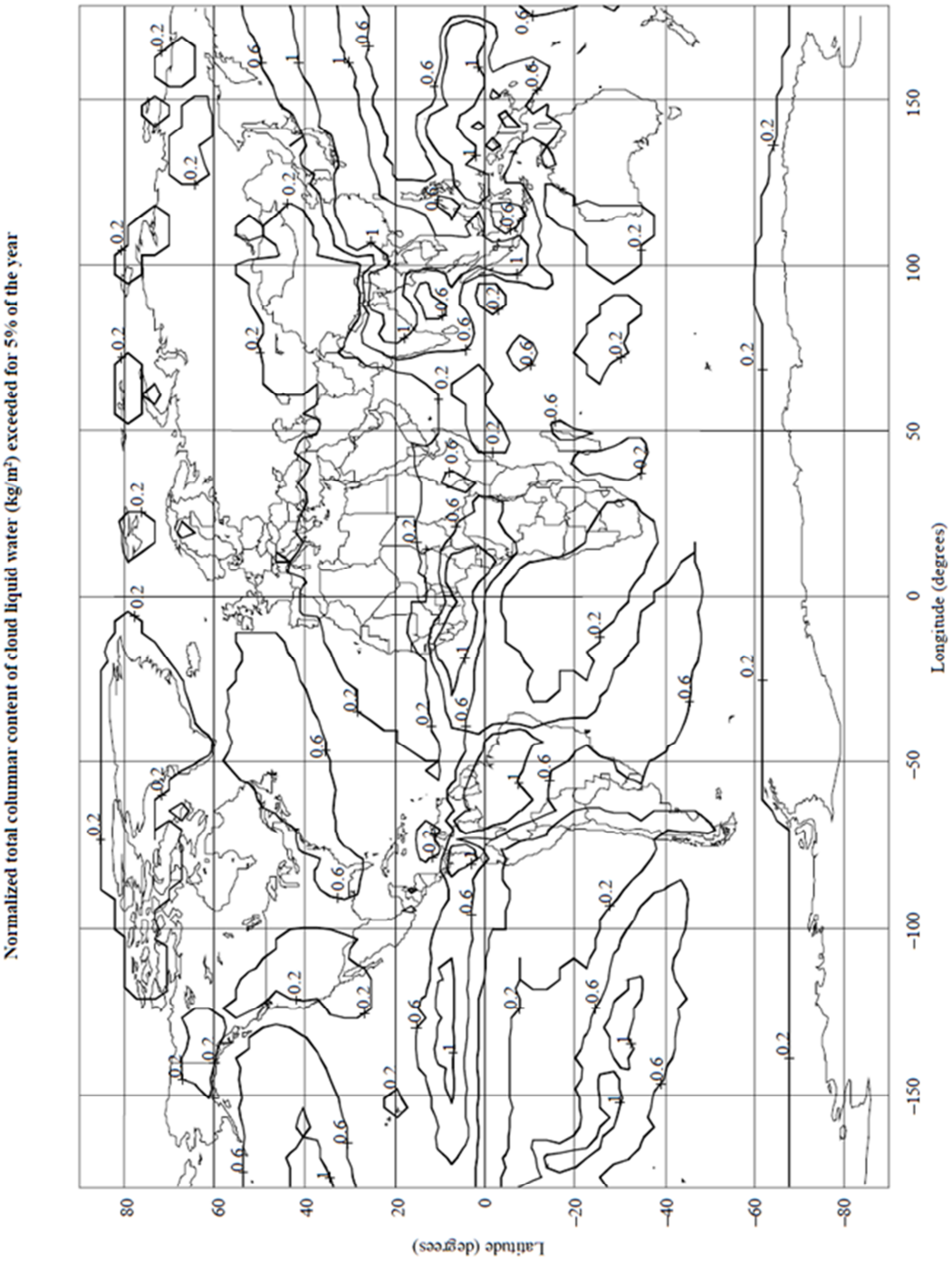

Figure A. 4 Normalized LWP for 1% probability (840.3)

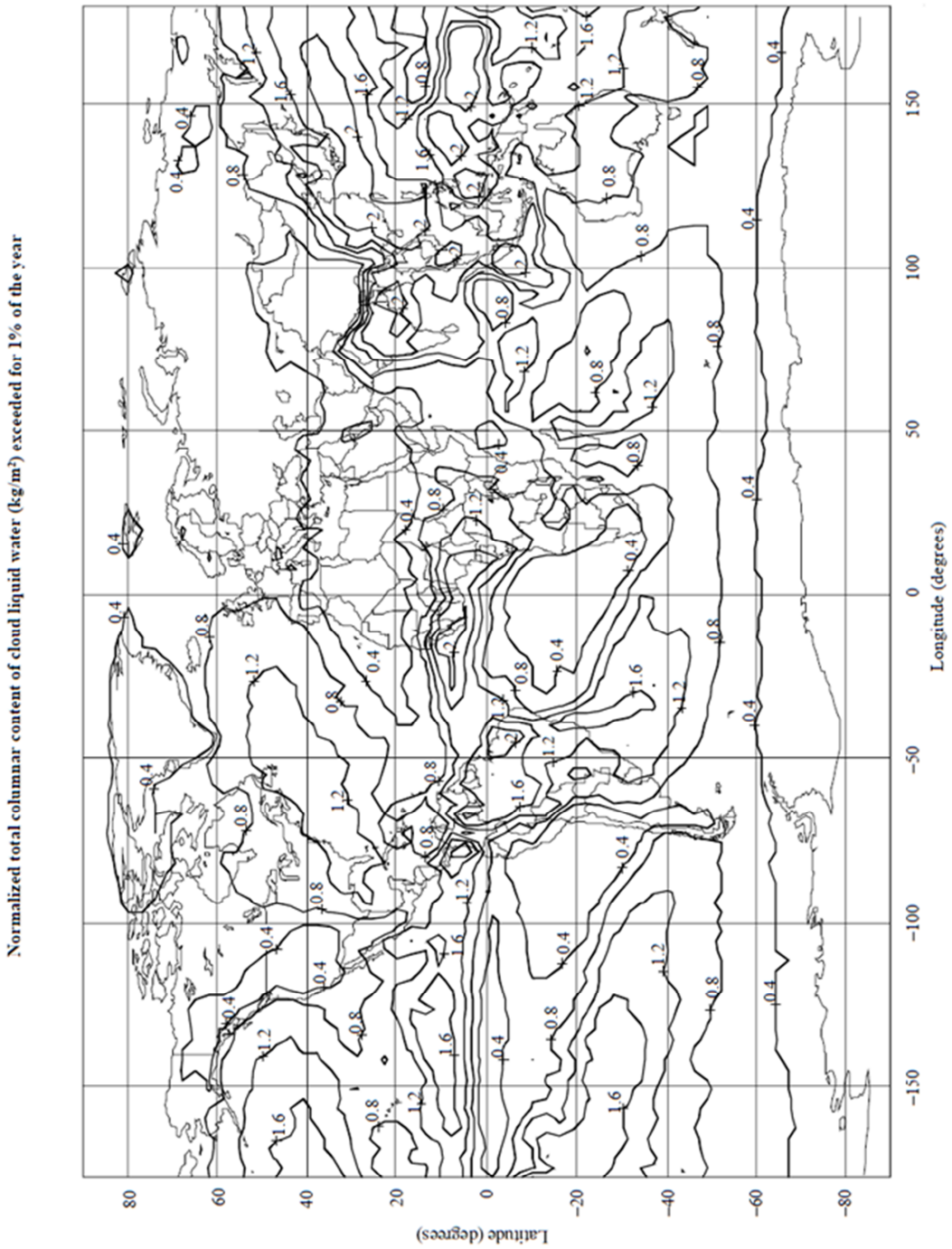

A.2 Normalized LWP maps (ITU-R 840.4)

Figure A. 5 Normalized LWP for 0.1% and 0.5% probability (840.4)

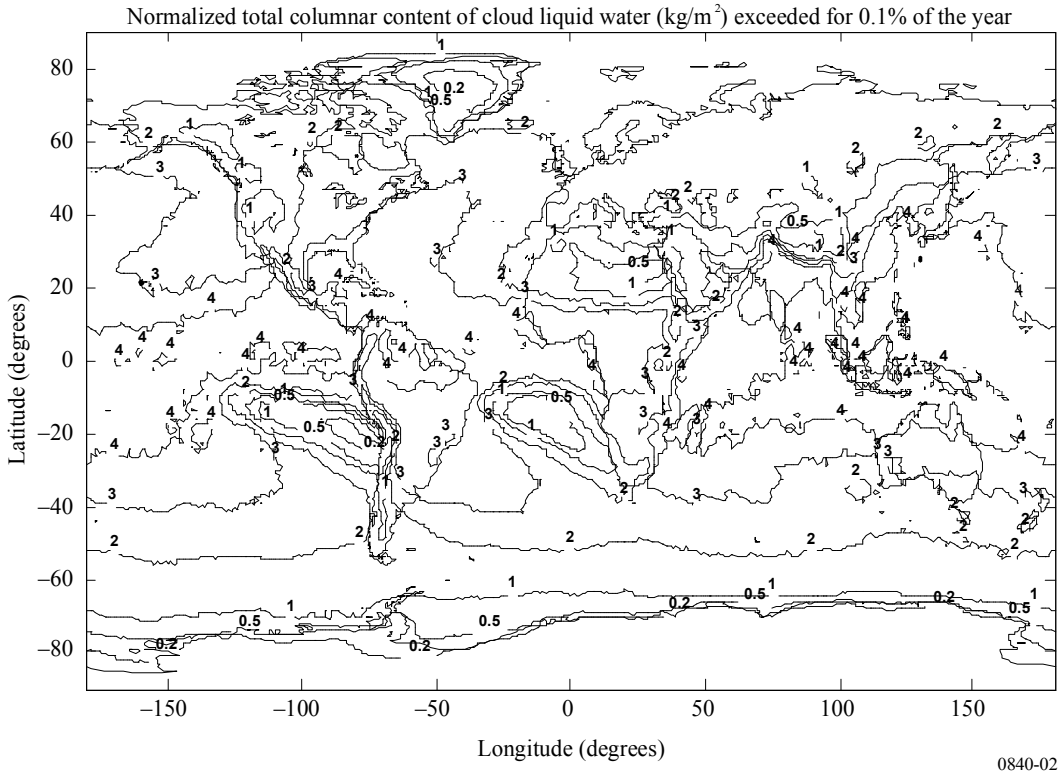

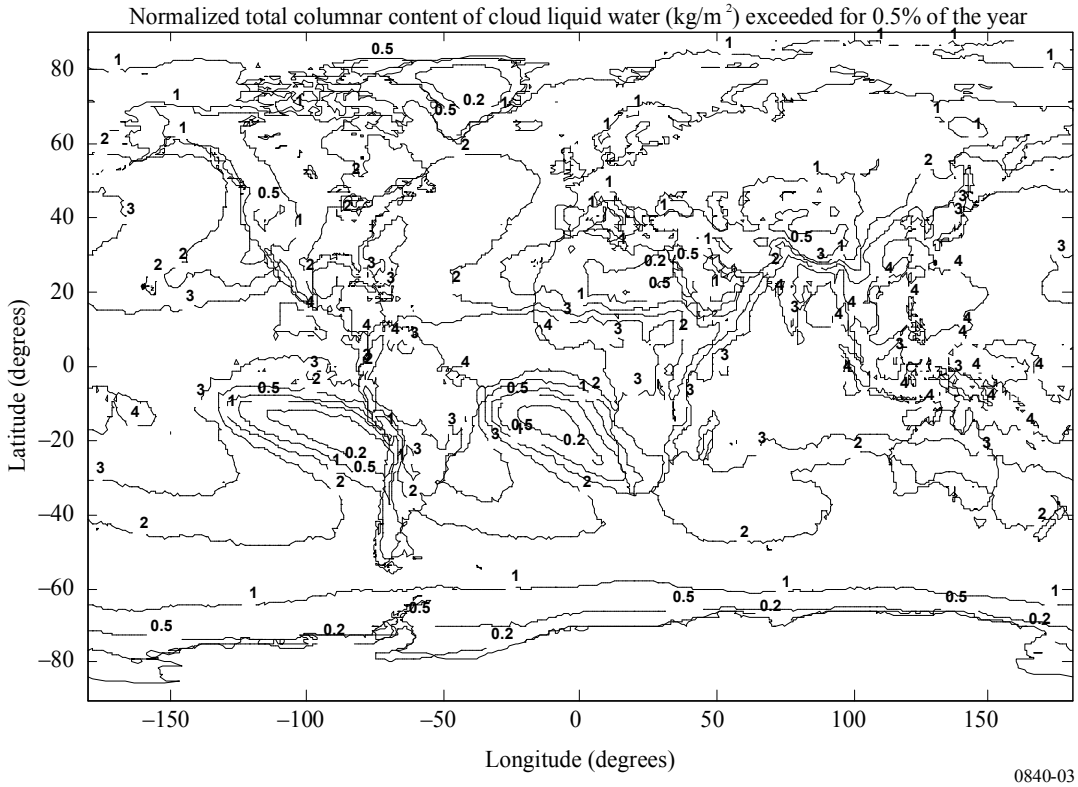

Figure A. 6 Normalized LWP for 1% and 5% probability (840.4)

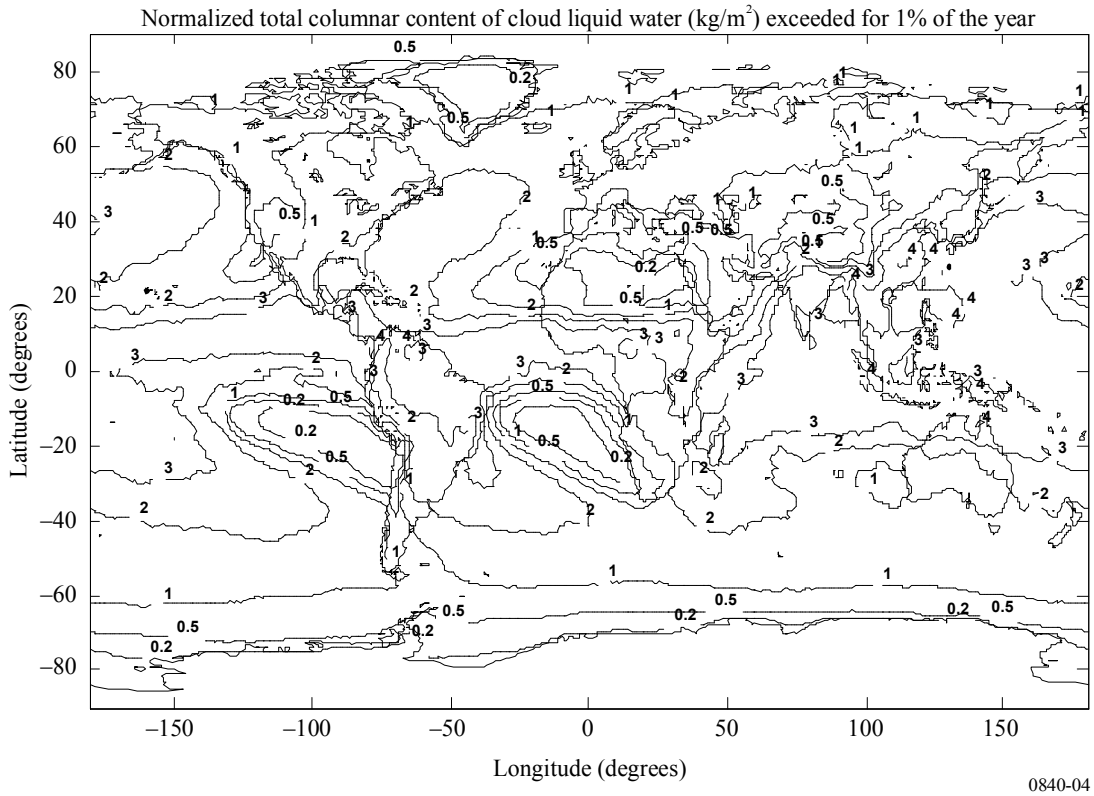

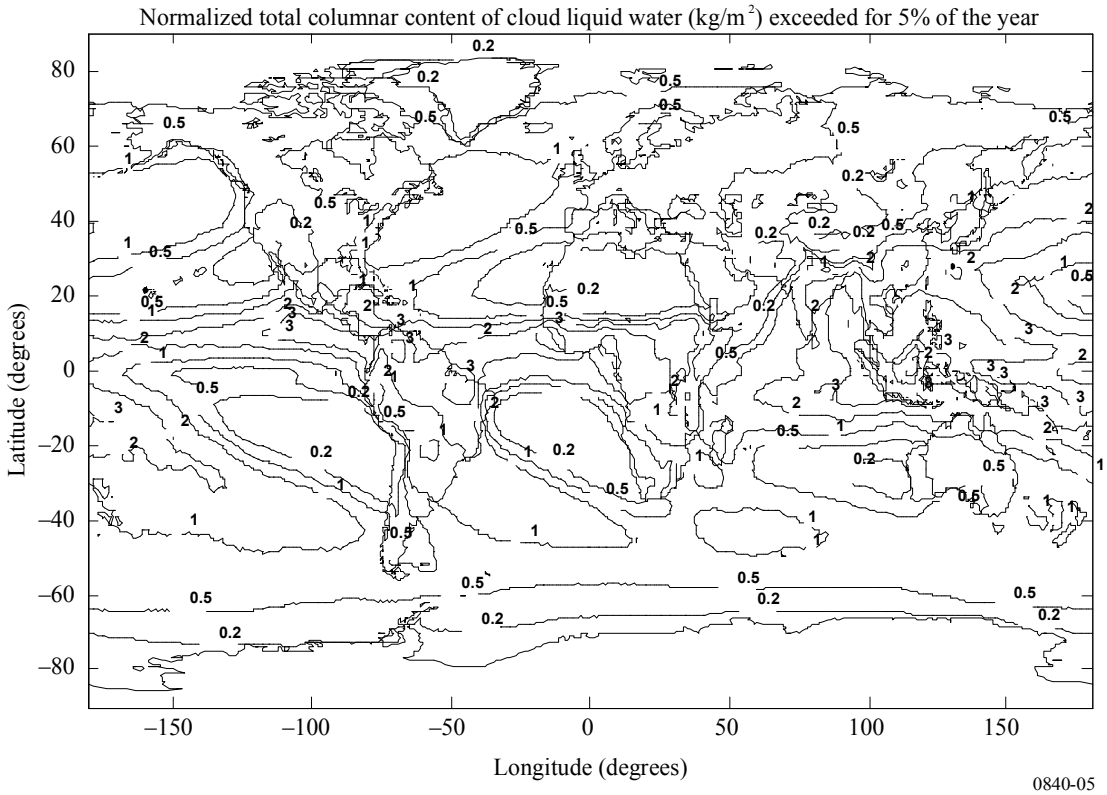

Figure A. 7 Normalized LWP for 10% and 20% probability (840.4)

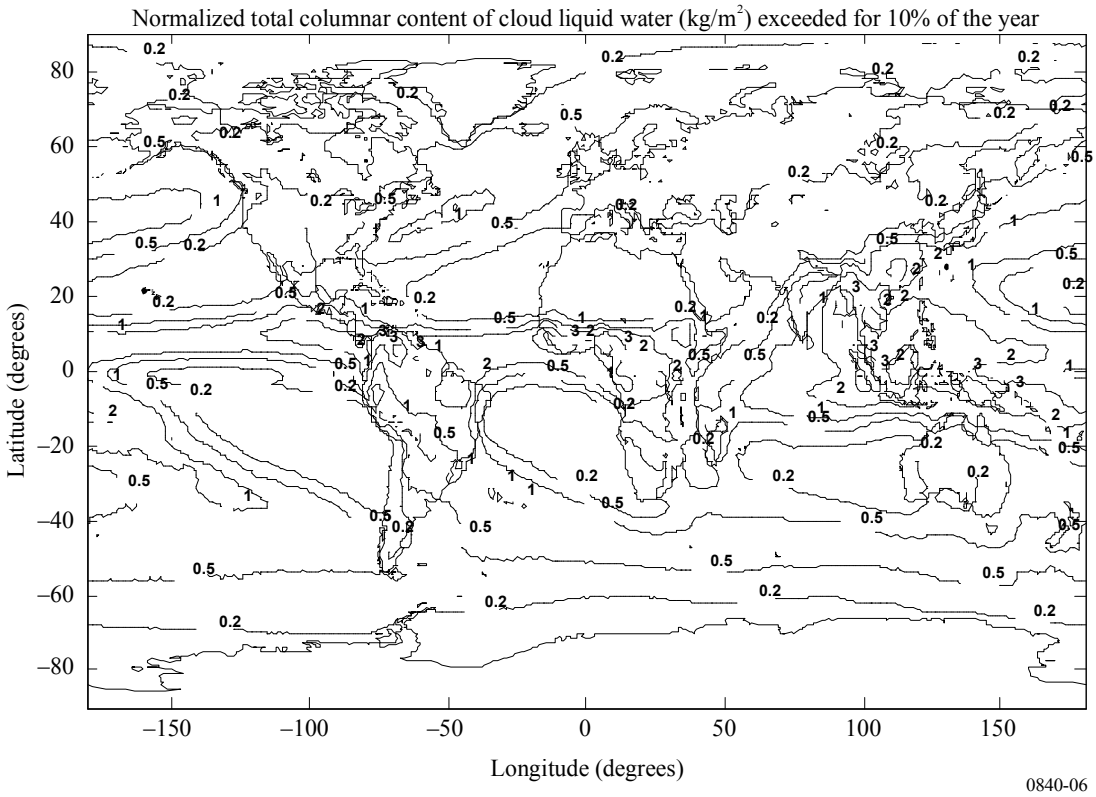

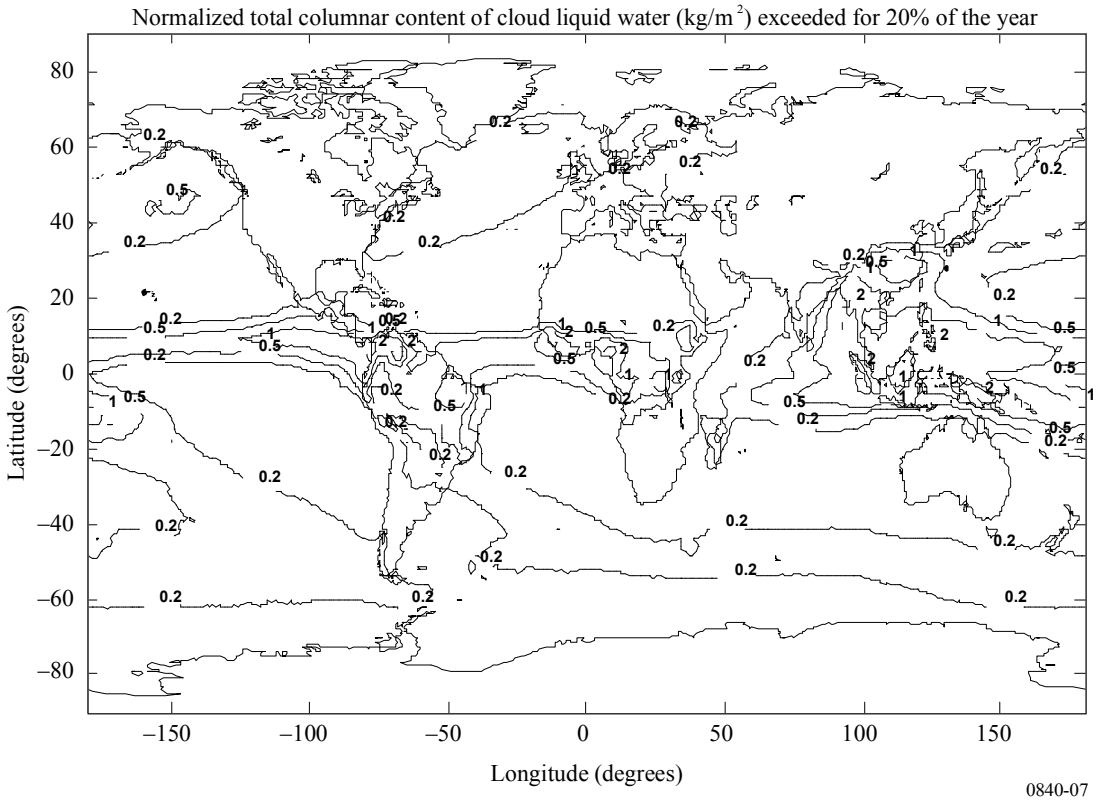

Appendix B

Table B. 1 UK Hourly Observations data format

HEADER	PARAMETER	FIELDS	COLUMNS	UNITS	COMMENTS
ID	Station Ref. Number	1	1-8	-	Station identification
IDTYPE	-	2	9-17	-	Station identification
MET_DOM	Meteorological Domain	3	18-28	-	Message types
YEAR	Year	3	29-35	-	4 characters
MON	Month	4	36-43	-	1 or 2 characters (from 1 to 12)
DAY	Day	5	44-51	-	1 or 2 characters (from 1 to 31max)
HOUR	Hour	6	52-59	-	Hour of observation from 0 to 2300
DIR	10 minutes wind direction	7	60-67	Degree true	From 0 to 360 degrees, clockwise. Note that zero values in both wind speed and wind direction fields indicate that there was no wind blowing at the time of observation. See Met Office documentation
SPEED	10 minutes wind speed	8	68-75	Knots	NB. A mean wind for the hour up until the reporting time. Note that zero values in both wind speed and wind direction fields indicate that

					there was no wind blowing at the time of observation. See Met Office documentation
PRST	Present weather	9	76-81	WMO Code	See Met Office documentation
PAS1	Most significant Past weather	10	82-87	WMO code	See Met Office documentation
PAS2	Least significant Past weather	11	88-93	WMO code	See Met Office documentation
TCA	Total cloud amount	12	94-98	WMO code	See Met Office documentation
LCT	Low cloud type	13	99-103	WMO Code	See Met Office documentation
MCT	Medium cloud type	14	104-108	WMO Code	See Met Office documentation
HCT	High cloud type	15	109-113	WMO Code	See Met Office documentation
CBA	Cloud base amount	16	114-118	WMO code	See Met Office documentation
CBH	Cloud base height	17	119-126	DAM	DAM = Decameters See Met Office documentation
VIS	Horizontal visibility	18	127-133	DAM	DAM = Decameters See Met Office documentation
MSLP	Mean Sea Level Pressure	19	134-146	0.1 mb	Atmospheric pressure is expressed in millibars (1 millibar = 100 pascals = 100 newtons per square metre). Precision aneroid barometers are now in general use for measuring pressure and a

					correction for altitude is applied to obtain the value at mean sea level (MSL).
CA1	Cloud amount - level 1	20	147-151	WMO code	See WMO documentation
CT1	Cloud type - level 1	21	152-156	WMO code	See WMO documentation
CB1	Cloud base - level 1	22	157-164	DAM	DAM = decameters See WMO documentation
CA2	Cloud amount - level 2	23	165-169	WMO code	See WMO documentation
CT2	Cloud type - level 2	24	170-174	WMO code	See WMO documentation
CB2	Cloud base - level 2	25	175-182	DAM	DAM = Decameters See WMO documentation
CA3	Cloud amount - level 3	26	183-187	WMO code	See WMO documentation
CT3	Cloud type - level 3	27	188-192	WMO code	See WMO documentation
CB3	Cloud base - level 3	28	193-200	DAM	DAM = Decameters See WMO documentation
CA4	Cloud amount - level 4	29	201-205	WMO code	See WMO documentation
CT4	Cloud type - level 4	30	206-210	WMO code	See WMO documentation
CB4	Cloud base - level 4	31	211-218	DAM	DAM = Decameters See WMO documentation
VVIS	Vertical visibility	32	219-226	DAM	DAM = Decameters See Met Office documentation
TEMP	Dry-bulb air temperature	33	227-234	0.1 Degrees Celsius	See Met Office documentation
DEW	Dew-point	34	235-242	0.1	The dew point

	temperature			Degrees Celsius	temperature (in degrees Celsius) is the temperature to which the air must be cooled to produce saturation with respect to water at its existing atmospheric pressure and humidity.See Met Office documentation
WETB	Wet-bulb temperature	35	243-250	0.1 Degrees Celsius	The web-bulb temperature is the lowest temperature (in degrees Celsius) that can be obtained by evaporating water into the air. It measures the humidity of the air.See Met Office documentation
STNP	Station level pressure	36	251-262	0.1 mb	Atmospheric pressure (in mb) as measured at the station level. Correction for altitude is not applied.
ALTP	Altimeter pressure	37	263-270	mb	-
SOG	State of ground	38	271-275	WMO Code	-
MGS	10 minutes maximum gust speed	39	276-283	knots	See Met Office documentation

Appendix C

Table C. 1 Flag values of synoptic data files.

Type / Genus of cloud:
WMO code 0500: Genus of cloud

/ - cloud not visible owing to darkness, fog, duststorm, sandstorm or other
analogous phenomena
0 - cirrus (CI)
1 - cirricumulus (CC)
2 - cirrostratus (CS)
3 - altocumulus (AC)
4 - altostratus (AS)
5 - nimbostratus (NS)
6 - stratocumulus (SC)
7 - stratus (ST)
8 - cumulus (CU)
9 - cumulonimbus (CB)

Total cloud amount:

WMO code 2700: Cloud cover / amount

/ - cloud is indiscernible for reasons other than fog or other meteorological
phenomena, or observation is not made.
0 - sky clear
1 - 1 okta : 1/10 - 2/10
2 - 2 oktas : 2/10 - 3/10
3 - 3 oktas : 4/10
4 - 4 oktas : 5/10
5 - 5 oktas : 6/10
6 - 6 oktas : 7/10 - 8/10
7 - 7 oktas or more, but not 8 oktas : 9/10 or more, but not 10/10
8 - 8 oktas : 10/10
9 - sky obscured by fog or other meteorological phenomena

Low cloud type:
WMO code 0513: Clouds of genera Stratocumulus, Stratus, Cumulus, etc.

/ - stratocumulus, stratus, cumulus and cumulonimbus invisible owing to darkness,
fog, blowing dust or sand, or other phenomena
0 - no stratocumulus, stratus, cumulus or cumulonimbus
1 - cumulus with little vertical extent and seemingly flattened, or ragged
cumulus, other than of bad weather, or both
2 - cumulus of moderate or strong vertical extent, generally with protuberances

in the form of domes or towers, either accompanied or not by other cumulus or stratocumulus, all having bases at the same level
3 - cumulonimbus, the summits of which, at least partially, lack sharp outlines but are neither clearly fibrous (cirriform) nor in the form of an anvil; cumulus, stratocumulus or stratus may also be present
4 - stratocumulus formed by the spreading out of cumulus; cumulus may also be present
5 - stratocumulus not resulting from the spreading out of cumulus
6 - stratus in a more or less continuous later, or in ragged shreds, or both but no stratus fractus of bad weather
7 - stratus fractus of bad weather or cumulus fractus of bad weather, or both (pannus), usually below altostratus or nimbostratus
8 - cumulus and stratocumulus other than that formed from the spreading out of cumulus; the base of the cumulus is at a different level from that of the stratocumulus
9 - cumulonimbus, the upper part of which is clearly fibrous (cirriform) often in the form of an anvil; either accompanied or not by cumulonimbus without anvil or fibrous upper part, by cumulus, stratocumulus, stratus or pannus

---

020011 CLOUD AMOUNT

0 0
1 1 OKTA OR <1
2 2 OKTAS
3 3 OKTAS
4 4 OKTAS
5 5 OKTAS
6 6 OKTAS
7 7 OKTAS (<8)
8 8 OKTAS
9 SKY OBSCURED METEOROLOGICAL
10 SKY PARTLY OBSCURED BY FOG AND/OR OTHER METEOROLOGICAL PHENOMENA
11 SCATTERED
12 BROKEN
13 FEW

020012 CLOUD TYPE

0 CI
1 CC
2 CS
3 AC
4 AS
5 NS
6 SC
7 ST
8 CU
9 CB

Appendix D

Figure D. 1 Full set of 7-years cycle error (CT)

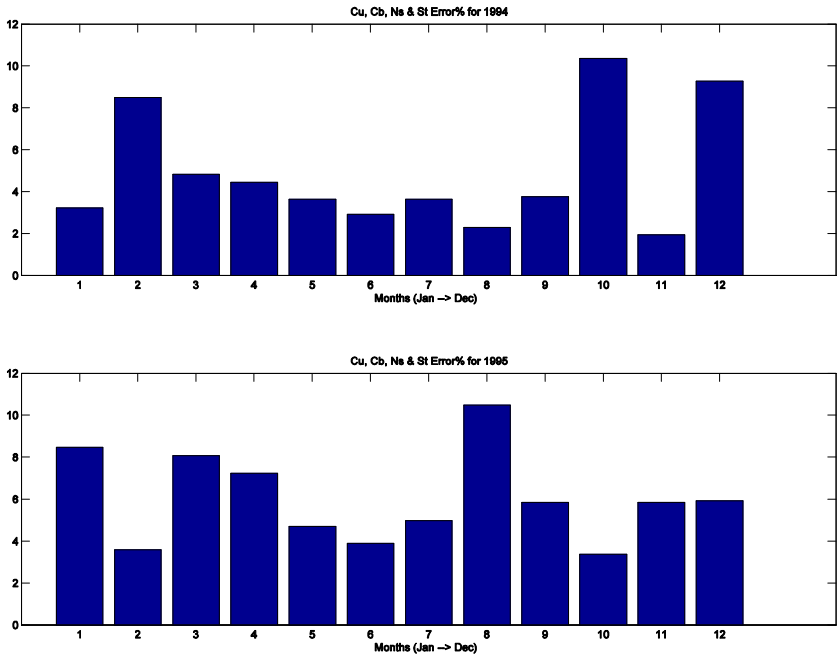

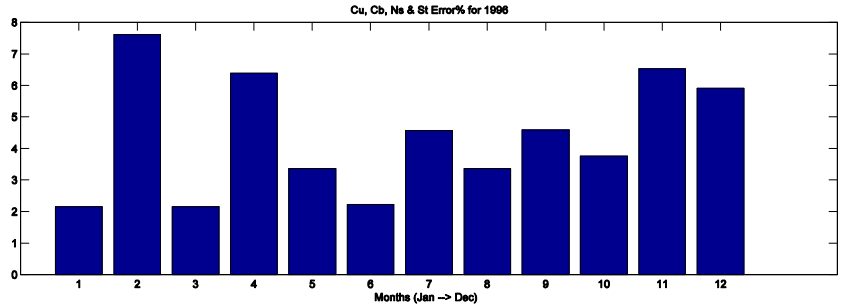
Cu, Cb, Ns & St Error% for 1996
Months (Jan --> Dec)

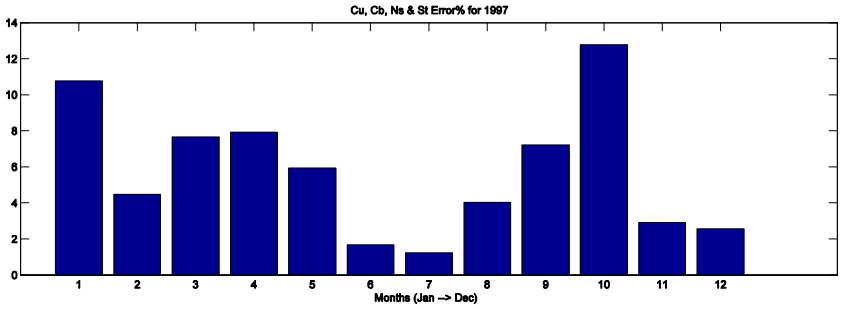
Cu, Cb, Ns & St Error% for 1997
Months (Jan --> Dec)

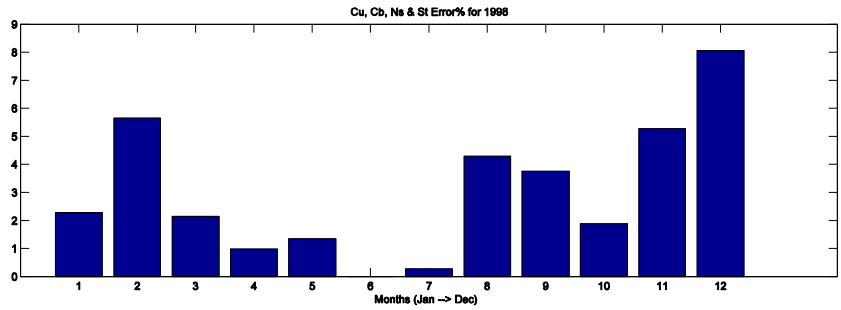
Cu, Cb, Ns & St Error% for 1998
Months (Jan --> Dec)

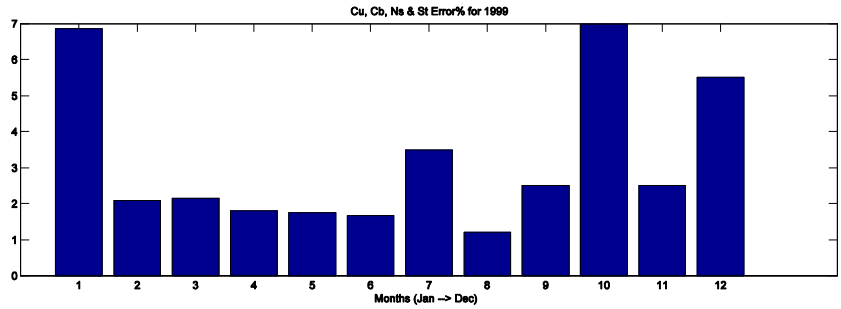
Cu, Cb, Ns & St Error% for 1999
Months (Jan --> Dec)

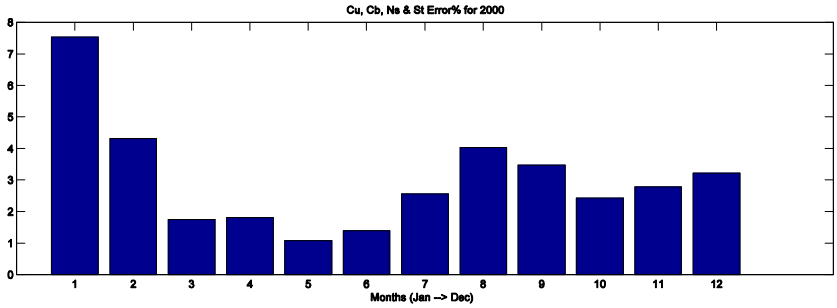

Figure D. 2 Full set of 7-years cycle error (LCT)

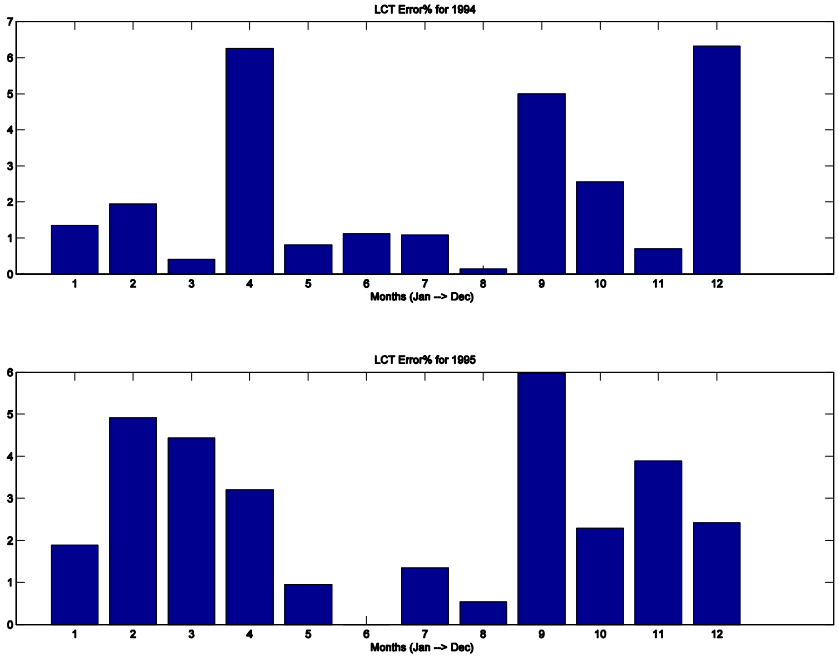

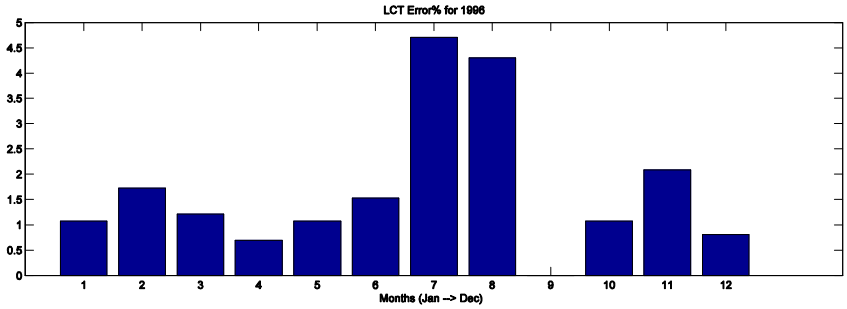
LCT Error% for 1996
0
0.5
1
1.5
2
2.5
3
3.5
4
4.5
5
1
2
3
4
5
6
7
8
9
10
11
12
Months (Jan --> Dec)

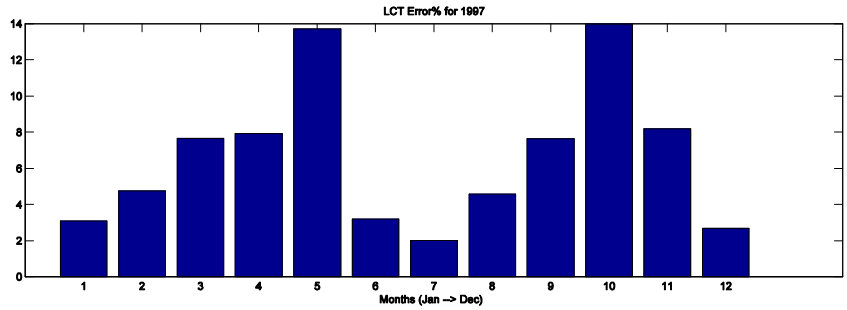
LCT Error% for 1997
0
2
4
6
8
10
12
14
1
2
3
4
5
6
7
8
9
10
11
12
Months (Jan --> Dec)

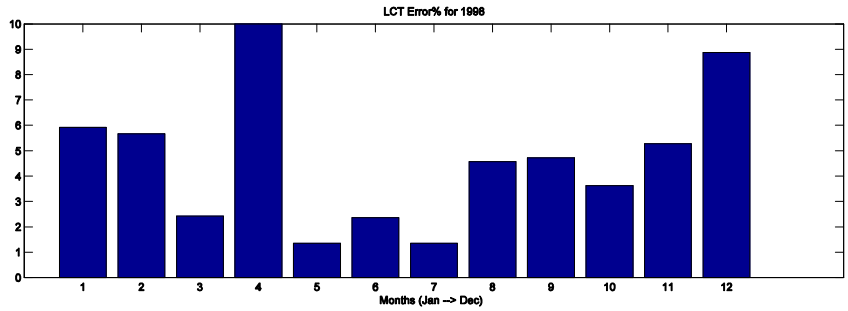
LCT Error% for 1998
0
1
2
3
4
5
6
7
8
9
10
1
2
3
4
5
6
7
8
9
10
11
12
Months (Jan --> Dec)

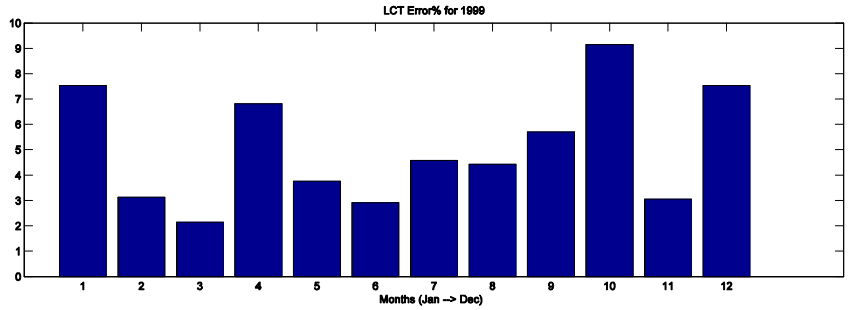
LCT Error% for 1999
0
1
2
3
4
5
6
7
8
9
10
1
2
3
4
5
6
7
8
9
10
11
12
Months (Jan --> Dec)

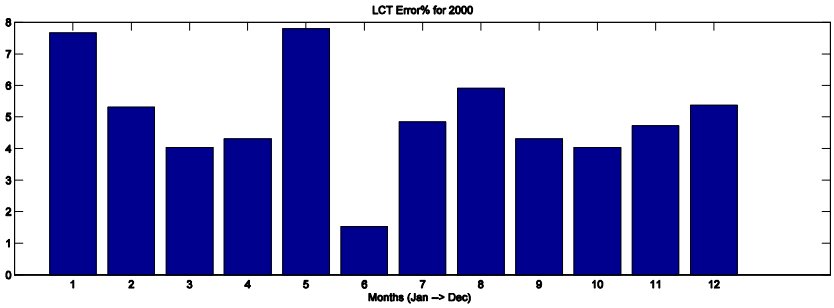
LCT Error% for 2000
0
1
2
3
4
5
6
7
8
1
2
3
4
5
6
7
8
9
10
11
12
Months (Jan --> Dec)

Appendix E

NCAR variables calculations for ERA-INTERIM.xps

Appendix F

F.1 ICSSC-2010 Conference paper (Published)

Adobe Acrobat Document

F.2 EuCAP 2012, PRAGUE (Published)

Acrobat Document

[1] Martin, D. H. (2000), *Communication satellites,* 4th ed, Aerospace Press, El Segundo, CA.

[2] Elbert, B. R. (1999), *Introduction to satellite communication,* 2nd ed, Artech House, USA.

[3] Evans, B. G. (2000), Satellite communication systems, 3rd edition, Short Run Press Ltd., UK.

[4] Maral, G. and Bousquet, M. (2002), *Satellite communications systems : systems, techniques and technology,* 4th ed, Wiley, Chichester.

[5] TechnologyUK, 'Radio and Terrestrial Microwave', (2012), available at: http://www.technologyuk.net/telecommunications/communication_technologies/radio_and_terrestrial_microwave.shtml (accessed 05/17).

[6] Vidyasagar Sir, 'Fundamentals of satellite communication system',(2012), available at: http://vsagar.com/2011/12/10/fundamentals-of-satellite-communication-system/ (accessed 05/18).

[7] Kolawole, M. O. (2002), *Satellite communication engineering,* Marcel Dekker, New York.

[8] meteorological office, UK. (2008), available at: www.metoffice.gov.uk (accessed 11/23).

[9] Mike Willis, 'Propagation tutorial', (2012), available at: http://www.mike-willis.com/Tutorial/propagation.html (accessed 05/09)

[10] Allnutt, J. A. (1989), *Satellite-to-ground radiowave propagation,* Peter Peregrinus Ltd Company, london, UK.

[11] Great Britain, M. O. (1981), *A course in elementary meteorology,* Second Impression ed, H.M. Stationery Off, London.

[12] University of Omaha-UNOmaha, 'Cloud Formation', (2012), available at: http://maps.unomaha.edu/Peake/3510/cloudform.html (accessed 04/17).

[13] Guissard, A. (1980), Study of the influence of the atmosphere on the performance of an imaging microwave radiometer, ESTEC Contract 4124/79/NL/DG (SC) Rep, Université Catholique de Louvain, European Space Agency.

[14] Brussard, G. and Watson, P. A. (1995), *Atmospheric modelling and millimetre wave propagation,* 1st ed, Chapman and Hall, London, UK.

[15] Debye, P., (1929), *Polar molecules*, Chemical Catalogue Company, NY, USA.

[16] Mathews, P. A. (1965), *Radio wave propagation, VHF and above,* Chapman and Hall.

[17] Pruppacher, H. R. and Pitter, R. L. (1971), "semi-empirical determination of the shape of cloud and raindrops", *J. Atmos. Sci.,* , no. 28, pp. 86-94.

[18] Mie, G. (1908), *Ann. Phys.,* vol. 25, no. 4, pp. 377.

[19] Saxon, D. S. (1955), Lectures on the scattering light, 9, UCLA Department of Meteorological Sciences.

[20] Born, M. and Wolf, E. (1986), *Principles of Optics,* Pergamon, Oxford.

[21] Kerker, M. (1969), *The Scattering of Light,* Academia Press, New York.

[22] Ishimaru, A. (1997), *Wave propagation and scattering in random media,* IEEE press, New York.

[23] Ramo, S., Whinnery, J. R. and Van Duzer, T. (1984), *Fields and Waves in Communication Electronics,* 2nd ed, Wiley, New York.

[24] Stratton, J. (1941), *Electromagnetic Theory,* McGraw-Hill, New York.

[25] Liebe, H. J., Manabe, T. and Hufford, G. A. (1989), "Millimeter-wave attenuation and delay rates due to fog/cloud conditions", *IEEE Trans. Antennas Propag,* vol. 37, no. 12, pp. 1617-23.

[26] Falcone, V.J. and Abreu, L.W., (1979), *Atmospheric attenuation of millimeter and submillimeter waves*, EASCON '79 Record. IEEE Publ. 79CH 1476-1 AES ed., IEEE, New York.

[27] Gunn, K.L. and East, T.W., 1954, "The Microwave Properties of Precipitation Particles", Quart. J. Royal Meteor. Soc., 80, pp. 522-545.

[28] Staelin. D.H., 1966, "Measurements and Interporetation of the Microwave Spectrum of the Terrestrial Atmosphere near 1-Centimeter Wavelength", J. Geophys. Res., 71, no. 12. June, pp. 2875-2881.

[29] Slobin, S., 1982, "Microwave Noise Temperature and Attenuation of Clouds: Statistics of These Effects at Various Sites in United States, Alaska, and Hawaii", Radio Science, 17 no. 6. Nov-Dec, pp.1455-1464.

[30] Altshuler, E. And Marr, R., 1989, "Cloud Attenuation at Millimeter Wavelengths", IEEE Trans. Ant. Prop., 37, no. 11, pp. 1473-1479.

31 Gerace, G. C. and Smith, E. K. (1990), "A comparison of cloud models (EM wavescattering)", Antennas and Propagation Magazine, IEEE, vol. 32, no. 5, pp. 32-38.

32 Dissanayake, A., Allnutt, J. and Haidara, F. (1997), "A prediction model that combines rain attenuation and other propagation impairments along Earth-satellite paths", Antennas and Propagation, IEEE Transactions on, vol. 45, no. 10, pp. 1546-1558.

33 Salonen, E. and Uppala, S. (1991), "New prediction method of cloud attenuation", Electronics Letters, vol. 27, no. 12, pp. 1106-1108.

34 ITU-R, Recommendation P.840-3, "Attenuation due to clouds and fog", October 1999.

35 ITU-R, Recommendation P.840-4, "Attenuation due to clouds and fog", October 2009.

36 Al-Ansafi, K., Garcia, P., Riera, J. M. and Benarroch, A. (2003), "One-year cloud attenuation results at 50 GHz", Electronics Letters, vol. 39, no. 1, pp. 136-137.

37 S.G. Warren, C. J. Hahn, J. London, R. M. Chevrin, and R. L. Jenne, "Global distribution of total cloud cover and cloud type amounts over land," Nat. Ctr. Atmospheric Res. (NCAR), Tech. Notes, NCAR/TN-273, Oct. 1986.

38 R. J. Doviak and D. S. Zrnic, Doppler radar and weather observations Orlando. New York: Academic, 1984.

39 Liebe, H. J. (1989), "MPM-an atmospheric millimeter-wave propagation model", Int. J. Infrared and Millimeter Waves, vol. 10, no. 6, pp. 631-650.

40 Manabe, T., Liebe, H. J. and Hufford, G. A. (1987), "Complex permittivity of water between 0 and 30 THz", Vol. Twelfth Int. Conf. on Infrared and Millimeter Waves, Lake Buena Vista, Florida, IEEE, pp. 229.

41 Geleyn, J., F.:'Some diagnostics of the cloud /radiation interaction in ECMWF forecasting model'. ECMWF Workshop on radiation and cloud-radiation interaction in numerical modeling, 15th-17th October 1980, ECMWF, pp. 133-162.

42 ITU-R website Study Groups SG3, "FASCICLE CONCERNING THE STATISTICAL DISTRIBUTIONS OF INTEGRATED WATER VAPOUR AND LIQUID WATER CONTENTS GIVEN IN RECOMMENDATIONS ITU-R P.836-4 AND ITU-R P.840-4", Dec 2010.

43 A. Martellucci, "Use and development of climatological and experimental databases for radiowave propagation modelling in SatCom and SatNav systems", invited paper, Proceedings of 3rd European conference on antennas and propagation, EuCAP 2009, 23-27 March 2009, Berlin, Germany, pp. 2002-2006

44 European Space Agency (ESA) COST Action 255, "Radiowave Propagation Modelling for SatCom Services at Ku-Band and Above", Final Report, ESA Publication Division, 2002, chapter 2.1

[45] ESA, "ITALSAT Propagation Handbook," European Space Agency.

[46] Savvaris, A. (2004), *Accurate Prediction of Scintillation Degradation Applicable to Satellite Communication Systems Design* (PhD thesis), University of Glamorgan, .

[47] A. Savvaris, "Transfer Report: Accurate Prediction of Scintillation Degradation Applicable to Satellite Communication Systems Design," University of Glamorgan, Pontypridd 2002.

[48] RCRU, "Report of the RCRU at RAL for the Year 1997, Annual report," Rutherford Appleton Laboratory (RAL) 1997.

[49] J. M. Woodroffe, R. C. H. Morgan, and J. R. Newbury, "Preliminary Results from an ITALSAT Propagation Experiment at 49.5GHz in the UK," presented at Olympus Utilisation Conference (WPP-60), Seville, Spain, 1993.

[50] Science and Technology Facilities Council (STFC), Chilbolton Facility for Atmospheric and Radio Research, [Wrench, C.L.]. Chilbolton Facility for Atmospheric and Radio Research (CFARR) data, [Internet]. British Atmospheric Data Centre, 2003-,April 2010. Available from http://badc.nerc.ac.uk/data/chilbolton/.

[51] Ventouras, S., P. G. Davies, and J. R. Norbury (1995), "Olympus based propagation measurements in southern UK", IEE Conf. Publ., 407, 27-31.

[52] S. Ventouras, S. A. Callaghan, and C. L. Wrench (2006), "Long-term statistics of Tropospheric attenuation from the Ka/U band ITALSAT satellite experiment in the United Kingdom", Radio Sci., 41, RS2007 , doi:10.1029/2005RS003252.

[53] UK Meteorological Office. MIDAS Land Surface Stations data (1853-current), [Internet].NCAS British Atmospheric Data Centre, 2006, April 2010. Available from http://badc.nerc.ac.uk/view/badc.nerc.ac.uk__ATOM__dataent_ukmo-midas/.

[54] , ERA Interim, Daily Fields, Full Resolution , available at: http://data-portal.ecmwf.int/data/d/interim_full_daily (accessed 12/14/2011).

[55] Dee, D. P., Uppala, S. M., Simmons, A. J., Berrisford, P., Poli, P., Kobayashi, S., Andrae, U., Balmaseda, M. A., Balsamo, G., Bauer, P., Bechtold, P., Beljaars, A. C. M., van de Berg, L., Bidlot, J., Bormann, N., Delsol, C., Dragani, R., Fuentes, M., Geer, A. J., Haimberger, L., Healy, S. B., Hersbach, H., Hólm, E. V., Isaksen, L., Kållberg, P., Köhler, M., Matricardi, M., McNally, A. P., Monge-Sanz, B. M., Morcrette, J. -., Park, B. -., Peubey, C., de Rosnay, P., Tavolato, C., Thépaut, J. -. and Vitart, F. (2011), "The ERA-Interim reanalysis: configuration and performance of the data assimilation system", Quarterly Journal of the Royal Meteorological Society, vol. 137, no. 656, pp. 553-597.

[56] Assis, M.S., Einloft, C.M., "A Simple Method for Estimating Rain Attenuation Distributions." Proc. URSI, La Baule, p.301, 1977.

[57] Bryant G.F., Adimula I., Riva C., and G. Brussaard, "Rain Attenuation Statistics from Rain Cell Diameters and Heights", submitted to International Journal of Satellite Communications, 1999.

[58] Crane R.K. "Prediction of attenuation by rain", IEEE Transaction on Communications, COM-28, pp. 1717-1733, 1980.

[59] Flavin R.K., "Satellite link rain attenuation in Brisbane and a proposed new model for Australia", Telstra Research Laboratories, Report N. 8375, 1996.

[60] ITU-R, "Propagation data and prediction methods required for the design of Earth-space telecommunication systems", Propagation in Non-Ionised Media, Recommendation 618-1to9, Geneva, (1986-1990-1992-1994-1995-1997-1999-2001-2003-2007).

[61] Mandeep J.S., TANAKA K.: 'Effects of atmospheric parameters on satellite link', Int. J. Infrared Millimeter Waves, 2007, 28, (10), pp. 789-795

[62] Mandeep J.S., Ojo J.S., Emiliani L.D.: 'Statistics of annual and diurnal cloud attenuation over equatorial climate', IET Commun., 2009, Vol. 3, Iss. 4, pp. 630-635

[63] Raina M. K.: 'Atmospheric Emission Measurements of Attenuation by Microwave Radiometer at 19.4 GHz', IEEE Trans. on Antennas and propagation, 1996, Vol. 44, No. 2, pp.188-191

[64] Dissanayake A., Allnutt J., Haidara F.: 'Cloud attenuation modelling for SHF and EHF applications', Int. J. Satell. Commun. 2001, Vol. 19, pp. 335-345

[65] Maitra A., Chakraborty S.: 'Cloud Liquid Water Content and Cloud Attenuation Studies with Radiosonde Data at a Tropical Location', J. Infrared Milli Terahz Waves, 2009, No. 30, pp. 367-373

[66] Savvaris A., Otung I.E., "Preliminary Preprocessing of ITALSAT Data at 20, 40 and 50 GHz", URSI 2000 Symposium.

[67] E. Salonen, C.Riva, and J.P.V Poiares Baptista, "A global model for total fade distribution of atmospheric phenomena", Millennium Conference on Antennas & Propagation, AP2000, ESA SP-444 PROCEEDINGS, 9-14 April 2000, Davos, Switzerland.

[68] I. Otung, *Communication Engineering Principles*: Palgrave, 2001.

[69] A. Bateman, *Digital Communications - Design for the Real World*: Addision Wesley, 1999.

[70] ITU-R F.557-4, Geneva, 1997.

[71] C. K. Kassianides, "A Study of the Effects of Scintillation on Digital Satellite Communication Systems," in *School of Electronics*. Pontypridd: University of Glamorgan, 2002.

[72] F. Xiong, "Modem Techniques in Satellite Communications," *IEEE Communications Magazine*, pp. 84-98, August 1994.

[73] ITU-R P.1623, "Prediction method of fade dynamics on Earth-space paths", ITU, Geneva, Switzerland, 2003.

[74] European Space Agency (ESA) COST Action 255, "Radiowave Propagation Modelling for SatCom Services at Ku-Band and Above", Final Report, ESA Publication Division, 2002, chapter 5.3

[75] *Hörle J., 'Up-link power control of satellite Earth stations as a fade countermeasure of 20/30 GHz communications systems', Int. Jour. Of Sat. Com., Vol. 6, June 1988, pp. 323-330*

[76] R. J. Acosta, "Rain Fade Compensation Alternatives for Ka-band Communication Satellite," presented at 3rd Ka-Band Ultilization Conference, Sorrento, Italy, 15-18 Sep. 1997.

[77] M. J. Willis and B. G. Evans, "Fade Countermeasures at Ka band for Olympus," *Int. Journal of Satellite Communication*, vol. 3, pp. 301-311, 1988.

[78] L. Castanet, J. Lemonton, and M. Bousquet, "Fade Mitigation Techniques for New SatCom Services at Ku-band and Above: a Review," presented at 5th International Workshop on Radiowave Propagation Modelling for SatCom Services at Ku-band and Above, Netherlands, 28-29 Oct. 1998.

[79] H. Fukuchi, "Quantitative Analysis of the Effect of Adaptive Satellite Power Control as a Rain Attenuation Countermeasure," presented at IEEE International Symposium on Antennas and Propagation, 1994.

[80] Poiares Baptista P., Paraboni A., "Active compensation techniques for spacecraft antennas", ESA publication, "Preparing for the future", vol. 5, n°1, March 1995

[81] C. D. Hughes and M. Tomlinson, "The Use of Spread-Spectrum Coding as a Fading Countermeasure at 20/30 GHz," *ESA Journal*, vol. 11, pp. 73-81, 1988

[82] J. G. Proakis, *Digital Communications*, Third Edition ed: Mc Graw-Hill Int. Ed., 1995.

[83] M. Filip and E. Vilar, "Implementation of Adaptive Modulation as a Fade Countermeasure," *Int. Journal of Satellite Communication*, vol. 8, pp. 33-41, June 1990

[84] B. C. Gremont, M. Filip, and E. Vilar, "Simulation of a High Frequency Satellite Link with a Fade Countermeasure," presented at International Conference on Antennas and Propagation (ICAP 1999), York, UK, 1999

[85] E. Matricciani, "Prediction of Site Diversity Performance in Communications Systems Affected by Rain Attenuation: Extension of Two Layer Rain Model," *Euro. Trans. on Telecomms and Related Technologies*, vol. 5, pp. 327-336, May-June 1994.

[86] D. B. Hodge, "An Improved Model for Diversity Gain on Earth-Space Propagation Paths," *Radio Science*, vol. 17, pp. 1393-1399.

[87] Chambers, A. (2008), *Viability of High Availability V band Satellite Communication using Hybrid Fade Mitigation* (PhD thesis), University of Glamorgan, .

[88] Tiedtke, M. (1993), "Representation of clouds in large-scale models", Mon. Wea. Rev., 121, 3040-3061.

[89] National Center for Atmospheric Research, 'ERA-Interim Vertical Coordinate Conventions and Numerical Attributes', http://dss.ucar.edu/datasets/ds627.0/docs/Eta_coordinate/, 20 Oct. 2008. (accessed 12/14/2011).

[90] D. Vanhoenacker-Janvier, C. J. Gibbins, C. J. Walden, C. L. Wrench, S. Ventouras, J. Spiegel(1), C. Oestges, D. Mertens, A. Martellucc, 'CHARACTERIZATION AND MODELLING OF PROPAGATION EFFECTS IN 20-50 GHZ BAND', XXVIIIth General Assembly of International Union of Radio Science Proceedings, new delhi, 2005.

[91] Paraboni, A., Riva, C., Capsoni, C., Luini, L., Castanet, L., Jeannin, N., Martellucci, A., Pontes, M., Schonhuber, M. & Emiliani, L. 2011, 'Propagation modelling and mapping of rain, clouds and water vapour to cope with spatial and temporal variability', Proceedings of the 5th European Conference on Antennas and Propagation, EUCAP 2011, pp. 3242.

[92] I. E. Otung, "Accurate prediction of scintillation degradation applicable to satellite communication system design," University of Glamorgan 1998.